

Collisionless magnetic reconnection : the Contour Dynamics approach

Citation for published version (APA):

van der Plas, E. V. (2007). *Collisionless magnetic reconnection : the Contour Dynamics approach*. [Phd Thesis 2 (Research NOT TU/e / Graduation TU/e), Applied Physics and Science Education]. Technische Universiteit Eindhoven. <https://doi.org/10.6100/IR629516>

DOI:

[10.6100/IR629516](https://doi.org/10.6100/IR629516)

Document status and date:

Published: 01/01/2007

Document Version:

Publisher's PDF, also known as Version of Record (includes final page, issue and volume numbers)

Please check the document version of this publication:

- A submitted manuscript is the version of the article upon submission and before peer-review. There can be important differences between the submitted version and the official published version of record. People interested in the research are advised to contact the author for the final version of the publication, or visit the DOI to the publisher's website.
- The final author version and the galley proof are versions of the publication after peer review.
- The final published version features the final layout of the paper including the volume, issue and page numbers.

[Link to publication](#)

General rights

Copyright and moral rights for the publications made accessible in the public portal are retained by the authors and/or other copyright owners and it is a condition of accessing publications that users recognise and abide by the legal requirements associated with these rights.

- Users may download and print one copy of any publication from the public portal for the purpose of private study or research.
- You may not further distribute the material or use it for any profit-making activity or commercial gain
- You may freely distribute the URL identifying the publication in the public portal.

If the publication is distributed under the terms of Article 25fa of the Dutch Copyright Act, indicated by the "Taverne" license above, please follow below link for the End User Agreement:

www.tue.nl/taverne

Take down policy

If you believe that this document breaches copyright please contact us at:

openaccess@tue.nl

providing details and we will investigate your claim.



**Collisionless
Magnetic
Reconnection**

the Contour Dynamics approach

E.V. van der Plas

**Collisionless magnetic reconnection,
the Contour Dynamics approach**

PROEFSCHRIFT

ter verkrijging van de graad van doctor aan de
Technische Universiteit Eindhoven, op gezag van de
Rector Magnificus, prof.dr.ir. C.J. van Duijn, voor een
commissie aangewezen door het College voor
Promoties in het openbaar te verdedigen
op vrijdag 28 september 2007 om 16.00 uur

door

Emiel Valentijn van der Plas

geboren te Amsterdam

Dit proefschrift is goedgekeurd door de promotoren:

prof.dr. N.J. Lopes Cardozo
en
prof.dr. W.J. Goedheer

Copromotor:
dr. H.J. de Blank

CIP-DATA LIBRARY TECHNISCHE UNIVERSITEIT EINDHOVEN

Plas, Emiel V. van der

Collisionless magnetic reconnection : the Contour Dynamics approach /
by Emiel Valentijn van der Plas. - Eindhoven : Technische Universiteit Eindhoven, 2007.
Proefschrift. - ISBN 978-90-386-1614-8

NUR 925

Trefw.: plasma-instabiliteiten / kernfusiereactoren / magnetohydrodynamica /
magnetoplasma's / plasmakinetica.

Subject headings: tearing instability / fusion reactors / magnetohydrodynamics /
magnetic reconnection / plasma kinetic theory.

The work described in this dissertation is part of a research program of the Stichting voor Fundamenteel Onderzoek der Materie (FOM) with financial support from the Nederlandse Organisatie voor Wetenschappelijk Onderzoek (NWO) and Euratom. The work was carried out at the FOM-Institute for Plasma Physics Rijnhuizen in Nieuwegein, the Netherlands. The views and opinions expressed herein do not necessarily reflect those of the European Commission.

Soon you will forget everything, soon everybody will forget you.
Marcus Aurelius, Personal Notes.

Contents

1	Introduction	1
1.1	Reconnection	1
1.2	Relevance	2
1.3	Modelling of magnetic reconnection	5
1.4	This thesis	6
1.4.1	Physical question	6
1.4.2	Method	7
1.5	Outline	9
1.6	List of publications	10
	References	10
2	Model equations	13
2.1	Single particle trajectories and drift motion	13
2.1.1	Gyro-orbits and guiding centre motion	13
2.1.2	The $\mathbf{E} \times \mathbf{B}$ drift	14
2.1.3	The polarization drift	14
2.1.4	The diamagnetic drift	15
2.2	The Vlasov equation	16
2.3	The drift-kinetic approximation	18
2.3.1	Reduction by strong magnetization	18
2.3.2	Convective form of the drift-kinetic equation	20
2.3.3	Discretization of the perturbed distribution function	20
2.3.4	Isothermal fluid equations	22
2.4	The cold ion approximation	24
2.4.1	The polarization drift approach	24
2.4.2	The particle approach	26
2.5	The generalized Ohm's law	27
2.6	Kinetic waves in a strongly magnetized plasma	28
2.6.1	Waves in drift-kinetic theory	29
2.6.2	The plasma dispersion function	30
2.6.3	Waves in the two-fluid drift-Alfvén model	33
2.6.4	The fluid reduction of the kinetic equations	34
	References	36
3	Kinetic collisionless tearing instability in slab geometry	37
3.1	Introduction	39
3.2	The drift-kinetic model	40
3.3	Equilibrium	42
3.4	Linear stability	44
3.4.1	Fluid case	44
3.4.2	Kinetic case	46
3.5	Connection to Δ'	47
3.6	Discussion of the fluid limit of the kinetic equations	48

3.7	Influence of a temperature gradient on the linear stability	49
3.7.1	Perturbed eigenfunctions	50
3.7.2	Linear phase shift near marginal stability	51
3.8	Nonlinear phase shift	52
3.9	Discussion	57
	References	58
3.A	Proof of the uniqueness of the tearing mode solution	60
3.B	Estimates for the plasma dispersion function	62
4	Temperature gradients in fast collisionless magnetic reconnection	65
4.1	Introduction	67
4.2	Drift-kinetic model	67
4.3	Equilibrium, linear stability	68
4.4	Influence of a temperature gradient	70
4.5	Nonlinear shift	70
4.6	Discussion	72
	References	73
5	Collisionless tearing mode in cylindrical geometry	75
5.1	Introduction	77
5.2	The two-fluid drift-Alfvén model	78
5.3	Contour Dynamics	78
5.4	Equilibrium, linear stability	80
5.5	Numerical method	83
5.6	Numerical results	84
5.6.1	Comparison to the linear dispersion relation	84
5.6.2	Nonlinear saturation of the magnetic islands	87
5.6.3	Scale collapse	88
5.6.4	Effect of the electron temperature	89
5.6.5	Complete internal $m = 1$ reconnection	89
5.7	Discussion	90
	References	91
5.A	The stability of a current-vortex patch	93
5.A.1	A circular current-vortex patch	93
5.A.2	Linear perturbation of two concentric current-vortex patches	94
5.A.3	Stability of a single current-vortex patch	94
5.A.4	Stability of a pair of concentric patches	95
5.A.5	Stability of a pure current patch	95
5.A.6	Stability of a single current patch using eigenfunctions	96
6	Kinetic effects in a cylindrical tearing mode	97
6.1	Introduction	99
6.2	The drift-kinetic model	100
6.3	Initial conditions	101
6.4	Contour Dynamics	102
6.5	Equilibrium, linear stability	103
6.6	Numerical method	106

6.7	Numerical results	108
6.7.1	Comparison with the two-fluid model	108
6.7.2	Comparison with ∇T -effects in slab geometry	111
6.7.3	Dynamical behaviour of the X-point	113
6.8	Discussion	116
	References	117
6.A	Evolution of the macroscopic quantities	118
7	Discussion and conclusions	119
7.1	Method	119
7.2	Linear stability	119
7.3	Nonlinear effects of a temperature gradient	120
7.4	Numerical results	121
7.5	Discussion and outlook	122
	References	124
A	Cylindrical limit of slab results	127
A.1	Equilibrium	127
A.2	Perturbations	129
A.3	Boundary conditions: the dispersion relation	131
	References	133
	Summary	135
	Samenvatting	141
	Acknowledgements	147
	Curriculum Vitae	149

1 Introduction

1.1 Reconnection

“There is hardly a term in plasma physics which exhibits more scents, facets and also ambiguities, and which at times seems to be used with a touch of magic. The basic picture is that of two field lines frozen in and carried along with the fluid, until they come close to each other at some point where, due to weak non-ideal effects in Ohm’s law, they are cut and reconnected in a different way.”

D. Biskamp, *Magnetic Reconnection in Plasmas*, [1]

Everything is plasma.

Actually, not everything. In our everyday life only few examples of plasma come to mind, such as incandescent tubes and recently plasma screens. But when we look beyond our relatively cool and dense little planet, almost everything is plasma: stars, interstellar matter, protostars, matter that is either so hot or so dilute and rarefied that the constituent atoms have shed their electrons, resulting in a gas of positively charged nuclei and negatively charged electrons, interacting through the Coulomb-force but otherwise freely moving and independently of each other.

Interstellar space is full of plasma, irradiated by stars and cosmic rays, pulled at by galaxies, black holes or young stellar objects, swirling it around but not quite holding onto it and letting it go in the form of jets that escape again in a very straight fashion for sometimes many tens of light-years. Our Sun itself charges itself up as a giant dynamo and hurls plasma at us in the form of solar wind against which we are shielded by the Earth’s magnetic field, causing aurora Borealis (northern light), and magnetic substorms in our magnetopause.

In all these phenomena the ionized particles were violently dislocated from the magnetic field line to which they at one time were intimately bound. This violent overthrow, rerouting the infrastructure of the plasma, is called *magnetic reconnection* (see Fig. 1.1).

To understand what magnetic reconnection is, and under what circumstances it occurs, we first look at the situation in which it does not occur. An ideal plasma is a plasma that is an ideal electric conductor. Because of the relative freedom of the charged particles, this is not a very far-fetched idea. In this case the plasma particles and magnetic field lines are indissolubly connected. When the magnetic field is perturbed, the plasma responds by generating a current that tries to nullify the original disturbance. This is demonstrated in superconducting materials, that expel an external magnetic field with so much success that a magnet actually stays afloat above them, unable to push in its magnetic field. When the material becomes resistive, the magnetic field sinks in, and the magnet lands on top. The same happens to a plasma when the particles do collide, and thus experience friction and resistivity. The current that had formed decays and the magnetic field becomes prone to change. Change here means that it may undergo *topological* change: the magnetic field lines can be envisaged to be cut loose, and then reconnected again enabling the magnetic field to relax into a differently organized state.

This process is responsible for the transformation of differential rotation of e.g. the Sun into a giant dynamo, and the unleashing of coronal mass ejections, that lead to magnetic storms that make astronauts dive away behind a lead wall and create havoc amongst the global positioning satellites. It is also responsible for the reorganization of the magnetic field within

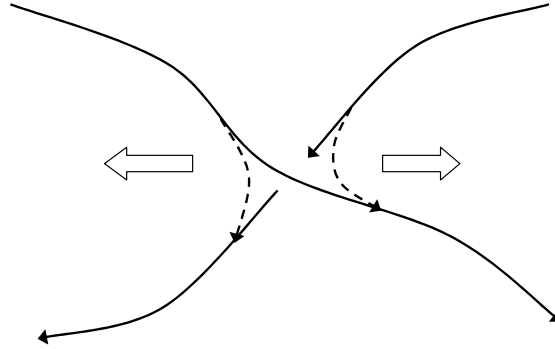


Figure 1.1: The basic process of magnetic field line reconnection: the relaxation of magnetic tension by the reorganization of the magnetic field.

fusion plasmas in present day laboratory experiments, threatening magnetic confinement by creating exponentially growing helical structures within the plasma that do not support a large temperature gradient.

However, under these circumstances, due to the high temperature, particle collisions become so scarce that the sheer speed with which the reconnection process unfolds poses a riddle: How can the structure of the magnetic field change so drastically in a time that is so short that only few plasma particles can collide? The mean collision time between electrons can be up to a factor 10 larger than the timescale in which the reconnection process takes place. When this is the case, the process is called *collisionless reconnection*.

There are several mechanisms that may cause reconnection to occur in the absence of collisions, such as (electromagnetic) turbulence, and wave-particle interactions such as Landau damping. One that seems promising in predicting fast reconnection is electron inertia: the finite electron mass results in the fact that the current sheet that should prevent reconnection from happening is drawn up too late. In this fashion the field lines have come loose and reconnected before the shielding electrons get into motion.

Slowish electrons yield a possible mechanism for collisionless reconnection, but still a lot of questions remain. As stated before, a magnetic field line within a certain part of the plasma ‘carries’ electrons with a certain temperature. But what happens when this field line is cut open and connected to a field line with electrons of a very different temperature? Especially in fusion experiments the temperature gradient can be enormous, larger than anywhere else in the universe, even. What do electrons with different energies do during the reconnection process? This will be one of the main questions addressed in this thesis.

1.2 Relevance

Reconnection takes place in various types of plasmas: plasmas can either be too hot or too dilute to display collisional, resistive behaviour. The main application of the research that will be presented here is *nuclear fusion*. Nuclear fusion is the process during which two lighter atomic nuclei collide and merge into a heavier one. The reaction products carry the energy that is released in such a process as kinetic energy, i.e. by going extremely fast. The process that is the most feasible candidate to produce fusion power in a reactor is between two

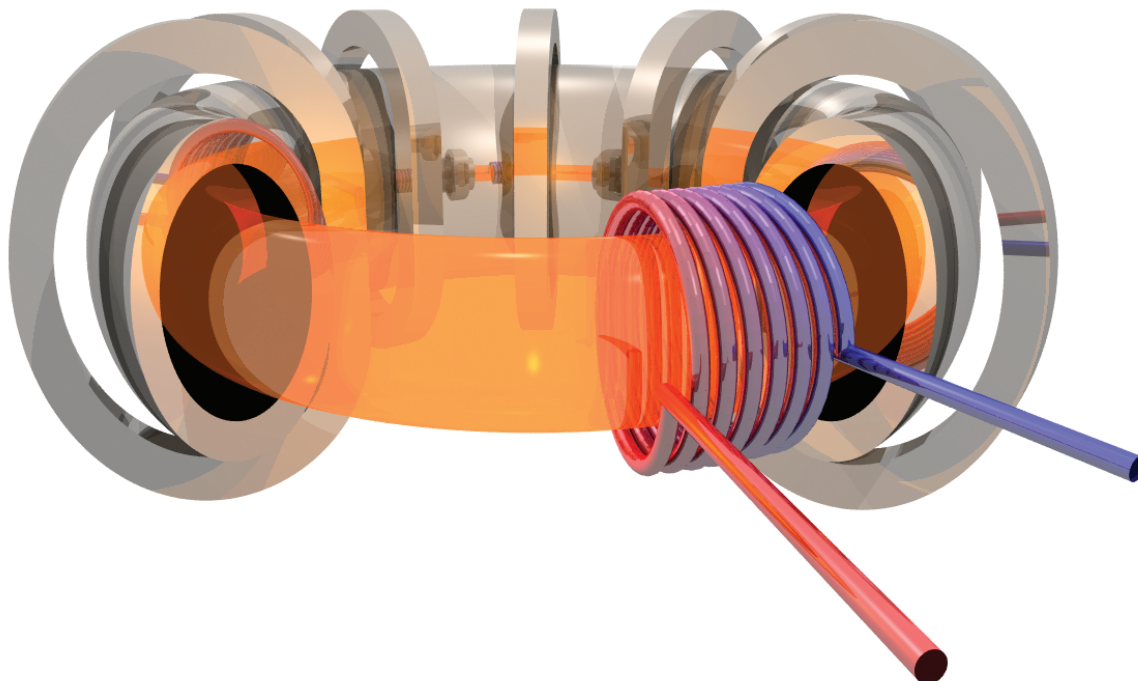


Figure 1.2: A schematic drawing of a tokamak. Shown are the toroidal magnetic field coils, the vessel, the heat exchanger and the plasma (in orange).
(Figure: FOM Rijnhuizen)

hydrogen isotopes, deuterium (D) and tritium (T) to yield helium and a neutron,



Because of energy and momentum conservation, most of the kinetic energy will be carried by the neutron. Deuterium consists of a nucleus with a positively charged proton and a neutron and a negatively charged electron surrounding it, and tritium has a proton and two neutrons in its nucleus. The process is hindered by the Coulomb-force: the nuclei are both positively charged and hence repel each other. This means that the nuclei have to have a very high velocity to overcome this barrier.

The Sun also relies on nuclear fusion as its energy source, and confines plasma at a temperature of 15 million degrees Kelvin in its core with its huge gravity field pulling the plasma inward. This leads to a relatively slow, smouldering fusion reaction.

Here on Earth, we have to do better. And hotter. We want to maintain a fusion reaction with minimum input power and maximum yield, which means that we have to heat the D-T plasma to a much higher temperature. When the ions have a mean energy of 15 keV, corresponding to roughly 150 million degrees Kelvin, enough particles have such a high energy that they can pass through the Coulomb barrier by quantum mechanical tunneling. To achieve such temperatures is hard, but not impossible. To keep the plasma insulated, present day fusion reactor concepts use a toroidally shaped magnetic field. The best candidate for delivering net fusion power in the near future is called the *tokamak* (see Fig. 1.2), a machine with a strong magnetic field in the *toroidal* direction (the long way around the torus), and

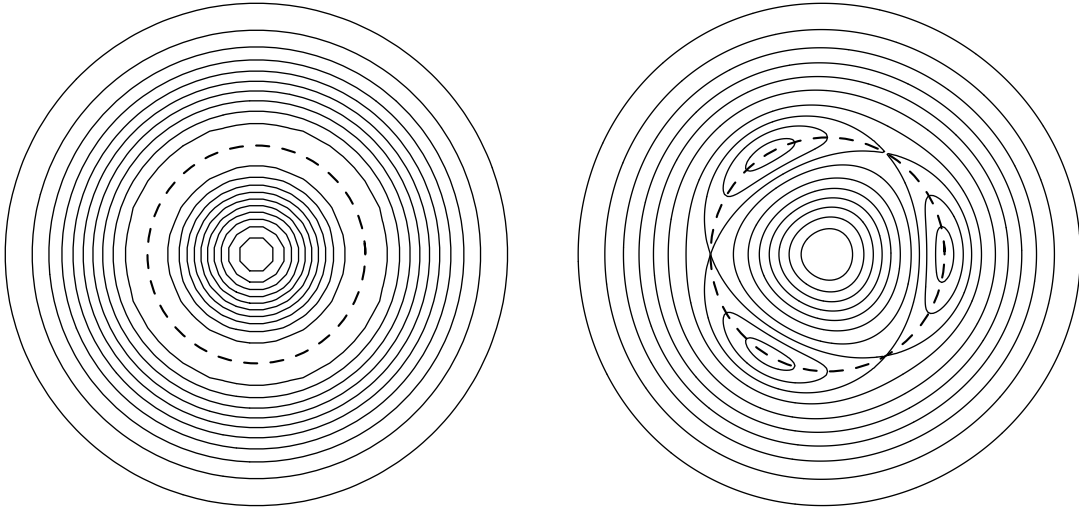


Figure 1.3: On the left the circles represent a poloidal cross section of the closed flux surfaces, and the dashed line shows the resonant surface. On the right the surfaces around the resonant surfaces are torn by a tearing mode with mode number $m = 3$. A chain of magnetic islands appears.

a current through the plasma, generated either inductively or non-inductively, results in a smaller *poloidal* component. The now helical magnetic field lines are thus organized on nested concentric surfaces, also called *flux surfaces*. The radial profile of the current density induces a poloidal field that is different for each flux surface, leading to the situation where the magnetic field has a different direction on each flux surface, yielding a profile of the magnetic winding number, q . The magnetic field strength B is large compared to the plasma pressure p , even in the next generation machine ITER. This is also called the *low- β regime*, with $\beta = 2\mu_0 p/B^2$. The plasma in ITER will have approximately $\beta \approx 0.03$. Some other machine concepts, such as reverse field pinches, can operate in intermediate or high β .

A tokamak is a complicated machine. The chemicals the wall is made of may pollute the plasma, the magnetic field is generated by a finite number of coils, and therefore rippled, and because of the fact that the toroidal magnetic field is stronger on the inboard-side (the high field side) than on the outboard-side (the low field side) of the torus, particles do no longer follow a field line helically but sometimes stop and turn around when the magnetic field becomes too high, changing the transport properties of the plasma. A tokamak is constantly being fuelled and heated, in a localized way, so that the magnetic winding number q can be adjusted to be non-monotonic. Depending on the profile of the winding number and on the heat distribution, instabilities may arise. These instabilities set the plasma into motion, and some may cause the reconnection of magnetic field lines.

The research presented in this thesis is ultimately aimed at achieving a more thorough understanding of collisionless reconnection, which is responsible for one particular plasma phenomenon that may occur in tokamak plasmas, viz. the *tearing mode*.

This so-called tearing mode is a perturbation of the flux surfaces, resulting in the local break-up (or ‘tearing’) of the flux surface structure, creating a region of helical magnetic islands. In Fig. 1.3 a poloidal cross section of the plasma is depicted before and after such a

break-up. It can be started by only a small perturbation after which it grows exponentially, and is therefore called an “instability”.

This can have several consequences for the plasma confinement: the perturbation of the plasma may lead to the onset of plasma turbulence, creating chaotic small scale structures. Furthermore, the perturbation of one flux surface can induce the break-up of neighboring flux surfaces, resulting in magnetic island chains with different mode numbers. When those island chains grow and start to overlap radially this can be the starting point of *magnetic field ergodization*. The magnetic field lines are no longer confined to their two-dimensional toroidal surfaces, but can fill up a three-dimensional volume, extending over a large radial distance. Because of the excellent parallel conductivity along the field lines, this leads to enhanced transport of particles from the core of the plasma to the edge. When the tearing mode affects the layer in the plasma where the magnetic field returns to the exact same spot after one toroidal rotation, i.e. where the magnetic winding number $q = 1$, generally near the core of the plasma, it can completely or partly turn the enclosed flux inside out, effectively spilling the heat of the central plasma outwards and relaxing it to the temperature of the edge of this region. When this happens repetitively, this is called the *sawtooth* oscillation in tokamak-jargon, referring to the time-trace of the central temperature which builds up and crashes periodically. If the islands grow too large it is possible that an instability at e.g. the $q = 2$ surface causes a plasma *disruption*: the plasma discharge ends at once, releasing all of the magnetic energy stored in the magnetic field. This may cause considerable damage to the inside of the machine, and is something one does not want to happen to an expensive nuclear facility too often.

1.3 Modelling of magnetic reconnection

A lot of effort is put into the study of tearing modes, as they may cause particle and heat transport and threaten the plasma confinement within tokamaks. Experiments are being undertaken that attempt to visualize magnetic islands and to control their onset and growth by applying spatially and temporally localized heating at the center of the island [2].

Reconnection in tokamaks is characterized by the fact that there is a dominant, nowhere vanishing, toroidal ‘guide’-field in the plasma. Because of the fast transport and equilibration along the magnetic field lines the dynamics that concern the tearing mode are reduced to the plane perpendicular to the magnetic field. This contrasts to the astrophysical applications, where generally reconnection is located at regions where $\mathbf{B}(\mathbf{x}) \rightarrow 0$, yielding large gyro-orbits so that particles can decouple from the magnetic field, thus facilitating magnetic reconnection [3, 4].

The assumption of a strong guide field implies that the plasma β is low, which makes the coupling to whistler-type modes negligible as the scale length on which they play a role becomes vanishingly small. In the low- β ordering the kinetic Alfvén wave can couple to the tearing mode.

The excitation of the tearing mode can be modelled in various ways. The perturbation of the flux surfaces can be assumed to stem from an external source, either by means of a forcing of e.g. external magnetic field coils or growing secondary magnetic island chains. This is named *forced* magnetic reconnection [5]. Another way is to describe reconnection as a result of an instability in a plasma that consists of an external, ideal, region that is considered to be far away from the reconnection region, and an internal region that is treated

as a resistive or otherwise unideal boundary layer [6, 7]. Both approaches are able to model a smooth current profile, in which either an external force or the instability because of the current profile itself drive the reconnection of magnetic field. Neoclassical tearing modes can be considered a combination of both, where the mode starts as a perturbation of a linearly stable equilibrium, but becomes unstable as a consequence of the driving feedback of the bootstrap current that depends on the width of the magnetic island that is created.

In this thesis a tearing mode is excited locally by imposing a steep current gradient at two locations, so that they constitute a current layer. In this way the whole plasma region is treated on the same footing, and no further assumptions need to be made regarding the scales.

The literature on reconnection in tokamaks has addressed a number of different mechanisms that enable magnetic field lines to reconnect. A lot of research is done in resistive models [8]. When it became clear that reconnection can occur in near-collisionless plasmas on time scales that are much shorter than the resistive time scale, that corresponds to the mean electron-ion collision time, different collisionless physical mechanisms were investigated, such as reconnection as a result of Landau resonances [9], and electron inertia. The latter has been studied in both a two-fluid context [7, 10] as well as with a kinetic model for the electrons [11]. Electron inertia proved a good candidate to yield fast reconnection rates that were comparable to those found in tokamak experiments.

The effect of the ion temperature on the process of magnetic reconnection has been studied extensively. The consequences of a finite ion gyro-radius have been studied within the framework of the two-fluid drift-Alfvén model [12]. When the ion gyro-radius becomes so large that the effects can no longer be described perturbatively, a kinetic model is called for to calculate the influence of the ion dynamics on the stability and dynamics of a tearing mode. The effects of energetic ions, as they emerge during intense plasma heating and in a burning fusion plasma, have been studied by looking at the consequences of an anisotropic ion pressure [13]. These include the effects of trapped ions. Although the ion temperature effects are not negligible, in this thesis the electron dynamics are studied separately, assuming a passive ion-response to parallel electron compression.

The approach to model collisionless magnetic reconnection that is presented in this thesis is novel, and its results should be compared to results obtained with the same model equations, but by a different approach, as e.g. reported in [11]. Here, a kinetic model is used to calculate the evolution in time of a tearing mode in a smooth equilibrium in a straight, double periodic domain. It is noted that the computational effort that is needed is a limiting factor. Our approach makes use of local excitation of the mode by perturbing steep current gradients, which yields a self-consistent and analytically tractable model that is valid on the infinite plane. The numerical implementation requires the use of a discrete number of contours that represent the parallel velocity, instead of a smooth and continuous velocity distribution as in [11].

1.4 This thesis

1.4.1 Physical question

Fast magnetic reconnection is observed in laboratory fusion experiments, as well as in the rarefied plasmas in the Earth's magnetosphere [14]. The fact that this happens at timescales so much shorter than the collision times of the electrons motivated the study of electron inertia

as a fast reconnection mechanism [10, 15, 16]. Here, we will focus on reconnection in fusion plasmas, that are designed to sustain a very large temperature gradient across the magnetic field lines. However, in collisionless plasmas, electrons move and equilibrate rapidly along the reconnecting field lines, but have mean collision times perpendicular to the magnetic field that are long compared to the transit time of the system. Therefore, a temperature difference poses a fundamental physics problem whose solution requires a kinetic model, as electrons of different energies are shown to display different behaviour during this process [17].

In this thesis the behaviour of a collisionless reconnecting instability is studied, in a plasma with a strong magnetic guide field and where reconnection is made possible by finite electron inertia.

The main question addressed in this thesis will be:

What is the effect of a temperature gradient on reconnecting magnetic field lines in near-collisionless plasmas?

This question can be made more specific, considering the underlying physics:

- What is the role of collisionless electrons in this process?
- How do the reconnected electrons contribute to the current and temperature distributions inside the magnetic island?
- How is the macroscopic magnetic field modified?

To be able to answer these questions, the following subquestions need to be addressed:

- How do we set up a kinetic model that can take into account non-collisionality and a temperature gradient?
- What are the kinetic effects of the electron motion parallel to the magnetic field, and how do they affect the linear and nonlinear stability properties of a tearing mode in a straight current layer with or without a temperature gradient?
- What are the linear stability properties of a tearing mode in an annular current layer, what are the subsequent isothermal nonlinear effects, and how do they agree with numerical simulations based on the very same model?
- How does the anatomy of a nonlinear reconnecting mode in an annular current layer change when kinetic effects such as a temperature gradient are taken into account?

1.4.2 Method

Model

The nonlinear aspects of reconnection have proven to be essential to understand why it can be so fast. Also, temperature effects are expected to be dependent on the finite island size [17]. Therefore, we make use of a method that has shown to be suitable for the handling of nonlinear dynamics in fluid problems, viz. *contour dynamics*. This is a formalism that is used in studying two-dimensional fluid flow, calculating the evolution in time of the boundaries of an area with uniform vorticity, and more recently also applied to plasma fluid models [18, 19, 20, 21].

However, the combination of the weak collisionality of the plasma and the fact that we are interested in the effects of a temperature gradient requires a kinetic model. Therefore we

have developed a *kinetic contour dynamics* model. This is a novel model, and it takes some initial investigations to make sure that we can apply it to our problem.

First, a kinetic model is developed to provide a basic tokamak-like background. It assumes a dominant magnetic field in one direction and a smaller perpendicular component, and a plasma $\beta \ll 1$. The ion dynamics are reduced so that they only respond passively to local charge imbalance by parallel electron compression. The fact that the equilibration along the magnetic field lines happens at very short time scales reduces the dynamics of interest, making it effectively two-dimensional. The model describes the electron dynamics perpendicular to the magnetic field, and is applicable to timescales that are large compared to the characteristic time of plasma oscillations, ω_{pe}^{-1} and the electron gyro-frequency Ω_e . The electron velocity parallel to the magnetic field is described by a distribution function that may depend on time and space [11, 17].

The isothermal two-fluid plasma model [12] is retrieved as a limit of the drift-kinetic model by replacing the full electron velocity distribution function by an equilibrium part and a discrete amount of electrons with plus and minus the thermal velocity, that thus constitutes a current in a specified region.

Here it is noted that contour dynamics is predominantly a method that determines the choice of the initial conditions of a plasma problem. By specifying finite spatial areas with uniform electron velocity distribution, the boundaries specify discretized contours, and hence all the analysis that will follow can be considered contour dynamics. On the other hand, by means of discretization in velocity space only the kinetic formalism can reduce to fluid formalism. When discretization in both real and velocity space is applied, the method can be used in numerical simulations.

Linear stability

This model, described in detail in Chapter 3, is applied to an equilibrium current distribution that is uniform, except for discontinuities in one direction of inhomogeneity at certain places. In fact, because the distribution is uniform almost everywhere, the discontinuity is the only place where the equilibrium may be perturbed. Because this jump is a boundary for electrons with a specific velocity parallel to the magnetic field, one may say that for every parallel velocity the electrons can be represented by a specific *contour*. The assumption that these electrons behave like an incompressible fluid completes the correspondence between the methods used in incompressible 2D Euler-flow and kinetic modelling of collisionless reconnecting instabilities in magnetized plasma.

The equilibrium that is used, upon which the perturbations and the ensuing instabilities take place, is generally chosen to be of rather simple geometry, slab or cylinder, and harbours the scale length d_e in it, the electron inertial skin depth, which is a consequence of assuming finite electron inertia as the mechanism that causes reconnection.

To be able to perform nonlinear analysis of the dynamics of this system, we have to be certain of the linear stability properties of the equilibrium. In slab geometry, the full drift-kinetic model becomes tractable enough to derive a linear dispersion relation for the frequency or growth rate of an instability, and study the influence of a number of parameters, among which the difference or mismatch between the velocity distribution functions of the electrons from either originating area of the reconnecting magnetic field lines. Also statements about the form and symmetry of the resulting magnetic islands in the nonlinear stage are made, once steady reconnection ($\partial^2\psi/\partial t^2 = 0$) is reached. In cylindrical geometry, linear stability

analysis can be performed using the two-fluid drift-Alfvén equations.

Numerics

The idea of applying contour dynamics to problems in plasma physics is not new [19, 20, 21]. However, no attempt was made to study magnetic reconnection with this method. We have gratefully made use of the computer code that was developed by P.W.C. Vosbeek [18, 22], which was made available to us by L.P.J. Kamp of the TU Eindhoven. We adapted this code to model a discretized electron velocity distribution along the magnetic field lines, making it possible to discern between the behaviour of very fast and more or less co-moving electrons. The discretization in velocity space is discussed in section 2.3.3. In this way we can study the nonlinear dynamics in the plane perpendicular to the magnetic guide field causing collisionless magnetic reconnection and model the effects of a spatially varying distribution of parallel velocity, such as a temperature gradient. More subtle phase-space effects such as Landau damping are beyond the scope of this thesis. Numerically, it is more straightforward to study the cylindrical equilibria, as they form a spatially bounded area on the infinite plane.

The choice of this approach to model nonlinear collisionless reconnection provides us with a transparent physical model which makes the linear and nonlinear analysis and the numerical simulations comparable to a high degree.

1.5 Outline

Chapter 2 introduces some background on the type of plasma physics that will be discussed in this thesis.

Chapters 3 and 4 treat the same subject, but Chapter 3 is set up as a more introductory and complete paper, providing derivations, discussions and proofs, whereas Chapter 4 has the form of a compact report. They consider the linear stability properties of a straight current slab for the full drift-kinetic equations. The effect of a temperature gradient is discussed in both the linear and nonlinear stage of an unstable tearing mode.

In Chapter 5 the analysis is extended to cylindrical geometry, considering the linear stability of an annular current equilibrium using the isothermal two-fluid equations. A numerical contour dynamics code is used to calculate the nonlinear evolution in time of this equilibrium. The analytical results have been compared to growth rates that can be obtained using the contour dynamics code. Some nonlinear phenomena have been observed and quantified.

The code was extended so that it can handle arbitrarily many contours in velocity space, making it possible to study kinetic effects and to model a collisionless plasma with a temperature gradient. The numerical results are reported in Chapter 6. These results are compared to the theoretical predictions made in Chapters 3 and 4.

The results of the work presented in this thesis are discussed in Chapter 7. In Appendix A the equivalence of the cylindrical and the slab results is shown, making sure that they are limiting cases of each other.

1.6 List of publications

Below is a list of publications related to this thesis.

Journal publications

E. V. van der Plas, H. J. de Blank. Temperature gradients in fast collisionless magnetic reconnection. *Phys. Rev. Lett.* 98:265002, 2007.

E. V. van der Plas, H. J. de Blank. Kinetic model of a collisionless tearing instability in slab geometry, to be submitted to *Phys. Plasmas*.

E. V. van der Plas, H. J. de Blank. Collisionless tearing mode in cylindrical geometry, to be submitted to *Plasma Phys. Control. Fusion*.

E. V. van der Plas, H. J. de Blank. Kinetic effects in a cylindrical tearing mode using Contour Dynamics, in preparation.

Conference proceedings

E. V. van der Plas and H. J. de Blank. Kinetic drift effects in magnetic reconnection, *31st EPS Conference on Plasma Physics*, 28 June - 2 July 2004, London (UK), P-2.073.

E. V. van der Plas, L. P. J. Kamp and H. J. de Blank. Contour dynamics modelling of kinetic magnetic reconnection, *33rd EPS Conference on Plasma Physics*, 19 - 23 June 2006, Rome (Italy), P-5.156.

H. J. de Blank and E. V. van der Plas, Contour Dynamics: Kinetic electron simulation of collisionless reconnection, *34th EPS Conference on Plasma Physics*, 2 - 6 July 2007, Warsaw (Poland), P-4.081.

References

- [1] D. Biskamp. *Magnetic reconnection in Plasmas*. 2000.
- [2] I. G. J. Classen, E. Westerhof, C. W. Domier, A. J. H. Donne, R. J. E. Jaspers, Jr. N. C. Luhmann, H. K. Park, M. J. van de Pol, G. W. Spakman, and M. W. Jakubowski TEXTOR team. *Phys. Rev. Lett.*, 98(3):035001, 2007.
- [3] T. G. Cowling. Magnetic Stars. In L. H. Aller and D. B. McLaughlin, editors, *Stellar Structure - Stars and Stellar Systems*, page 425, 1965.
- [4] J. M. Green. *J. Geophys. Res.*, 93:8583–90, 1988.
- [5] T. S. Hahm and R. M. Kulsrud. *Phys. Fluids*, 28:2412, 1985.
- [6] H. P. Furth, J. Killeen, and M. N. Rosenbluth. *Phys. Fluids*, 6:459, 1963.
- [7] M. Ottaviani and F. Porcelli. *Phys. Rev. Lett.*, 71:3802, 1993.

-
- [8] E. N. Parker. *J. Geophys. Res.*, 62:509–520, 1957.
- [9] B. Coppi, J. W.-K. Mark, L. Sugiyama, and G. Bertin. *Phys. Rev. Lett.*, 42:1058, 1979.
- [10] M. Ottaviani and F. Porcelli. *Phys. Plasmas*, 2:4104, 1995.
- [11] T. V. Liseikina, F. Pegoraro, and E. Yu. Echkina. *Phys. Plasmas*, 11:3535, 2004.
- [12] T. J. Schep, F. Pegoraro, and B. N. Kuvshinov. *Phys. Plasmas*, 1:2843, 1994.
- [13] F. Porcelli. *Phys. Rev. Lett.*, 66(4):425–428, 1991.
- [14] V. M. Vasyliunas. *Rev. Geophys. Space Phys.*, 13:303, 1975.
- [15] J. Wesson. *Nuclear Fusion*, 30:2545, 1990.
- [16] E. Cafaro, D. Grasso, F. Pegoraro, F. Porcelli, and A. Saluzzi. *Phys. Rev. Lett.*, 80:4430, 1998.
- [17] H. J. de Blank and G. Valori. *Plasma Phys. Control. Fusion*, 45:A309, 2003.
- [18] P. W. C. Vosbeek and R. M. M. Mattheij. *J. of Comput. Phys.*, 133:222, 1997.
- [19] N. J. Zabusky, M. H. Hughes, and K. V. Roberts. *J. of Comput. Phys.*, 30:96, 1979.
- [20] J. Bergmans, B. N. Kuvshinov, V. P. Lakhin, and T. J. Schep. *Phys. Plasmas*, 7:2388, 2000.
- [21] J. H. Mentink, J. Bergmans, L. P. J. Kamp, and T. J. Schep. *Phys. Plasmas*, 12:052311, 2005.
- [22] P. W. C. Vosbeek. *Contour Dynamics and Applications to 2D Vortices*. Ph.d. thesis, Technical University Eindhoven, 1998.

2 Model equations

In this chapter some of the basic plasma phenomena will be brought to the footlight that are essential to fully appreciate the work presented in this thesis.

First, by showing how individual particles move in electromagnetic fields, we will progress towards more collective effects such as drift flows and waves. This introduction is not intended to be complete, but merely touches upon the basic subjects.

2.1 Single particle trajectories and drift motion

2.1.1 Gyro-orbits and guiding centre motion

The equation of motion for a particle of type α where $\alpha = i, e$ stands for ion or electron, with mass m_α and charge q_α in an electromagnetic field can be given by

$$\frac{d\mathbf{x}}{dt} = \mathbf{v}, \quad \frac{d\mathbf{v}}{dt} = \frac{q_\alpha}{m_\alpha}(\mathbf{E} + \mathbf{v} \times \mathbf{B}), \quad (2.1)$$

with the last term the *Lorentz* force. Ignoring the source equations for the moment, the fields comply to Maxwell's equations,

$$\nabla \times \mathbf{E} = -\frac{\partial \mathbf{B}}{\partial t}, \quad (2.2)$$

$$\nabla \cdot \mathbf{B} = 0. \quad (2.3)$$

If we consider the case with a homogeneous, static, magnetic field in the z -direction and no electric field, then we can split the velocity in a parallel part $v_{\parallel} = \mathbf{v} \cdot \mathbf{b}$ with $\mathbf{b} = \mathbf{B}/B$ the unit vector in the direction of \mathbf{B} , and a perpendicular part v_{\perp} . We can solve the system given by Eq. (2.1) by

$$v_x = v_{\perp} \sin \Omega t, \quad v_y = v_{\perp} \cos \Omega t, \quad (2.4)$$

and integrate to yield $\rho = \{\rho_x, \rho_y, 0\}$, with

$$\rho_x = \rho_\alpha \cos \Omega_\alpha t, \quad \rho_y = \rho_\alpha \sin \Omega_\alpha t, \quad (2.5)$$

where

$$\Omega_\alpha = \frac{q_\alpha B}{m_\alpha}, \quad \rho_\alpha = \frac{v_{\perp}}{\Omega_\alpha}, \quad (2.6)$$

are the *gyro-* or *Larmor* frequency and radius, so that

$$\rho_\alpha = -\frac{m_\alpha}{q_\alpha B^2} \mathbf{v} \times \mathbf{B}. \quad (2.7)$$

This describes a particle at $\mathbf{x} = \{x, y, z\} = \mathbf{R} + \rho_\alpha$, that is gyrating with a frequency Ω_α , and a radius ρ_α around a point in space, its *guiding centre*, at \mathbf{R} .

The guiding centre may undergo all kinds of movements, and because of the thermal velocity the particle might move extremely fast, but the basis remains the same: a particle gyrates around a field line, and the radius becomes smaller for smaller mass and larger magnetic field.

Note furthermore that the direction in which positively charged particles are gyrating is opposite to that of negatively charged particles.

If we apply some constant force \mathbf{F} on the particle, the equation of motion of the particle Eq. (2.1) becomes

$$\frac{d\mathbf{v}}{dt} = \frac{q_\alpha}{m_\alpha}(\mathbf{E} + \mathbf{v} \times \mathbf{B}) + \frac{1}{m_\alpha}\mathbf{F}. \quad (2.8)$$

The motion due to the applied force can be separated from the gyration if we transform to the guiding centre reference frame. The velocity becomes

$$\begin{aligned} \mathbf{v}_g \equiv \frac{d\mathbf{R}}{dt} &= \mathbf{v} + \frac{1}{q_\alpha B^2}(q_\alpha \mathbf{v} \times \mathbf{B} + \mathbf{F}) \times \mathbf{B}, \\ &= v_{\parallel} \mathbf{b} + \frac{\mathbf{F} \times \mathbf{B}}{q_\alpha B^2}. \end{aligned} \quad (2.9)$$

So an arbitrary force \mathbf{F} leads to an acceleration along the magnetic field line and a charge dependent *drift*, i.e. a velocity perpendicular to the (dominant) magnetic field. A drift can generally be seen as the consequence of an asymmetry in the force-field during a gyro-orbit. A particle speeds up when the the force is in line with the motion, and so the gyro-radius increases, whereas it decreases again when the orbit has reached its zenith. In this way the particle slides sideways, perpendicular to both the applied force and the magnetic field.

Because of the charge q_α in the expression for drift velocities, they are opposite for electrons and ions and generally lead to charge separation and currents, except when the force \mathbf{F} is proportional to q_α .

2.1.2 The $\mathbf{E} \times \mathbf{B}$ drift

If an electric field is present in the plasma, as a result of a perturbation or current that is driven through it, the plasma particles will be subject to an electric force $q_\alpha \mathbf{E}$. If we assume this field to be constant, and fill this in in Eq. (2.9), the charge drops out and we get

$$\mathbf{v}_E = \frac{\mathbf{E} \times \mathbf{B}}{B^2}. \quad (2.10)$$

This is called the $\mathbf{E} \times \mathbf{B}$ -*drift*. This is a velocity that is perpendicular to both the electric and the magnetic field. Though this is derived from a simplified particle trajectory picture, this velocity actually gives rise to a drift, or a flow of the plasma. This does not lead to charge separation, and hence currents.

2.1.3 The polarization drift

If the electric field is constant in space but not in time, $\partial \mathbf{E} / \partial t \neq 0$, the $\mathbf{E} \times \mathbf{B}$ -drift is not constant either. Instead it pulls the electrons perpendicularly to the magnetic field to and fro, and one can consider this as a force corresponding to the change in the $\mathbf{E} \times \mathbf{B}$ -velocity,

$$\mathbf{F} = m_\alpha \frac{dv_E}{dt} = \frac{m_\alpha}{B^2} \frac{\partial \mathbf{E}}{\partial t} \times \mathbf{B}.$$

This force \mathbf{F} then yields a secondary drift of its own, similar to the $\mathbf{E} \times \mathbf{B}$ -drift,

$$\mathbf{v}_{p,\alpha} = \frac{m_\alpha}{q_\alpha B^2} \frac{\partial \mathbf{E}}{\partial t}.$$

This we call the *polarization drift*. As can be deduced from the fact that the charge q_α is still in the expression, the drift results in charge separation, or a current.

2.1.4 The diamagnetic drift

The previous drift phenomena are the consequence of a force perpendicular to the magnetic field line along which the plasma particle is gyrating, and can be understood as the motion of a single particle in an external field. Some drifts, on the other hand, arise as the result of the gradient of the macroscopic quantities, such as the plasma pressure or the magnetic field. To briefly introduce them, we turn to the momentum balance equation of the ion fluid,

$$m_i n_i \mathcal{D}_t \mathbf{v}_i = q_i n_i (\mathbf{E} + \mathbf{v} \times \mathbf{B}) - \nabla p_i - \nabla \cdot \Pi_i, \quad (2.11)$$

with $\mathcal{D}_t = \partial_t + \mathbf{v}_i \cdot \nabla$, $n_i \approx n_e = n$ the particle density and Π_i is the gyroviscous part of the pressure tensor. If we take the cross product of this equation with the magnetic field unity vector $\mathbf{b} = \mathbf{B}/B_0$ and divide by $q_i n_i B_0$, we get

$$\frac{m_i}{q_i B_0^2} \mathcal{D}_t \mathbf{v}_i \times \mathbf{B} = \frac{1}{B^2} (\mathbf{E} \times \mathbf{B}) - \frac{1}{q_i n_i B^2} \nabla p_i \times \mathbf{B} - \frac{1}{n_i B^2} \nabla \cdot \Pi_i \times \mathbf{B}. \quad (2.12)$$

In this relation we can identify the following terms: first of all the first term on the right hand side, which corresponds to the $\mathbf{E} \times \mathbf{B}$ -velocity \mathbf{v}_E .

If the magnetic field is assumed to be strong and almost constant, \mathbf{v}_E is the dominant contribution to the nonlinear $\mathbf{v}_i \cdot \nabla \mathbf{v}_i$ term on the left hand side. In that case the left hand side of Eq. (2.12) reduces to the previously given definition of the ion polarization drift.

Then, the second term on the right hand side is called the *ion diamagnetic* drift, which also has an electron counterpart. It arises out of the fact that a charged particle that is gyrating around a magnetic field line \mathbf{B} corresponds to a current itself, and generates a magnetic field in the direction opposite to the applied field. The contributions of particles gyrating around neighboring field lines cancel when the plasma is homogeneous. When we sum over all the particles, we find the magnetization $\mathbf{M} = -n \langle m\mu \rangle \mathbf{b}$. Here, μ is the magnetic moment defined by $v_\perp^2/2B$. When a plasma has a thermal distribution $\langle \frac{1}{2} m v_\perp^2 \rangle = T$, we can write the magnetization as a function of the pressure p ,

$$\mathbf{M} = -\frac{p}{B} \mathbf{b}.$$

If the pressure is not constant, this gives rise to a current, the so-called *diamagnetic current*,

$$\mathbf{j} = \nabla \times \mathbf{M} = -\frac{\nabla p \times \mathbf{B}}{B^2}, \quad (2.13)$$

where again the magnetic field \mathbf{B} is taken to be constant. If divided by electron or ion charge and density, this becomes the diamagnetic drift velocity (for ions or electrons),

$$\mathbf{v}_{D,\alpha} = -\frac{\nabla p \times \mathbf{B}}{q_\alpha n B^2}. \quad (2.14)$$

Here again it is stressed that this is a drift that would not pull on a single particle: it is the consequence of the fact that at one point there are more particles gyrating than at the point next to it, resulting in a net movement of the fluid. If \mathbf{B} is curved and has a considerable gradient, we have to let the curl in Eq. (2.13) act on \mathbf{B} as well. This gives terms that correspond to the velocities that are called the curvature drift and ∇B drift.

When the diamagnetic drift velocity \mathbf{v}_D is also convoluted in the $\mathbf{v}_i \cdot \nabla \mathbf{v}_i$ term on the left hand side, we get a diamagnetic contribution to the polarization drift velocity. However, this

term cancels exactly against the gyroviscous term, the last term on the right hand side of Eq. (2.12). This is called the *gyroviscous cancellation*. When \mathbf{B} is large and constant, the \mathbf{v}_E contribution is dominant over \mathbf{v}_D , and the gyroviscous term is smaller by at least two orders of magnitude.

2.2 The Vlasov equation

The equations for single particle motion describe the dynamics of individual, non-interacting particles, and by definition, a plasma consists of a large number of intimately interacting particles displaying collective behaviour. The behaviour of only a limited number of particles with a simplified model of their relative forces already turns out to be quite hard to calculate. One way of dealing with the multitude of variables and degrees of freedom is invoking a distribution function $f_\alpha(\mathbf{x}, \mathbf{v}, t)$. This function is defined such that the amount of particles species α with velocity \mathbf{v} at \mathbf{x} on time t is $\iint d^3x d^3v f_\alpha$.

Such a distribution is normalized such that integration over all of phase-space gives

$$\iint d^3x d^3v f_\alpha = n_\alpha(t),$$

the total number of ions or electrons at time t . This is assumed to be constant. If we could determine $f(\mathbf{x}, \mathbf{v}, t)$ we would know the electromagnetic fields from that point onwards, because a particle distribution evolves according to (here) classical mechanics. A volume in phase-space moves according to the Boltzmann equation,

$$\frac{\partial f_\alpha}{\partial t} + \frac{\partial}{\partial \xi_i} \left(\frac{\partial \xi_i f_\alpha}{\partial t} \right) = C_\alpha, \quad (2.15)$$

where $\xi_i = \{\mathbf{x}, \mathbf{v}\}$ are the six-dimensional phase-space coordinates, and C_α is a collision term, changing the distribution function in time. In the case of plasma, collisions are not very likely to occur in the same sense as in a neutral gas. It is more appropriate to think of it as a short-range interaction term, causing small angle deflections that may sum up to large angle deflections. This can be modelled using a Fokker-Planck type collision operator. However, when the temperature in a magnetized plasma becomes high enough, it will experience vanishingly small Spitzer resistivity, proportional to $T^{-3/2}$. In this regime, the short-range interaction term C_α will be neglected. The Boltzmann equation can be simplified if

$$\frac{\partial}{\partial \mathbf{x}} \frac{d\mathbf{x}}{dt} = \frac{d\mathbf{x}}{dt} \frac{\partial}{\partial \mathbf{x}}, \quad \frac{\partial}{\partial \mathbf{v}} \frac{d\mathbf{v}}{dt} = \frac{d\mathbf{v}}{dt} \frac{\partial}{\partial \mathbf{v}},$$

where the first equality follows trivially if the space variables are orthogonal. The second term holds since the Lorentz-term in the interaction is always perpendicular to \mathbf{v} , and because we neglect resistive and radiative terms, that may be proportional to $\eta \mathbf{v}$. Thus we arrive at the *Vlasov equation*,

$$\frac{\partial f_\alpha}{\partial t} + \mathbf{v} \cdot \nabla f_\alpha + q_\alpha (\mathbf{E} + \mathbf{v} \times \mathbf{B}) \cdot \frac{\partial f_\alpha}{\partial \mathbf{v}} = 0. \quad (2.16)$$

We wish to obtain a closed set of equations to calculate the evolution in time for the distribution function and the electromagnetic fields. This is done by combining the Vlasov equation

and Maxwell's equations in the following way: we established that

$$\begin{aligned} n_\alpha(\mathbf{x}, t) &= \int d^3v f_\alpha(\mathbf{x}, \mathbf{v}, t), \\ \mathbf{u}_\alpha(\mathbf{x}, t) &= \int d^3v \mathbf{v} f_\alpha(\mathbf{x}, \mathbf{v}, t), \end{aligned}$$

so that the charge and current density become

$$\begin{aligned} \rho_\alpha(\mathbf{x}, t) &= \sum_\alpha q_\alpha n_\alpha, \\ \mathbf{J}(\mathbf{x}, t) &= \sum_\alpha q_\alpha n_\alpha \mathbf{u}_\alpha. \end{aligned}$$

In this way we can extract macroscopic quantities by taking moments from the Boltzmann or Vlasov equation. In other words, a macroscopic variable $\langle g \rangle$ that depends on (\mathbf{x}, t) is the result of averaging the function $g(\mathbf{x}, \mathbf{v}, t)$ over velocity space,

$$\langle g \rangle_\alpha \equiv \int d^3v g(\mathbf{x}, \mathbf{v}, t) f_\alpha(\mathbf{x}, \mathbf{v}, t).$$

This only works when f_α goes to zero fast enough for $v \rightarrow \infty$.

The zeroeth moment of the Vlasov equation thus yields the continuity equation,

$$\frac{\partial n_\alpha}{\partial t} + \nabla \cdot (n_\alpha \mathbf{u}_\alpha) = 0. \quad (2.17)$$

The first moment, multiplying f_α with $m_\alpha \mathbf{v}$, gives the momentum balance equation,

$$\frac{\partial}{\partial t} (n_\alpha m_\alpha \mathbf{u}_\alpha) + \nabla \cdot (n_\alpha m_\alpha \langle \mathbf{v} \mathbf{v} \rangle_\alpha) - q_\alpha n_\alpha (\mathbf{E} + \mathbf{u}_\alpha \times \mathbf{B}) = 0. \quad (2.18)$$

Finally, the energy equation is obtained by multiplying with $m_\alpha v^2$,

$$\frac{\partial}{\partial t} (n_\alpha m_\alpha \langle v^2 \rangle_\alpha) + \nabla \cdot (n_\alpha m_\alpha \langle \mathbf{v} v^2 \rangle_\alpha) - q_\alpha n_\alpha \mathbf{E} \cdot \mathbf{u}_\alpha = 0. \quad (2.19)$$

Here we see clearly that the n -th moment equation always requires knowledge of the $n+1$ -th moment. This means that if we want to actually calculate something, we have to truncate this infinite hierarchy somewhere. This is usually done after the second moment, and transport theory is used to model the term that involves the third moment.

At this point the further study of these equations will not be pursued. Instead, an approach is taken that leans more heavily on the form of the electron distribution function $f \equiv f_e$.

Even though there are many classes of solutions to Eq. (2.16), one that is particularly important is the Maxwellian equilibrium distribution function, representing local thermal equilibrium,

$$f = n \prod_{i=x,y,z} \sqrt{\frac{m}{2\pi k T_i}} e^{-\frac{1}{2} m v_i^2 / k T_i} = n \prod_{i=x,y,z} \frac{e^{-v_i^2 / v_{t,i}^2}}{\sqrt{\pi} v_{t,i}},$$

with Boltzmann constant k , density n , and a different temperature T_i in every direction i . These temperatures can be defined by the mean velocities in each direction:

$$\overline{v_i^2} = \frac{k T_i}{m} = \frac{1}{2} v_{t,i}^2, \quad i = x, y, z,$$

or $v_t = \sqrt{2kT/m}$.

In a magnetized plasma, velocities and temperatures are highly anisotropic. It is instructive to define a component parallel and perpendicular to the (dominant) magnetic field, so that

$$f = n \frac{e^{-v_{\parallel}^2/v_{t\parallel}^2} e^{-v_{\perp}^2/v_{t\perp}^2}}{\sqrt{\pi} v_{t\parallel} \pi v_{t\perp}^2},$$

with definitions $kT_{\parallel} = \frac{1}{2} m v_{t\parallel}^2$ and $kT_{\perp} = \frac{1}{2} m v_{t\perp}^2$. Then

$$\begin{aligned} \overline{v_{\perp}^2} &= \frac{1}{\pi v_{t\perp}^2} \int_0^{\infty} dv_{\perp} 2\pi v_{\perp}^3 e^{-v_{\perp}^2/v_{t\perp}^2} = 2v_{t\perp}^2 \int_0^{\infty} dx x^3 e^{-x^2} = v_{t\perp}^2 = \frac{2kT_{\perp}}{m}, \\ \overline{v_{\parallel}^2} &= \frac{1}{\sqrt{\pi} v_{t\parallel}} \int_{-\infty}^{\infty} dv_{\parallel} v_{\parallel}^2 e^{-v_{\parallel}^2/v_{t\parallel}^2} = \frac{1}{2} v_{t\parallel}^2 = \frac{kT_{\parallel}}{m}. \end{aligned}$$

so that $\overline{v^2} = \overline{v_{\parallel}^2} + \overline{v_{\perp}^2} = \frac{1}{2} v_{t\parallel}^2 + v_{t\perp}^2$. Note that $\int d^3v = \int_{-\infty}^{\infty} dv_{\parallel} \int_0^{\infty} dv_{\perp} 2\pi v_{\perp}$.

2.3 The drift-kinetic approximation

Solving coupled partial differential equations for the distribution function and the fields in three dimensions is very complex. However, in a tokamak plasma, the anisotropy that is introduced by the strong magnetic guidefield vastly simplifies the equations. Without loss of generality we will call the direction of the dominant part of the magnetic field the z -direction. Furthermore, we assume that the fields do not vary on short time or length scales, such as the electron (inverse) gyro-frequency or radius. This means that instead of the general kinetic equations in $\{\mathbf{x}, \mathbf{v}, t\}$, which still contains all the phase-information of the gyro-motions of the electrons, we can average over the phase-angle and the perpendicular velocity. In this way we obtain a distribution function that keeps track of the position of the guiding centre \mathbf{R} and the parallel velocity v_{\parallel} in time.

2.3.1 Reduction by strong magnetization

The magnetic field in a tokamak can locally be assumed to be of the following form,

$$\mathbf{B} = B_0 \mathbf{e}_z + \nabla\psi \times \mathbf{e}_z, \quad (2.20)$$

where \mathbf{e}_z corresponds to the toroidal angle, going the long way around the torus, and x, y are perpendicular components, corresponding to r, θ in the poloidal plane. Here, B_0 is considered constant, and $|\nabla\psi| \ll B_0$ a considerably smaller perpendicular component, representing the poloidal field created by the toroidal current in a tokamak. In other words, $B_{x,y} \sim \varepsilon B_0$, with $\varepsilon \ll 1$. Here we note that we can distinguish between the $x - y$ plane and the direction perpendicular to the magnetic field, which from here will be labeled \perp , not to be confused with the microscopic perpendicular component associated with the helical motion of plasma particles around the field line. The corresponding electric field is

$$\mathbf{E} = -\mathbf{e}_z(\nabla\phi - \partial_t\psi). \quad (2.21)$$

In general we can say that the velocity in the parallel direction, along the field line, is also considerably larger than the drift-velocity across, so $v_{\perp} \sim \varepsilon v_{\parallel}$, and if we project on the z -axis

and its perpendicular plane we have

$$\begin{aligned} v_z &= v_{\parallel} + \mathcal{O}(\varepsilon^2), \\ \mathbf{v}_{x,y} &= v_{\perp} + v_{\parallel} \frac{\mathbf{B}_{x,y}}{B} + \mathcal{O}(\varepsilon^2). \end{aligned}$$

As $v_{\parallel} \sim \mathcal{O}(1)$, the v_{\parallel} -term in the perpendicular velocity is kept. Because B_0 is constant and $|\nabla\psi| \ll B_0$, we may neglect the ∇B and curvature drifts. If we assume that the dominant component of the perpendicular velocity is the $\mathbf{E} \times \mathbf{B}$ -drift, we can decompose the velocity as follows

$$\begin{aligned} \mathbf{v} &= \mathbf{v}_{\perp} + v_{\parallel} \frac{\mathbf{B}}{B}, \\ &= \frac{\mathbf{E} \times \mathbf{B}}{B^2} + v_{\parallel} \frac{B_0 \mathbf{e}_z + \nabla\psi \times \mathbf{e}_z}{B}, \\ &\approx \frac{\nabla\phi + v_{\parallel} \nabla\psi}{B_0} \times \mathbf{e}_z + v_{\parallel} \mathbf{e}_z. \end{aligned}$$

At this point we introduce the *Poisson brackets*. They are defined as

$$[f, g] \equiv \mathbf{e}_z \cdot \nabla f \times \nabla g = \partial_x f \partial_y g - \partial_y f \partial_x g, \quad (2.22)$$

with respect to the z -axis, where the last equal-sign only holds in cartesian coordinates. This notation allows us to write the $\mathbf{v} \cdot \nabla$ -operator as

$$\begin{aligned} \mathbf{v} \cdot \nabla &= \frac{1}{B_0} (\nabla\phi + v_{\parallel} \nabla\psi + v_{\parallel} \mathbf{e}_z) \cdot \nabla, \\ &= \frac{1}{B_0} ([\phi + v_{\parallel} \psi, \dots] + v_{\parallel} \partial_z). \end{aligned}$$

In much the same way the acceleration becomes

$$-\frac{e}{m_e} (\mathbf{E} + \mathbf{v} \times \mathbf{B}) = -\frac{e}{m_e} (\partial_t \psi - \partial_z \phi + \frac{1}{B_0} [\phi, \psi]).$$

This yields the following form of the kinetic equation for collisionless plasmas in the drift approximation [1, 2, 3],

$$\frac{\partial f}{\partial t} + \frac{1}{B_0} ([\phi + v_{\parallel} \psi, f] + v_{\parallel} \partial_z f) + \frac{e}{m_e} \left(\frac{1}{B_0} [\psi, \phi] + \partial_z \phi - \partial_t \psi \right) \frac{\partial f}{\partial v_{\parallel}} = 0, \quad (2.23)$$

known as the *drift-kinetic equation*.

This equation has reduced the number of degrees of freedom considerably, and smoothened the fast and spiky dynamics of a set of electromagnetically interacting point particles, but still hosts the infamous particle-wave resonances. Most importantly, it is tailored to study the instabilities that this thesis focusses on, and resolves the issues of combining extreme low collisionality and the interest in the effects of a temperature gradient.

It can be closed by taking the zeroeth and first moment equation as sources,

$$\nabla^2 \phi = \frac{\Omega_i}{n_0} \int dv_{\parallel} f(\mathbf{x}, v_{\parallel}, t), \quad (2.24)$$

$$\nabla^2 \psi = -e \int dv_{\parallel} v_{\parallel} f(\mathbf{x}, v_{\parallel}, t), \quad (2.25)$$

the ion response equation (see section 2.4) and the parallel momentum balance equation, respectively.

2.3.2 Convective form of the drift-kinetic equation

The set of equations (2.9, 2.24, 2.25) can be simplified further by assuming that the z -direction is an ignorable coordinate. One can align the velocity coordinate to z by transforming to the canonical momentum in the z -direction,

$$v_z = v_{\parallel} + \frac{e}{m_e}\psi. \quad (2.26)$$

This simplifies Eq. (2.9) for the new distribution function $f(\mathbf{x}, v_z, t)$ to [4]

$$\mathcal{D}_t f \equiv \frac{\partial f}{\partial t} + \frac{1}{B_0}[\Phi, f] = 0, \quad (2.27)$$

with streamfunction

$$\Phi = \phi + v_z\psi - \frac{e}{2m_e}\psi^2, \quad (2.28)$$

as all derivatives with respect to z vanish. Eq. (2.24) remains unchanged, but Eq. (2.25) becomes

$$\nabla^2\psi - d_e^{-2}\psi = \int dv_z v_z f(\mathbf{x}, v_z, t), \quad (2.29)$$

with $d_e = c/\omega_{pe} = \sqrt{m_e/e^2n}$ the electron inertial skindepth. This introduces a shielding of the current density on the lengthscale d_e .

One of the most striking characteristics of this formulation is the Lagrangian convective form of Eq. (2.27), that reminds of two-dimensional Eulerian fluid flow. It has the form of a total Lagrangian derivative $\mathcal{D}_t f = 0$, where the quantity f is advected by streamfunction Φ , but keeps it unchanged in the comoving frame. This is a very important property, that we will exploit more than once. It enables us to use the powerful technique of *contour dynamics* that has been used for 2D fluid flow [5, 6] and plasma dynamics using a two-fluid model [7], but now applies to the kinetic formulation as well.

2.3.3 Discretization of the perturbed distribution function

Solving the system of equations (2.27, 2.24, 2.29) is still a formidable complex task, as it requires knowledge of the exact form of the distribution function f . This complexity may be reduced by linearization, splitting f into an constant equilibrium part f_0 and a smaller fluctuating part $f_1 \ll |f_0|$,

$$f = f_0(\mathbf{v}) + f_1(\mathbf{x}, \mathbf{v}, t).$$

This may already be enough to yield tractable analysis in suitably chosen geometries, but in order to use e.g. numerical contour dynamics, it is essential to take one extra step. We can discretize f_1 as the sum of a number of δ -functions of v with weights that may depend on space and time.

In Chapter 5 and 6 we shall consider a model with weights that are spatially constant except for jumps at a finite number of *contours*. These contours thus define the boundaries between two areas with a differently perturbed electron distribution f_1 .

We can write the equilibrium and perturbed part of the distribution function as follows:

$$f_0(v_z) = \frac{n}{\sqrt{\pi}v_t} e^{-v_z^2/v_t^2},$$

$$f_1(\mathbf{x}, v_z, t) = \sum_{i=0}^{N-1} f_{1,i}(\mathbf{x}, t) \delta(v_z - v_i),$$

where N is the depth of the discretization in velocity space, or the number of contours used as an initial condition to model a jump. The moments of the perturbed distribution function are

$$h_j = \int dv_z v_z^j f_1 = \sum_{i=0}^{N-1} v_i^j f_{1,i}(\mathbf{x}, t). \quad (2.30)$$

Hence, for given values of the support velocities v_0, \dots, v_{N-1} , the first N moments h_0, \dots, h_{N-1} determine the weights $f_{1,0}, \dots, f_{1,N-1}$.

If we want to impose a perturbation to the equilibrium distribution function, one degree of freedom remains: dependent on how we choose the v_i , the weights $f_{1,i}(\mathbf{x}, t)$ are determined.

One approach is to define moments in a way that low order moments correspond to basic deviations from a Maxwellian distribution and higher order moments reflect less likely deviations. This can be achieved by using orthogonal functions instead of v_i^n . Hermite polynomials $H_n(x)$ are polynomials that satisfy

$$\int_{-\infty}^{\infty} H_m(x) H_n(x) e^{-x^2} dx = 2^n \sqrt{\pi} n! \delta_{m,n}. \quad (2.31)$$

Now, we define Hermitian moments as

$$h_j^H = \int H_j(v/v_t) f_1 dv, \quad (2.32)$$

so that a perturbation $\sim v^m \exp(-v^2/v_t^2)$ of the distribution function only perturbs the lowest $m+1$ moments h_0^H, \dots, h_m^H . Because of the orthogonality of the Hermite polynomials, a perturbation $\sim H_m(v/v_t) \exp(-v^2/v_t^2)$ would only perturb the moment h_m^H .

If we apply this to the sum of δ -functions that should impose a perturbation to f_0 , we note that this procedure cannot eliminate all moments higher than N . However, by choosing v_i as the zeroes of the N -th Hermite polynomial, the next, $N+1$ -th moment vanishes: $h_N^H = 0$. The first N moments, however, do not vanish, and are given by

$$h_j^H = \sum_{i=0}^{N-1} f_i H_j(v_i/v_t), \quad j = 0, \dots, N-1. \quad (2.33)$$

The first four moments have a well-known physical interpretation,

- 0: density perturbation $n_{e,1} = h_0^H$,
- 1: velocity (current) perturbation $j_1 = -en_{e,0}v_{e,1} = \frac{1}{2}v_t h_1^H$,
- 2: temperature perturbation $n_{e,0}T_1 = \frac{1}{4}v_t^2 m_e h_2^H$,
- 3: heat flow $q = \frac{1}{8}v_t^3 m_e h_3^H$.

The simplest case, $N=1$, corresponds to the Euler system. Only one type of contour exists, that limits an area with higher electron density, corresponding to an elevated level of vorticity. No current perturbation is possible. For $N=2$, the isothermal two-fluid model is retrieved [2, 7, 8]. By making a negative perturbation at negative v_z and a positive for positive v_z (or vice versa), this results in a shifted Maxwellian, corresponding to a current perturbation. With $N=3$, it is possible to capture non-isothermal effects. It is, however, equivalent to an isothermal electron model with a different temperature, to which an extra δ -function at $v=0$ is added to model the ion potential vorticity [2, 3]. Truly kinetic modelling therefore starts for $N \geq 4$.

2.3.4 Isothermal fluid equations

The full drift-kinetic equations can be used to resolve phenomena that are fast or slow compared to the thermal speed of the bulk plasma. When e.g. a wave with a phase velocity that is slow compared to the thermal speed travels through the plasma, the affected plasma particles have the time to thermalize, i.e. relay the information that the wave is compressing or diluting the plasma locally to the plasma in the direct surroundings. Such a perturbation is then called *isothermal*.

Or, if λ_{mfp} is the mean free path of an electron, and t_c a typical time (e.g. a transit time, $v_t t_c = l_c$, with l_c the size of the system), then

$$\text{isothermal:} \quad \frac{\omega}{k} \ll \frac{\lambda_{\text{mfp}}}{t_c}.$$

The other limit, where very fast wave phenomena compress and dilute plasma so fast that they cannot interchange information at all, is called *adiabatic*.

$$\text{adiabatic:} \quad \frac{\omega}{k} \gg \frac{\lambda_{\text{mfp}}}{t_c}.$$

For adiabatic processes, thermal conduction is unimportant, and the adiabatic gas law applies,

$$\partial_t p n^{-5/3} = 0. \quad (2.34)$$

The regime in between these two limiting cases is captured by the resonances in the drift-kinetic equation.

There have been many attempts to construct a collisionless limit of the plasma fluid equations [2, 9]. In this thesis however, the focus will not be on the details of the intricate challenges that arise when a gas consisting of particles that do not collide on timescales that we are considering, needs to be described as a fluid, which entails instant thermalization. Even though the assumptions of a collisionless fluid are hard to meet, the equations prove most useful.

Here, the fluid equations will be derived as the zeroth and first moment of the drift-kinetic equation with the discretized $N = 2$ electron velocity distribution function,

$$f \equiv f_{\text{iso}} = f_0 + f_1 \quad (2.35)$$

with

$$f_0 = \frac{n_{e,0}}{\sqrt{\pi}v_t} e^{-v_{\parallel}^2/v_t^2}, \quad f_1 = -\frac{j_1}{2ev_t} \{\delta(v_{\parallel} - v_t) - \delta(v_{\parallel} + v_t)\}, \quad (2.36)$$

so that

$$\int dv_{\parallel} f = n_e, \quad (2.37)$$

$$-e \int dv_{\parallel} v_{\parallel} f = j_1, \quad (2.38)$$

$$\frac{m_e}{n_e} \int dv_{\parallel} v_{\parallel}^2 f = m_e v_t^2 = T_e, \quad (2.39)$$

become electron density, current density and electron temperature. Here we note that the ratio of pressure over density is fixed at $m_e v_t^2$.

The perturbed part of the electron distribution function is described as a sum of two delta-distributions in velocity space, corresponding to the two contours that can be drawn around the area in which this perturbation plays a role. When the distribution function would be discretized using N velocities, the weights w_i of these perturbations could be chosen such that only the first moment h_1^H of the distribution function becomes non-zero. Here, $N = 2$ yields the simplest isothermal description, which can analytically be manipulated to give the two-fluid drift-Alfvén model equations.

Performing the integration over parallel velocity over Eq. (2.23) multiplied by unity,

$$\begin{aligned} 0 &= \partial_t \int dv_{\parallel} f + \frac{1}{B_0} [\phi, \int dv_{\parallel} f] + \frac{1}{B_0} [\psi, \int dv_{\parallel} v_{\parallel} f] + \partial_z \int dv_{\parallel} v_{\parallel} f \\ &= \partial_t n + \frac{1}{B_0} [\phi, n] - \frac{1}{eB_0} [\psi, j_{\parallel}] - \frac{1}{e} \partial_z j_{\parallel}, \\ \Rightarrow 0 &= \partial_t N + \frac{1}{B_0} [\phi, N] - v_A^2 \left(\frac{1}{B_0} [\psi, \nabla^2 \psi] + \partial_z \nabla^2 \psi \right), \end{aligned}$$

where we used that the current density only has a parallel component $env_t \approx \nabla^2 \psi$, and in the last line multiplied by $\Omega_i/n_0 = eB_0/m_i n_0$ to obtain an equation in the vortical quantity $N = \Omega_i n/n_0$.

The same can be done for a parallel momentum balance equation, multiplying Eq. (2.23) by mv_{\parallel} ,

$$\begin{aligned} 0 &= \partial_t \int dv_{\parallel} v_{\parallel} f + \frac{1}{B_0} [\phi, \int dv_{\parallel} v_{\parallel} f] + \frac{1}{B_0} [\psi, \int dv_{\parallel} v_{\parallel}^2 f] + \partial_z \int dv_{\parallel} v_{\parallel}^2 f \\ &\quad - \frac{e}{m} (\partial_t \psi + \frac{1}{B_0} [\phi, \psi] - \partial_z \phi) \int dv_{\parallel} v_{\parallel} \frac{\partial f}{\partial v_{\parallel}} \\ &= -\frac{1}{e} \partial_t \nabla^2 \psi - \frac{1}{eB_0} [\phi, \nabla^2 \psi] + \frac{1}{B_0} [\psi, nv_t^2] + \partial_z (n_e v_t^2) \\ &\quad + \frac{en_e}{m_e} (\partial_t \psi + \frac{1}{B_0} [\phi, \psi] - \partial_z \phi), \\ \Rightarrow 0 &= \partial_t (d_e^2 \nabla^2 \psi - \psi) + \frac{1}{B_0} [\phi, d_e^2 \nabla^2 \psi - \psi] - \frac{1}{B_0} [\psi, N \rho_s^2] - \partial_z (N \rho_s^2), \end{aligned}$$

where $\rho_s = \sqrt{m_e m_i v_t^2}/eB_0$ the ion-sound Larmor radius. It is demonstrated here that when the distribution function $f(\mathbf{x}, v_{\parallel}, t)$ is discretized by taking two well-chosen values, the fluid equations emerge. Also, taking two values is exactly enough to provide for two non-zero moment equations. The third, being the equation for heat conduction, vanishes as this discretization only allows isothermal dynamics,

$$\int dv_{\parallel} (v_{\parallel}^2 - v_t^2) f_{\text{iso}} \equiv 0.$$

In this way the hierarchy of needing the $(N + 1)$ -th moment to close the N -th moment equation is resolved. We obtain

$$\partial_t N + \frac{1}{B_0} [\phi, N] = v_A^2 \left(\frac{1}{B_0} [\psi, \nabla^2 \psi] + \partial_z \nabla^2 \psi \right), \quad (2.40)$$

$$\partial_t (d_e^2 \nabla^2 \psi - \psi) + \frac{1}{B_0} [\phi, d_e^2 \nabla^2 \psi - \psi] = \frac{1}{B_0} [\psi, N \rho_s^2] + \partial_z (N \rho_s^2). \quad (2.41)$$

This is not a closed set of equations, as we have two equations for three unknowns. The third equation stems from the modelling of the ion response to electron density perturbations, and is discussed in section 2.4.

2.4 The cold ion approximation

The dynamics of the electrons in a plasma is described by a fluid or a kinetic model, which takes into account the degrees of freedom along the magnetic field lines of the electrons as they move through the plasma. In the work presented in this thesis, however, the ions are often considered to be *cold* relative to the electrons. This choice of words may however sound misleading, as the process of nuclear fusion between ions is supposed to happen at temperatures of roughly 15 keV, hundreds of millions of degrees.

In the strong guide field ordering we observe that we can neglect the electron gyroradius ρ_e for phenomena on the drift scale, but generally we cannot do the same for the ion gyro-radius ρ_i . To model ion gyromotion correctly, some rigor is in order, and a kinetic model for the perpendicular motion of the ions is called for, as e.g. in [10].

Another possibility is to neglect the ion gyroradius all the same, and consider them to be cold. This is not entirely justified physically, but the effects of taking into account the finite ion Larmor radius have been studied in both two-fluid context [2] and in a complete kinetic model for the ions [10, 11], and can be looked at more or less separately from the electron dynamics, which is the primary subject of investigation in this thesis.

Here, our aim is to focus on the phenomena that concern the parallel electron dynamics. The drift ordering focusses on timescales $\omega_{pe}^{-1} < \tau < \Omega_i^{-1}$, so we do not resolve the jittery movement of plasma waves. However, electrons can be considered to move approximately along flux tubes parallel to the magnetic field. An ion density perturbation could lead to a region of positive space charge, to which electrons react by compression along the flux tube, or vice versa. This does not occur instantly because distances (wave lengths) along the field line are large compared to perpendicular length scales. With this in mind we do not model the dynamics of the ions separately, but we assume them to be passive as time scales are short with respect to the ion gyro-frequency Ω_i , subtly changing their gyro-orbits to assure local charge neutrality.

In most of the physical applications the electron temperature is roughly the same as the ion temperature, so

$$T_e \approx T_i, \quad \rightarrow \quad v_{t,e} \gg v_{t,i}$$

by at least one order of magnitude $\sim \sqrt{m_i/m_e}$. Furthermore, the parallel acceleration of electrons by the electromagnetic field goes with Ω_e , and with Ω_i for ions, which is a difference of order m_i/m_e , which implies that the change in v_e as a result of a perturbation of the space charge is larger than the change in v_i by two orders of magnitude.

So assuming ions to be cold merely states that they do not move in the same way electrons do, and that they behave according to simplified reduced dynamics. These can be derived from several types of arguments.

2.4.1 The polarization drift approach

The starting point of this line of reasoning is the ion momentum balance equation,

$$m_i n_i \mathcal{D}_t \mathbf{v}_i = q_i n_i (\mathbf{E} + \mathbf{v} \times \mathbf{B}) - \nabla p_i - \nabla \cdot \Pi_i, \quad (2.42)$$

where $\mathcal{D}_t = \partial_t + \mathbf{v}_i \cdot \nabla$, and Π_i is the gyroviscous part of the pressure tensor. Dividing by $n_i m_i$ and taking the curl of this equation yields

$$\nabla \times \mathcal{D}_t \mathbf{v}_i = \nabla \times (\mathbf{v}_i \times \vec{\Omega}_i) + \frac{1}{n_i^2} \nabla n_i \times \nabla p_i, \quad (2.43)$$

where the notation $\vec{\Omega}_i = q_i \mathbf{B} / m_i$, reminiscent of the ion gyrofrequency, is introduced. When we apply the vector identity

$$\nabla \times (\mathbf{v}_i \cdot \nabla \mathbf{v}_i) = \mathbf{v}_i \cdot \nabla \vec{\omega} + \vec{\omega} \nabla \cdot \mathbf{v}_i - \vec{\omega} \cdot \nabla \mathbf{v}_i,$$

with $\vec{\omega} \equiv \nabla \times \mathbf{v}_i$ the ion vorticity, and if we assume that the pressure gradient is parallel to the density gradient, the *barotropic fluid* approximation, we may write Eq. (2.43) as

$$\mathcal{D}_t (\vec{\omega} + \vec{\Omega}_i) + (\vec{\omega} + \vec{\Omega}_i) \nabla \cdot \mathbf{v}_i = (\vec{\omega} + \vec{\Omega}_i) \cdot \nabla \mathbf{v}_i. \quad (2.44)$$

Here we may use the ion continuity equation $\mathcal{D}_t n_i + n_i \nabla \cdot \mathbf{v}_i = 0$ to eliminate $\nabla \cdot \mathbf{v}_i$, so that

$$\mathcal{D}_t \left(\frac{\vec{\omega} + \vec{\Omega}_i}{n_i} \right) = \left(\frac{\vec{\omega} + \vec{\Omega}_i}{n_i} \right) \cdot \nabla \mathbf{v}_i. \quad (2.45)$$

If we furthermore assume that $\mathbf{B} \approx B_0 \mathbf{e}_z$, we can say that the ion velocity in the z -direction v_{iz} is not directly driven by the 2-D dynamics perpendicular to \mathbf{B} . Only parallel density fluctuations may couple to the perpendicular equations, and the fast equilibration parallel to magnetic field lines results in the fact that this is a very small effect. This means that in the z -direction, we can put $v_{iz} \approx 0$. This reduces Eq. (2.45) to

$$\mathcal{D}_t U \equiv \mathcal{D}_t \left(\frac{\omega_z + \Omega_i}{n_i} \right) = 0. \quad (2.46)$$

Here, Ω_i is no longer a vector quantity and thus has become the ion Larmor frequency. The quantity U that is conserved here is called the *potential vorticity*. In fact, only assuming $k_{\parallel} = 0$ and using Ertel's theorem [12] also yields this conservation law.

If we compare this to the derivation of the drift phenomena in section 2.1.4, we note that this term arises out of the ion polarization drift term. In this case, the $\mathbf{E} \times \mathbf{B}$ -drift is absorbed in the time derivative of $\vec{\Omega}_i$ and the diamagnetic drift drops out when taking the curl.

When the ion vorticity is small with respect to the ion gyrofrequency, e.g. when B_0 is large, Eq. (2.46) becomes

$$\mathcal{D}_t \left(\frac{\omega_z}{\Omega_i} - \frac{\delta n}{n_0} \right) = 0, \quad (2.47)$$

where $n_i = n_0 + \delta n$. This is called the *quasi-geostrophic* approximation, which states that $|\delta n| \ll n_0$. Here we suppress the subscript i , as the plasma is supposed to be quasi-neutral on the timescales that are considered here, so that $n_i = n_e$.

If in Eq. (2.42) the $\mathbf{E} \times \mathbf{B}$ -drift is dominant, then

$$\mathbf{v}_i \approx \frac{1}{B_0} \nabla \phi \times \mathbf{e}_z \quad \Rightarrow \quad \vec{\omega} = \frac{1}{B_0} \nabla^2 \phi \mathbf{e}_z.$$

When we fill this in Eq. (2.47), we get

$$\mathcal{D}_t \left(\frac{\nabla^2 \phi}{B_0 \Omega_i} - \frac{\delta n}{n_0} \right) = 0, \quad (2.48)$$

where now $\mathcal{D}_t \equiv \partial_t + [\phi, \dots]$. This is called the *geostrophic* approximation.

An interpretation of this equation is that electron density fluctuations are equal in size to the ion ($\mathbf{E} \times \mathbf{B}$ -flow) vorticity. In other words, when electrons may undergo fast phenomena, the ions cancel the local space charge by changing their vortical motion. To be a little more specific, we can look at the microscopic picture.

2.4.2 The particle approach

To express the density fluctuations in terms of vorticity, we construct a field of which the rotation of the ion is a particular solution. If we consider a region with a constant charge density, causing an electric field $\mathbf{E} = -\nabla\phi = -B_0\delta\omega\mathbf{x}$, corresponding to a potential

$$\phi = \frac{1}{2}B_0\delta\omega(x^2 + y^2),$$

this would describe the rotation of plasma as the consequence of the $\mathbf{E} \times \mathbf{B}$ -velocity, with a constant vorticity $\nabla^2\phi/B_0 = 2\delta\omega$. The gyrofrequency ω of an individual particle is found by solving the equation of motion Eq. (2.1), but now with a background electric field, so that

$$m_i\ddot{\mathbf{x}} = q\mathbf{v} \times \mathbf{B} + q\mathbf{E}$$

becomes

$$-\omega^2 = -\omega\Omega_i - \delta\omega\Omega_i. \quad (2.49)$$

When $\delta\omega = \nabla^2\phi/2B_0 = 0$ the vorticity is just $\omega = \Omega_i$. The electric field obviously alters the motion of the gyrating ions, by an amount of perturbed vorticity $\delta\omega$,

$$\omega \approx \Omega_i + \delta\omega,$$

which can be found by substitution in Eq. (2.49),

$$(\Omega_i + \delta\omega)^2 = \Omega_i(\Omega_i + \delta\omega) - \Omega_i\delta\omega,$$

when the δ^2 term is neglected. So the (perturbed) electric field can induce ion vorticity. To see how this is coupled to the density we look back at the definition of the ion Larmor radius Eq. (2.6),

$$\rho_i = \frac{v_{\perp,i}}{\Omega}, \quad \Rightarrow \quad \delta\rho_i = -\rho_i \frac{\delta\omega}{\Omega} \approx -\rho_i \frac{1}{2} \frac{\nabla^2\phi}{B_0\Omega_i},$$

we see that the extra vorticity has an effect on the radius of gyration of the ions, that now encircle an area

$$A = \pi\rho_i^2 \quad \Rightarrow \quad \frac{\delta A}{A} = 2\frac{\delta\rho_i}{\rho_i} = -\frac{\nabla^2\phi}{B_0\Omega_i},$$

and the argument to couple this to density goes roughly like this: the larger the area that is circled by an ion, the less ions per area,

$$\frac{\delta n}{n} = -\frac{\delta A}{A} = \frac{\nabla^2\phi}{B_0\Omega_i}.$$

So, in words, parallel perturbations of the electron pressure may cause (temporary) electric fields that cause the surrounding ions to change their gyro-radius a little, thus changing the

ion density to compensate the charge imbalance. The electron pressure is no longer visible in the equations since we are used to take the curl of the momentum balance equation to consider vorticities instead of momentum, which does not mean pressure does not play a role.

How do these ways of looking at electron-ion interaction mesh? To see that ions indeed gyrate in a way that a temporarily higher electron density in a flux tube in the middle induces them to increase the ion density there, we can think of it as a time-varying electric field. The accumulation of electrons (the parallel electron pressure perturbation) takes some time to build up, so you get with the field of a space charge

$$\delta\mathbf{E} \sim -\delta\omega\mathbf{x}, \quad \text{and} \quad \partial_t\mathbf{x} = -\frac{1}{\Omega_i}\partial_t\mathbf{E},$$

a velocity *towards* the flux tube, or

$$\delta\mathbf{x} \sim -\frac{1}{\Omega_i}\delta\mathbf{E}.$$

So in this way we can think as well in terms of vorticity as in terms of a relatively passive ion response to electron density perturbations, of the cold ion approximation.

2.5 The generalized Ohm's law

As it is assumed that there is no electrical resistivity in the plasma that we consider, it is not bad practice to be precise in how electrical fields are dealt with by the plasma. In an ideal plasma, without resistivity, viscosity or inertia, we may simply say that electric fields cannot exist: they are immediately annihilated by the infinitely mobile fluid, so, in a moving frame,

$$\mathbf{E} + \mathbf{v} \times \mathbf{B} = 0.$$

This can be translated to the by now more common notation, using the fields ϕ and ψ ,

$$\partial_t\psi + \partial_z\phi + \frac{1}{B_0}[\phi, \psi] = 0. \quad (2.50)$$

It was claimed in the introduction that field lines in an ideal plasma that intersected a volume at some time t , at later times would still intersect the exact same volume, or, in other words, that the magnetic field is *frozen into the plasma*. This can now be shown using this expression.

First, a flux surface need not be exactly identical to a surface on which ψ is constant. We can see that a parallel disturbance of ϕ breaks the Lagrangian covariance in Eq. (2.50). A flux surface can be constructed by demanding that

$$\mathbf{B} \cdot \nabla\chi = 0 \quad \Rightarrow \quad B_0\partial_z\chi + [\psi, \chi] = 0. \quad (2.51)$$

Here, the new flux coordinate χ is assumed to be constant along a magnetic field line.

Second, the flux through a surface at a time t should be the same after the surface flows with the plasma for a time δt , so “frozen in” can be quantified thus,

$$\partial_t\chi + \frac{1}{B_0}[\phi, \chi] = 0. \quad (2.52)$$

If we define the following covariant derivatives in the usual way,

$$\begin{aligned}\mathcal{D}_t &= \partial_t + \frac{1}{B_0}[\phi, \cdot], \\ \nabla_{\parallel} &= \partial_z + \frac{1}{B_0}[\psi, \cdot],\end{aligned}$$

then the Jacobi identity of these two operators becomes

$$\mathcal{D}_t \nabla_{\parallel} A - \nabla_{\parallel} \mathcal{D}_t A = [\partial_t \psi + \partial_z \phi + \frac{1}{B_0}[\phi, \psi], A].$$

So, when Ohm's ideal law applies, the right hand side becomes identical to zero, so then $\mathcal{D}_t \nabla_{\parallel} A = \nabla_{\parallel} \mathcal{D}_t A$. Furthermore, if we consider $A = \chi$, and χ labels flux surfaces at some time t , then it will keep doing so, or

$$(\partial_t + \frac{1}{B_0}[\phi, \cdot])(B_0 \partial_z \chi + [\psi, \chi]) = 0.$$

This implies that $\nabla_{\parallel} \mathcal{D}_t A = 0$, or (2.52) along a field line, must also hold, so that magnetic flux is frozen into the plasma as long as the ideal Ohm's law applies. This concludes the excursion into ideal magnetohydrodynamics.

When dissipative effects or electron inertia are taken into account, they enter through the generalized Ohm's law,

$$\mathbf{E} + \mathbf{v} \times \mathbf{B} = \eta \mathbf{J} + d_e^2 \frac{d\mathbf{J}}{dt} - \frac{1}{ne}(\nabla p_e - \mathbf{J} \times \mathbf{B}). \quad (2.53)$$

The first two terms on the right hand side break the flux-preserving symmetry, and can cause *reconnection* to occur, so that the magnetic field lines inside a $\chi = c$ surface can be broken up and reconnected again. The last two terms modify the electric field, but can not induce reconnection by themselves.

In this thesis, η will be considered negligible, and we will focus on the inertial term as a mechanism for collisionless reconnection. When two magnetic field lines with a different orientation, that are then frozen into the plasma, are pushed together, the resulting electric field accelerates electrons to prevent the cancellation of the magnetic flux. The finite electron inertia prohibits this current from arising instantaneously, thus facilitating reconnection.

2.6 Kinetic waves in a strongly magnetized plasma

In this section we will consider plane waves in an infinite periodic slab geometry. This analysis can be applied to both fluid and kinetic equations alike, and in the presence of a temperature or density gradient. This may already give an indication of some of the kinetic modifications that one may expect to arise when we depart from fluid theory.

In this section it will be shown how the structure of the dispersion relation for waves in strongly magnetized plasmas differs when we compare kinetic and fluid theory. The parallel velocity distribution function yields a complex relation that shows the interplay between a particle population and waves, which is captured in the plasma dispersion function if the distribution is Maxwellian. It has already been shown in section 2.3.4 that the fluid equations can be derived from the drift-kinetic equation in a straightforward manner using the perturbed

distribution function that is discretized in velocity space only with $N = 2$. Here it will be shown that the correspondence lies even closer, and that it is possible to obtain the fluid results from the kinetic dispersion relation by the substitution of a ‘discretized’ dispersion function, which is based on the discretized distribution function, but itself is smooth. This gives some insight on how fluid theory captures most of the isothermal kinetic dynamics, but does away with the resonances.

Note that in this approach no use is made of contours, that correspond to the boundary in space of a region with a perturbed distribution function. The geometry here is simplified to perform a general linear analysis of possible waves. This leaves room to introduce some other excursions from isotropy, such as an equilibrium density and temperature gradient.

2.6.1 Waves in drift-kinetic theory

We consider a plane plasma slab, with a magnetic guide-field $\mathbf{B} = B_0 \mathbf{e}_z + \nabla\psi \times \mathbf{e}_z$, where $\nabla\psi \ll B_0$. The Maxwell-Vlasov equation for the distribution function $f(x, v_{\parallel}, t)$, with v_{\parallel} parallel to the magnetic field, in the drift-approximation given by Eq. (2.23), is repeated here for convenience,

$$\partial_t f + [\phi, f] + v_{\parallel}(\partial_z f + [\psi, f]) + \frac{e}{m_e}([\psi, \phi] + \partial_z \phi - \partial_t \psi) \frac{\partial f}{\partial v_{\parallel}} = 0. \quad (2.54)$$

All perturbed quantities may be split into an equilibrium and a fluctuating part,

$$A \equiv A_0(x, v_{\parallel}) + A_1(x, y, z, t)$$

in which $A_0 \gg A_1$, and with A_0 the solution to the equilibrium equations, and a fluctuating part $A_1 \sim \exp(i(\omega t - \mathbf{k} \cdot \mathbf{x}))$ that describes the plane wave disturbances.

The unperturbed, equilibrium distribution function may be of the form (cf. section 2.2),

$$f_0(x, v_{\parallel}) = \frac{1}{\sqrt{\pi}} \frac{n_0}{v_t} e^{-v_{\parallel}^2/v_t^2} \quad \text{with} \quad \frac{1}{2} m_e v_t^2 = k T_{e\parallel}, \quad (2.55)$$

though most of the analysis does not depend on the specific form of the distribution function. For the present analysis, the equilibrium may contain gradients in density and temperature, here chosen in x -direction, and without loss of generality,

$$\partial_x n_0 = -\frac{n_0}{L_n} \quad \partial_x v_t = -\frac{v_t}{2L_T}. \quad (2.56)$$

This leads to the expression for the gradient in the distribution function

$$\partial_x f_0 = f_0 \left(-\frac{1}{L_n} + \frac{1}{2} \frac{1}{L_T} \right) + \frac{v_{\parallel}}{2L_T} \frac{\partial f}{\partial v_{\parallel}}.$$

The partial derivative to the parallel velocity is only evaluated under the integral sign, by partial integration, so that no information about the specific form of the distribution function is needed beforehand.

Here, we will focus on dynamics where the electrons are not assumed to move so quickly that they induce charge separation, creating plasma waves with the plasma frequency $\omega_{pe}^2 = n_e e^2 / \epsilon_0 m_e$. The ion response to parallel electron compressibility is modelled by the

cold ion approximation, that was introduced in section 2.4, and is quantified in Eq. (2.46): $\mathcal{D}_t U = 0$, or

$$\partial_t(\nabla^2 \phi - N) + [\phi, \nabla^2 \phi - N] = 0 \quad (2.57)$$

with $N \equiv \Omega_i \log n$. If N is a function of x , we get a contribution from the bracket $[\phi, N] \neq 0$.

We close the drift-kinetic equation by taking the zeroeth and first moment of it, providing us with the sources for the potential vorticity equation and Ampère's equation,

$$\nabla^2 \phi = \frac{\Omega_i}{n_0} \int dv_{\parallel} f, \quad (2.58)$$

$$\nabla^2 \psi = -e \int dv_{\parallel} v_{\parallel} f, \quad (2.59)$$

respectively. Linearizing Eqs. (2.54, 2.58, 2.59), we get

$$(\omega - v_{\parallel} k_z) f_1 + \left[k_y f_0 \left(\frac{1}{L_n} - \frac{1}{2L_T} \right) - k_y \frac{v_{\parallel}}{2L_T} \frac{\partial f_0}{\partial v_{\parallel}} \right] (\phi_1 + v_{\parallel} \psi_1) = \Omega_e \frac{\partial f_0}{\partial v_{\parallel}} (\omega \psi_1 + k_z \phi_1) \quad (2.60)$$

and

$$-k_{\perp}^2 \phi_1 = \frac{\Omega_i}{n_0} \int dv_{\parallel} f_1 + \left[\phi_1, \frac{\Omega_i}{\omega n_0} \right] \quad (2.61)$$

$$-k_{\perp}^2 \psi_1 = -\frac{e}{B_0} \int dv_{\parallel} v_{\parallel} f_1 \quad (2.62)$$

If we linearize the potential vorticity equation for the ion response for an equilibrium with a density gradient, we obtain, by $[\phi, N] = -\partial_y \phi \partial_x N = k_y \phi_1 \Omega_i / L_n$:

$$\omega(-k_{\perp}^2 \phi_1 - N) - \frac{\omega_*}{\omega \rho_s^2} \phi_1 = 0,$$

with $\omega_* = k_y v_t^2 / m_e L_n$ the density component of the diamagnetic frequency. The ion-sound Larmor radius,

$$\rho_s = \frac{v_t}{e B_0} \sqrt{m_i m_e},$$

is a length scale that does often surface in drift theory. It corresponds to how disturbances in the electron density couple to the ion gas, the electrons being so much more volatile than the ions.

2.6.2 The plasma dispersion function

The drift-kinetic equation manages the information on where particles are and how fast they are moving. In this sense it contains *particle-wave resonances*, phenomena such as (inverse) Landau damping, that can be visualized by plasma particles surfing from a plasma wave that loses its energy this way, or, inversely, fast fusion-born particles exciting a localized plasma tsunami.

The plasma dispersion function is a function that ‘scans’ a Gaussian distribution with a resonant denominator. Its definition is

$$Z(\zeta) \equiv \frac{1}{\sqrt{\pi}} \int_{-\infty}^{\infty} dt \frac{e^{-t^2}}{t - \zeta}.$$

This is a function that corresponds solely to a Gaussian or Maxwellian distribution function, and we will use this function in subsequent analysis. This does not mean that conclusions become very different when a different distribution function is used; we just cannot use the symbol $Z(\zeta)$ anymore, nor its characteristics.

Now, we renormalize in order to get dimensionless quantities:

$$\begin{aligned} u &= v_{\parallel}/v_t & \phi &= \frac{\phi_1}{v_t \rho_e} = \frac{\Omega_e}{v_t^2} \phi_1 \\ \zeta &= \frac{\omega}{k_z v_t} & \psi &= \frac{\psi_1}{\rho_e} = \frac{\Omega_e}{v_t} \psi_1 \\ \zeta_* &= \frac{k_y}{k_z} \frac{v_t}{\Omega_e L_n} & F_0 &= \frac{v_t}{n_0} f_0 \quad \left(\int du F_0 = 1 \right) \\ \zeta_T &= \frac{k_y}{k_z} \frac{v_t}{\Omega_e L_T} & F_1 &= \frac{v_t}{n_0} f_1 \end{aligned}$$

The drift-kinetic equation Eq. (2.54) then becomes:

$$F_1 = -\frac{1}{u-\zeta} \left[\left[-\left(\zeta_* - \frac{1}{2} \zeta_T \right) F_0 + \frac{1}{2} \zeta_T u \frac{\partial F_0}{\partial u} \right] (\phi + u\psi) + \frac{\partial F_0}{\partial u} (\phi + \zeta\psi) \right]$$

and the dimensionless counterparts of Eqs. (2.58, 2.59) are given by

$$(-k_{\perp}^2 - \frac{\zeta_*}{\zeta})\phi = \frac{1}{\rho_s^2} \int du F_1 \quad (2.63)$$

$$-k_{\perp}^2 \psi = -\frac{1}{d_e^2} \int du u F_1. \quad (2.64)$$

Here, the electron inertial skin depth $d_e = \sqrt{m_e/n_0 e^2}$ is the length scale at which electromagnetic disturbances are screened in the plasma by the electrons. Note that $d_e^2/\rho_s^2 = v_A^2/v_t^2$.

If we express the integrals in Eqs. (2.63, 2.64) using the plasma dispersion function, we get

$$\begin{aligned} (-k_{\perp}^2 \rho_s^2 - \frac{\zeta_*}{\zeta})\phi &= \int du F_1 = \\ & \left[-\left(\zeta_* - \frac{1}{2} \zeta_T \right) \int du \frac{F_0}{u-\zeta} - \left(1 - \frac{1}{2} \zeta_T \zeta \right) \int du \frac{1}{u-\zeta} \frac{\partial F_0}{\partial u} \right] (\phi + \zeta\psi) \\ & + \frac{1}{2} \zeta_T \int du \frac{\partial F_0}{\partial u} (\phi + u\psi) + \psi \left[-\left(\zeta_* - \frac{1}{2} \zeta_T \right) \int du F_0 + \frac{1}{2} \zeta_T \zeta \int du \frac{\partial F_0}{\partial u} \right] \\ & = (\phi + \zeta\psi) \left[-\left(\zeta_* - \frac{1}{2} \zeta_T \right) Z(\zeta) - \left(1 - \frac{1}{2} \zeta_T \zeta \right) Z'(\zeta) \right] - \zeta_* \psi \end{aligned} \quad (2.65)$$

$$k_{\perp}^2 d_e^2 \psi = \int du u F_1 = \zeta \int du F_1 + \zeta_* \phi \quad (2.66)$$

Here, the prime denotes derivation with respect to its argument. Inspection of Eq. (2.66) shows that

$$\psi = -\zeta \frac{\rho_s^2}{d_e^2} \phi,$$

so that we can fill this in in Eq. (2.65), yielding

$$\rho_s^2 k_{\perp}^2 + \frac{\zeta_*}{\zeta} + \left(1 - \zeta^2 \frac{\rho_s^2}{d_e^2} \right) \left[-\left(\zeta_* - \frac{1}{2} \zeta_T \right) Z(\zeta) - \left(1 - \frac{1}{2} \zeta_T \zeta \right) Z'(\zeta) \right] + \zeta_* \zeta \frac{\rho_s^2}{d_e^2} = 0, \quad (2.67)$$

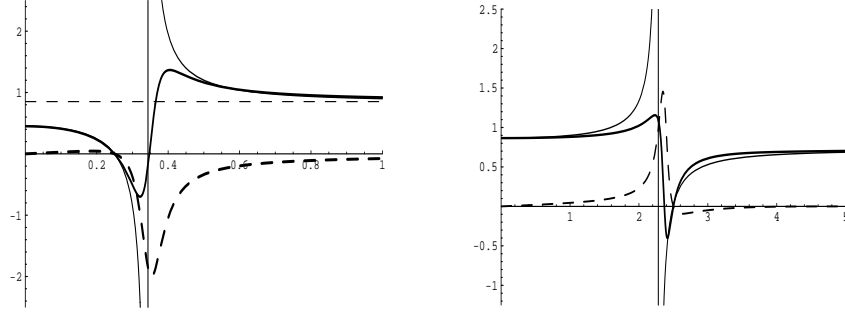


Figure 2.1: Left we see $\omega(\zeta)$ in the kinetic case (**bold**) and the fluid approximation (thin line). The dashed line indicates the imaginary part of $\omega(\zeta)$. We see that the singularities around the Alfvénic velocities are resolved in the kinetic case (in this figure, $d_e < \rho_s$). On the right hand side we see the same picture, for the same ω_T . Here, $d_e > \rho_s$.

as the required dispersion relation.

For $\zeta_* = \zeta_T = 0$, the dispersion relation becomes

$$\rho_s^2 k_\perp^2 = - \left(\frac{1}{\rho_s^2} - \frac{\zeta^2}{d_e^2} \right) Z'(\zeta). \quad (2.68)$$

We can rewrite the dispersion relation as the frequency/growth rate being a function of the parameter ζ ¹. This means rewriting the parameters ζ_* and ζ_T , as they contain a k_z ,

$$\zeta_* = \frac{\omega_*}{k_z} = \frac{\omega_*}{\omega} \zeta, \quad \zeta_T = \frac{\omega_T}{\omega} \zeta.$$

Now we can rewrite Eq. (2.68) to yield

$$\omega(\zeta) = \left(1 - \zeta^2 \frac{\rho_s^2}{d_e^2} \right) \frac{-(\omega_* - \frac{1}{2}\omega_T)\zeta Z(\zeta) + \frac{1}{2}\omega_T \zeta^2 Z'(\zeta) - \omega_*}{-\rho_s^2 k_\perp^2 + \left(1 - \zeta^2 \frac{\rho_s^2}{d_e^2} \right) Z'(\zeta)}. \quad (2.69)$$

In the derivation of this relation no assumption was made about the specific form of the distribution function F_0 , other than that we use the symbol Z for the plasma dispersion function, that is defined for a Maxwellian distribution. If we want to make a comparison with e.g. the fluid model, we suppose that the distribution function F_0 is Maxwellian, and that we are far away from the particle-wave resonance of the plasma dispersion function, so $|\zeta| \gg 1$, so that waves do not interchange energy with the thermal electrons.

¹This means that if in the usual $\omega(k)$ representation

$$\omega(k) \sim (\omega - k_z V)$$

so that there is a solution with a wave propagating in the z -direction with a phase velocity V , this shows up in the $\omega(\zeta)$ representation as

$$\omega(\zeta) \sim \frac{\omega}{\omega - k_z V} = \frac{\zeta}{\zeta - V},$$

i.e. as a pole.

If we take the limit $\zeta \rightarrow \infty$, the plasma dispersion function reduces to

$$Z(\zeta) \rightarrow -\frac{1}{\zeta} - \frac{1}{2\zeta^3} - \dots$$

and, similarly, its derivative,

$$Z'(\zeta) \rightarrow \frac{1}{\zeta^2} + \frac{3}{2\zeta^4} + \dots$$

This leads to the reduced dispersion relation for large ζ , with

$$\omega(\zeta) \xrightarrow{\zeta \rightarrow \infty} \frac{\omega_* + \omega_T}{1 + k_{\perp}^2 d_e^2}. \quad (2.70)$$

This is an interesting result, because there are no specific kinetic corrections to this so-called kinetic *diamagnetic drift-frequency*, apart from the finite d_e correction which also shows up in fluid theory, as we shall see.

2.6.3 Waves in the two-fluid drift-Alfvén model

We introduce a version of the nonlinear drift-Alfvén fluid equations: in ϕ, ψ and $N \equiv \Omega_i \log n$:

$$\partial_t(\nabla^2 \phi - N) + [\phi, \nabla^2 \phi - N] = 0, \quad (2.71)$$

$$\partial_t(\psi - d_e^2 \nabla^2 \psi) + [\phi, \psi - d_e^2 \nabla^2 \psi] = -\rho_s^2 [N, \psi] + \partial_z(\phi - \rho_s^2 N), \quad (2.72)$$

$$\partial_t N + [\phi, N] = v_A^2 ([\psi, \nabla^2 \psi] + \partial_z \nabla^2 \psi), \quad (2.73)$$

which are again three equations to solve three variables. Here, the density part of the potential vorticity N is treated as an independent variable. The linearized version of Eqs. (2.71 - 2.73) read

$$\omega(-k_{\perp}^2 \phi - N) = \frac{\omega_*}{\rho_s^2} \phi \quad (2.74)$$

$$\omega(1 + k_{\perp}^2 d_e^2) \psi = -k_z(\phi - \rho_s^2 N) - \omega_* \psi \quad (2.75)$$

$$\omega N - v_A^2 k_z k_{\perp}^2 \psi = -\frac{\omega_*}{\rho_s^2} \phi \quad (2.76)$$

If we put $v_t = 1$, so that $d_e^2/\rho_s^2 = v_A^2$, and $\zeta = \omega/k_z$, this yields the fluid dispersion relation,

$$\omega(\zeta) = \frac{\omega_*}{1 + k_{\perp}^2 d_e^2} \frac{\zeta^2 - d_e^2/\rho_s^2}{\zeta^2 - \frac{d_e^2}{\rho_s^2} \frac{1 + k_{\perp}^2 \rho_s^2}{1 + k_{\perp}^2 d_e^2}}.$$

The limit for large ζ is identical to the kinetic case when we take out the temperature gradient in Eq. (2.70),

$$\omega(\zeta) \xrightarrow{\zeta \rightarrow \infty} \frac{\omega_*}{1 + k_{\perp}^2 d_e^2}. \quad (2.77)$$

The fluid equations Eqs. (2.71 - 2.73) are derived with the assumption that the plasma is isothermal, so it does not come as a surprise that the temperature part of the diamagnetic frequency ω_T does not arise.

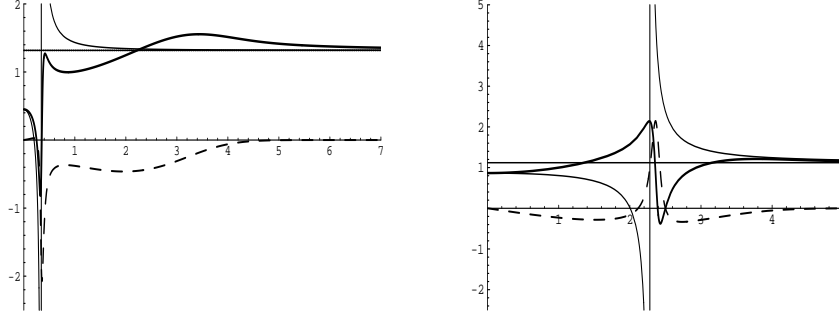


Figure 2.2: Again the dispersion relation $\omega(\zeta)$ is plotted. Here we see in the left figure that ($d_e > \rho_s$) the limit for large ζ is the same for the fluid expression and the kinetic description (**bold**) as the imaginary part tends to zero quite fast, but the behaviour for small ζ very different. Right we see that there is a regime where, if $d_e > \rho_s$ and ω_T becomes too large, that the fluid equation ‘flips’ (back), whereas the kinetic equation does not, and the solutions do not converge until ζ becomes large.

2.6.4 The fluid reduction of the kinetic equations

We would like to compare the $\omega(\zeta)$ relation obtained in the kinetic approach to its fluid counterpart.

If we do not use the complete plasma-dispersion function $Z(\zeta)$ which still holds all particle-wave resonances, but instead fill in the isothermal discretized $n_{\text{cont}} = 2$ distribution function as introduced in section 2.3, where only the thermal speeds (in the $\pm \mathbf{e}_z$ direction) are retained, we get

$$\begin{aligned} Z_F(\zeta) &= \int du \frac{F_{N=2}}{u - \zeta} = \int du \frac{1}{u - \zeta} \frac{1}{2} [\delta(u - 1) + \delta(u + 1)] \\ &= \frac{\zeta}{1 - \zeta^2}, \end{aligned} \quad (2.78)$$

where $F_{N=2}$ is the dimensionless version of the discretized distribution function. Looking at Eq. (2.54), or Eqs. (2.65) and (2.66), we note that they contain a derivative of the distribution function with respect to the parallel velocity, that leads to the primed version of the plasma dispersion function. This is not possible for Z_F , since we can not take a derivative of the delta distribution with respect to its argument, so instead we take

$$Z_F' = \frac{1}{\zeta^2 - 1}, \quad (2.79)$$

which yields equivalence of the fluid equations and the kinetic equations when $\omega_T = 0$. Eq. (2.79) is obtained by partial integration, thus delaying the substitution with the delta distributions, and it complies to $Z_F' = -\zeta Z_F$. Therefore, here the prime does not mean differentiation with respect to the argument, but merely suggests correspondence to $Z'(\zeta)$.

Using the substitutions of the plasma dispersion function (2.78, 2.79) we can construct a fluid-like dispersion relation out of the kinetic dispersion relation Eq. (2.69),

$$\omega(\zeta) = \frac{\omega_*(\zeta^2 \rho_s^2 - d_e^2)}{\rho_s^2 \zeta^2 + d_e^2 (k_{\perp}^2 \rho_s^2 (\zeta^2 - 1) - 1)}. \quad (2.80)$$

The dispersion relation for $\omega_* = \omega_T = 0$ from Eq. (2.68) becomes

$$\omega^2 = k_z^2 v_A^2 \frac{1 + k_\perp^2 \rho_s^2}{1 + k_\perp^2 d_e^2},$$

which is the exact fluid result for the limit of low plasma β : $\beta \ll 1$, see e.g. the discussion and Eq. (26) in [13].

Eq. (2.80) no longer contains the (inverse) temperature gradient length ω_T , since by using this single-temperature distribution function it can no longer support a difference in temperature. In Eq. (2.69) this can be seen more clearly if we highlight a part of the equation,

$$\omega(\zeta) = \left[\omega_*(1 + Z) + \frac{1}{2} \omega_T \zeta (Z + \zeta Z') \right] A,$$

with A the rest of the equation. If $Z' = -\zeta Z$, then no temperature gradient remains in the dispersion relation.

When we look for a way to introduce a temperature gradient in the fluid equations, the only place where we find temperature in a way that the length scale enters the linearized equations is in the Ampère equation (2.72). There is a term $\rho_s^2 [N, \psi]$, that we can imagine to be $[\rho_s^2 N, \psi]$. If we keep in mind that $\rho_s^2 \sim v_t^2$, then we can say that, if gradients are defined in a similar way as in the kinetic case, cf. (2.56),

$$[\rho_s^2 N, \psi] = \partial_x (\rho_s^2 N_0) \partial_y \psi_1 = \left(-\frac{1}{L_T} - \frac{1}{L_n} \right) \rho_s^2 N_0 (i k_y \psi_1).$$

This leads to an expression for $\omega(\zeta)$

$$\omega(\zeta) = \frac{\zeta^2 (\omega_* + \omega_T) \frac{\rho_s^2}{d_e^2} - \omega_*}{\zeta^2 (1 + k_\perp^2 d_e^2) \frac{\rho_s^2}{d_e^2} - (1 + k_\perp^2 \rho_s^2)},$$

which not only leads to the correct asymptotical behaviour for $\zeta \rightarrow \infty$, but is also identical to the kinetic case if we use the ‘fluid’ distribution functions for $\omega_T = 0$ (which is reasonable since ω_T is supposed to drop out in this limit).

References

- [1] H. J. de Blank and G. Valori. *Plasma Phys. Control. Fusion*, 45:A309, 2003.
- [2] T. J. Schep, F. Pegoraro, and B. N. Kuvshinov. *Phys. Plasmas*, 1:2843, 1994.
- [3] B. N. Kuvshinov, V. P. Lakhin, F. Pegoraro, and T. J. Schep. *J. Plasma Physics*, 59:727, 1998.
- [4] T. V. Liseikina, F. Pegoraro, and E. Yu. Echkina. *Phys. Plasmas*, 11:3535, 2004.
- [5] N. J. Zabusky, M. H. Hughes, and K. V. Roberts. *J. of Comput. Phys.*, 30:96, 1979.
- [6] P. W. C. Vosbeek and R. M. M. Mattheij. *J. of Comput. Phys.*, 133:222, 1997.
- [7] J. H. Mentink, J. Bergmans, L. P. J. Kamp, and T. J. Schep. *Phys. Plasmas*, 12:052311, 2005.
- [8] J. Bergmans, B. N. Kuvshinov, V. P. Lakhin, and T. J. Schep. *Phys. Plasmas*, 7:2388, 2000.
- [9] R. D. Hazeltine, M. Kotschenreuther, and P. J. Morrison. *Phys. Fluids*, 28(8):2466–2477, 1985.
- [10] R. Horiuchi and T. Sato. *Phys. Plasmas*, 4(2):277–289, 1997.
- [11] M. Tanaka. *Phys. Plasmas*, 3(11):4010–4017, 1996.
- [12] W. Horton. *Phys. Rep.*, 192:1–3, 1990.
- [13] V. V. Mirnov, C. C. Hegna, and S. C. Prager. *Phys. Plasmas*, 11:4468, 2004.

3 Kinetic model of a collisionless tearing instability in slab geometry

Abstract

Temperature gradients are shown to deform and shift the magnetic islands that grow during fast collisionless reconnection when electron inertia decouples the plasma motion from the magnetic field. A kinetic model of the electrons describes the collisionless processes during the reconnection of field lines that originate in regions with different temperatures. Using a novel model of the reconnecting instability as a surface mode, the kinetic effects are treated analytically in both the linear and nonlinear stages of the instability of a current-carrying low- β plasma slab in a strong magnetic guide field. This configuration is shown to be unstable with respect to tearing modes of large enough wavelength, and stable with respect to short wavelength and kink-like perturbations. A temperature gradient across the chain of magnetic islands yields a new criterion for marginal stability and a diamagnetic shift of the chain with respect to the initial perturbations.

3.1 Introduction

Fast magnetic reconnection under near collisionless conditions is observed in the Earth's magnetosphere [1] and in laboratory plasmas. Fast internal plasma relaxations (sawteeth), occurring in near thermonuclear fusion conditions in tokamaks, were found to grow on a timescale that could not be explained by resistivity alone [2], and have motivated the study of electron inertia as a fast reconnection mechanism [3, 4, 5, 6, 7]. In thermonuclear magnetic confinement, reconnection is of particular concern as it connects field lines that originate in plasma regions with different temperatures, thus reducing thermal insulation. In collisionless plasmas, where electrons move rapidly along the reconnecting field lines, a temperature difference between the connecting field lines poses a fundamental physics problem whose solution requires a kinetic model. A temperature difference δT was shown [8] to modify the magnetic geometry near the x-points that form during reconnection. However, whereas Ref. [8] presents this effect in the vicinity of the magnetic x-point during reconnection at a constant rate, the present paper shows the effects of temperature differences on a reconnecting instability (tearing mode) that produces finite-size magnetic islands.

We show that in both the linear and nonlinear stages of the tearing instability, temperature differences cause a phase shift of the magnetic island chain with respect to the distant magnetic perturbations, together with island deformations consistent with the x-point deformations reported in [8]. The nonlinear phase shift may prove important in magnetic plasma confinement, where reconnection affects the heat loss most when multiple island chains form. Interactions between primary island chains can create secondary and higher order islands and eventually a chaotic magnetic field that fills the volume ergodically. Via phase shifts between primary and higher order island structures, temperature gradients can affect the onset of chaos. This mechanism is as yet unquantified and differs from the more direct ways in which the temperature gradient affects the onset of instabilities, growth rates of tearing modes [9, 10], and the level of plasma turbulence.

A fluid four-field model that incorporates all the fluid nonlinearities [11] has been studied extensively, and resulted in a compact representation in a two-fluid model [12] that allowed for the identification of its Hamiltonian structure and consequently conserved quantities.

It has also been shown [13] that the absence of dissipation in such a fluid model leads to the formation of current and vorticity layers that become increasingly small and seem to implode with time. It turns out that this finite-time singularity can be resolved by replacing the fluid description by a drift-kinetic model, assuming a kinetic electron response of the electrons parallel to the magnetic guide field [8].

In this ordering [12, 14, 15] a magnetic guide field dominates so that parallel equilibration occurs at a time scale much smaller than the perpendicular dynamics, and a distribution function is assumed for the parallel velocity of the electrons. In this way, the model can self-consistently cope with both the (perpendicular) non-collisionality and the fact that the plasma sustains a considerable temperature gradient.

To study the nature of a kinetic collisionless reconnecting tearing mode, in this paper a force-free equilibrium is considered that is periodic in the y -direction, and piecewise homogeneous in the x -direction. In this way regions of uniform canonical momentum in the z -direction, taken to be an ignorable coordinate, are created. The analysis is analogous to a one-dimensional version of contour dynamics [16]. This equilibrium automatically satisfies any formulation of the Vlasov equations as there are no gradients. This allows for a fully analytical approach to the question of linear kinetic stability. An exact dispersion relation in

the linear regime can be obtained, which is sensitive to small temperature gradients.

The jumps, though highly artificial and unphysical, can be considered far away from the actual (linear) mode, as it arises in between two interfaces that can be arbitrarily far apart in this description. No assumptions of periodicity in the x -direction have to be made, and all quantities vanish for $|x| \rightarrow \infty$. This is very different from the Harris-sheet pinch approach [17].

This model set-up proves to be unstable with respect to a tearing mode, and stable to the kink mode. More importantly, it is stable for phenomena with short wavelengths, up until a stability barrier. This means that when an unstable mode with a specific parameter set is studied in a periodic domain, there will not be an infinity of modes with a larger wavenumber that need to be taken into account as well. A domain can be chosen such that there is only one unstable mode present.

The dispersion relation of such a mode can be given in a closed form, but is in the kinetic case more complex than when a two-fluid description of this system is used. It can be shown that far away from wave-particle resonances similar behaviour is predicted by both descriptions, but some essentially kinetic features of the kinetic tearing mode are recovered as well.

A point of careful scrutiny is the validity of the strong guide-field limit used here. This limit is analyzed in the Δ' description in Refs. [18, 19] with a fluid model that includes compression and the Hall term, which are important at scales below the ion skin depth $d_i = d_e \sqrt{m_i/m}$, but for sufficiently low β Refs. [18, 19] recover the drift-Alfvén system as used in Refs. [5, 6, 7]. In the present model the equilibrium scales are below d_i . A complete stability analysis of the equilibrium (3.9) using the fluid model of Refs. [18, 19] shows that the effects of compression and the Hall term are indeed significant, but only in narrow layers of width $d_e \sqrt{\beta}$ around the current jumps. For $\beta \ll 1$ these effects are negligible in the dispersion relation, and neither affect the reconnecting mode nor create another instability of the equilibrium (3.9).

One of the major challenges has been to prove that the stability boundary that can be found using two-fluid theory remains the only stability boundary in the kinetic case, even though the anatomy of the unstable mode has changed in several complicating ways. The proof is attached as an appendix, and is rigorous as long as the current inside the current layer is carried by electrons that move considerably slower than their thermal speed.

The kinetic description also allows for the inclusion of a temperature gradient in a self-consistent way. In this paper we show how the stability boundary of the tearing mode is changed by this temperature gradient, and how it results in an x -dependent shift of the reconnection layer in the electron diamagnetic direction.

The paper is organized as follows. First, the drift-kinetic equations are outlined in section 3.2. Then, the specifics of the equilibrium are given in section 3.3. The dispersion relations based on the two-fluid model and the kinetic model are detailed and compared in sections 3.4 and 3.6. The influence of the application of a small temperature gradient to the equilibrium is described in the linear and the nonlinear stage of the mode in sections 3.7 and 3.8, and the results will be discussed and summarized in section 3.9.

3.2 The drift-kinetic model

The magnetic island geometry is described with a 2D model with a strong magnetic guide field in the z -direction and smaller perpendicular perturbations that only depend on (x, y) : $\mathbf{B} = B_0 \mathbf{e}_z + \mathbf{e}_z \times \nabla \psi$, with $|\nabla \psi| \ll B_0$, in order to model a low- β tokamak. This

ordering neglects magnetic curvature and particle trapping due to ∇B . The electric field is $\mathbf{E} = \mathbf{e}_z \partial \psi / \partial t - \nabla \phi$ and ϕ, ψ are the electric and magnetic potentials. The electrons and their velocities $\parallel \mathbf{B}$ are described by a distribution function $\tilde{f} = \tilde{f}(t, \mathbf{x}, v_{\parallel})$ that satisfies the collisionless drift-kinetic equation

$$\partial_t \tilde{f} + \frac{1}{B_0} [\phi, \tilde{f}] + v_{\parallel} \nabla_{\parallel} \tilde{f} = \frac{e}{m_e} (\partial_t \psi - \nabla_{\parallel} \phi) \frac{\partial \tilde{f}}{\partial v_{\parallel}}. \quad (3.1)$$

The bracket is defined as $[g, h] = \mathbf{e}_z \cdot \nabla g \times \nabla h$ and $\nabla_{\parallel} = \partial_z + [\psi,]$ is the derivative along the total magnetic field \mathbf{B} . Larmor radius effects are neglected here, and the magnetic moment has been integrated over.

The ions respond to parallel fluctuations of the electron density by moving perpendicularly to the magnetic field with the polarization drift to maintain quasi-neutrality, while the parallel ion flow is negligible. This is described by a fluid model for the perpendicular motion of the ions in which we neglect ion Larmor radius effects. This leads to the ion vorticity equation

$$\frac{1}{B_0} \nabla^2 \phi = \frac{\Omega_i}{n_0} \delta n,$$

where in addition the drift ordering is assumed, so that $n \approx n_0$, consistent with $\nabla^2 \phi \ll \Omega_i$. Thus, the ion vorticity equation describes electron density perturbations as a source for the electric field, just as Ampère's law relates the magnetic field to the current density. This leads to a closed system with three equations for ϕ, ψ and f .

We consider cases in which the z -coordinate is ignorable, $\partial_z = 0$, so that we can change the velocity coordinate to the canonical momentum,

$$v_z = v_{\parallel} + \frac{e}{m} \psi,$$

and write Eq. (3.1) as

$$\partial_t f + [\Phi, f] = 0, \quad (3.2)$$

with $f = f(t, \mathbf{x}, v_z)$ and $\Phi = (\phi + v_z \psi - (e/2m_e)\psi^2)/B_0$ a v_z -dependent streamfunction. This means that any function of $G(f, v_z)$ is a solution of Eq. (3.2). The first two moments of the new electron distribution function,

$$\int dv_z f = n_0 + \frac{1}{e v_A^2} \nabla^2 \phi, \quad (3.3)$$

$$-e \int dv_z v_z f = \nabla_e^2 \psi, \quad \nabla_e^2 \equiv \nabla^2 - d_e^{-2}, \quad (3.4)$$

with electron inertial skin depth $d_e = \sqrt{m/e^2 n_0}$ and Alfvén velocity $v_A = B_0 / \sqrt{n_0 m_i}$, provide the sources for the electric and magnetic fields in the plasma. The conservation laws of this system, discussed in e.g. Ref. [8], relies on the smallness of ion Larmor radius effects (the cold-ion limit). Finite ion Larmor radius effects, as presented in e.g. Ref. [12], give rise to a more complicated mathematical structure (although the opposite limit of large Larmor radii gives the comparably simple equation, the Boltzmann response of adiabatic ions).

The system of equations (3.2, 3.3) can also be closed by a fluid equation instead of (3.4) and still maintain all kinetic properties. By taking the first two moments of the kinetic

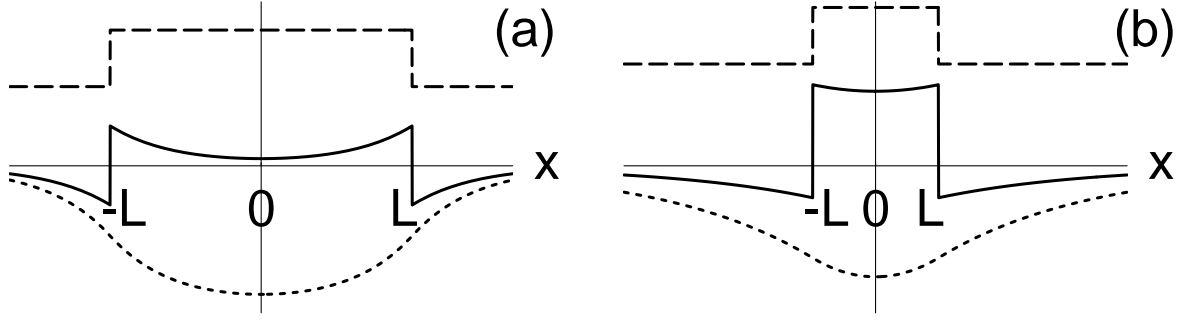


Figure 3.1: Equilibria with a current layer of width $2L$, for $L = 2d_e$ (a) and $L = 0.5d_e$ (b). Dashed curves: x -dependence of the electron distribution function f at fixed v ; solid curves: the current density $\nabla^2\psi_0(x)$, showing a current layer at $|x| < L$ and screening at distances $> d_e$; dotted curves: ψ_0 .

equation one obtains the isothermal fluid equations

$$\partial_t \nabla^2 \phi + [\phi, \nabla^2 \phi] = v_A^2 [\psi, \nabla^2 \psi], \quad (3.5)$$

$$\partial_t \nabla_e^2 \psi + [\phi, \nabla_e^2 \psi] = -\frac{v_t^2}{v_A^2} [\nabla^2 \phi, \psi]. \quad (3.6)$$

Here, $v_t = \sqrt{2T_e/m_e}$ is the parallel electron thermal velocity. These equations also constitute the two-fluid model [12]. By including either Eq. (3.3) or (3.4) the kinetic effects such as particle-wave resonances are accounted for.

3.3 Equilibrium

The system of equations (3.2)–(3.4) describes reconnection due to electron inertia in the strong guide-field (low- β) limit. In order to apply this model nonlinearly, i.e., for finite size islands, we avoid the usual Δ' analysis [20], where the reconnection drive at large scales is described with MHD. Instead, the driving force is modelled by positioning current density jumps at a distance $\sim d_e$ of each other, resulting in a sheared magnetic field around $x = 0$. The locations of the jumps are spatially separated from the reconnection layer where the magnetic islands grow and thermal effects are concentrated, but there is no separation of scales. The equilibrium electron distribution function is chosen as simple as possible for this kinetic model: spatially constant except for jumps at $x = \pm L$ well outside the reconnection region,

$$f_0 = \frac{n_0}{v_t \sqrt{\pi}} \times \begin{cases} e^{-v_z^2/v_t^2}, & |x| > L, \\ e^{-(v_z/v_t - \zeta_0)^2}, & |x| < L. \end{cases} \quad (3.7)$$

The sources in Eqs. (3.3) and (3.4) are a constant density n_0 and a source for the current density that equals $j_0 \equiv en_0 v_t \zeta_0$ in the layer $-L < x < L$ and vanishes elsewhere,

$$\int dv_z f_0 = n_0, \\ -e \int dv_z v_z f_0 = \begin{cases} 0 & \text{for } |x| > L, \\ j_0 & \text{for } |x| < L. \end{cases}$$

The current density $\nabla^2\psi$ differs from this piecewise constant function because via the ∇_e^2 operator in Eq. (3.4), electron inertia screens the currents on distances larger than d_e , as shown in Fig. 3.1(a,b). The current density vanishes towards $x = \pm\infty$. The parallel electron thermal velocity is defined by

$$T_e = \frac{1}{2}m_e v_t^2 = \frac{m_e}{n_0} \int dv_z v_z^2 f_0. \quad (3.8)$$

Note that the two-fluid model is immediately recovered when for the electron thermal distribution function a Dirac delta distribution at $\pm v_t$ is inserted, so that electrons only move with plus or minus the electron thermal speed [12]. In this framework there are two conserved generalized vorticities, $\omega_{\pm} = \nabla^2\phi \mp v_A^2/v_t \nabla_e^2\psi$, advected by their own respective streamfunctions Φ_{\pm} . By superposition of regions of the two types of current-vorticity, of equal weight but opposite sign, a region of pure current density can be constructed, like the current slab as described here. The evolution of the borders or *contours* of such a region of generalized vorticity is again determined by the positions of its own contour and that of the contours of the region of the other type of generalized vorticity [21]. The kinetic case is similar, only with an infinite amount of contours. In this perspective it is clear that the work presented here is an analytical application of contour dynamics which has been used in several numerical studies [22, 23].

Here we add that there is no equilibrium electric potential, and (so) no ion potential vorticity as a result of $\mathbf{E} \times \mathbf{B}$ drift. This is equivalent to stating that we consider ourselves in the frame where the ions stand still.

These demands can be met by constructing a force-free equilibrium, in which we make sure that the $[\psi, \nabla^2\psi]$ bracket (or $\mathbf{j} \times \mathbf{B}$ -term) cancels. We can solve for the equilibrium ψ_0 by observing that

$$\nabla_e^2\psi_0 = \frac{1}{2}j_0 \sum_{\pm} \text{sign}(L \pm x).$$

Solving for ψ_0 , one find that the equilibrium magnetic potential and current density are

$$\psi_0(x) = \frac{1}{2}d_e^2 j_0 \sum_{\pm} \text{sign}(L \pm x)(1 - e^{-|L \pm x|/d_e}). \quad (3.9)$$

and

$$\nabla^2\psi_0(x) = \frac{1}{2}j_0 \sum_{\pm} \text{sign}(L \pm x)e^{-|L \pm x|/d_e}. \quad (3.10)$$

In this way we have constructed a smooth ψ_0 that goes to zero for $x \rightarrow \pm\infty$, and that hosts a region of nonzero mean electron velocity for $|x| < L$. This results in a localized current density $j(x)$ that is shielded on the scale of d_e , the electron inertial skin depth, and thus becomes invisible for large $|x|$. Integrated over the whole domain there is no net current density.

In this configuration it is therefore not suitable to assign a value of Δ' to this equilibrium, as this quantity is defined as the mismatch between the left and right asymptotic derivative at $x = 0$, or the integrated current density inside the current layer as perceived from the so-called ‘outer’ region, far away from the reconnection zone at $x = 0$. In this case $\partial_x\psi_0 \rightarrow 0$ for $x \rightarrow \pm\infty$. This equilibrium is not destabilized by outer forcing.

When $L \gg d_e$, the term ‘current layer’ becomes less descriptive of the equilibrium, and we end up with two current jumps on the edge of a region of small perpendicular magnetic field ψ'_0 . The dynamics of this configuration become trivial in this limit, as the perturbations at $x = \pm L$ can no longer couple to yield a mode.

3.4 Linear stability

The equilibrium and the dynamics are completely determined by the location of the jumps in the generalized current density, as all quantities are constant in between and in the rest of the domain. So, since f is piecewise constant and the kinetic equation (3.2) is purely advective, an instability can perturb f only by perturbing the contours at $x_{\pm} = \pm L$. The fluid equations are obtained from taking moments of the kinetic equation, so the same will hold. The perturbations of the form $A = A_0(x) + A_1(x) \exp(i(ky - \omega t))$, again assuming z ignorable and y periodic and infinite, may be called surface waves. From here, a prime will denote derivation with respect to x .

If we want to calculate the plasma response to these perturbations, we have to solve the system of differential equations (3.3) and (3.4) in the kinetic case, or, in the fluid case, (3.5) and (3.6).

3.4.1 Fluid case

The fluid case will be treated first, as it is more straightforward in terms of symmetry and tractability. If we linearize Eqs. (3.5) and (3.6) we get

$$-\omega \nabla^2 \phi_1 = v_A^2 k (\psi'_0 \nabla_e^2 \psi_1 - \psi_1 \nabla_e^2 \psi'_0), \quad (3.11)$$

$$-\omega \nabla_e^2 \psi_1 = k \frac{v_t^2}{v_A^2} \psi'_0 \nabla^2 \phi_1 + k \phi_1 \nabla_e^2 \psi'_0. \quad (3.12)$$

The construction of the equilibrium is such, that the fluid equations decouple away from the interfaces of the current layer, because $\nabla_e^2 \psi'_0 = j_0(\delta(x+L) - \delta(x-L))$. Thus, away from $x = \pm L$, Eqs. (3.11) and (3.12) reduce to $\nabla^2 \phi_1 = 0$ and $\nabla_e^2 \psi_1 = 0$, with general solutions that decay for $|x| \rightarrow \infty$ of the form

$$\phi_1 = (\phi_L e^{-k|x+L|} + \phi_R e^{-k|x-L|}) e^{i(ky - \omega t)}, \quad (3.13)$$

$$\psi_1 = (\psi_L e^{-k_e|x+L|} + \psi_R e^{-k_e|x-L|}) e^{i(ky - \omega t)}, \quad (3.14)$$

with $k_e = \sqrt{k^2 + d_e^{-2}}$. The discontinuous derivatives at $x = \pm L$ are determined by

$$\begin{aligned} \nabla^2 \phi_1 &= -2k (\delta(x+L)\phi_L - \delta(x-L)\phi_R) e^{i(ky - \omega t)}, \\ \nabla_e^2 \psi_1 &= -2k_e (\delta(x+L)\psi_L - \delta(x-L)\psi_R) e^{i(ky - \omega t)}. \end{aligned}$$

Away from the interfaces, these source functions vanish so that the fluid equations decouple.

The boundary conditions at $x = \pm L$ prevent the system from being trivial: all terms of Eqs. (3.11) and (3.12) contain Dirac delta distributions: we can explicitly write the values of the fields at the location of the contours, $x = \pm L$,

$$\begin{aligned} \phi_1(-L) &\sim \phi_L + e^{-2kL} \phi_R, & \phi_1(L) &\sim e^{-2kL} \phi_L + \phi_R, \\ \psi_1(-L) &\sim \psi_R + e^{-2k_e L} \psi_L, & \psi_1(L) &\sim e^{-2k_e L} \psi_L + \psi_R, \\ \psi'_0(-L) &= -\frac{k_{\parallel}}{k}, & \psi'_0(L) &= \frac{k_{\parallel}}{k}, \end{aligned}$$

with $k_{\parallel} = kB_y(L) = kd_e j_0 / 2B_0$ the maximum parallel wave number.

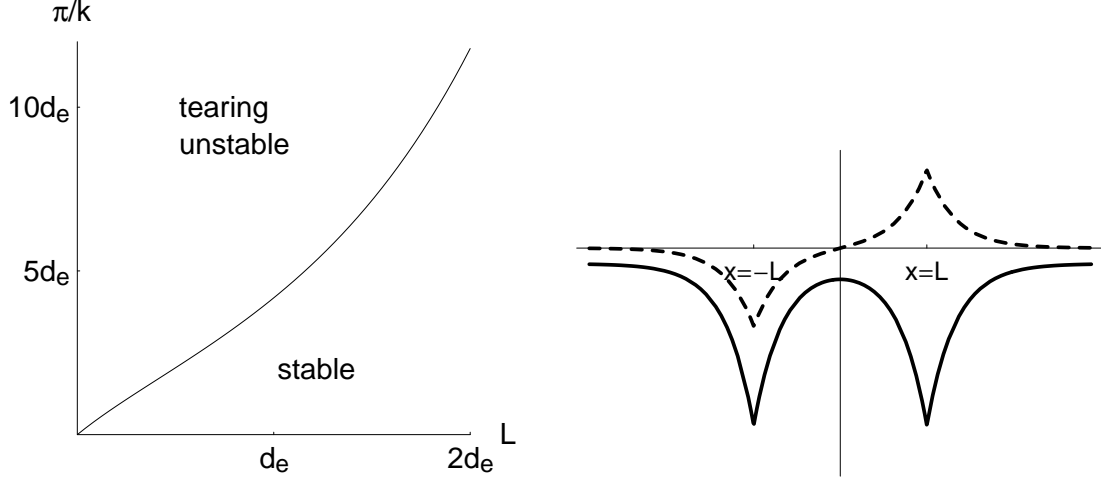


Figure 3.2: On the left the stability of the current layer ($R_+ = 0$) as a function of normalized layer width L/d_e and wavelength π/kd_e is shown. At the stability boundary, $\omega = 0$. On the right the profiles of ϕ_1 (dashed curve) and ψ_1 (solid curve), showing jumps in the derivatives at $x = \pm L$.

Now demanding the fluid equations to hold for the perturbation of nontrivial fields ϕ, ψ at both the interfaces simultaneously, we obtain the constraints for the response of the plasma, i.e. a dispersion relation. Normalizing the frequency to the Alfvén frequency,

$$\zeta = \frac{\omega}{k_{\parallel} v_t},$$

one finds the dispersion relation

$$\mathcal{D}_F(\zeta) = (\zeta^2 - \zeta_+^2 R_+) (\zeta^2 - \zeta_-^2 R_-) = 0, \quad (3.15)$$

where we introduce the shorthand notation

$$\begin{aligned} \zeta_{\pm}^2 &= 1 + \frac{v_A^2}{v_t^2} \frac{1 \mp e^{-2kL}}{kd_e \epsilon}, \\ R_{\pm}(k) &= 1 - \frac{1 \pm e^{-2k_e L}}{k_e d_e \epsilon}, \\ \epsilon &= 1 - e^{-2L/d_e}, \end{aligned}$$

The dispersion relation has solutions

$$\zeta^2 = \zeta_{\pm}^2 R_{\pm}. \quad (3.16)$$

Here, the minus-sign corresponds to a mode that is odd in the magnetic perturbation ψ_1 ($\psi_L = -\psi_R$) and even in the perturbed electrostatic potential ϕ_1 ($\phi_L = \phi_R$), the parity of a kink mode.

The plus-sign corresponds to the mode that is odd in ϕ_1 and even in ψ_1 , the parity of a tearing mode: a chain of magnetic islands with wavelength $2\pi/k$ is formed, with reconnection at $x = 0$.

Note furthermore that in the dispersion relation the kink and the tearing part are completely decoupled, so that the eigenfunctions Eq. (3.13) and (3.14) are exact.

The stability of the modes is completely determined by the factor R_{\pm} . For the tearing mode, an unstable solution is obtained when $\omega^2 < 0$ when $R_+ < 0$, as $\zeta_{\pm}^2 > 0$ always. This is a purely geometric criterion, as R_{\pm} is a function of the ratios of the scale lengths of the mode with respect to the inertial skin depth, kd_e , L/d_e only.

For the kink mode, $R_-(k) = 0$ has no solutions for real k , so only stable solutions exist.

3.4.2 Kinetic case

In order to include temperature gradients in the model, a fluid model does not suffice in the collisionless limit. If two magnetic field lines that originate from regions of the plasma with different temperatures reconnect, collisionless electrons from the ‘hot’ and ‘cold’ branches of the reconnected field lines will redistribute themselves over the field line at different speeds. This leads to the possibility of temperature gradient induced density and current density perturbations [8]. It is the effect of such perturbations on the reconnection process that we shall investigate in this section. Clearly, a kinetic model of the parallel electron velocity is required. Therefore, the model necessarily includes resonant interactions between waves and electrons and Landau damping.

We shall now linearize the kinetic system of equations (3.2), (3.3), and (3.4) for the equilibrium (3.7). The linearized kinetic equation is

$$f_1 = -k \frac{\phi_1 + (v_z - \Omega_e \psi_0) \psi_1}{\omega - k(v_z - \Omega_e \psi_0) \psi'_0} f'_0, \quad (3.17)$$

where the derivative of the equilibrium distribution is

$$f'_0 = \frac{n_0}{\sqrt{\pi} v_t} \left(e^{-v_z^2/v_t^2} - e^{-(v_z/v_t - \zeta_0)^2} \right) (\delta(x+L) - \delta(x-L)). \quad (3.18)$$

The linear system is closed by expressing ϕ_1 and ψ_1 in terms of f_1 by means of the linearized Eqs. (3.3) and (3.4). However, instead of evaluating two integrals of f_1 over velocity space, it suffices to linearize only Eq. (3.3) and then relate ϕ_1 and ψ_1 via the fluid equation (3.11), which is the lowest moment of the linearized kinetic equation. Substituting (3.17) in the linearized vorticity equation (3.3)

$$\nabla^2 \phi_1 = \frac{\Omega_i}{n_0} \int dv_z f_1, \quad (3.19)$$

yields

$$\begin{aligned} \nabla^2 \phi_1 &= \frac{\Omega_i}{n_0} \int dv_z \left(-k \frac{\phi_1 + (v_z - \Omega_e \psi_0) \psi_1}{\omega - k \psi'_0 (v_z - \Omega_e \psi_0)} f'_0 \right) \\ &= -\frac{\Omega_i}{\psi'_0 v_t} \left(\phi_1 + \frac{\omega \psi_1}{k \psi'_0} \right) (\delta(x+L) - \delta(x-L)) \times \\ &\quad \frac{1}{\sqrt{\pi}} \int dv_z \frac{e^{-(v_z/v_t - \zeta_0)^2} - e^{-v_z^2/v_t^2}}{\omega/k \psi'_0 + \Omega_e \psi_0 - v_z}. \end{aligned} \quad (3.20)$$

where $\psi'_0(\pm L) = \pm k_{\parallel}/k$. As in the fluid case, the instability is a surface mode so that the above equation has only contributions for $x = \pm L$, and the eigenfunctions have the form (3.13, 3.14). Substituting these expressions and evaluating the integrals at $x = \pm L$ yields

$$\begin{aligned} 2k\phi_L &= \frac{v_A^2}{v_t^2} \left(\phi_1(-L) + \zeta v_t \psi_1(-L) \right) I_L, \\ 2k\phi_R &= \frac{v_A^2}{v_t^2} \left(\phi_1(L) + \zeta v_t \psi_1(L) \right) I_R, \end{aligned}$$

where

$$\begin{aligned} I_L &= -\frac{1}{2\zeta_0} \left(Z(\zeta + \zeta_\epsilon + \frac{1}{2}\zeta_0) - Z(\zeta + \zeta_\epsilon - \frac{1}{2}\zeta_0) \right), \\ I_R &= -\frac{1}{2\zeta_0} \left(Z(\zeta - \zeta_\epsilon + \frac{1}{2}\zeta_0) - Z(\zeta - \zeta_\epsilon - \frac{1}{2}\zeta_0) \right), \end{aligned}$$

and

$$Z(\zeta) \equiv \frac{1}{\sqrt{\pi}} \int_{-\infty}^{\infty} dt \frac{e^{-t^2}}{t - \zeta}, \quad \zeta_\epsilon = \frac{\epsilon - 1}{2} \zeta_0.$$

Solving these equations and Eq. (3.11) in $x = \pm L$ for the four unknowns $\phi_{L,R}$, $\psi_{L,R}$ yields the dispersion relation

$$\mathcal{D}(\zeta, k) = (I_L + I_R + q_+)(I_L + I_R + q_-) - (I_L - I_R)^2 = 0, \quad (3.21)$$

with

$$q_{\pm} = \left((R_{\pm}^{-1} - 1)\zeta^2 - \zeta_{\pm}^2 + 1 \right)^{-1}. \quad (3.22)$$

Unlike the fluid dispersion relation (3.15), this equation has no explicit solutions in ζ , as $Z(\zeta)$ is a complex-valued transcendental function. Inspection shows that $\{R_{\pm} = 0, \zeta = 0\}$ is a solution, as it was in the fluid case.

Again, we see that the dispersion relation contains a mode that is even in ψ_1 and odd in ϕ_1 , and one that is just the opposite, but now a term proportional to $(I_L - I_R)^2$ couples the two. This means that the eigenfunctions (3.13 and 3.14) are now approximate only.

Inspection shows that $R_{\pm} = 0$ are still stability boundaries, with marginal stability at $\zeta = 0$. Not entirely to be expected, though, is the fact that this is the *only* stability boundary in this complex valued and coupled system. In the appendix we prove that for small enough but finite values of ζ_0 there are no other solutions to the dispersion relation, and hence no other unstable modes in this model system.

3.5 Connection to Δ'

The common definition of Δ' in literature is the total amount of current inside a resistive or non-ideal boundary layer,

$$\Delta' = \left| \frac{d \ln \psi_1}{dx} \right|_{x=0^-}^{x=0^+},$$

i.e. the jump of the logarithmic derivative across this layer. But, as discussed, in the case studied here this current cancels out as a result of the inertial shielding of the jets.

We can apply an adjusted version of the Δ' -formalism to this equilibrium by expressing the stability boundary as follows

$$\Delta'_{\text{new}} \equiv \frac{\delta\psi'_1}{\psi_1} \Big|_{x=L} > \frac{\delta\psi''_0}{\psi'_0} \Big|_{x=L},$$

where $\delta\psi'_1$ and $\delta\psi''_0$ are the jumps of ψ'_1 and ψ''_0 at $x = L$. Then

$$\frac{\delta\psi'_1}{\psi_1} \Big|_{x=L} = -\frac{2k_e}{1 - e^{-2k_e L}},$$

and

$$\frac{\delta\psi''_0}{\psi'_0} \Big|_{x=L} = j_0 \frac{k}{k_{\parallel}},$$

giving the exact same stability boundary. Note that this criterion differs from the usual form ($\Delta' > 0$) that is found in equilibria with smooth current profiles. The complexity of the differential form then often requires asymptotic matching, and constant ψ''_0 or even ψ_0 inside the matching region.

The difference can be explained by the very different approach that is chosen in this paper. Instead of assuming a smooth distribution function, and therefore smooth ϕ , ψ -profiles, the primary focus lies in the region $|x| < L$. The tearing instability is now not driven by current inhomogeneity far away from the reconnection region, but by a surface mode at $|x| = L$.

Here, the border between the inner and outer region is drawn differently: the distance between the jumps in the electron distribution function, $2L$, does not distinguish between different regimes or different sets of equations, but can be used as an estimate of the maximum island width w where linear theory may still apply. The stability criterion $R_+(L/d_e, kd_e) = 0$ is a function of the ratio L/d_e and the product kd_e only. For any value L/d_e a wave number k can be chosen such that the corresponding mode is arbitrarily close to marginal stability.

3.6 Discussion of the fluid limit of the kinetic equations

The kinetic description of the stability of the current layer equilibrium is more challenging in a few ways than the fluid description, and it seems appropriate to track the differences in the anatomy of the mode to which the equilibrium has become unstable.

First of all, the dispersion relation has become complex valued. This means that in general the solutions are not either oscillatory or exponentially growing or evanescent, but a combination of both. This is a direct consequence of taking an integral with a resonant denominator, resulting in a complex valued plasma dispersion function.

Secondly, the kinetic dispersion relation mixes modes with opposite parity, unlike the fluid relations. The mode that is even in ψ and odd in ϕ , the tearing mode, excites the kink mode through the mixing term that is proportional to $(I_L - I_R)^2$. This term follows from the transformation to the canonical momentum in the z -direction, $v_z = v_{\parallel} - \Omega_e \psi$, that leads to a $(\phi - (e/2m_e)\psi^2)/B_0$ term in the streamfunction Φ . This term couples the parities of the fields in a way that does not show up in the fluid analysis.

To understand why the point of marginal stability is unchanged in the kinetic description of the mode, we look at the equation that is responsible for the stability criterion once more, Eq. (3.11), which describes the linearized $\mathbf{j} \times \mathbf{B}$ force balance, and the stability of the tearing mode in specific. Near marginal stability, $\zeta^2 \sim R_+ \sim 0$, so that we can use ω as a small

ordering parameter. Following this ordering, the electrostatic perturbation ϕ_- is one order in ζ smaller than the magnetic perturbation ψ_+ . If we apply this ordering for the whole system of equations, we see that the coupling terms in Eq. (3.21) are maximally of order $\zeta_0\zeta$ for ϕ_+ and $\zeta_0\zeta^2$ for ψ_- . Here we used the small- ζ expansion to estimate $I_L - I_R$ as given in Appendix 3.B,

$$I_L - I_R \approx 8\zeta_\epsilon\zeta - 2i\sqrt{\pi}\zeta_\epsilon,$$

which has a nonvanishing imaginary part for $\zeta \rightarrow 0$. Near marginal stability, at $\zeta = 0$, this does not result in a change in the dispersion relation.

When we want to see if the kinetic modes can be identified with the fluid solutions as found before, we can take the limit $\omega/kv_t \rightarrow \infty$, so that all wave phenomena travel much faster than the thermal electrons, $\omega/k \gg v_t$. In that case the effects of particle-wave resonances become negligible.

In the kinetic dispersion relation, the limit

$$\lim_{\zeta \rightarrow \infty} Z(\zeta) \approx -\frac{1}{\zeta} - \frac{1}{2\zeta^3} + \mathcal{O}\left(\frac{1}{\zeta^5}\right),$$

is a well defined limit of the plasma dispersion function. Here, the argument of the dispersion function is dimensionless, $\zeta = \omega/k_{\parallel}v_t$. Then, if we look at the dispersion relation Eq. (3.21),

$$(I_L + I_R + q_+)(I_L + I_R + q_-) = (I_L - I_R)^2,$$

we see that if we are looking for a comparison with the fluid dispersion relation, we have to look at the uncoupled case, $I_L - I_R \rightarrow 0$, since there are no terms proportional to ζ_ϵ , ζ_0 in the fluid case.

From the definition Eq. (3.22) we can rewrite the solutions of (3.21) so that

$$\frac{I_L + I_R}{q_{\pm}} + 1 \approx \left(-\frac{1}{\zeta} - \frac{1}{2\zeta^3}\right) \left((R_{\pm}^{-1} - 1)\zeta^2 - \zeta_{\pm}^2 + 1 \right) + 1 = 0.$$

which gives $\zeta^2 = (\zeta_{\pm}^2 + \frac{1}{2})R_{\pm} - \frac{3}{2}$. This is to be compared with the fluid result (3.16): $\zeta_F^2 = \zeta_{\pm}^2 R_{\pm}$. The two expressions agree in the limit $\zeta_{\pm} \gg 1$, so either by letting $L \rightarrow 0$ (so that $\epsilon \rightarrow 0$) or assuming $v_A \gg v_t$. The former limit merely confirms that the limit in which the layer becomes considerably smaller than d_e is equally ill-posed for both fluid and kinetic theory, but the latter limit corresponds to the statement that magnetic pressure should be considerably higher than thermal pressure, i.e. the plasma $\beta \ll 1$.

3.7 Influence of a temperature gradient on the linear stability

Before treating the kinetic nonlinear physics of finite-size islands, we consider the effect of a small temperature gradient in the x -direction on the linear kinetic tearing mode. Introducing such a gradient in the equilibrium distribution,

$$f_0 = \frac{n_0}{\sqrt{\pi}v_t(x)} e^{-v^2/v_t^2(x)},$$

one finds

$$f'_0 \approx \frac{1}{L_T} \left(\frac{v^2}{v_t(0)^2} - \frac{1}{2} \right) \frac{n_0}{\sqrt{\pi}v_t(0)} e^{-v^2/v_t^2(0)}$$

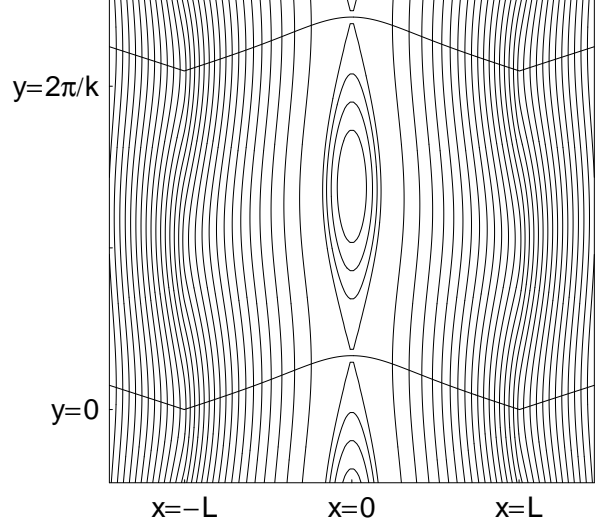


Figure 3.3:

The effect of a temperature gradient on the linear perturbation ψ_1 of the magnetic potential of the tearing mode is illustrated here by showing $\psi_0 + \psi_1$ for a small but finite perturbation. The x -dependence of the phase shift in the y -direction is indicated by two lines.

for small gradients with $v_t(x) \approx v_t(0)$. We use this approximation in the following. The temperature gradient T'_0 gives rise to the electron drift frequency

$$\omega_* = -\frac{kT'_0}{eB}. \quad (3.23)$$

The effects of ω_* on the stability of the tearing mode have been extensively discussed in the literature, see e.g. [9, 10, 24]. Instead, in the following we shall concentrate on the effects of ω_* on the eigenfunctions of the tearing mode.

3.7.1 Perturbed eigenfunctions

The gradient in the equilibrium distribution function perturbs the linear distribution function, $f_1 = (\phi_1 + v_z \psi_1) f'_0 k / \omega$. Away from kinetic resonances, i.e. assuming $\omega^2 \gg k_{\parallel}^2 v_t^2$, this becomes

$$f_1 \approx \frac{k}{\omega} (\phi_1 + v_z \psi_1 - \Omega_e \psi_1 \psi_0).$$

From Eq. (3.4), or equivalently Eqs. (3.11) and (3.19), we obtain for the perturbed eigenfunction $\psi_1 \sim \exp i(ky - \omega t)$,

$$\begin{aligned} \psi_1'' - (k^2 + d_e^{-2})\psi_1 &= -e \int dv_z v_z f_1, \\ &\approx -e \frac{k}{\omega} \psi_1 \int dv_z v_z f'_0, \\ &\equiv -e \frac{k}{\omega} \left(\frac{n_0 T'_0}{m_e} \right) \psi_1, \end{aligned}$$

which we write as $\psi_1'' - \tilde{k}^2 \psi_1 = 0$, with solution

$$\psi_1 \sim e^{\pm \tilde{k}x + i(ky - \omega t)},$$

where

$$\tilde{k} = \sqrt{k^2 + d_e^{-2} \left(1 + \frac{\omega_*}{\omega} \right)}. \quad (3.24)$$

The frequency of the growing mode will generally be complex, $\omega = \omega_r + i\gamma$, which means that the application of a finite temperature gradient results in a complex $\tilde{k} = \tilde{k}_r + i\tilde{k}_i$. The eigenfunctions of the tearing symmetry inside the current layer ($-L < x < L$) will then have a general form of

$$\psi_1 \sim \cosh(\tilde{k}_r x + i\tilde{k}_i x) e^{i(ky - i\omega t)}. \quad (3.25)$$

One sees that \tilde{k}_i introduces an oscillatory term in the x -dependence of ψ_1 . Such oscillatory behaviour was first reported in [24], where temperature as well as density gradients were considered. Here we offer a different interpretation of the same effect, as an x -dependent phase shift in the electron diamagnetic direction of the eigenfunction (3.14). This shift δy depends on the temperature gradient through ω_* in \tilde{k}_i , and is illustrated in Fig. 3.3. It is given by

$$\delta y(x) = \arctan(\tanh(\tilde{k}_r x) \tan(\tilde{k}_i x)) \approx \frac{\tilde{k}_i}{\tilde{k}} |x|, \quad (3.26)$$

where the last expression holds in the limit $|x| \gg k_r^{-1}$, far away from the x-point of the island.

3.7.2 Linear phase shift near marginal stability

To properly quantify the diamagnetic shift of the magnetic island chain we have to take into account the fact that marginal stability has shifted as well. The temperature gradient has led to a new, phase velocity dependent, version of the magnetic wave number \tilde{k} . If we can deduce the frequency at which the tearing mode becomes unstable for some known ω_* , then we can estimate the phase shift of the magnetic island with respect to the perturbations at the edges of the current layer.

When the growth rate is large, in the sense that for a complex frequency $\omega = \omega_r + i\gamma$, with $\gamma \gg \omega_*$, ω_r , we have directly from the definition

$$\tilde{k}^2 = k^2 + \frac{1}{d_e^2} \left(1 + \frac{\omega_*}{\omega_r + i\gamma}\right) \quad (3.27)$$

that

$$\tilde{k}_i = -\frac{\omega_*}{2\gamma \tilde{k}_r d_e^2}. \quad (3.28)$$

When on the other hand $\gamma \ll \omega_*$, ω_r , a more careful approach is called for. We are interested in the behaviour of the shift for various regimes of T'_0 , but we can also look at this as the difference between how fast modes are (in terms of a growth rate, in the linear case) compared to the thermal velocity. This takes us to the dispersion relation, where we note that only R_+ is a function of \tilde{k} , so that for small temperature gradients, we can say that for $\gamma \ll \omega_*$, ω_r ,

$$\omega_+^2 = \zeta_+^2 R_+(\tilde{k}) \approx \zeta_+^2 \left(R_+(k_e) + \frac{dR_+}{d\tilde{k}} \frac{d\tilde{k}}{d\gamma} \gamma + \dots \right) \quad (3.29)$$

If we partially evaluate this expansion,

$$R_+ = R_+(k_e) + R_1 \frac{\omega_*}{2k_e d_e^2} \frac{-i\gamma}{\omega_r^2} + \mathcal{O}(\gamma^2),$$

where in the last denominator we have neglected the γ^2 terms. Here,

$$R_1 \equiv \frac{dR_+}{dk_e}.$$

When we resubstitute this into the dispersion relation we get

$$\omega_+^2 = \zeta_+^2(R_+(k_e) - i\frac{\gamma\omega_*}{2k_e d_e^2 \omega_r^2} R_1 + \mathcal{O}(\gamma^2)),$$

which can be split into a real and an imaginary part:

$$\begin{aligned} \text{Real:} \quad & \omega_r^2 - \gamma^2 - \zeta_+^2 R_+(k_e) = 0, \\ \text{Imaginary:} \quad & 2\omega_r \gamma - \zeta_+^2 \left(\frac{\gamma\omega_*}{2\omega_r^2 k_e d_e^2} \right) R_1 = 0. \end{aligned}$$

From the imaginary part of the dispersion relation we get

$$\omega_r = -\sqrt[3]{\frac{\zeta_+^2 \omega_*}{4k_e d_e^2} R_1} = \omega_c. \quad (3.30)$$

This is the linear stability boundary for the collisionless tearing mode in the presence of a small temperature gradient. For $\omega_* \rightarrow 0$ we retrieve the former boundary at $\omega = 0$.

The phase shifts in the small and large growth rate regimes can be summarized as

$$\delta y = -\frac{|x|}{k} \times \begin{cases} \omega_*/(2\gamma k_e d_e^2), & \text{if } \gamma \gg \omega_c, \\ 2\gamma\omega_c/R_1\zeta_+^2, & \text{if } \gamma \ll \omega_c. \end{cases} \quad (3.31)$$

The last expression shows that the phase shift vanishes for small growth rates.

3.8 Nonlinear phase shift

Once the reconnection process is well underway, the magnetic island will start to have a finite width w , and as already a finite amount of flux has reconnected, regions of increasing temperature difference start to be drawn into the x-point area. A steepening temperature gradient will accumulate across the x-point. It is reasonable to consider the case in which two flux tubes of such finite δT will reconnect.

In the reconnected flux tube, the electrons originating from the high temperature side, with say $T = T_+$, will flow into the magnetic island with a larger thermal velocity than the electrons that originate from the low T side with temperature T_- .

The plasma will still follow lines of constant Φ , so for each value of v_z there will be a separatrix with $\Phi = 0$ that separates the hot from the cold plasma. This leads to a position-dependent distribution function, which, as shown in [25], results in a perturbed current density inside the island. Because the island now has a finite width, this imbalance in the current density causes an up-down asymmetry of the separatrices of the magnetic island.

If we assume at some stage that the reconnection process proceeds at a quasi-steady rate, the kinetic equation (3.2) reduces to

$$[\Phi, f] = 0. \quad (3.32)$$

This means that the distribution function does not evolve in time, and that we consider a stationary structure in which the plasma flows along lines of constant Φ , without taking into account saturation phenomena. We can trivially solve this equation by supposing a constant distribution function on either side of the island chain,

$$f = f_0 \pm \tilde{f}, \quad (3.33)$$

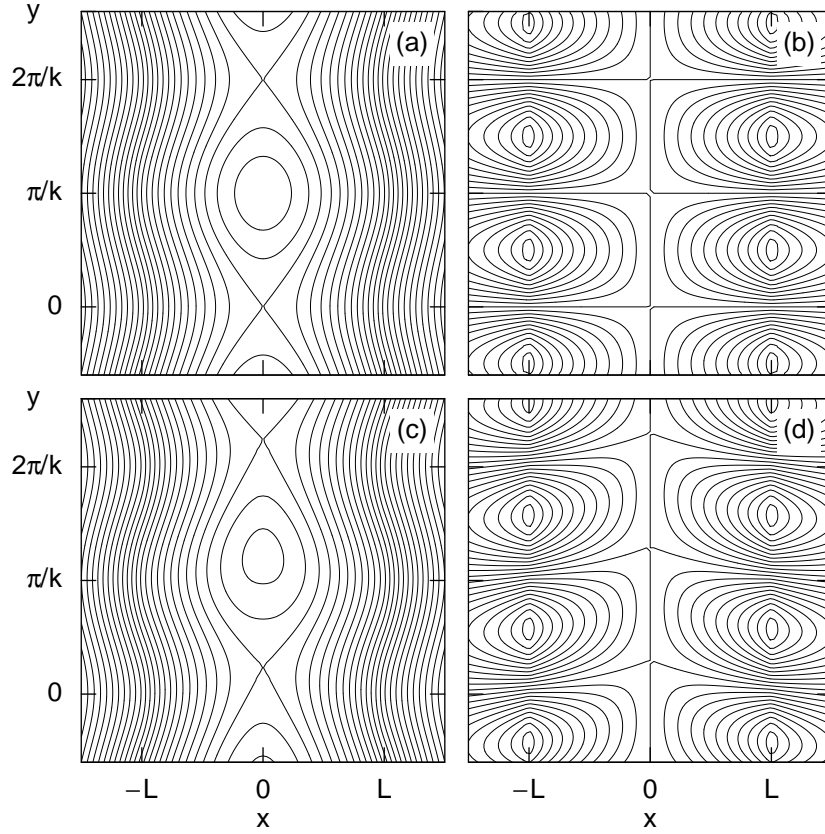


Figure 3.4: The perturbed fields of a tearing mode, ψ (a) and ϕ (b). The current density is discontinuous at $x = \pm L$. In the presence of a temperature difference across the magnetic island, the island becomes up-down asymmetric and is shifted by δy with respect to the outer mode structure, as can be seen in $\psi_0 + \psi_1 + \tilde{\psi}$ (c) and $\phi_1 + \tilde{\phi}$ (d).

with

$$\frac{1}{2} \int dv_z v_z^2 \tilde{f} = n_0(T_+ - T_-).$$

These two distribution functions meet at a separatrix, but, as outlined in [8], this is given by

$$\Phi(v_z, x, y) = 0,$$

which is a line that runs through the x-point and inside the island, and is different for each value of v_z . The distribution function as a function of (x, y) becomes

$$f(v_z, x, y) = f_0(v_z) + \tilde{f}(v_z) \text{sign}(v_z - v_s), \quad (3.34)$$

where

$$v_s(x, y) = -\frac{\phi}{\psi} + \frac{e}{2m}\psi,$$

is the resonant value of v_z at a given position (x, y) , or, the value of v_z for which the distribution functions meet at that position.

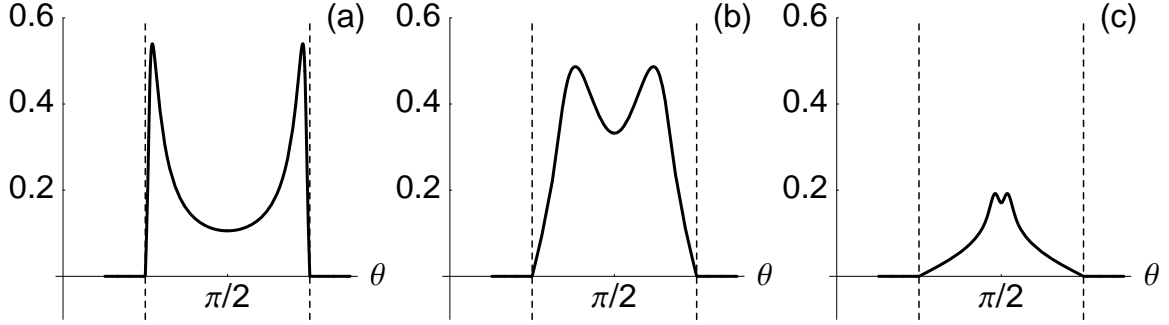


Figure 3.5: Angular distribution of the current density (a.u.) in the x-point vicinity, assuming a constant reconnection rate, based on the kinetic analysis in [8]. The dashed lines indicate the separatrix positions. The three cases shown have $v_t = kw\phi_L/8\psi_L$ (a), $v_t = kw\phi_L/\psi_L$ (b), and $v_t = 8kw\phi_L/\psi_L$ (c).

To calculate the perturbed current density inside the island as a result of the position dependent distribution function, we can say that

$$\begin{aligned}
 \tilde{j} &= -e \int_{-\infty}^{\infty} dv_z v_z (f - f_0), \\
 &= -e \left(\int_{-\infty}^{v_s} dv_z v_z \tilde{f} + \int_{v_s}^{\infty} dv_z v_z (-\tilde{f}) \right) \\
 &= e\delta T \left(\frac{1}{m_e} + \frac{v_s^2}{T_0} \right) f_0(v_s) \text{sign}(y).
 \end{aligned} \tag{3.35}$$

This current perturbs the original magnetic island geometry through Ampère’s law (3.4), stating that where there is more positive current, the outflow angle of the separatrix narrows, and vice versa.

The degree in which this perturbed current density deforms the separatrices and induces a diamagnetic shift in the y -direction depends on the ratio of the velocity of the mode and the thermal velocity. This ratio makes the current distribution to be either confined to a small region near the y -axis or spread out to the entire width of the island. In Ref. [8] this was illustrated for the simplified case of a steady-state reconnection rate. In that case, the current density in the vicinity of the x-point is a function of the angle $\theta = \arctan(y/x)$ only. Figure 3.5 shows the angular distribution of the current density based on the analysis in Ref. [8], for three values of the reconnection rate.

First, if we consider the reconnection process to be fast in the sense that

$$\frac{\phi_L}{\psi_L} \gg \frac{v_t}{kw},$$

(Fig. 3.5(c)) the perturbed current is concentrated near $x = 0$, in a layer much narrower than the island width $2w$. If we assume the perturbed current to have the form

$$\tilde{j}(x, y) = \frac{A}{k} \sin(ky) \delta(x), \tag{3.36}$$

ignoring higher order Fourier harmonics in the y -direction that may arise near the o-point, so that the amount of perturbed current can be given by

$$\int \tilde{j}(x, y) dx = Ay. \quad (3.37)$$

From Eq. (3.35) we then obtain

$$A = \delta T \frac{en_0}{m_e} \frac{\psi_L}{\phi_L}.$$

The corresponding magnetic field perturbation is given by

$$\tilde{\psi} = -\frac{A}{2kk_e} \sin(ky) e^{-k_e|x|}. \quad (3.38)$$

This adds up to a total field $\psi = \psi_0 + \psi_1 + \tilde{\psi}$, of which we can determine how its x-point is shifted with respect to the contour perturbations that initiated the tearing mode. This shift, which vanishes for large x and is maximal for $x = 0$, is given by

$$\begin{aligned} \delta y(x) &= \frac{1}{k} \arcsin \left(\frac{A}{2kk_e \psi_L} \frac{e^{-k_e|x|}}{(e^{-k_e|x+L|} + e^{-k_e|x-L|})} \right) \\ &\lesssim \frac{A}{2k^2 k_e \psi_L}. \end{aligned} \quad (3.39)$$

When on the other hand the island grows slowly compared to the thermal velocity, $\phi_L/\psi_L \ll v_t/kw$, then the electrons that carry the perturbed current will have fanned out completely, filling up the full width of the island with this current imbalance. We then assume that the current near the x-point is constant,

$$\tilde{j}(x, y) = \frac{en_0}{m_e v_t \sqrt{\pi}} \delta T \operatorname{sign}(y), \quad (3.40)$$

and changes sign at the o-point in the middle of the island. This limit is illustrated in Fig. 3.5(a). The peaks of $j(\theta)$ near the separatrices become logarithmic singularities in the limit, with a negligible contribution to the magnetic field.

Now, to calculate the behaviour of $\tilde{\psi}$ as a function of δT we have to solve Ampère's equation again by letting (3.40) be its source. We can do this analytically by taking $\tilde{j}(x, y)$ to be centered at the y -axis again for the sake of the algebra. So, if

$$\int \tilde{j}(x, y) dx = A'y,$$

and

$$\begin{aligned} \int \tilde{j}(x, y) dx &= \int_{-w \sin(k|y|/2)}^{w \sin(k|y|/2)} \frac{A'}{k} \sin(ky) \delta(x) dx, \\ &= \frac{A'}{k} |\sin(ky)|, \\ &\approx A'|y|. \end{aligned}$$

This should be the same as

$$\begin{aligned} \int \tilde{j}(x, y) dx & \int_{-w \sin(k|y|/2)}^{w \sin(k|y|/2)} \frac{en_0}{m_e v_t \sqrt{\pi}} \delta T \operatorname{sign}(y), \\ & \approx w|ky| \frac{en_0}{m_e v_t \sqrt{\pi}} \delta T. \end{aligned}$$

Thus we obtain for the case of a relatively slowly evolving tearing mode

$$A' = \frac{en_0 k w}{2m_e v_t \sqrt{\pi}} \delta T. \quad (3.41)$$

Summarizing the both limiting cases, we can say that the shift δy is

$$\delta y = \frac{en \delta T}{2mk^2 k_e} \times \begin{cases} 1/\phi_L & \phi_L/\psi_L \gg v_t/kw, \\ kw/(2\sqrt{\pi}v_t\psi_L) & \phi_L/\psi_L \ll v_t/kw. \end{cases} \quad (3.42)$$

Now we have calculated the diamagnetic shift of a chain of magnetic islands in four different regimes: in the linear case for large and small growth rate and in the nonlinear stage for a mode that is fast and slow compared to the thermal velocity. We can relate those regimes by considering the role of the amplitude of the tearing mode.

From the linear dispersion relation Eq. (3.21), we can obtain an expression for the linear growth rate,

$$\frac{\phi_L}{\psi_L} = i\gamma \frac{k_e k_{\parallel} v_A^2}{k \zeta_+^2}, \quad (3.43)$$

and we can also relate the island width to the linear magnetic perturbation because

$$w^2 = \frac{2\psi_L}{j_0} e^{-L/d_e}. \quad (3.44)$$

Using these relations we can rewrite Eq. (3.42)

$$\delta y = -\frac{\omega_*}{2k_e d_e} \frac{\epsilon(1-\epsilon)}{kk_{\parallel}} \times \begin{cases} \frac{\zeta_+^2 v_A^2}{k_e k_{\parallel}^2} \frac{1}{\gamma w} & \gamma w \gg k_{\parallel} v_t/k, \\ \frac{1}{2\sqrt{\pi}v_t} & \gamma w \ll k_{\parallel} v_t/k. \end{cases} \quad (3.45)$$

This draws a more complete picture of what we can expect in different regimes and how they interconnect. When an equilibrium such as we have described becomes marginally unstable with respect to the tearing mode, it will generally be in a linear regime with a small growth rate, and a shift proportional to the growth rate itself will emerge. The growth rate may increase considerably, e.g. by the inertia effects as treated in [5], and the corresponding shift will become directly proportional to the *local* diamagnetic frequency ω_* and linearly inversely proportional to the growth rate.

But after a finite amount of time the island will have obtained a finite width w , and the nonlinear effects are to be taken into account. When the island is still growing fast, the nonlinear shift is also proportional to ω_* , and inversely proportional to the product of the growth rate and the island width, a speed. When this speed starts to decrease, e.g. because the island starts to saturate, $\gamma \rightarrow 0$, still a finite shift δy of the island chain remains.

This means that this ‘settling’ of a diamagnetic shift of magnetic islands may play a role well out of the linear and in a nonlinear, saturated, stage of a plasma in which several interacting chains of magnetic islands of different helicity may be present. When low order rational island chains grow secondary islands are created. Their mutual poloidal phase angle has consequences for the path leading to stochastization when field lines fill a volume of space ergodically.

3.9 Discussion

Although fluid models yield good qualitative and quantitative descriptions of a number of aspects of magnetic reconnection, even in the near-collisionless regime, a number of effects, most notably wave-particle resonances and non-thermal effects, require a kinetic approach. The results of the present paper focus on the kinetic effects of the parallel motion of the electrons along the field lines, as it is this motion that is most directly affected by a topology change of the field lines. The effects presented in this paper are supplemented with results obtained in the limit case of an isothermal fluid model, in order to identify which effects can be called essentially kinetic.

In order to study the kinetic model in the nonlinear regime, the technique of contour dynamics was used, which leads to an unorthodox choice of the initial current profile. This simple but non-trivial equilibrium is found to be unstable with respect to a reconnecting instability, that can be triggered by a surface mode along the central current layer.

Collisionless reconnection of magnetic field lines at different temperatures yields a phase shift in the electron diamagnetic direction of the growing magnetic island chain relative to the far fields. In the linear regime, this shift is related to the oscillatory behaviour of the tearing mode eigenfunctions in the presence of density or temperature gradients reported in [24]. The present paper arrives at a more general result, also valid in the nonlinear regime, e.g. in the case of island saturation. The phase shift is a function of both the reconnection rate (growth rate in the linear case), and the ratio of the eigenfunctions ϕ_1/ψ_1 . In case of a linear mode, these two parameters are related.

The phase shifts in the different linear and nonlinear regimes are summarized in Eqs. (3.31) and (3.45). For large γ the phase shift decreases as γ^{-1} in both the linear case (3.31) and the nonlinear case (3.45), while for small γ the linear phase shift is proportional to γ . Therefore this shift, most pronounced at larger distances $|k_e x| > 1$, decreases as the reconnection rate slows down. However, when the magnetic island grows into the nonlinear regime, a constant phase shift (3.45), independent of w , remains near the island where $|k_e x| < 1$, due to the finite temperature difference that builds up near the island.

While the dispersion relation (3.21) is specific for the equilibrium (3.7), the redistribution of electrons after reconnection (3.34) is valid more generally, e.g. when the free energy for the instability originates well outside the reconnection zone. Then the criterion for instability is $\Delta' > 0$, both in kinetic theory and in the collisionless fluid limit [6]. Thus, also Eq. (3.31) for the phase shift is generally applicable, with γ and k in (3.31) related via the dispersion relation for the case of interest. Likewise, within the range of validity of the kinetic model [8, 15], Eq. (3.45) are applicable for arbitrary nonlinear evolution of the island width caused by an instability or external forcing, by specifying w and γ independently.

A final point of attention is the validity of the strong guide-field limit used here. This limit is analyzed in the Δ' description in Refs. [18, 19] with a fluid model that includes compression and the Hall term, i.e. coupling to the Whistler wave, which are important at scales below the ion skin depth $d_i = d_e \sqrt{m_i/m}$, but for sufficiently low β Refs. [18, 19] reobtain the drift-Alfvén system as used in Refs. [6, 7]. In the present model the equilibrium scales are below d_i . A complete stability analysis of the equilibrium (3.9) using the fluid model of Refs. [18, 19] shows that the effects of compression and the Hall term are indeed significant, but only in narrow layers of width $d_e \sqrt{\beta}$ around the current density jumps. For $\beta \ll 1$ these effects are negligible in the dispersion relation, and neither affect the reconnecting mode nor create another instability of the equilibrium (3.9). In this view, we conclude that the tearing modes

to which the Δ' description applies are subject to Whistler wave physics because the relevant scale length d_i lies between the (MHD) driving force at longer scale lengths and the shorter reconnection scale length.

The model in the present paper uses an equilibrium with steep current gradients that provide a driving force at short scales. This is a reductionist technique, isolating the kinetic physics on the reconnecting field lines from the Hall-MHD physics at large scales.

Acknowledgements

This work, supported by the European Communities under the contract of Association between EURATOM/FOM, was carried out within the framework of the European Fusion Programme with financial support from NWO. The views and opinions expressed herein do not necessarily reflect those of the European Commission.

References

- [1] V. M. Vasyliunas. *Rev. Geophys. Space Phys.*, 13:303, 1975.
- [2] A. W. Edwards, D. J. Campbell, W. W. Engelhardt, H.-U. Fahrbach, R. D. Gill, R. S. Granetz, S. Tsuji, B. D. J. Tubbing, A. Weller, J. Wesson, and D. Zasche. *Phys. Rev. Lett.*, 57:210, 1986.
- [3] J. Wesson. *Nuclear Fusion*, 30:2545, 1990.
- [4] F. Porcelli. *Phys. Rev. Lett.*, 66(4):425–428, 1991.
- [5] M. Ottaviani and F. Porcelli. *Phys. Rev. Lett.*, 71:3802, 1993.
- [6] M. Ottaviani and F. Porcelli. *Phys. Plasmas*, 2:4104, 1995.
- [7] E. Cafaro, D. Grasso, F. Pegoraro, F. Porcelli, and A. Saluzzi. *Phys. Rev. Lett.*, 80:4430, 1998.
- [8] H. J. de Blank and G. Valori. *Plasma Phys. Control. Fusion*, 45:A309, 2003.
- [9] B. Coppi, J. W.-K. Mark, L. Sugiyama, and G. Bertin. *Phys. Rev. Lett.*, 42:1058, 1979.
- [10] J. F. Drake, N. T. Gladd, C. S. Liu, and C. L. Chang. *Phys. Rev. Lett.*, 44:994, 1980.
- [11] R. D. Hazeltine, M. Kotschenreuther, and P. J. Morrison. *Phys. Fluids*, 28(8):2466–2477, 1985.
- [12] T. J. Schep, F. Pegoraro, and B. N. Kuvshinov. *Phys. Plasmas*, 1:2843, 1994.
- [13] G. Valori, D. Grasso, and H. J. de Blank. *Physics of Plasmas*, 7(1):178–184, 2000.
- [14] B. B. Kadomtsev and O. P. Pogutse. *Sov. Phys. JETP*, 38:283–290, 1974.
- [15] T. V. Liseikina, F. Pegoraro, and E. Yu. Echkina. *Phys. Plasmas*, 11:3535, 2004.
- [16] N. J. Zabusky, M. H. Hughes, and K. V. Roberts. *J. of Comput. Phys.*, 30:96, 1979.

- [17] F. Ceccherini, C. Montagna, F. Pegoraro, and G. Cicogna. *Phys. Plasmas*, 12:052506, 2005.
- [18] V. V. Mirnov, C. C. Hegna, and S. C. Prager. *Phys. Plasmas*, 11:4468, 2004.
- [19] R. Fitzpatrick and F. Porcelli. *Phys. Plasmas*, 11:4713, 2004.
- [20] H. P. Furth, J. Killeen, and M. N. Rosenbluth. *Phys. Fluids*, 6:459, 1963.
- [21] J. Bergmans, B. N. Kuvshinov, V. P. Lakhin, and T. J. Schep. *Phys. Plasmas*, 7:2388, 2000.
- [22] D. G. Dritschel. *J. Comput. Phys.*, 77(1):240–266, 1988.
- [23] P. W. C. Vosbeek and R. M. M. Mattheij. *J. of Comput. Phys.*, 133:222, 1997.
- [24] G. Ara, B. Basu, B. Coppi, G. Laval, M. N. Rosenbluth, and B. V. Waddell. *Ann. Phys.*, 112:443, 1978.
- [25] H. J. de Blank. *Phys. Plasmas*, 8:3927, 2001.

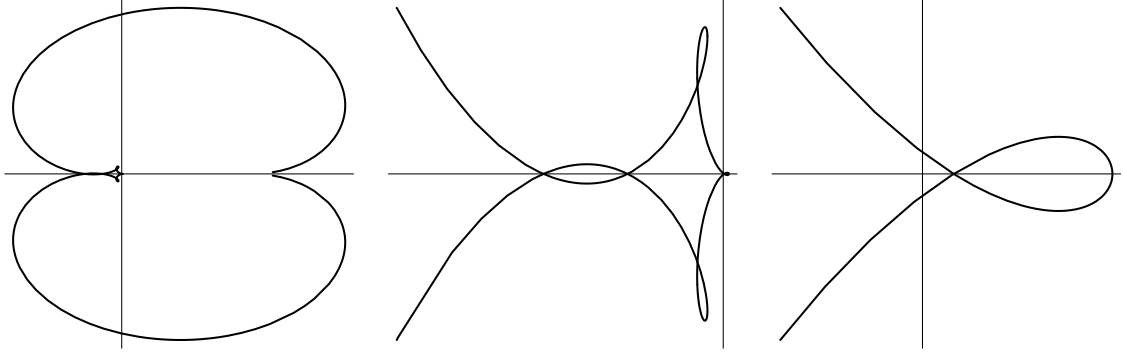


Figure 3.6: Example of a Nyquist diagram for the dispersion relation (3.21), showing the complex \mathcal{D} -plane for real values of ζ . The left figure shows the complete curve and the other two figures are successive magnifications near the origin. Here, the wavenumber k is chosen so that the configuration is just above marginal stability, $R_+(\tilde{k}) > R_+(\tilde{k}_c)$. The magnified figures help to show that the winding number of the curve around the origin is zero, i.e., for these parameters there is no unstable solution.

3.A Proof of the uniqueness of the tearing mode solution

The model system presented here is only interesting for more general purposes, like numerical research, if we know what other instabilities it hosts. If one chooses parameters such that the current layer is tearing-unstable to study collisionless magnetic reconnection with this mode, one wants to be sure there is no small-wavelength instability that may even grow faster. This would blur the vision on the tearing mode, and one might wonder whether it is not better to choose a completely realistic current profile altogether.

In this section it will be shown that for a small enough equilibrium current compared to the thermal velocity, i.e. for small enough $\zeta_0 = j_0/env_t$, there is no other solution to the complete dispersion relation than the tearing mode that was discussed.

The dispersion relation, Eq. (3.21) is a complex function of a generally complex variable. A second solution should part from the real axis at the point of marginal stability, so we are looking for a solution of the dispersion relation for real ζ .

Nyquist proposed a method to determine whether an expression has solutions (roots) in the complex plane. If one were to draw the image of ζ for $\omega \in \mathbb{R}$ under $\mathcal{D}(\zeta)$, this would give a contour in the complex plane. The Nyquist theorem then states that the number of times that this contour circles the origin is equal to the amount of complex roots of $\mathcal{D}(\zeta) = 0$.

This is a way to test for stability, but gives no proof that there cannot exist a region that hosts an instability within the regions that were tested. So a more rigorous approach is needed. The real and imaginary parts of the dispersion relation (3.21) are respectively

$$(Z_{R+} + q_+)(Z_{R+} + q_-) - Z_{R-}^2 - Z_{I+}^2 + Z_{I-}^2 = 0, \quad (3.46)$$

$$Z_{I+}(2Z_{R+} + q_+ + q_-) - 2Z_{I-}Z_{R-} = 0, \quad (3.47)$$

where $Z_{R\pm} = \text{Re}(I_L \pm I_R)$ and $Z_{I\pm} = \text{Im}(I_L \pm I_R)$. We can take a combination of these equations to eliminate, say, q_+ ,

$$Z_{I+}\text{Re}(\mathcal{D}) - (Z_{R+} + q_-)\text{Im}(\mathcal{D}) = 0,$$

to arrive at a quadratic equation for q_- ,

$$(q_- - A)^2 - B = 0, \quad (3.48)$$

with

$$A = -Z_{R+} + \frac{Z_{R-}Z_{I-}}{Z_{I+}},$$

$$B = (1 + Z_{R-}^2/Z_{I+}^2)(Z_{I-}^2 - Z_{I+}^2),$$

and solutions $q_- = A \pm \sqrt{B}$. Note that the choice to eliminate q_+ instead of q_- was arbitrary, and so the \pm sign indicates the distinction between q_{\mp} . This solution q_- of equation (3.48) is a function of ζ , ϵ , and ζ_0 . We can calculate upper and lower boundaries for the plasma dispersion function (see section (3.B)), and by taking the proper combination we can find

$$q_- < q_{-\max} \equiv A_{\max} + \sqrt{B_{\max}}$$

with

$$A_{\max} = 2 + \frac{2\zeta_0^2}{G},$$

$$B_{\max} = 4\zeta_\epsilon^2(\pi + (4\zeta_\epsilon/G)^2),$$

$$G = 1 - \frac{1}{4}\zeta_0^2 - \frac{3}{4}\zeta_\epsilon^2.$$

Here G is a denominator of order unity. The second inequality for holds for $\zeta = 0$: we note that that we can find the extrema of the estimated q_{\max} by differentiating (and by inspection), as it is a polynomial, monotonous function, and find that these are located at $\zeta = 0$. For small ζ , ζ_0 , and ζ_ϵ , the solutions q_{\pm} approximate the value $-Z_{R+} \approx 2$, which is larger than zero.

This analysis of the value of q_{\pm} is derived by looking at the dispersion relation, and by solving it formally. The dispersion relation, however, consisted of terms that were already defined before by the problem that we were trying to solve originally, the characteristics of a straight current layer in a collisionless plasma.

In order for the q_{\pm} as defined by (3.22) to be positive, it is clear that since $R_- > 0$ always, that for small enough ζ at least $q_- < 0$, whereas the solution above decrees $q_- \rightarrow 2$ for small arguments. This means that there is no solution to $\mathcal{D} = 0$ possible for $\zeta > \zeta_{\min}$, with

$$\zeta_{\min} = \sqrt{\frac{\zeta_{\pm}^2 - 1}{R_{\pm}^{-1} - 1}} > 0.$$

Furthermore, to be certain that both $q_{\pm}^{-1} > 0$,

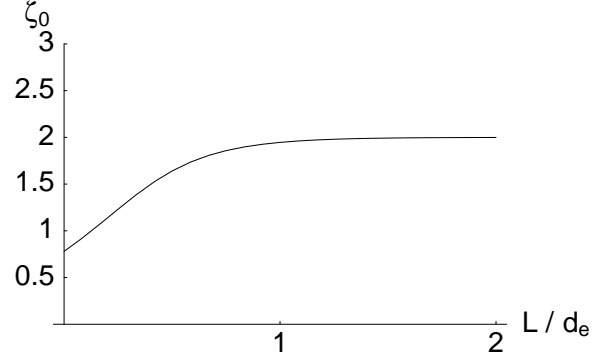
$$\frac{1}{R_{\pm}} - 1 > 0 \quad \Rightarrow \quad R_{\pm} > 0,$$

as $\zeta_{\pm}^2 - 1 > 0$ always, which means that it is necessary that $k > k_c$, the marginal value for the tearing-stable region ($R_+(k_c) \equiv 0$). As $R_- > R_+$, $R_+^{-1} < R_-^{-1}$ and $\zeta_+ < \zeta_-$,

$$q_- = \left(\frac{1}{R_-} - 1\right)\zeta_-^2 - \zeta_-^2 + 1 < \left(\frac{1}{R_+} - 1\right)\zeta_+^2 - \zeta_+^2 + 1 = q_+, \quad \forall \zeta \in \mathbb{R}.$$

Figure 3.7:

The existence of a solution of $q_{-\min} = q_{-\max}$ as a function of L/d_e (horizontal) and ζ_0 (vertical). Below the line no solution is possible, as there $q_{-\max} > q_{-\min}$. The figure shows that for $\zeta_0 < 0.72$ there is no solution for any value of L/d_e , and this critical value of ζ is found for $L \rightarrow 0$.



These are the ingredients that constitute a lower bound from the definition of q_- .

If the upper bound of the solution to the dispersion relation q_- crosses the lower bound of the definition of q_- , there may be a solution that represents a mode in the system that we are considering. Note, however, that this reasoning only holds as long as we are certain that $q_+ > 0$! Otherwise, the ζ for which the solution is reached might go to zero, and R_-^{-1} may be infinite: the ordering that we use becomes unusable.

Using these expressions we can find an upper and a lower bound for q_- , and thus we can solve for ϵ and ζ_0 to find a q_- that holds for both inequalities,

$$q_{-\min} < q_-(\epsilon, \zeta_0) < q_{-\max}. \quad (3.49)$$

With these two versions of q_- the equation (3.49) can be solved for every value of ζ_e and ϵ . But it is necessary to remember that the lower bound $q_{-\min}$ also depends on $R_-(k_c d_e, L/d_e)$, so to make a transparent estimate we solve this equation for $\zeta_0, L/d_e$ (remember that $\epsilon = 1 - \exp(-2L/d_e)$), of which Fig. (3.A) is an illustration. It is clear that for $L/d_e \rightarrow 0$ the smallest maximal value of ζ_0 is to be found, which is $\zeta_{0,\max} = 0.7$. Equating the upper and lower bound yields Fig. (3.A), which is minimal in ζ_0 when L/d_e (and therefore ϵ) goes to zero. Then the largest ζ_0 for which with certainty can be claimed there are no solutions to $q_{-\min} = q_{-\max}$, is $\zeta_0 \approx 0.7$.

Now, we check for which value of ζ_0 the lower boundary of q_+ is still larger than zero.

$$q_{+\min} = A_{\min} - \sqrt{B_{\max}}$$

where

$$A_{\min} = 2 - \frac{1}{3}\zeta_0^2 - \frac{4}{3}\zeta_\epsilon^2 + \zeta_\epsilon^2(8 - 2\zeta_0^2 + 32\zeta_\epsilon^2)(1 - \frac{1}{3}\zeta_0^2 + \frac{8}{3}\zeta_\epsilon^2).$$

The inequality by filling in $\zeta = \zeta_\epsilon$, as the quantity $q_{+\min}$ is monotonous in $(\zeta, \epsilon, \zeta_0)$ for small values of the argument, and certainly before it becomes zero at $\zeta_0 = 0.57$. As this is a lower value than the $\zeta_{0,\max}$ found before, this proof is only valid up to $\zeta_0 = 0.57$. For higher values of ζ_0 we cannot guarantee there are no other modes possible in this plane slab configuration.

3.B Estimates for the plasma dispersion function

The definition of the plasma dispersion function for $(\zeta) > 0$ is

$$Z(\zeta) = \frac{1}{\sqrt{\pi}} \int_{-\infty}^{\infty} dt \frac{e^{-t^2}}{t - \zeta}, \quad (3.50)$$

consistent with

$$Z'(\zeta) = -2(1 + \zeta Z), \quad Z(0) = i\sqrt{\pi}. \quad (3.51)$$

The real part $\text{Re}(Z) = Z_R$ is an odd function, $-Z_R(\zeta) = Z_R(-\zeta)$, which has only one zero, $\zeta = 0$, for real values of ζ . Thus one easily sees that

$$\zeta Z_R \leq 0, \quad \forall \zeta \in \mathbb{R}. \quad (3.52)$$

From (3.51) and (3.52) one can conclude that $Z'_R \leq 2$. This equation can be used in the integral

$$Z_R = \int_0^\zeta dt \frac{dZ_R}{dt}, \quad (3.53)$$

to arrive at the inequality

$$\zeta Z_R \geq -2\zeta^2.$$

This can be placed back into (3.51) to yield

$$Z'_R \leq -2 + 4\zeta^2 \quad \text{etc.} \quad (3.54)$$

In this way we can generate upper and lower estimates for the plasma dispersion function and its derivatives. These boundaries can be to put bounds on the quantities $Z_{R\pm}$ and $Z_{I\pm}$, which involves the plasma dispersion function with arguments $\zeta \pm (\epsilon \pm 1)\zeta_0$. Some care is needed since these arguments may change sign in the type of integrals used below.

First we tackle Z_{R-} by writing it as the integral

$$\begin{aligned} Z_{R-} &= \frac{1}{2\zeta_0} \int_{-\zeta_0/2}^{\zeta_0/2} d\zeta_1 \left(Z'_R(\zeta + \zeta_0 + \zeta_1) - Z'_R(\zeta - \zeta_0 + \zeta_1) \right) \\ &= \frac{1}{2\zeta_0} \int_{-\zeta_0/2}^{\zeta_0/2} d\zeta_1 \int_{-\zeta_\epsilon}^{\zeta_\epsilon} d\zeta_2 Z''_R(\zeta + \zeta_1 + \zeta_2) \\ &= \frac{1}{2\zeta_0} \int_0^\zeta dt \int_{-\zeta_0/2}^{\zeta_0/2} d\zeta_1 \int_{-\zeta_\epsilon}^{\zeta_\epsilon} d\zeta_2 Z'''_R(t + \zeta_1 + \zeta_2). \end{aligned}$$

Here we can use the property that Z'''_R is an even function for which the method outlined in Eqs. (3.51 - 3.54) gives the inequalities

$$8 - 32\zeta^2 \leq Z'''_R(\zeta) \leq 8.$$

By applying these inequalities to the integrand of the triple integral expression for Z_{R-} , one finds

$$8\zeta_\epsilon \left(1 - \frac{1}{3}\zeta_0^2 - \frac{4}{3}\zeta_\epsilon^2 - 4\zeta^2 \right) \leq \frac{dZ_{R-}}{d\zeta} \leq 8\zeta_\epsilon,$$

which can be integrated to give

$$8\zeta_\epsilon \zeta \left(1 - \frac{1}{3}\zeta_0^2 - \frac{4}{3}\zeta_\epsilon^2 - \frac{4}{3}\zeta^2 \right) \leq Z_{R-} \leq 8\zeta_\epsilon \zeta \quad (3.55)$$

for $\zeta > 0$. In a similar fashion the following estimates can be made for small argument ζ :

$$\begin{aligned} -2 &\leq Z_{R+} \leq -2 + 4\zeta^2 + \frac{1}{3}\zeta_0^2 + \frac{4}{3}\zeta_\epsilon^2, \\ -2\sqrt{\pi}\zeta &\leq Z_{I+} \leq -2\sqrt{\pi}\zeta \left(1 - \zeta^2 - \frac{1}{4}\zeta_0^2 - 3\zeta_\epsilon^2 \right), \\ -2\sqrt{\pi}\zeta_\epsilon &\leq Z_{I-} \leq -2\sqrt{\pi}\zeta_\epsilon \left(1 - 3\zeta^2 - \frac{1}{4}\zeta_0^2 - \zeta_\epsilon^2 \right). \end{aligned}$$

4 Temperature gradients in fast collisionless magnetic reconnection

Abstract

Temperature gradients are shown to deform and shift the magnetic islands that grow during fast collisionless reconnection when electron inertia decouples the plasma motion from the magnetic field. A kinetic electron model describes the collisionless processes during the reconnection of field lines originating in regions with different temperatures. Using a novel model of the reconnecting instability as a surface mode, the kinetic effects are treated analytically in the linear and nonlinear stages of the instability of a current-carrying low- β plasma slab in a strong magnetic guide field.

Published in:
Physical Review Letters **98**, 265002 (2007)
Authors: E.V. van der Plas, H.J. de Blank

4.1 Introduction

Fast magnetic reconnection is observed in near-collisionless plasmas in the Earth's magnetosphere [1] and in the laboratory. Fast internal plasma relaxations (sawteeth) observed in tokamaks near thermonuclear fusion conditions have motivated the study of electron inertia as a fast reconnection mechanism [2, 3, 4]. In thermonuclear magnetic confinement, reconnection is of particular concern as it connects field lines that originate in plasma regions with different temperatures, thus reducing thermal insulation. In collisionless plasmas, where electrons move rapidly along the reconnecting field lines, a temperature difference poses a fundamental physics problem whose solution requires a kinetic model. A temperature difference was shown [5] to modify the magnetic geometry near the magnetic x-points that form during reconnection. While that result was limited to the vicinity of x-points during reconnection at a constant rate, here we extend the description to a reconnecting instability that produces finite-size magnetic islands. We show that in both the linear and nonlinear stages of island growth, x-point deformations like those reported in [5] relate to a phase shift of the island chain with respect to the distant magnetic perturbations. The nonlinear phase shift may prove important in magnetic plasma confinement, where reconnection affects the heat loss most when multiple island chains form. Interactions between primary island chains can create secondary and higher order islands and a volume-filling chaotic magnetic field. Phase differences between these island chains affect the onset of chaos. Via phase shifts at small scales, temperature gradients can change the degree of ergodicity and hence plasma confinement, contrasting the more direct ways in which gradients affect growth rates of tearing modes [6, 7], other instabilities, and the level of plasma turbulence.

4.2 Drift-kinetic model

The island geometry is captured in a 2D model with a strong magnetic guide field in the z -direction with perturbations that only depend on (x, y) : $\mathbf{B} = B_0 \mathbf{e}_z + \mathbf{e}_z \times \nabla \psi$, with $|\nabla \psi| \ll B_0$, in order to model a low- β tokamak. This ordering neglects magnetic curvature and particle trapping due to ∇B . The electric field is $\mathbf{E} = \mathbf{e}_z \partial \psi / \partial t - \nabla \phi$ and ϕ, ψ are the electric and magnetic potentials. The electrons and their velocities $\parallel \mathbf{B}$ are described by a distribution function $f(t, x, y, v_{\parallel})$ that satisfies the collisionless drift-kinetic equation

$$\frac{\partial f}{\partial t} + \frac{1}{B_0} [\phi, f] + v_{\parallel} \nabla_{\parallel} f = \frac{e}{m} \left(\frac{\partial \psi}{\partial t} - \nabla_{\parallel} \phi \right) \frac{\partial f}{\partial v_{\parallel}}. \quad (4.1)$$

The bracket is defined as $[g, h] = \mathbf{e}_z \cdot \nabla g \times \nabla h$. Assuming the coordinate z to be ignorable, a velocity coordinate change to the canonical momentum $v_z = v_{\parallel} + e\psi/m$ reduces Eq. (4.1) to an advective equation [8]

$$\frac{\partial f}{\partial t} + [\Phi, f] = 0, \quad (4.2)$$

where $\Phi = (\phi + v_z \psi - \psi^2 e / 2m) / B_0$ is a v_z -dependent streamfunction. The fields depend on f via the ion vorticity equation and Ampère's law,

$$n_0 + \nabla^2 \phi / (e v_A^2) = \int f dv_z, \quad (4.3)$$

$$(\nabla^2 - d_e^{-2}) \psi = -e \int f v_z dv_z. \quad (4.4)$$

Here $d_e = \sqrt{m/e^2n}$ is the inertial skin depth and $v_A = B_0/\sqrt{m_i n_0}$ the Alfvén velocity. Equation (4.3) gives the quasineutral response of the ion polarization drift to electron density variations for frequencies below the ion gyrofrequency and negligible ion thermal motion [9].

We consider the reconnecting instability of a plasma with current concentrated in a straight slab. First, we describe the instability without temperature gradient, later introducing such a gradient ∇T perturbatively. The effect of ∇T on the stability is considered to be negligible compared to the strong instability due to the current profile which overcomes the stabilizing kinetic effects in the collisionless limit reported in Refs. [6, 7].

4.3 Equilibrium, linear stability

The system of equations (4.2)–(4.4) describes reconnection due to electron inertia in the strong guide-field (low- β) limit. In order to apply this model nonlinearly, i.e., for finite size islands, we avoid the usual Δ' analysis [10], where the reconnection drive at large scales is described with MHD. Instead, the driving force is modelled by positioning current density jumps at scales $\sim d_e$. The locations of the jumps are spatially separated from the reconnection layer where the magnetic islands grow and thermal effects are concentrated, but there is no separation of scales. The equilibrium electron distribution function is chosen as simple as possible for this kinetic model: spatially constant except for jumps at $x = \pm L$ well outside the reconnection region,

$$f_0 = \frac{n_0}{v_t \sqrt{\pi}} \times \begin{cases} e^{-v_z^2/v_t^2}, & |x| > L, \\ e^{-(v_z/v_t - \zeta_0)^2}, & |x| < L. \end{cases} \quad (4.5)$$

The density is spatially constant while the current source equals $-e \int f_0 v_z dv_z = en_0 v_t \zeta_0 \equiv j_0$ in the layer $-L < x < L$ and vanishes elsewhere. The current density $\nabla^2 \psi$ differs from this piecewise constant function because in Eq. (4.4), electron inertia screens the currents on distances larger than d_e , as shown in Fig. 4.1(a,b). The equilibrium potentials are $\phi_0 = 0$ and

$$\psi_0(x) = \frac{d_e^2}{2} j_0 \sum_{\pm} \text{sign}(L \pm x) (1 - e^{-|L \pm x|/d_e}). \quad (4.6)$$

We linearize Eqs. (4.2)–(4.4) for perturbations of the form $A = A_0(x) + A_1(x) \exp(iky - i\omega t)$. Since the kinetic equation (4.2) is purely advective and f_0 is constant except at $x = \pm L$, f_1 is localized at $x = \pm L$, i.e., the perturbations are surface modes, with exact eigenfunctions

$$f_1(x, v_z) = f_L(v_z) \delta(x + L) + f_R(v_z) \delta(x - L), \quad (4.7)$$

$$\phi_1(x) = (\phi_L e^{-k|x+L|} + \phi_R e^{-k|x-L|}) e^{kL}, \quad (4.8)$$

$$\psi_1(x) = (\psi_L e^{-k_e|x+L|} + \psi_R e^{-k_e|x-L|}) e^{k_e L}. \quad (4.9)$$

The modified wave number $k_e = \sqrt{k^2 + d_e^{-2}}$ arises in the linearized Ampere law,

$$\psi_1'' - k_e^2 \psi_1 = -e \int f_1 v_z dv_z, \quad (4.10)$$

where a prime denotes the x -derivative. With these eigenfunctions, the dispersion relation for $\omega(k)$ is

$$(I_+ + I_- + q_+)(I_+ + I_- + q_-) = (I_+ - I_-)^2, \quad (4.11)$$

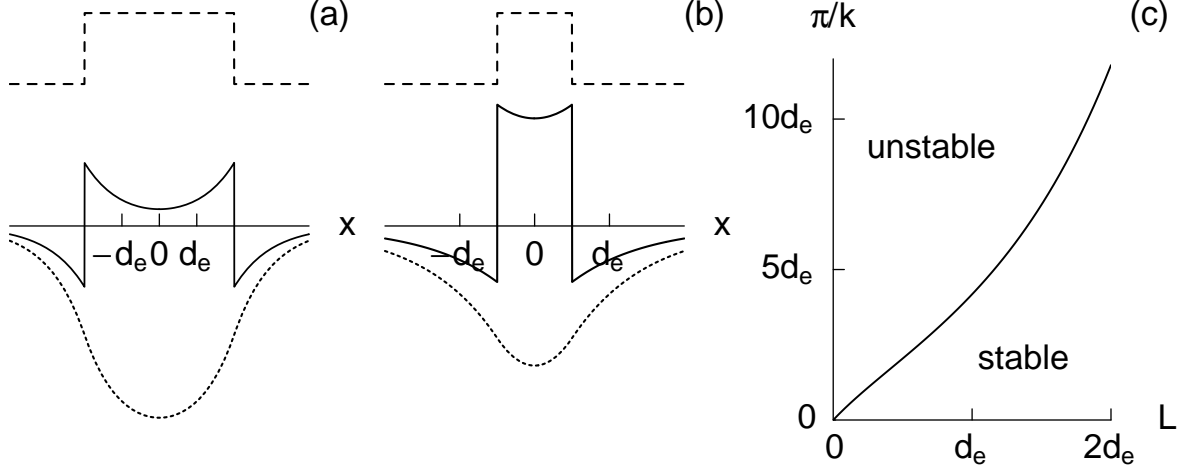


Figure 4.1: Equilibria with a current layer of width $2L$, for $L = 2d_e$ (a) and $L = 0.5d_e$ (b). Dashed curves: x -dependence of the electron distribution function f at fixed v ; solid curves: the current density $\nabla^2\psi_0(x)$, showing a current layer at $|x| < L$ and screening at distances $> d_e$; dotted curves: ψ_0 . Frame (c): Stability of the current layer as a function of layer width and wavelength. At the stability boundary $\omega = 0$.

with

$$I_{\pm} = \frac{1}{2}\zeta_0^{-1} \left(Z(\zeta_{\pm} + \frac{1}{2}\zeta_0) - Z(\zeta_{\pm} - \frac{1}{2}\zeta_0) \right), \quad (4.12)$$

$$\zeta_{\pm} = \omega / (v_t k_{\parallel}) \pm \frac{1}{2}\zeta_0(1 - \epsilon), \quad (4.13)$$

$$q_{\pm}^{-1} = (v_t k_{\parallel})^{-2} (\omega^2 / R_{\pm} - \Omega_{\pm}^2 - \omega^2) + 1, \quad (4.14)$$

$$\Omega_{\pm}^2 = k_{\parallel}^2 \left(v_t^2 + v_A^2 \frac{1 \mp e^{-2kL}}{kd_e\epsilon} \right), \quad (4.15)$$

$$R_{\pm}(k) = 1 - \frac{1 \pm e^{-2k_e L}}{k_e d_e \epsilon}, \quad (4.16)$$

$\epsilon = 1 - e^{-2L/d_e}$, the maximal parallel wave number $k_{\parallel} = kB_y(L)/B_0 = kd_e\epsilon j_0/2B_0$, and $Z(\zeta)$ the plasma dispersion function. Although the dispersion relation (4.11) is complex-valued in general, it has a very simple stability boundary for the tearing mode, viz. $R_+(k) = 0$, where $\omega = 0$. This stability boundary, shown in Fig. 4.1(c), is proved to be unique for moderate electron currents, $\zeta_0 < 0.5$ (i.e. barring beam phenomena). In particular, the analogous stability boundary for the kink mode, $R_-(k) = 0$, has no solutions for real values of k . For $\zeta_0 \ll 1$, one finds that the dispersion relation reduces to two uncoupled equations $I_+ \approx I_- \approx -\frac{1}{2}q_{\pm}$ for the eigenmodes with $\phi_L = \mp\phi_R$ and $\psi_L = \pm\psi_R$. The even- ψ and odd- ψ modes have tearing and kink mode parity, respectively. For finite ζ_0 , the term on the right in Eq. (4.11) couples the modes with kink and tearing parity, breaking their (anti)symmetry. This is a kinetic effect: At high frequencies, away from particle-wave resonances, the kinetic model (4.2)–(4.4) reduces to the isothermal 2-fluid model of Refs. [3, 4, 9]. The fluid limit $\zeta_{\pm} \gg 1$ of Eq. (4.12) is $I_{\pm} = \zeta_{\pm}^{-2} = \zeta^{-2}$, yielding uncoupled tearing and kink parity modes with frequencies

$$\omega_{\pm}^2 = \Omega_{\pm}^2 R_{\pm}. \quad (4.17)$$

4.4 Influence of a temperature gradient

Before treating the kinetic nonlinear physics of finite-size islands, we consider the effect of a small temperature gradient on the linear kinetic tearing mode. Introducing an equilibrium temperature gradient T'_0 gives $f_1 = (\phi_1 + v_z \psi_1) f'_0 k / \omega$ and modifies Eq. (4.10) into $\psi''_1 \approx \tilde{k}^2 \psi_1$, with a wavelength $\tilde{k} \equiv \sqrt{k_e^2 + \omega_* / \omega d_e^2}$ that depends on the electron diamagnetic drift frequency $\omega_* = -k T'_0 / eB$. The frequency is complex, $\omega = \omega_r + i\gamma$, so that the linear effect of the temperature gradient is a complex $\tilde{k} \approx k_e + ik_i$ with $k_i \ll k_e$. This gives the eigenfunction $\psi_1(x)$ in Eq. (4.9) an x -dependent complex phase. For $|x| \leq L$ and $\psi_L = \psi_R$ one finds $\psi_1 \sim \cosh(k_e x + ik_i x) \exp(iky)$. The oscillations in the x -direction were also reported in Ref. [11], which in addition includes the diamagnetic effect of a density gradient. The oscillation can be viewed as a phase shift of the magnetic perturbations at $|x| \gg k_e^{-1}$ with respect to the magnetic islands, of $\delta y(x) = |x| k_i / k$ in the y -direction. A fast growing mode with $\gamma \gg \omega_*$, ω_r has $k_i = -\omega_* / (2\gamma k_r d_e^2)$. In the opposite limit $\gamma \ll \omega_*$, ω_r a Taylor expansion of $R_+(\tilde{k})$ shows the effect of ω_* ,

$$R_+(\tilde{k}) = R_+(k_e) - i \frac{\omega_* \gamma}{2k_e d_e^2 \omega_r^2} R_1 + O(\gamma^2),$$

where $R_1 = dR_+/d\tilde{k}$ is in the range $1 < \tilde{k} R_1 < 1 + d_e/L$. Substitution in the fluid dispersion relation (4.17) yields

$$\omega_r = \omega_c \equiv [\omega_* \Omega_+^2 R_1 / (4k_e d_e^2)]^{1/3}.$$

The phase shifts in both regimes can be summarized as

$$\delta y = -\frac{|x|}{k} \times \begin{cases} \omega_* / (2\gamma k_e d_e^2), & \gamma \gg \omega_c, \\ 2\gamma \omega_c / R_1 \Omega_+^2, & \gamma \ll \omega_c. \end{cases} \quad (4.18)$$

The last expression shows that the phase shift vanishes for small growth rates.

4.5 Nonlinear shift

We shall now show that in the fully nonlinear regime, a finite phase shift is present even for vanishing growth rates. Contrary to the linear phase shift, which is proportional to $|x|$, this nonlinear shift is only present close to the magnetic island. It is caused by the finite temperature difference δT across the island when the island grows to a finite width comparable with d_e . Using the conservation properties of our equations [5, 8, 12] we can deal with the following nonlinearities: (i) the advective nonlinearity of Eq. (4.2), and (ii) the temperature difference δT across the magnetic x-points. However, temperature gradients are introduced only perturbatively: terms nonlinear in ∇T are not considered.

In the nonlinear stage, the reconnection process draws flux tubes together that originate in regions of the plasma with different temperatures. On the reconnected flux tubes, the collisionless electrons originating on the high- T and low- T sides move into the magnetic island with different thermal velocities. The nonlinear kinetic effect shown in Ref. [5] is that this imbalance of the electron velocities perturbs the current density in the island, causing an asymmetry in the y -direction. This can be seen by considering the vicinity of the magnetic x-point. In the nonlinear stage the x-point angles are finite. Assuming that the reconnection process proceeds at a quasi-steady rate, the kinetic equation (4.2) reduces to $[\Phi, f] = 0$, i.e., the electron distribution function near the x-point does not evolve and hence is aligned with

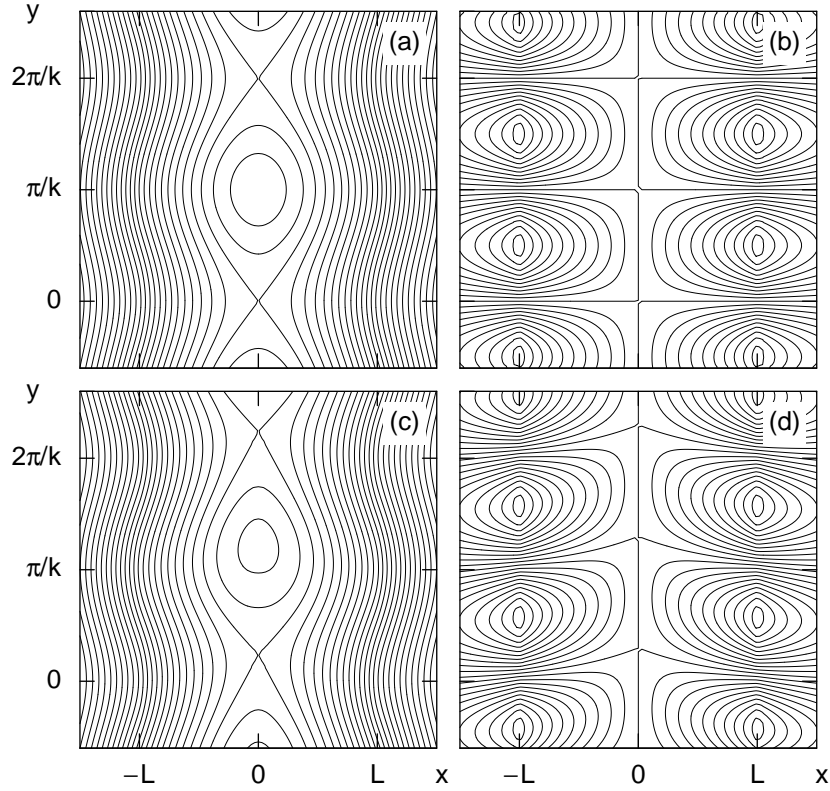


Figure 4.2: The perturbed fields of a tearing mode, ψ (a) and ϕ (b). The current density is discontinuous at $x = \pm L$. In the presence of a temperature difference across the magnetic island, the island becomes up-down asymmetric and is shifted by δy with respect to the outer mode structure, as can be seen in $\psi_0 + \psi_1 + \tilde{\psi}$ (c) and $\phi_1 + \tilde{\phi}$ (d).

the stream-function, $f(t, x, y, v_z) = f(v_z, \Phi(v_z, x, y))$. In the plasma that streams towards the x-point from the high- T side this equation is trivially satisfied by a constant, hot, distribution function $f(v_z) = f_0 + \tilde{f}$ and the plasma that approaches the reconnection zone from the low- T side has a constant distribution $f_0 - \tilde{f}$. As outlined in Ref. [5], the two distribution functions meet at the separatrix of the stream function, which is inside the island. However, for each value of v_z , the separatrix $\Phi(v_z, x, y) = 0$ is a different curve through the x-point. Therefore, inside the island the distribution function is position-dependent,

$$f(v_z, x, y) = f_0(v_z) + \tilde{f}(v_z) \text{sign}(v_z - v_s(x, y)), \quad (4.19)$$

where $v_s = \psi e/2m - \phi/\psi$ is defined by $\Phi(v_s, x, y) = 0$. The island separatrices correspond to $v_s = \pm\infty$. Integrating $v_z f$ over v_z yields a position-dependent current perturbation inside the island,

$$\tilde{j}(x, y) = e \delta T \left(\frac{1}{m} + \frac{v_s^2}{T_0} \right) f_0(v_s) \text{sign}(y). \quad (4.20)$$

Via Ampère's law (4.4), this current perturbation perturbs the field ψ both inside and outside the island.

Up to this point, the technique for combining the distribution functions of reconnecting field lines is applicable to general magnetic configurations with an X-line in astrophysics and in the laboratory. For the closed magnetic field of a tokamak, we now compute the field perturbation from Eq. (4.20) in two limiting cases. First, if reconnection proceeds fast ($\phi_L/\psi_L \gg \hat{v}_t \equiv v_t/kw$), the perturbed current is concentrated near $x = 0$ in a layer much narrower than the island width $2w$ with, for small y ,

$$\int \tilde{j} dx = Ay, \quad \text{and} \quad A \equiv \frac{en\psi_L}{m\phi_L} \delta T,$$

We neglect higher Fourier harmonics in the island period ky and consider the current to be concentrated at $x = 0$,

$$\tilde{j}(x, y) = (A/k) \sin(ky) \delta(x). \quad (4.21)$$

This leads to a magnetic field perturbation

$$\tilde{\psi} = -(A/2kk_e) e^{-k_e|x|} \sin(ky).$$

The total field $\psi = \psi_0(x) + \psi_1(x) \cos(ky) + \tilde{\psi}$ has a phase shift in the y -direction (see Fig. 4.2) which vanishes for large x and has a maximal value at $x = 0$,

$$\delta y = \frac{1}{k} \arcsin\left(\frac{A}{2kk_e\psi_L}\right) \approx \frac{A}{2k^2k_e\psi_L}.$$

In the other limit of slow island growth, $\phi_L \ll \hat{v}_t\psi_L$, the perturbed current is broad. Near the x-point it is almost constant, $\tilde{j} = \delta T en / (mv_t\pi^{1/2}) \text{sign}(y)$. This means that $\int \tilde{j} dx$ at fixed y depends on the local island width $w|\sin(ky/2)|$. Noting that \tilde{j} changes sign in the island center and again neglecting higher harmonics in ky , we once more solve Ampère's law $\nabla^2\tilde{\psi} = \tilde{j}$ approximately by considering \tilde{j} to be concentrated in $x = 0$ as in Eq. (4.21). Thus we find $A = \delta T en / (2m\hat{v}_t\pi^{1/2})$ in the limit of slow island growth. The two limit cases can be listed as

$$\delta y = \frac{en \delta T}{2mk^2k_e} \times \begin{cases} 1/\phi_L, & \phi_L \gg \hat{v}_t\psi_L, \\ 1/\hat{v}_t\psi_L, & \phi_L \ll \hat{v}_t\psi_L. \end{cases} \quad (4.22)$$

In order to compare the linear (4.18) and nonlinear (4.22) phase shifts, and discuss the role of the island width, we relate the ratio of the perturbed fields to the linear growth rate, $\phi_L/\psi_L = i\gamma k_e k_{\parallel} v_A^2 / (k\Omega_+^2)$, relate the island width to the linear perturbation, $w^2 = 8(\psi_L/j_0)e^{-L/d_e}$, and assume that the temperature difference near the x-point scales linearly with the island width, $\delta T \sim T_0'w$. The phase shifts for fast and slow reconnection in the nonlinear stage are then

$$\delta y = c_1\omega_*/k^2\gamma w, \quad \gamma \gg k_{\parallel}\hat{v}_t, \quad (4.23)$$

$$\delta y = c_2\omega_*/kk_{\parallel}v_t, \quad \gamma \ll k_{\parallel}\hat{v}_t, \quad (4.24)$$

where c_1, c_2 are functions of kd_e and L/d_e of order unity.

4.6 Discussion

In conclusion, collisionless reconnection of magnetic field lines at different temperatures yields a phase shift in the electron diamagnetic direction of the growing magnetic island chain

relative to the far fields. The phase shifts in the different linear and nonlinear regimes are summarized in Eqs. (4.18), (4.23), and (4.24). For large γ the phase shift decreases as γ^{-1} in both the linear case (4.18) and the nonlinear case (4.23), while for small γ the linear phase shift is proportional to γ . Therefore this shift, most pronounced at larger distances $|k_e x| > 1$, decreases as the reconnection rate slows down. However, when the magnetic island grows into the nonlinear regime, a constant phase shift (4.24), independent of w , remains near the island where $|k_e x| < 1$, due to the finite temperature difference that builds up near the island.

While the dispersion relation (4.11) is specific for the equilibrium (4.5), the redistribution of electrons after reconnection (4.19) is valid more generally, e.g. when the free energy for the instability originates well outside the reconnection zone. Then the criterion for instability is $\Delta' > 0$, both in kinetic theory and in the collisionless fluid limit [3]. Thus, also Eq. (4.18) for the phase shift is generally applicable, with γ and k in (4.18) related via the dispersion relation for the case of interest. Likewise, within the range of validity of the kinetic model [5, 12], Eqs. (4.23) and (4.24) are applicable for arbitrary nonlinear evolution of the island width caused by an instability or external forcing, by specifying w and γ independently.

A final point of attention is the validity of the strong guide-field limit used here. This limit is analyzed in the Δ' description in Refs. [13, 14] with a fluid model that includes compression and the Hall term, which are important at scales below the ion skin depth $d_i = d_e \sqrt{m_i/m}$, but for sufficiently low β Refs. [13, 14] reobtain the drift-Alfvén system as used in Refs. [3, 4]. In the present model the equilibrium scales are below d_i . A complete stability analysis of the equilibrium (4.6) using the fluid model of Refs. [13, 14] shows that the effects of compression and the Hall term are indeed significant, but only in narrow layers of width $d_e \sqrt{\beta}$ around the current density jumps. For $\beta \ll 1$ these effects are negligible in the dispersion relation, and neither affect the reconnecting mode nor create another instability of the equilibrium (4.6).

Acknowledgements

This work, supported by the European Communities under the contract of Association between EURATOM/FOM, was carried out within the framework of the European Fusion Programme with financial support from NWO.

References

- [1] V. M. Vasyliunas. *Rev. Geophys. Space Phys.*, 13:303, 1975.
- [2] J. Wesson. *Nuclear Fusion*, 30:2545, 1990.
- [3] M. Ottaviani and F. Porcelli. *Phys. Plasmas*, 2:4104, 1995.
- [4] E. Cafaro, D. Grasso, F. Pegoraro, F. Porcelli, and A. Saluzzi. *Phys. Rev. Lett.*, 80:4430, 1998.
- [5] H. J. de Blank and G. Valori. *Plasma Phys. Control. Fusion*, 45:A309, 2003.
- [6] B. Coppi, J. W.-K. Mark, L. Sugiyama, and G. Bertin. *Phys. Rev. Lett.*, 42:1058, 1979.
- [7] J. F. Drake, N. T. Gladd, C. S. Liu, and C. L. Chang. *Phys. Rev. Lett.*, 44:994, 1980.
- [8] H. J. de Blank. *Phys. Plasmas*, 8:3927, 2001.

- [9] T. J. Schep, F. Pegoraro, and B. N. Kuvshinov. *Phys. Plasmas*, 1:2843, 1994.
- [10] H. P. Furth, J. Killeen, and M. N. Rosenbluth. *Phys. Fluids*, 6:459, 1963.
- [11] G. Ara, B. Basu, B. Coppi, G. Laval, M. N. Rosenbluth, and B. V. Waddell. *Ann. Phys.*, 112:443, 1978.
- [12] T. V. Liseikina, F. Pegoraro, and E. Yu. Echkina. *Phys. Plasmas*, 11:3535, 2004.
- [13] V. V. Mirnov, C. C. Hegna, and S. C. Prager. *Phys. Plasmas*, 11:4468, 2004.
- [14] R. Fitzpatrick and F. Porcelli. *Phys. Plasmas*, 11:4713, 2004.

5 Collisionless tearing mode in cylindrical geometry

Abstract

Magnetic reconnection due to electron inertia is responsible for very fast and violent phenomena in magnetized plasmas in which magnetic energy is converted into electron kinetic energy on very short time scales. Considering an annular current region that stands model for current that may be associated with the helical transform ψ_* , we assume current density jumps in the radial direction. In this way we may use the powerful Contour Dynamics (CD) methods to study linear stability and nonlinear evolution of a tearing unstable equilibrium using a two fluid model. We obtain analytical expressions for the linear dispersion relation, that are in good agreement with the CD simulations.

5.1 Introduction

The violent transformation of magnetic energy into electron kinetic energy in a plasma known as magnetic reconnection, occurs in various instances in nature, such as geomagnetic substorms [1], solar flares [2], and the heating of the corona of the sun [3]. It converts magnetic energy into kinetic energy of electrons in very small reconnection zones, where magnetic flux originating from different regions in the plasma is broken up and recombined. The finite inertia can decouple the motion of the electrons from the magnetic field lines and so establish fast reconnection even in collisionless conditions, such as very hot or rarefied plasmas.

Though collisionless reconnection first saw applications in the field of astrophysics, where rarefied and diluted plasmas displayed phenomena on a timescale that was generally too short for resistive processes to take place, in the last two decades fusion experiments also raise the same challenges. The central part of a tokamak can be prone to the so-called sawtooth-instability, a process in which the plasma within the $q = 1$ surface is completely redistributed, thermalized, and according to some models [4, 5] completely turned inside out. The time in which this happens can be as little as a tenth of the mean Coulomb-collision time [6]. It was shown that fast collisionless reconnection can be achieved when electron inertia is accounted for as a current limiting factor [7, 8].

For larger values of q perturbations may lead to instabilities such as (neoclassical) tearing modes that form a chain of helical magnetic islands around the torus. These magnetic islands are long lived, coherent structures that can be described as localized and stationary solutions of the equations that govern the plasma motion. When they reach a critical size they become a threat for the magnetic confinement of the plasma.

Recently [9] equilibria with piecewise constant generalized vorticity constituting a periodic straight current layer have been proven to be unstable to a reconnecting mode with tearing symmetry. A surface perturbation that runs along the layer excites the mode that undergoes exponential growth in the subsequent linear stage. The dispersion relation for this mode can be derived from kinetic or fluid equations using the assumption that we have a strong magnetic guide field in a low- β plasma, so that we can describe the perpendicular dynamics of the plasma independent from the fast thermal motion along the field lines. In this way a class of Lagrangian advection equations was found.

In this paper the linear stability of cylindrical equilibria will be considered, by means of a dispersion relation pertaining to the collisionless two-fluid drift approximation. The thus predicted growth rates will be compared to numerical simulations using a contour dynamics code with symplectic time integration.

The paper is organized as follows. First, the two-fluid drift equations are outlined in section 5.2. Then, in section 5.3 it will be sketched how a convenient formulation of the two-fluid drift equations can be modelled using the Contour Dynamics (CD) technique. Subsequently, an equilibrium will be constructed that satisfies the equations in an intuitive way, that can be made unstable to tearing modes. The linear dispersion relations based on the two-fluid model are detailed in section 5.4. Some details on the numerical simulation tool will be given in section 5.5. The results of the simulations using the CD method will be discussed and summarized in section 5.6 and 5.7.

5.2 The two-fluid drift-Alfvén model

We consider a strongly magnetized, low- β plasma, with a strong magnetic guide field that is given by $\mathbf{B} = B_0 \mathbf{e}_z + \mathbf{e}_z \times \nabla \psi$ and an electric field $\mathbf{E} = \mathbf{e}_z \partial_t \psi - \nabla \phi$, where ϕ , ψ are the electrostatic and magnetic vector potential, respectively. We assume $\nabla \psi \ll 1$, so that the dynamics are strongly anisotropic.

The plasma is described as an electron and an ion fluid. The electrons are assumed to be collisionless, and their inertia is taken into account. We study two-dimensional motion only, independent of the z -coordinate. No magnetic curvature effects and particle trapping due to ∇B will be taken into account here.

The ions are assumed to be cold in the sense that they respond to parallel fluctuations of the electron density by moving perpendicularly to the magnetic field with the $\mathbf{E} \times \mathbf{B}$ -drift to maintain quasi-neutrality. In this way the electron density and the vorticity are linked similar to how the current and magnetic field are connected.

This response can be obtained from the compressibility of the ion polarization drift. From $v_{p,i} = -\partial_t \phi / (B_0 \Omega_i)$, with Ω_i the ion cyclotron frequency, we can deduce from the continuity equation that for small fluctuations from the ion density n_0 , we get that $\Omega_i \delta n / n_0 = \nabla^2 \phi / B_0$, or $\nabla^2 \phi \ll \Omega_i$.

Following [10, 11, 12], the electron fluid is described by the parallel component of the continuity and the electron momentum balance equation [12],

$$\frac{dn}{dt} + \nabla_{\parallel} n v_z = 0, \quad (5.1)$$

$$m_e n \frac{dv_z}{dt} = -enE_{\parallel} - \nabla_{\parallel} p_e, \quad (5.2)$$

with

$$\frac{d}{dt} = \frac{\partial}{\partial t} + [\phi, \cdot], \quad \nabla_{\parallel} = \frac{d}{dz} + [\psi, \cdot],$$

and $[A, B] = \mathbf{e}_z \cdot \nabla A \times \nabla B$. We assume the current density j to be negligible in the plane perpendicular to the dominant magnetic field, so that $j \approx \nabla_{\perp}^2 \psi$. The parallel electron velocity v_z is advected with the $\mathbf{E} \times \mathbf{B}$ -velocity, which is assumed to be the dominant perpendicular flow, and parallel ion flow is neglected.

This leads to a system of equations [10],

$$\partial_t \nabla^2 \phi + [\phi, \nabla^2 \phi] = v_A^2 [\psi, \nabla_e^2 \psi], \quad (5.3)$$

$$\partial_t \tilde{\nabla}^2 \psi + [\phi, \nabla_e^2 \psi] = -\frac{v_t^2}{v_A^2} [\nabla^2 \phi, \psi], \quad (5.4)$$

with $\nabla_e^2 = \nabla^2 - d_e^{-2}$, v_t the electron thermal velocity, $v_A^2 = B_0^2 / m_i n_0$ the Alfvén velocity and $d_e = c / \omega_{pe}$ the electron inertial skin depth.

5.3 Contour Dynamics

The equations (5.3, 5.4) can be cast in a Lagrangian form of two purely advective equations for generalized vorticities [10], that are being advected by their own respective generalized streamfunction,

$$\partial_t \omega_{\alpha} + [\Phi_{\alpha}, \omega_{\alpha}] = 0, \quad (5.5)$$

where $\alpha = +, -$ denotes the type of vorticity, given by $\omega_\alpha = \nabla^2\phi - (v_A^2/v_\alpha)\nabla_e^2\psi$, and their streamfunctions by $\Phi_\alpha = \phi + v_\alpha\psi$, where the parallel velocity $v_\pm = \pm v_t$.

The Lagrangian formulation allows the simplification that is exploited when using contour dynamics. Inverting the definition for the generalized vorticity (5.5), we obtain the stream function as integrals over the vorticity distributions $\omega_\pm(\mathbf{x})$,

$$\Phi_\alpha(\mathbf{x}, t) = \sum_{\beta=+,-} \int d^2\mathbf{x}' G_{v_\alpha v_\beta}(|\mathbf{x} - \mathbf{x}'|) \omega_\beta(\mathbf{x}'), \quad (5.6)$$

where the Green's function for the unbounded domain [13] is given by

$$G_{vv'}(r) \equiv \frac{1}{2\pi} \left(\ln r + \frac{vv'}{v_A^2} K_0\left(\frac{r}{d_e}\right) \right), \quad (5.7)$$

with $r = |\mathbf{x} - \mathbf{x}'|$, $v_i = \pm v_t$ and K_0 the modified Bessel function of the second kind. This expression was used as an interaction potential between point vortices in [12]. By assuming the (generalized) vorticity to be constant within a well-defined region C , bounded by a contour ∂C , the dynamics are completely defined. Such a piecewise uniform distribution of generalized vorticity will remain piecewise uniform by Eq. (5.5), and so the topology of the initial distribution is also conserved in time.

The Green's function $G_{vv'}(r)$ can be seen as the streaming potential of the contour type v_i at \mathbf{x} as a consequence of a contour line element of a patch of vorticity type v_j at \mathbf{x}' . The streamfunction as a consequence of a distribution of N patches becomes [14]

$$\Phi_j(\mathbf{x}, t) = \sum_{i=1}^N \omega_i \int_{C_i(t)} d^2\mathbf{x}' G_{v_i v_j}(|\mathbf{x} - \mathbf{x}'|), \quad (5.8)$$

with C_i a piecewise uniform generalized vorticity distribution of a contour with velocity type v_i . The velocity of the j -th contour is then calculated by applying Stokes' theorem and integrating by parts [13, 14],

$$\mathbf{u}_j(\mathbf{x}, t) = - \sum_{i=1}^N \omega_i \oint_{\partial C_i(t)} d\ell' G_{vv'}(|\mathbf{x} - \mathbf{x}'|),$$

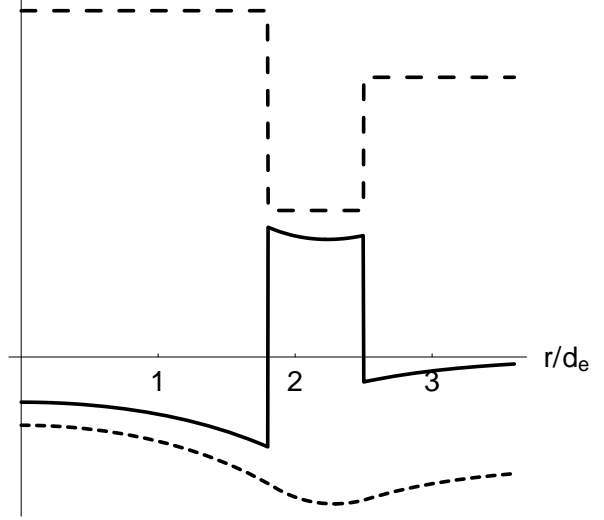
where the summation is over all contours ∂C_i and v_i is the velocity type of the i -th contour. This implies that the time evolution of a contour depends only of the location of the contours, including itself.

Because the surface enclosed by $\partial C_i(t)$ is conserved, all linear combinations of fluxes ω_α are conserved. This makes this approach very suitable for numerical purposes, as there are no external boundary conditions to be observed.

As mentioned before, the surface enclosed by the contour represents an amount of flux of $\int_{C_i} d^2x \omega_\alpha$ with $\omega_\alpha = \nabla^2\phi - (v_A^2/v_\alpha)\nabla_e^2\psi$, a combination of vorticity and current. By superposing contours of the $+$ and $-$ type we can construct regions of pure current density by giving them opposite weight. When the ω_\pm contours no longer fully overlap as a result of some (unstable) dynamics, regions of either ω_+ or ω_- start to form, that still contain current but have nonzero vorticity and can accelerate the mode.

Figure 5.1:

The fields of a current annulus equilibrium. Here, the dashed curve shows the x -dependence of the total generalized vorticity, the solid curve shows the current density $\nabla^2\psi_0$ as a layer between R_1 and R_2 that is shielded on a length scale d_e , and the dotted curve is ψ_0 .



5.4 Equilibrium, linear stability

We aim to study an equilibrium with a magnetic field aligned in the z -direction at some radius r_s in the plasma, in right-handed cylindrical coordinates (r, θ, z) , so that the equilibrium ψ_0 corresponds to a helical flux function ψ^* for a flux surface for some rational value of the safety factor, q .

We fulfill the requirements for equilibrium in a θ, z -independent cylindrical geometry automatically by making a linear combination of two concentric patches of radius R_1, R_2 , in such a way that $\phi = 0$ everywhere, i.e. no equilibrium background vorticity, and outside the patches there is no parallel current: $r > R_2 : \nabla_e^2 \psi_0 = 0$. To achieve this, two contours of equal strength and radius but of opposite type (α) are superposed at $r = R_1$ and $r = R_2$, so that we effectively have a system of four ω_α contours, with net vanishing vorticity and with magnetic vector potential

$$\psi_{0,j} = -d_e^2 j_j \begin{cases} 1 - \frac{R_j}{d_e} K_1\left(\frac{R_j}{d_e}\right) I_0\left(\frac{r}{d_e}\right) & \text{if } r < R_j, \\ \frac{R_j}{d_e} I_1\left(\frac{R_j}{d_e}\right) K_0\left(\frac{r}{d_e}\right) & \text{if } r > R_j, \end{cases}$$

for $j = 1, 2$, with I_i, K_i modified Bessel functions of the first and second kind. Though the current profile as depicted in Fig. 5.1 is peaked, and shows the shielding effects on a length scale d_e caused by the electron inertia, the ψ_0 constructed in this way is smooth and differentiable everywhere. The quantities

$$\begin{aligned} \hat{j}_1 &= \frac{\psi'_0(R_1)}{R_1} = j_1 I_{11} K_{11} + j_2 I_{11} K_{12} \frac{R_2}{R_1}, \\ \hat{j}_2 &= \frac{\psi'_0(R_2)}{R_2} = j_1 I_{11} K_{12} \frac{R_1}{R_2} + j_2 I_{12} K_{12}, \end{aligned}$$

give the relative gradient at R_1 and R_2 , the edges of the annulus. They need to be of opposite sign to have a neutral line within the annular region $R_1 < r < R_2$, or, in other words, for ψ_0 to have a minimum there. This means that $j_1 < 0 < j_2$. We have defined

$$I_{mj} \equiv I_m(R_j/d_e), \quad K_{mj} \equiv K_m(R_j/d_e), \quad j = 1, 2. \quad (5.9)$$

In this way we have constructed a smooth ψ_0 whose radial derivative goes to zero for $r \rightarrow 0, \infty$, and that hosts a region of nonzero mean electron velocity for $r < R_2$. This results in a localized current density $j(x)$ that is shielded on the scale of d_e , the electron inertial skin depth, and thus becomes invisible for large $|x|$. Integrated over the whole domain there is no net current density.

The limit $kR_1, kR_2 \gg 1$, and $R_1, R_2 \gg d_e$ while $R_2 - R_1 \ll R_1, R_2$ leads to the straight slab geometry that was investigated in [9].

Now that we have established an equilibrium, we seek to disturb it. We linearize Eqs. (5.3) and (5.4), yielding

$$-\omega \nabla^2 \phi_1 = v_A^2 (k\psi_0' \nabla_e^2 \psi_1 - k\psi_1 \nabla_e^2 \psi_0'), \quad (5.10)$$

$$-\omega \nabla_e^2 \psi_1 = \frac{v_t^2}{v_A^2} k\psi_0' \nabla^2 \phi_1 + k\phi_1 \nabla_e^2 \psi_0'. \quad (5.11)$$

where prime denotes derivation with respect to r . Here we note that we can only perturb the equilibrium by changing the location of the contours of ω_{\pm} . In the rest of the domain we have

$$\nabla^2 \phi_1 = 0,$$

with a general solution that is regular at $r = 0, r = \infty$,

$$\phi_1(r, \theta) = e^{i(m\theta - \omega t)} \sum_{j=1,2} \frac{\phi_{j,m}}{2m} \begin{cases} \left(\frac{r}{R_j}\right)^m, & r \leq R_j, \\ \left(\frac{R_j}{r}\right)^m, & r \geq R_j. \end{cases} \quad (5.12)$$

Similarly,

$$\nabla_e^2 \psi_1 \equiv \nabla^2 \psi_1 - d_e^{-2} \psi_1 = 0,$$

has regular solutions

$$\psi_1(r, \theta) = e^{i(m\theta - \omega t)} \sum_{j=1,2} \psi_{j,m} \begin{cases} K_{mj} I_m\left(\frac{r}{d_e}\right), & r \leq R_j, \\ I_{mj} K_m\left(\frac{r}{d_e}\right), & r \geq R_j. \end{cases} \quad (5.13)$$

These functions determine the shape of the perturbed fields, and make sure that they remain regular for $r \rightarrow 0, \infty$. They also contain a discontinuity in the first derivative. Evaluating the jumps at the inner and outer surfaces $r = R_1$ and $r = R_2$,

$$\psi_0'(R_j) = R_j \hat{j}_j, \quad (5.14)$$

$$\nabla_e^2 \psi_0' = \sum_{j=1,2} -j_j \delta(r - R_j), \quad (5.15)$$

$$\nabla^2 \phi_1 = \sum_{j=1,2} -\frac{2m}{R_j} \phi_{j,m} \delta(r - R_j), \quad (5.16)$$

$$\nabla_e^2 \psi_1 = \sum_{j=1,2} -\frac{\psi_{j,m}}{d_e} \delta(r - R_j), \quad (5.17)$$

these may give the coupling of the equilibrium with the perturbed field through Eqs. (5.10) and 5.11). Filling in the jump conditions (5.14) - (5.17), they can be written as

$$\omega \begin{pmatrix} \phi_{1,m} \\ \phi_{2,m} \end{pmatrix} = \mathbf{M}_{\psi} \begin{pmatrix} \psi_{1,m} \\ \psi_{2,m} \end{pmatrix}, \quad (5.18)$$

$$\omega \begin{pmatrix} \psi_{1,m} \\ \psi_{2,m} \end{pmatrix} = \mathbf{M}_{\phi} \begin{pmatrix} \phi_{1,m} \\ \phi_{2,m} \end{pmatrix}, \quad (5.19)$$

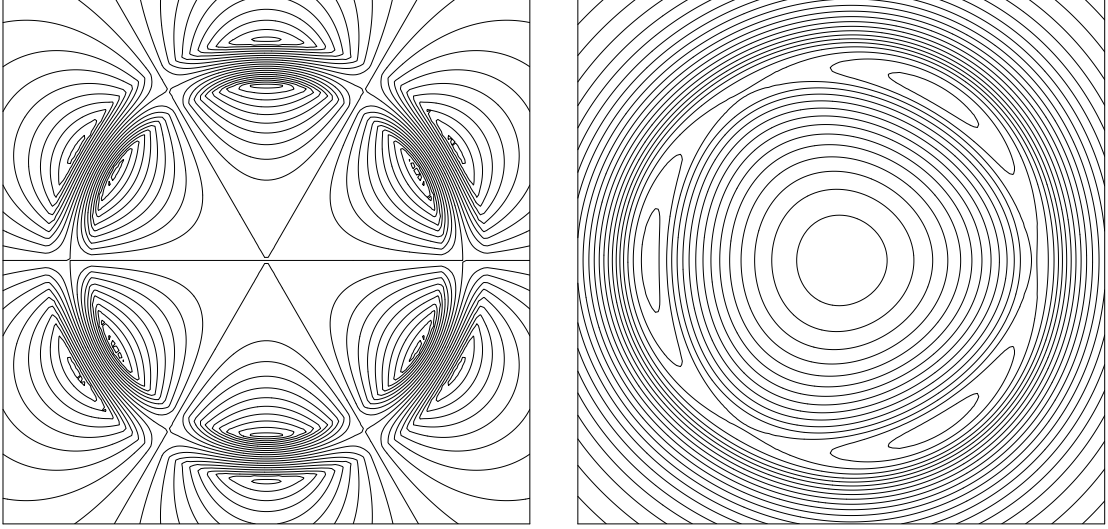


Figure 5.2: The linear $m = 3$ mode in a cylindrical current annulus, with eigenfunctions for the electrostatic potential ϕ (left) and the magnetic potential ψ (right).

with

$$\begin{aligned} \mathbf{M}_\psi &= -\frac{v_A^2}{2} \begin{pmatrix} j_1 I_{m1} K_{m1} - \hat{j}_1 & j_1 I_{m1} K_{m2} \\ j_2 I_{m1} K_{m2} & j_2 I_{m2} K_{m2} - \hat{j}_2 \end{pmatrix} \\ \mathbf{M}_\phi &= m \begin{pmatrix} j_1 + 2m\hat{j}_1 v_t^2 / v_A^2 & j_1 (R_1/R_2)^m \\ j_2 (R_1/R_2)^m & j_2 + 2m\hat{j}_2 v_t^2 / v_A^2 \end{pmatrix} \end{aligned} \quad (5.20)$$

Matching the jumps in the derivatives in the eigenfunctions at R_1 and R_2 leads to the dispersion relation in ω and $k = 2m/(R_1 + R_2)$,

$$\omega^4 - \omega^2 \text{Tr}(\mathbf{M}) + \det(\mathbf{M}) = 0, \quad (5.21)$$

with $\mathbf{M} = \mathbf{M}_\psi \mathbf{M}_\phi$.

We can identify three qualitatively different regimes in this description, with different stability characteristics. For $\text{Tr}(\mathbf{M}), \det(\mathbf{M}) > 0$ we have two unstable modes, for $\det(\mathbf{M}) < 0$ we have one unstable mode and for $0 < \det(\mathbf{M}) < \frac{1}{4} \text{Tr}(\mathbf{M})^2$ the current channel is stable. In the rest of the paper we will be interested in the part of parameter space where there is one unstable mode. When we investigate the behaviour of this mode we find that it is a reconnecting mode with tearing symmetry. We have to note, however, that the cylindrical geometry couples the even and odd perturbations.

In the linear case, when two interfaces are perturbed sinusoidally, it is possible to distinguish between a perfectly symmetric (tearing) and a perfectly anti-symmetric (kink) case. The difference between inner and outer circumference in a cylinder however couple these two, creating mixed tearing and kink modes. The mixed character lies in the fact that for the tearing modes the neutral line, on which the x- and o-points lie, are not exactly circular. We speak of a tearing mode because of the clear formation of magnetic islands, and because generally the eigenvalue corresponding to the tearing mode is considerably larger.

We note that this equilibrium is not forced into reconnection by an external driving force, which leads to the well known Δ' formalism through asymptotic matching techniques

[15, 16]. Instead the process is set in motion by standing surface perturbations at the surfaces $r = R_1, r = R_2$. In this configuration it is not suitable to assign a value of Δ' to this equilibrium, as this quantity is defined as the perceived current in the so-called ‘outer’ region, (or the mismatch $\lim_{x \rightarrow -\infty} d\psi/dx - \lim_{x \rightarrow +\infty} d\psi/dx$), far away from the reconnection zone at $x = 0$, with x a coordinate perpendicular to \mathbf{B} and in the direction of the inhomogeneity. In the equilibrium used here $d\psi_0/dx \rightarrow 0$ for $x \rightarrow \pm\infty$. As such, there is no boundary layer and no small parameter expansion.

5.5 Numerical method

The specifics of the numerical method are described in detail in [13, 14], so only some relevant or newly added features will be outlined here.

The input for the code consists of a set of boundaries of regions of piecewise constant generalized vorticity. Initial sinusoidal perturbations of the form $\sim \varepsilon \sin(m\theta)$ of an initially circular boundary can be specified per vortex patch, with $m \in \mathbb{N}$ and ε small enough to make sure that the behaviour can be considered linear at first. Choosing ε of the inner and outer patches of opposite sign results in a constricting, tearing perturbation. Note that in general the boundary of the whole patch is deformed, instead of different perturbations for the different generalized vorticities ω_{\pm} . This results in an initial deformation that is not an exact solution of the dispersion relation (5.21), but one that can be expressed as a sum of its eigenmodes.

In this way we arrive at a set of finite area vortex patches that are described by a discrete set of points or nodes and the jump in the corresponding vorticity with respect to the external value, taken to be zero.

The discretization of a contour is reconsidered by the code every timestep, inserting more nodes when the local curvature of a segment becomes too large, or when a line segment of the same vorticity type comes close, and deleting nodes vice versa. The velocity field of the discretized system is shown to be divergence-free nevertheless [14].

The motion of the contours is given by the Eqs. (5.5), and the points that constitute the contours can subsequently be calculated by a symplectic integration scheme. This means that the method, an implicit predictor-corrector scheme using a second-order midpoint rule, conserves the area of the initial contours very well [14].

When the amount of nodes per contour exceeds a preselected limit, the code breaks off. The intricate features can pose considerable computational cost when a highly nonlinear stage is reached, with the amount of computations scaling roughly with the amount of nodes squared.

The code harbours the possibility for Contour Surgery, meaning that when the tolerance for the closeness of two parts of a contour is surpassed, the code cuts the structure loose and ties the enclosing ends together, ignoring the conservation of initial topology. This feature is not used in our simulations and will not be discussed further, for details see [13].

The ϕ and ψ -fields as a function of \mathbf{x} , with $\phi = (\Phi_+ + \Phi_-)/2$ and $\psi = (\Phi_+ - \Phi_-)/2v_t$, can be calculated by testing whether \mathbf{x} is in- or outside a contour, and subsequently performing the integral

$$\Phi_j(\mathbf{x}) = \sum_i \omega_i \int_{C_i} d^2\mathbf{x}' G_{ij}(|\mathbf{x} - \mathbf{x}'|),$$

which is equivalent to

$$\Phi_j(\mathbf{x}) = \sum_i \omega_i \oint_{\partial C_i} \mathbf{e}_z \cdot d\mathbf{l}' \times (\mathbf{x} - \mathbf{x}') F_{ij}(|\mathbf{x} - \mathbf{x}'|),$$

with

$$F_{\alpha\beta}(r) = \frac{1}{r^2} \int_0^r dr' r' G_{v_\alpha v_\beta}(r').$$

The representation of this integral as a contour integral instead of a two-dimensional integral over the infinite plain has the advantage that no assumptions need to be made as to at what distance from the contours the velocity fields they create become negligible. Furthermore, the performance is enhanced, as it requires line integrals instead of surface integrals.

5.6 Numerical results

The set-up of the numerical simulations is as follows. Four concentric circular patches are superposed, two of radius R_1 and of strength ω_1 of their respective ω_\pm type, and two of radius $R_2 > R_1$ with equal but negative vorticity as their smaller counterparts. In this way an annular zone of pure current density with $j = (\omega_{+,1} - \omega_{-,1}) - (\omega_{+,2} - \omega_{-,2})$ for $R_1 < r < R_2$ is constructed. Analytically this equilibrium is tested for stability to perturbations with tearing symmetry of ‘poloidal’ wave number m using the linear dispersion relation (5.21). The parameters are chosen such that the current annulus equilibrium does not become unstable with respect to the kink-type mode.

When the equilibrium is unstable to one or more modes, a simulation is started with the corresponding parameters.

Furthermore, an equilibrium is almost always unstable with respect to more than one mode. One may choose to excite a mode that does not have the largest growth rate, as this is a free parameter in the input file. In the simulations that were performed by the authors no evidence was found that a mode started to develop a mixed character, i.e. with more than one mode number, not even in the deeply nonlinear stages. It is possible to excite a $m = 1, 2$ and $M \in \mathbb{N}$ mode simultaneously. In this situation the mode with the largest growth rate becomes dominant after few timesteps.

It is possible to ‘tailor’ the central ψ_0 profile to prevent collapse towards the centre as this now corresponds to a zone of zero magnetic shear. By placing one or more contours in the central region or by placing the equivalent of a current-wire or point-current vortex in the centre it is possible to ‘smoothen’ the current profile in order to obtain a more realistic starting point for the simulations. The following results have been obtained with flat central profiles, however.

5.6.1 Comparison to the linear dispersion relation

In general, it should be noted that the linear dispersion relation (5.21) can only be properly compared to a nonlinear simulation when the amplitude of the most unstable mode is small, compared to the width of the current layer, $w \ll R_2 - R_1$, but also compared to the radii themselves, $w \ll R_1, R_2$, because nonlinearly poloidal curvature effects may play a role. This refers to consequences of the difference between the length of a part of a field line on the inside and the outside of a magnetic island, that may diverge after the onset of the mode.

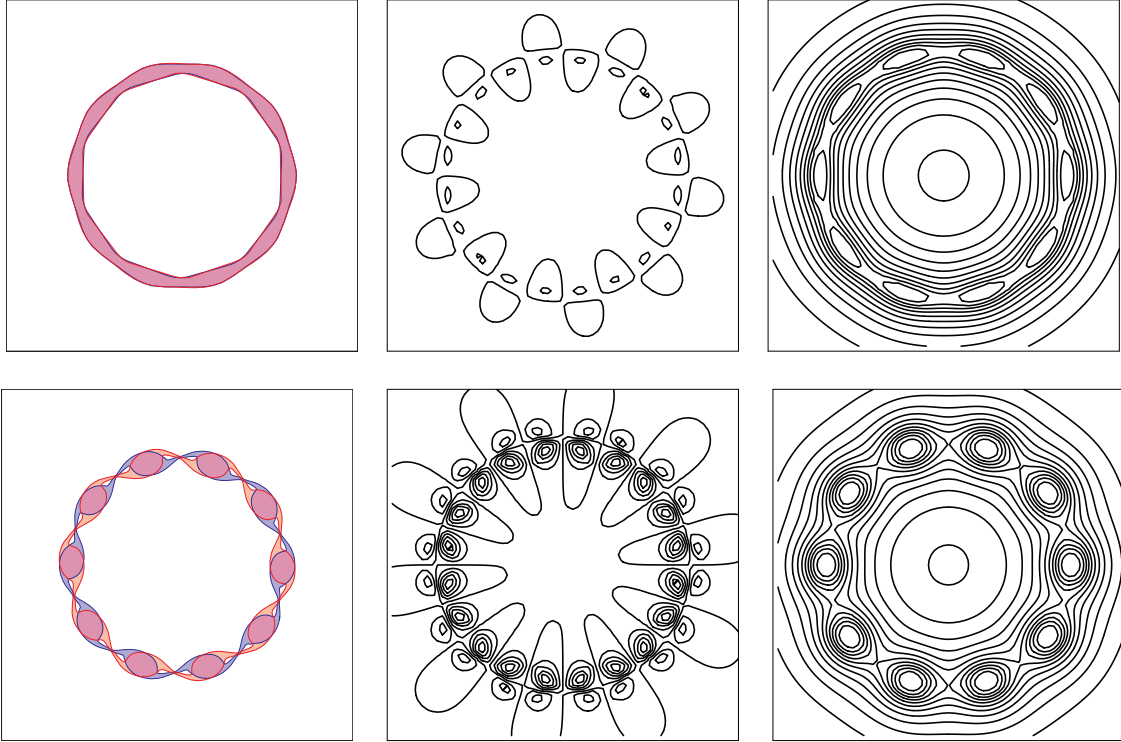


Figure 5.3: Contour dynamics simulation of an $m = 10$ perturbed equilibrium after $t = \tau_A$ (top) and $t = 3\tau_A$ (bottom). On the left we see the calculated contours, marking the borders of areas of uniform generalized vorticity. Red areas consist of ω_+ , blue areas of ω_- and purple areas are purely current-carrying parts. The middle column shows contours of the electrostatic potential ϕ and the right hand column the magnetic vector potential ψ .

When we calculate the reconnected flux as a function of time by deducting the flux at an o-point from the flux at an x-point,

$$\psi_{\text{rec}} = |\psi_o - \psi_x|,$$

we can estimate the growth rate yielded by the simulation by a logarithmic fit to the non-saturated states. This phase is depicted in the top rows of Figures 5.3, 5.4, 5.6 and to a lesser extent 5.8. But, as was pointed out, the initial deformation of the contours is not likely to be an exact eigenstate of the dispersion function. The dispersion relation (5.21) has four linearly independent solutions, two of which with tearing parity. The initial perturbation at $t = 0$ contains a superposition of the growing and decaying eigenfunctions, so that the perturbed vector potential for small t behaves as

$$\psi_1(t) = \psi_1(0) \cosh(\gamma t), \quad (5.22)$$

with $\psi_1(0)$ the perturbation at $t = 0$ and $\gamma = \text{Im}(\omega)$, the imaginary part of the eigenvalue corresponding to the tearing mode solution. This is equivalent to

$$\gamma t = \log \left(\frac{\psi(t)}{\psi_1(0)} + \sqrt{\left(\frac{\psi(t)}{\psi_1(0)} \right)^2 - 1} \right), \quad (5.23)$$

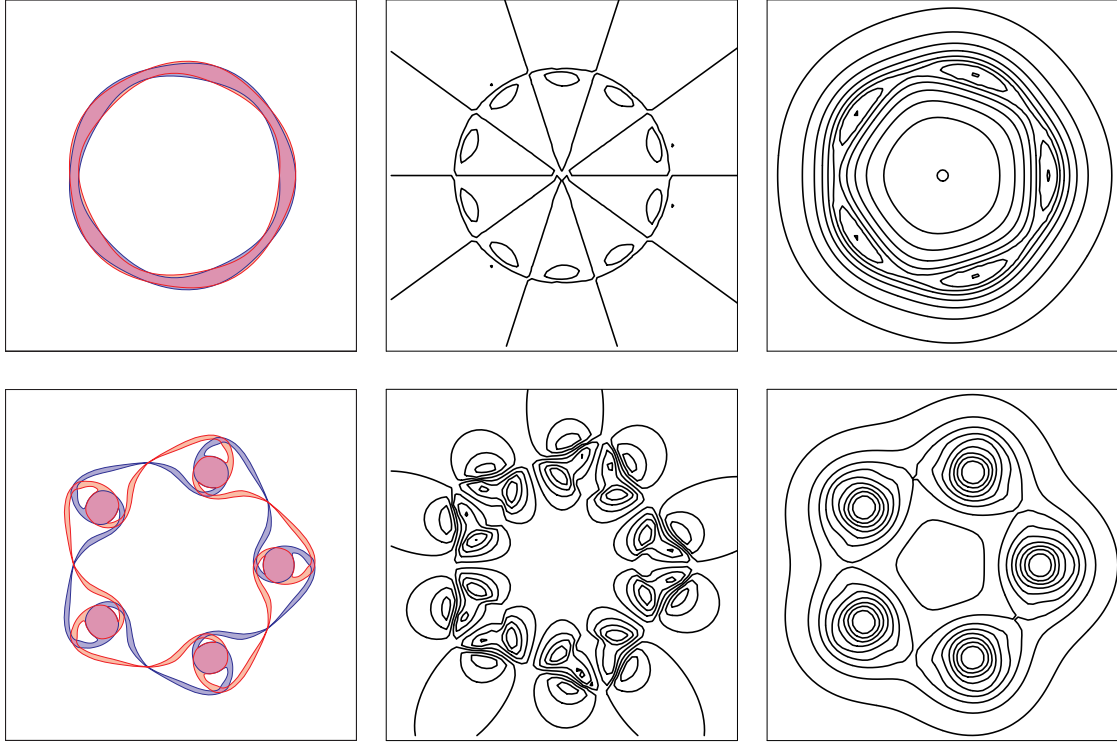


Figure 5.4: Contour dynamics simulation of an $m = 5$ perturbed equilibrium after $t = \tau_A$ (top) and $t = 5\tau_A$ (bottom).

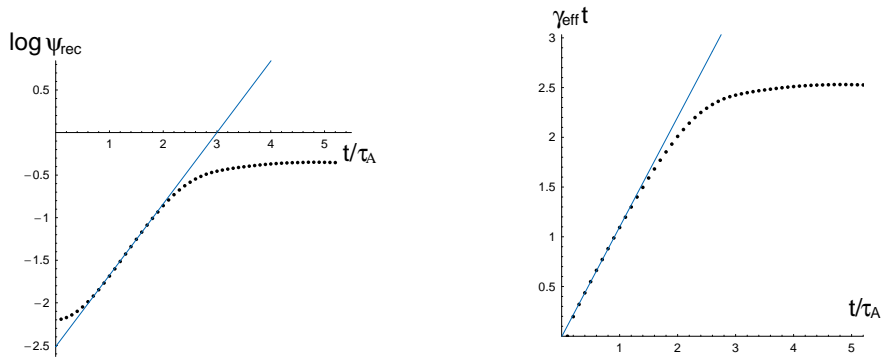


Figure 5.5: On the left the $\log \psi_{\text{rec}}$ versus time of the mode with $m = 5$ in Alfvén time units, $\tau_A = \rho_s/v_A$. The blue line is a fit considering the interval with the maximal slope, yielding $\gamma = 0.84$. On the right the $\gamma_{\text{eff}} t$ using Eq. (5.23) which gives $\gamma = 1.10$, in the linear stage, based on the same data.

illustrated in Fig. 5.5 for the case $m = 5$. This leads in general to a considerable correction compared to a linear fit at the point of inflection in the stage between early linear growth and saturation.

The fact that the initial perturbation has tearing symmetry does not rule out the possibility that also a mode with kink parity is excited. This mode is stable, but because it

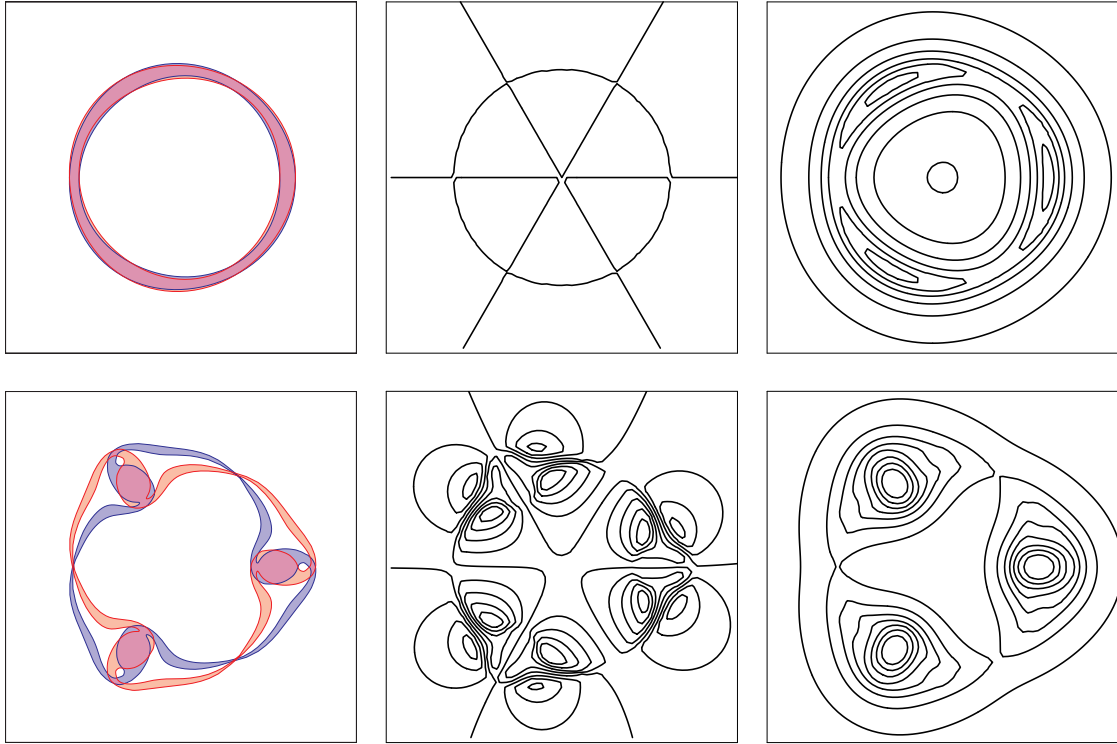


Figure 5.6: Contour dynamics simulation of an $m = 3$ perturbed equilibrium after $t = \tau_A$ (top) and $t = 5\tau_A$ (bottom).

would always be excited $\sim \cos\omega t$, it could give a noticeable modification of the growth rate, especially when the initial perturbation was not taken to be sufficiently small.

We consider a current annulus between $4 < r/d_e < 4.5$, with $j_j = \pm 1.5d_e^{-1}$. The growth rates of the tearing mode as predicted by the linear dispersion relation (γ_{dis}) and the ones found numerically (γ_{num}) are listed in Table 5.1. The growth rates are given in inverse Alfvén times τ_A^{-1} , with

$$\tau_A = \rho_s/v_A, \quad (5.24)$$

a typical Alfvén transit time through a unit cell of the simulation, that is normalized to $\rho_s = \sqrt{m_e m_i} v_t / eB_0$, the ion-sound Larmor radius.

We observe good correspondence between γ_{dis} and γ_{num} , especially for lower mode numbers. For $m = 10$, the deviation becomes more than 10 %.

It is possible that the fact that the initial condition is not an exact eigenfunction causes a mixing of tearing and kink parity modes that in turn cause this underestimation. However, the simulations and the dispersion relation are close enough to state that the model seems to describe what the simulation is showing in the early, linear phase.

5.6.2 Nonlinear saturation of the magnetic islands

We have generally let the simulations carry on until the criterion for the maximum nodes per contour broke it off, to see how the different types of nonlinear behaviour would develop.

From the analysis leading to the linear dispersion relation we can say that the island width

modenumber	R_1/d_e	R_2/d_e	$\gamma_{\text{dis}}(\tau_A^{-1})$	$\gamma_{\text{num}}(\tau_A^{-1})$
$m = 1$	1.8	2.5	0.47	0.47
$m = 3$	4.0	4.5	0.89	0.87
$m = 5$	4.0	4.5	1.15	1.10
$m = 10$	4.0	4.5	0.97	0.88

Table 5.1: Comparison of the analytically obtained growth rates from the linear dispersion relation γ_{dis} and the growth rates of the numerically simulated modes γ_{num} for different poloidal mode number m .

has to be significantly smaller than the total width of the current layer, $w < |R_2 - R_1|$, to be able to speak of linear or quasi-linear behaviour of the mode.

If we look e.g. at the case where $m = 5$, we see in the the top row of Fig. 5.4 that the islands already stretch out to the borders of the current layer, that can be seen in the left figure by the overlap of the contours of the blue and red ω_{\pm} -type, depicted in purple. This instance corresponds to $t = \tau_A$. If we now turn to Fig. 5.5, we see that at this point the mode is still exponentially growing and reconnecting.

When the amount of reconnected flux saturates, here, after approximately $t \approx 2.5\tau_A$, the magnetic islands have grown well beyond the width of the original current layer. When looking at the ϕ, ψ -fields, the new situation, seen in the left columns of e.g. Figs. 5.3, 5.4 and 5.6 does not change rapidly anymore, and seems stable. At this point we note that the remaining current cables at the centre of the magnetic islands are of dimension d_e , analogous to [13]. These cables host the most of the electrons. However, the contours of ω_{\pm} are still being advected under influence of their respective flowfields, especially near crossings of the two vorticity types (the blue and the red contours), creating thin filaments of length scales well below d_e . These filamentary structures eventually lead to the increase in nodes that makes the code break off.

5.6.3 Scale collapse

Once the islands start to saturate, the narrow filaments of the patches that are drawn across the x-point are stretched at ever smaller length scales, resulting in the extremely peaked current distributions as reported in [7, 17]. In slab geometry the current spike that forms as a result of the instability shrinks unboundedly and becomes a finite time singularity.

In our simulations, we see that for higher mode numbers the contours of ω_{\pm} at the x-point constrict, until the criterion for the amount of nodes per contour is violated.

When we turn to lower mode numbers, however, e.g. $m = 3$ in Fig. 5.6 we see how even in the earliest stages the linear mode is already curved around the cylinder.

This leads to an ever more pronounced in-out asymmetry of the mode, i.e. between the part facing inward and outward the cylinder. This asymmetry limits the sharply peaked growth and simultaneous scale collapse of the current distribution that is seen e.g. in [17]. The current layer shrinks well below the size of d_e , but reaches a minimum width well before the end of the simulation.

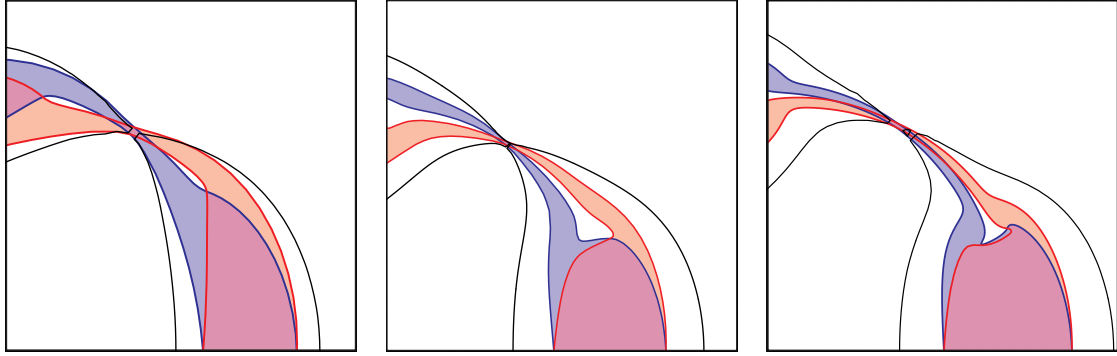


Figure 5.7: Details of the x-points for simulations of $m = 3$ perturbed equilibria in approximately the same phase of saturation with left $v_t = 2v_A$, middle $v_t = v_A$ and right $v_t = 0.5v_A$. The black line is the magnetic separatrix.

5.6.4 Effect of the electron temperature

The effect of electron temperature on the collisionless tearing mode was first reported in [11]. There, it was found that for $\rho_s/d_e > 1$, or, equivalently $v_t/v_A > 1$, the contours of ω_{\pm} should be approximately tangent to the separatrix of the magnetic island in ψ . In the opposite case, $v_t/v_A \rightarrow 0$, the angle between the contours of ω_{\pm} would also become 0, or π . In [17] it is discussed how the interplay between the electron thermal velocity and the velocity of the mode itself, ϕ/ψ , brings about this behaviour.

In short: when the thermal velocity of the electrons is large compared to the mode velocity of the mode, the electrons, with streamfunctions $\phi_{\pm} = \phi \pm v_t\psi$, will have a relatively strong tendency to follow the magnetic field lines. When on the other hand the mode is fast compared to the thermal velocity v_t , the dynamics of the electrons is mostly governed by the $\mathbf{E} \times \mathbf{B}$ -drift, interacting through ϕ , more or less independently of the dynamics of the mode, that interacts through ψ .

If we look at three different simulations, with $R_1 = 8d_e$, $R_2 = 10d_e$, but with decreasing ratio of v_t/v_A , we see this phenomenon taking effect: in Fig. 5.7 on the left side, for $v_t = 2v_A$, the blue and red contours of ω_{\pm} indeed approximately align with the separatrix of ψ , whereas for decreasing ratio v_t/v_A the contours move inwards, away from the magnetic separatrix, forming an ever thinner ribbon of current between the bulk current density distributions inside the islands. In the right figure in Fig. 5.7, the angle between the contours has become so small, or the current density distribution has become so thin in this stage of the simulation that the contours of ψ become distorted, resulting in the narrowing of the separatrices near the x-point. In this example the fact that the thermal velocity of the electrons is so much smaller than the velocity of the mode couples back to the shape of the mode itself.

5.6.5 Complete internal $m = 1$ reconnection

The sawtooth-instability in the centre of tokamaks has been associated with a large scale reconnection event within the $q = 1$ surface of the plasma. In 1975, Kadomtsev [4], presented a model on how a $m = 1, n = 1$ magnetic island could reconnect fully, replacing the original magnetic axis by the centre of the island, redistributing the plasma density and temperature as a result. This model has supporting evidence [18], but is probably a simplified picture [19].

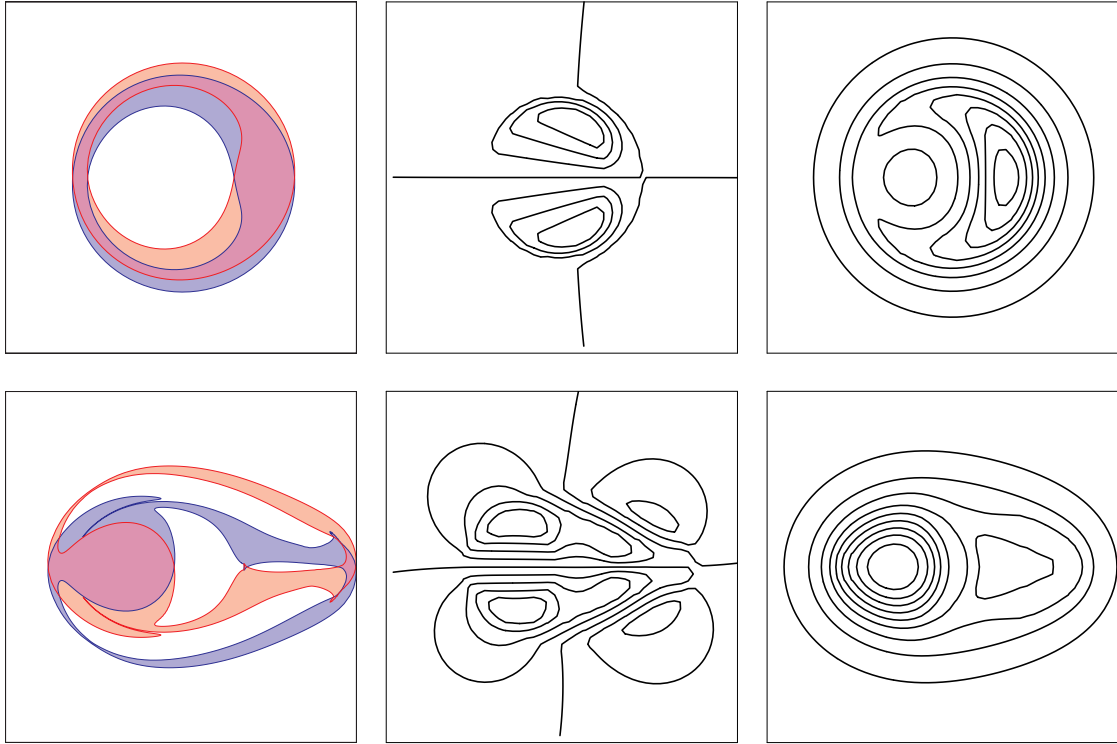


Figure 5.8: Contour dynamics simulation of $m = 1$ perturbed current equilibrium, after $t = 5\tau_A$ (top) and $15\tau_A$ (bottom).

Here, we have perturbed a current annulus with $R_1 = 1.8d_e$, $R_2 = 2.5d_e$, by displacing the central annulus infinitesimally in the negative x -direction. This is equivalent to an $m = 1$ perturbation. In the quasi-linear part of the simulation, in the left column of Fig. 5.8, we clearly see a $m = 1$ island appear in the ψ -contours, on the right. This island grows until it fills up almost all of the former inside of the cylinder or patch.

As there is no magnetic shear on the inside of the current patch, the motion of the $m = 1$ island is not inhibited in any way, and ‘bounces’ from the righthand side to the left. This is a result of the lack of magnetic shear in the centre of the annulus. When a current wire is placed to prevent this the island folds around it and smaller structures appear in the central region. This has not led to achieving a realistic ψ^* -profile, confining modes to a limited radial interval.

5.7 Discussion

A minimal model was presented to study tearing modes in cylindrical geometry. The collisionless drift two-fluid equations can be cast in an advective form that makes it possible to characterize a system by two types of contours, that are advected in their own respective flowfields.

In slab geometry, similar analysis was presented with a drift-kinetic model, containing all the information of the electron parallel velocity distribution function. The linear stability analysis then yields expressions for the linear dispersion relation containing the so-called

plasma dispersion function $Z(\zeta)$, in which particle-wave resonances are fully resolved. The argument ζ , is in this case dependent only on ω, k_{\parallel} and v_t , and the equilibrium parameter that measures the amount of current in the layer. In the cylinder, however, the argument ζ becomes dependent on r (more precise, k_{\parallel} becomes m/r). This makes the proof to exclude other modes that may or may not have larger growth rates very complicated, though some initial parameter studies have not revealed any other instabilities.

Therefore, the stability of a system with four degrees of freedom was studied: dependent on the formulation $\nabla^2\phi, \nabla_e^2\psi$ or ω_{\pm} , that were free to be chosen on the surfaces of R_1 and R_2 . This leads to four independent modes, and, as was mentioned in section 5.4, three generally accessible regions can be discerned. The choice of parameters that results in a ψ -profile with a neutral line between R_1 and R_2 , with an annular region carrying more current than the in- or outside, has always been stable with respect to the kink mode. Also, a fourth region, with $\text{Tr}(M)^2 - 4\det(M) > 0$, is (very likely) impossible to reach with real plasma parameters, but would correspond to overstable modes, i.e. modes with both an oscillatory and an exponentially growing or damping part. This can be proven rigorously using a two-fluid energy principle in cylindrical geometry, but this is beyond the scope of this paper.

The numerical results that are obtained with a fully nonlinear code are in very good agreement with the predictions made by linear theory. The time evolution of the reconnected flux shows that out of the initial conditions that were imposed to start up the mode with a preferred mode number, a linear combination of a damped and a growing mode starts to develop. This eventually leads to complete internal reconnection for the $m = 1$ case, or saturating islands for larger mode numbers.

Furthermore we see that the variation of the ratio of v_t/v_A , effectively changing the electron temperature in the simulation, confirms results by [11, 17], and suggests the formation of a thin, filamentary current ribbon in the x-point region, connecting the the x- and the o-points. In the nonlinear phase the lack of alignment of the current filaments flowing out of the x-point region leads to the distortion of the local magnetic field. This is clearly visible in the shape of the magnetic separatrix in the right figure in Fig. 5.7.

To summarize, the contour description of a current annulus within a plasma yields an excellent starting point for both the analytical and numerical study of collisionless tearing modes in cylindrical geometry.

Acknowledgements

This work, supported by the European Communities under the contract of Association between EURATOM/FOM, was carried out within the framework of the European Fusion Programme with financial support from NWO. The views and opinions expressed herein do not necessarily reflect those of the European Commission.

References

- [1] V. M. Vasyliunas. *Rev. Geophys. Space Phys.*, 13:303, 1975.
- [2] T. G. Cowling. Magnetic Stars. In L. H. Aller and D. B. McLaughlin, editors, *Stellar Structure - Stars and Stellar Systems*, page 425, 1965.
- [3] K. Shibata. *Advances in Space Research*, 17:9, 1996.

- [4] B. B. Kadomtsev. *Sov. J. Plasma Phys.*, 1:389, 1975.
- [5] A. Sykes and J. A. Wesson. *Phys. Rev. Lett.*, 37(3):140–143, 1976.
- [6] A. W. Edwards, D. J. Campbell, W. W. Engelhardt, H.-U. Fahrback, R. D. Gill, R. S. Granetz, S. Tsuji, B. D. J. Tubbing, A. Weller, J. Wesson, and D. Zasche. *Phys. Rev. Lett.*, 57:210, 1986.
- [7] M. Ottaviani and F. Porcelli. *Phys. Rev. Lett.*, 71:3802, 1993.
- [8] M. Ottaviani and F. Porcelli. *Phys. Plasmas*, 2:4104, 1995.
- [9] E. V. van der Plas and H. J. de Blank. *Phys. Rev. Lett.*, 98:265002, 2007.
- [10] T. J. Schep, F. Pegoraro, and B. N. Kuvshinov. *Phys. Plasmas*, 1:2843, 1994.
- [11] E. Cafaro, D. Grasso, F. Pegoraro, F. Porcelli, and A. Saluzzi. *Phys. Rev. Lett.*, 80:4430, 1998.
- [12] B. N. Kuvshinov, V. P. Lakhin, F. Pegoraro, and T. J. Schep. *J. Plasma Physics*, 59:727, 1998.
- [13] J. H. Mentink, J. Bergmans, L. P. J. Kamp, and T. J. Schep. *Phys. Plasmas*, 12:052311, 2005.
- [14] P. W. C. Vosbeek and R. M. M. Mattheij. *J. of Comput. Phys.*, 133:222, 1997.
- [15] H. P. Furth, J. Killeen, and M. N. Rosenbluth. *Phys. Fluids*, 6:459, 1963.
- [16] T. S. Hahm and R. M. Kulsrud. *Phys. Fluids*, 28:2412, 1985.
- [17] H. J. de Blank and G. Valori. *Plasma Phys. Control. Fusion*, 45:A309, 2003.
- [18] D. Wróblewski and R. T. Snider. *Phys. Rev. Lett.*, 71(6):859–862, 1993.
- [19] H. K. Park, A. J. H. Donne, Jr. N. C. Luhmann, I. G. J. Classen, C. W. Domier, E. Mazzucato, T. Munsat, M. J. van de Pol, and Z. Xia TEXTOR Team. *Phys. Rev. Lett.*, 96(19):195004, 2006.

5.A The stability of a current-vortex patch

In section 5.4 the linear stability of an annular current distribution was determined. This was achieved using eigenfunctions for ϕ and ψ . Here, it will be argued that using the formalism that corresponds to general contour dynamics brings us to the same conclusions.

The interaction potential between generalized vortex patches consists of a logarithmic part, i.e. a long-range potential, and a short-range interaction potential in the form of the modified Bessel function K_0 (MacDonald's function) of the normalized distance.

The drift-Alfvén model has stationary solutions in the form of circular vortex patches. The linear stability analysis of such patches is similar to the one performed in section 5.4, in the sense that the only linear perturbations of a circular patch are the infinitesimal perturbations of the circular boundary, the contour, of the form $\exp(im(\theta - \omega t))$ where m is a positive integer and θ is the polar angle. The difference is that the shape of the contours is not used a priori to determine eigenfunctions.

5.A.1 A circular current-vortex patch

In the drift-kinetic model the current/circulation ratio of a point-vortex can be characterized by a parallel velocity v_{\parallel} . This value defines on the one hand the mix of long-range and short-range potentials produced by the point-vortex, and on the other hand the velocity that the point-vortex attains in the presence of external electric and magnetic fields.

In the drift-Alfvén model this parallel velocity can have one of three discrete values, $v_i = 0, -v_t, v_t$. When the ion vorticity is assumed to be constant, this reduces to $v_i = \pm v_t$, corresponding to the streamfunctions ϕ_{\pm} .

The interaction potential between point vortices of types v_i, v_j and strengths ω_i, ω_j equals $V_{ij} = \omega_i \omega_j G_{1ij}(|\mathbf{x}_i - \mathbf{x}_j|)$, with G_{ij} the Green's function from Eq. (5.7),

$$G_{ij}(r) \equiv \frac{1}{2\pi} \left(\ln r + \frac{v_i v_j}{v_A^2} K_0\left(\frac{r}{d_e}\right) \right),$$

where $r \equiv |\mathbf{x}_1 - \mathbf{x}_2|$. The velocity of the second vortex due to the first vortex is given by

$$\omega_j \frac{d\mathbf{x}_j}{dt} = \mathbf{e}_z \times \nabla_j V_{ij}. \quad (5.25)$$

If we consider a vortex patch of radius r_i , type $v_{\parallel} = v_j$, and constant generalized vorticity ω_i . Due to this vortex patch a point vortex (test particle) of type $v_{\parallel} = v_j$ at position r_j will have an angular velocity

$$u_{\theta} = r_i \omega_i L_{ij}^1, \quad (5.26)$$

where we have defined

$$L_{ij}^m = L_{ji}^m \equiv \frac{1}{2m} \left(\frac{r_i}{r_j}\right)^m - \frac{v_i v_j}{v_A^2} I_{mi} K_{mj}. \quad (5.27)$$

for $r_i < r_j$, using the shorthand notation from Eq. (5.9). We take $r_i < r_j$, so that

$$u_{\theta} = r_i \omega_i \left(\frac{r_i}{2r_j} - \frac{v_i v_j}{v_A^2} I_{1i} K_{1j} \right).$$

The derivation of this interaction potential makes use of the integrals

$$\oint d\theta \cos(m\theta) K_0(r) = 2\pi I_{mi} K_{mj}, \quad (5.28)$$

and

$$\oint d\theta \cos(m\theta) \log r = \begin{cases} -\frac{\pi}{m} \left(\frac{r_i}{r_j}\right)^m, & m > 0, \\ 2\pi \log r_j, & m = 0, \end{cases} \quad (5.29)$$

where $r^2 = |\mathbf{x}_i - \mathbf{x}_j|^2 = r_i^2 + r_j^2 - 2r_i r_j \cos \theta$. In both integrals $r_i < r_j$. Hence for $m > 0$ we obtain

$$\oint d\theta \cos(m\theta) G_{ij}(|\mathbf{x}_i - \mathbf{x}_j|) = L_{ij}^m(r_i, r_j). \quad (5.30)$$

5.A.2 Linear perturbation of two concentric current-vortex patches

The starting point for the analysis will be the most general basic interaction, viz. between two vortex patches of types v_1 and v_2 , with vorticities ω_1 and ω_2 , and with radii r_1 and r_2 . We consider linear displacements of these patches given by

$$\tilde{r}_1(\theta, t) = r_1 + \varepsilon_1 e^{im(\theta - \omega t)}, \quad (5.31)$$

$$\tilde{r}_2(\theta, t) = r_2 + \varepsilon_2 e^{im(\theta - \omega t)}, \quad (5.32)$$

where ω , ε_1 , and ε_2 may be complex. Let us consider the effect of the second patch on the perturbation of the first patch. The perturbation at $r = r_2$ gives rise to a perturbed potential at the position (r_1, θ_1) , for test vortices of type $v_{\parallel} = v_1$, (cf. Eq. (5.8))

$$\tilde{\phi}(r_1, \theta_1, t) = \omega_2 r_2 \oint d\theta_2 \varepsilon_2 e^{im(\theta_2 - \omega t)} G_{12}(|\mathbf{x}_1 - \mathbf{x}_2|). \quad (5.33)$$

The perturbation of the potential leads to a radial velocity

$$\frac{\partial \tilde{r}_1}{\partial t} = -\frac{1}{r_1} \frac{\partial}{\partial \theta_1} (\tilde{\phi} + u_{\theta}(r_1) \tilde{r}_1). \quad (5.34)$$

at $r = r_1$. The first term is caused by the perturbation at $r = r_2$ and hence is proportional to $\varepsilon_2 \omega_2$. The second term is a Doppler shift associated with the angular rotation of the perturbation at $r = r_1$ due to the bulk of the second vorticity patch and therefore is proportional to $\varepsilon_1 \omega_2$. The integral in Eq. (5.33) can be evaluated using Eq. (5.30). One obtains

$$\frac{\partial \tilde{\phi}}{\partial \theta_1} = -im \varepsilon_2 r_2 \omega_2 L_{12}^m e^{im(\theta - \omega t)}. \quad (5.35)$$

Using the same notation, $u_{\theta}(r_1) = r_2 \omega_2 L_{12}^1$, and hence Eq. (5.34) becomes

$$\omega \varepsilon_1 r_1 = -\omega_2 r_2 (\varepsilon_2 L_{12}^m - \varepsilon_1 L_{12}^1). \quad (5.36)$$

5.A.3 Stability of a single current-vortex patch

We can apply the result (5.36) of the previous section to the case of a single vortex patch. Identifying the two patches in the previous section ($r_2 = r_1$, $\omega_2 = \omega_1$, $v_2 = v_1$) and taking $\varepsilon_2 = \varepsilon_1$, we obtain the dispersion relation

$$\omega = \omega_1 (L_{11}^1 - L_{11}^m). \quad (5.37)$$

It is clear from this relation that ω is real, i.e., the vortex patch is stable. One also sees that for $m = 1$ the frequency vanishes. It is not surprising that a vortex patch is metastable to an $m = 1$ perturbation, which is simply a rigid displacement.

5.A.4 Stability of a pair of concentric patches

Applying Eq. (5.36) to the self-interactions and the mutual interactions between the perturbations of two patches, one obtains the system of equations

$$\omega \begin{pmatrix} \varepsilon_1 r_1 \\ \varepsilon_2 r_2 \end{pmatrix} = \mathbf{M} \begin{pmatrix} \varepsilon_1 r_1 \\ \varepsilon_2 r_2 \end{pmatrix}, \quad (5.38)$$

where

$$M_{ij} = \delta_{ij} \sum_k \omega_k L_{ik}^1 - \omega_j L_{ij}^m. \quad (5.39)$$

Equation (5.38) is a quadratic eigenvalue equation for ω . This dispersion relation has real roots if its discriminant is positive. Hence the condition for stability is

$$(M_{11} - M_{22})^2 + 4M_{12} M_{21} > 0. \quad (5.40)$$

We first note that all configurations are stable for $m = 1$, i.e., for rigid displacements of the two vortex patches with respect to each other.

Secondly, we observe that a sufficient condition for stability is

$$M_{12} M_{21} = 4\omega_1 \omega_2 (L_{12}^m)^2 > 0.$$

Hence, all unstable configurations must have $\omega_1 \omega_2 < 0$.

Thirdly, one can consider the limit $r_1 \rightarrow 0$. We thus obtain the combination of a vortex patch and a central point-vortex. Keeping the total circulation $\Omega_1 = \pi \omega_1 r_1^2$ fixed, $M_{11} \rightarrow \infty$ because of the term $\omega_1 L_{11}^1$, whereas M_{12} , M_{21} , and M_{22} remain finite. As a result, the eigenvalues become $\omega = \infty$ and $\omega = M_{22}$. The infinite eigenvalue belongs to the eigenfunction that deforms the point-vortex, whereas the finite eigenvalue corresponds to deformations of the vortex-patch. The frequency is

$$\omega = \omega_2 (L_{22}^1 - L_{22}^m) + \Omega_1 \left(\frac{1}{2r_2^2} - \frac{v_1 v_2}{v_A^2} \frac{1}{2r_2 d_e} \mathbf{K}_1 \left(\frac{r_1}{d_e} \right) \right). \quad (5.41)$$

Comparing this with Eq. (5.37) for a single vortex patch, the frequency-shift due to the central vortex is evident.

5.A.5 Stability of a pure current patch

We can construct a patch that carries a current without vorticity by equating the radii of the two patches, $r_1 = r_2$, and setting $\omega_1 = -\omega_2$, so $v_1 = -v_2$. In that case

$$L_{11}^1 = L_{22}^1, \quad L_{12}^m = \frac{1}{2m} + \frac{v_2^2}{v_A^2} \mathbf{I}_{m2} \mathbf{K}_{m2},$$

so that

$$M_{11} = -M_{22} = \omega_2 \left(\frac{v_2^2}{v_A^2} \mathbf{I}_{12} \mathbf{K}_{12} + \frac{1}{2m} - \frac{v_2^2}{v_A^2} \mathbf{I}_{12} \mathbf{K}_{12} \right), \quad (5.42)$$

$$M_{12} = -M_{21} = \omega_2 L_{12}^m = \omega_2 \left(\frac{1}{2m} + \frac{v_2^2}{v_A^2} \mathbf{I}_{m2} \mathbf{K}_{m2} \right). \quad (5.43)$$

Then Eq. (5.38) reduces to

$$\begin{aligned}\omega^2 &= M_{22}^2 - \omega_2^2 M_{12}^2 \\ &= 2\omega_2^2 \frac{v_2^2}{v_A^2} \left(\frac{1}{m} + 2 \frac{v_2^2}{v_A^2} I_{12} K_{12} \right) (I_{12} K_{12} - I_{m2} K_{m2}).\end{aligned}\quad (5.44)$$

5.A.6 Stability of a single current patch using eigenfunctions

With this formalism, it is possible to obtain the full dispersion relation for the current annulus, given by Eq. (5.21). This would require extensive algebra, so for brevity here we compare the stability of a single current patch as described by Eq. (5.41) to the results using eigenfunctions. We note that ω should be replaced by $m\omega$ because of the definition of the perturbations defined by Eqs. (5.31), (5.32). In the case of eigenfunctions we consider the Eqs. (5.18) and (5.19), and turn off the inner patch by setting $j_1 = 0$. In this way, we obtain

$$\begin{aligned}\omega^2 &= \mathbf{M}_{\psi,22} \mathbf{M}_{\phi,22}, \\ &= \frac{1}{2} m v_A^2 j_2^2 \left(1 + 2m \frac{v_t^2}{v_A^2} I_{12} K_{12} \right) (I_{12} K_{12} - I_{m2} K_{m2}).\end{aligned}\quad (5.45)$$

This is the same result as obtained in Eq. (5.44), when we set $v_2 = v_t$ and identify $\omega_2 = \frac{1}{2} m j_2 v_A^2 / v_t$. This expresses that the method using eigenfunctions is equivalent to the formalism of interacting contours.

6 Kinetic effects in a cylindrical tearing mode using Contour Dynamics

Abstract

Magnetic reconnection converts magnetic into electron kinetic energy on sometimes faster than resistive timescales. Electron inertia is a candidate to provide a mechanism for fast collisionless reconnection. The low collisionality and temperature effects can be captured using a drift-kinetic model, which exploits the fact that electrons moving with the same canonical momentum behave as an incompressible fluid, and can be described and simulated by contour dynamics. The growth rate of the unstable tearing mode agrees with theoretical estimates from a linear dispersion relation from a two-fluid model. The effects of a temperature gradient result in a shift and diamagnetic rotation of the magnetic island structure, that are compared to analytical predictions based on a slab geometry. Island deformation as a result of a locally increasing temperature gradient is bound by the formation of a negative current region in the island due to the shielding effect of electron inertia.

6.1 Introduction

The problem of collisionless magnetic reconnection has been extensively studied in different fields of plasma physics, such as geo-astronomy [1], solar physics [2] and more recently also in the field of fusion applications [3], because the plasmas are so hot that they become virtually collisionless. Reconnection manifests itself through the transformation of magnetic into electron kinetic energy as the tearing and reconnection of magnetic field lines forms structures, such as magnetic islands in tokamaks. This can be such a violent process that it ends up in plasma instabilities that affect the confinement of the whole plasma, or even a plasma disruption, in which the plasma is lost completely. The timescale in which these phenomena develop in collisionless plasmas has challenged the physics community, as the resistivity in those circumstances is too low to produce the growth rates were observed in space [1] and in fusion experiments [4].

It was shown [3, 5] that taking into account finite electron inertia can provide fast magnetic reconnection rates even in collisionless plasma regimes. The underlying model can be cast in a Hamiltonian form, in which two or three fields are advected by their respective velocity fields. The reconnection process, however, involved the acceleration of electrons in exceedingly narrow current layers, displaying singular behaviour near the x-points. It was pointed out that this is an artefact of the equation of state, and that this behaviour is resolved when applying a kinetic approach [6].

There are more fundamental reasons to use a kinetic model to describe the particles during a collisionless phenomenon. In the absence of collisions, there is no mechanism that enables the equilibration of electrons with different energies during the reconnection process. Especially when a temperature gradient over the reconnection region is present, electrons originating from different regions with a different temperature, may get mixed as the field lines over which they travel are connected.

The nonlinear drift-kinetic model has been studied in reduced x-point geometry [6] and slab geometry [7]. It makes use of distribution function to describe the electron velocity parallel to the magnetic field. In this way, the model can unite the assumptions that in the perpendicular direction the plasma is both collisionless and at the same time sustains a finite temperature gradient. The two-fluid drift-Alfvén model [8] can be obtained as a special case of the drift-kinetic system when the perturbed distribution function is discretized in velocity space as consisting of populations of electrons that move with plus or minus the thermal velocity.

By assuming the direction of the dominant part of the magnetic field to be ignorable, a Lagrangian advective formulation of the drift-kinetic equations can be obtained by transforming to the canonical momentum in the z -direction. This has the form of a conservation law in which each combination of vorticity and current is pointwise conserved when it is advected by a stream function that depends on the parallel velocity.

The full drift-kinetic equations were used to obtain an exact linear dispersion relation in slab geometry [9]. To achieve an analytically tractable, the perturbed electron velocity distribution function was spatially discretized, by imposing jumps in the current density to mark the boundaries of the current layer. In the present paper, the perturbed distribution function is discretized in both real as velocity space, creating finite area regions with a uniform distribution function that in velocity space consists of a continuous equilibrium part and delta distributions for the perturbed part. In this way for each parallel velocity a *contour* can be specified that bounds the region in which this velocity is uniformly distributed.

This model is applied to a force-free equilibrium that is constructed by imposing jumps in the distribution function that correspond to a finite first moment or current density at two concentric circles. In this way an annular current region can be established that is unstable with respect to a tearing mode.

As a consequence of the advective formulation and the double discretization, we can make use of numerical contour dynamics. Contour dynamics has been applied to the two-fluid drift-Alfvén system [10, 11], but not to investigate magnetic reconnection. Here, we present an extended version of the code used in [10, 11, 12], that now can handle an arbitrarily fine discretization in velocity space. This enables us to impose a finite jump in the second moment, the electron temperature, as well. The consequences of a thus constructed temperature gradient can be compared to the analytical results that were reported in [9].

In this way it is possible to obtain the distributions e.g. the current and the temperature during the process of magnetic reconnection, and thus study the anatomy of a magnetic island that is generated by a collisionless tearing mode.

The paper is organized as follows. In section 6.2 the drift-kinetic model is introduced using a Lagrangian advective formulation which shows the resemblance to the 2-D Euler fluid equations. To be able to apply the contour dynamics formalism, the perturbed electron distribution function needs to be discretized, for which a method is proposed in section 6.3. The advective property of the Lagrangian formulation is exploited in section 6.4, where the contour dynamics formalism is outlined. In section 6.5 we give a short linear stability analysis of the equilibrium used for the two-fluid drift-Alfvén equations, as the full drift-kinetic equations do not yield a closed form of the dispersion relation in cylindrical geometry. Also, the effects of a temperature gradient on a slab equilibrium as shown in [9] are indicated. The numerical tool that was used to perform the numerical simulations is briefly outlined in section 6.6, and the results that were obtained are given in section 6.7. These results are summarized and discussed in section 6.8.

6.2 The drift-kinetic model

This section outlines a model that describes the dynamics of collisionless electrons that experience the effects of finite inertia. It includes the effects of parallel electron compression and all the fluid nonlinearities that are incorporated in Hazeltine's three-fluid model [13]. This model is generalized by using the drift-kinetic equation to describe the parallel motion of the electrons instead of an isothermal equation of state.

We consider a strongly magnetized, low β plasma, with a strong magnetic guide field $\mathbf{B} = B_0(\mathbf{e}_z + \mathbf{e}_z \times \nabla\psi)$ and an electric field $\mathbf{E} = B_0(\mathbf{e}_z\partial_t\psi - \nabla\phi)$, where ϕ , ψ are the electrostatic and magnetic vector potential, respectively. We assume $\nabla\psi \ll 1$, so that the dynamics are strongly anisotropic. The z -direction is taken to be ignorable, and we study two-dimensional motion only.

The ions are assumed to be cold in the sense that they respond to parallel fluctuations of the electron density by moving perpendicularly to the magnetic field with the $\mathbf{E} \times \mathbf{B}$ -drift to maintain quasi-neutrality. In this way the electron density and the vorticity are linked similar to how the current and magnetic field are connected. Because of the larger mass of ions, the electrons tend to carry the current, $j \approx -en_e v_z \approx \nabla_{\perp}^2 \psi$, and parallel ion flow is neglected. Furthermore we assumed the drift ordering to apply, so that $n \approx n_0$, consistent with $\nabla^2 \phi \ll \Omega_i$.

For the electrons we assume that they can be described by a distribution function $\tilde{f}(\mathbf{x}, v_{\parallel}, t)$, with v_{\parallel} the velocity parallel to the magnetic field, that satisfies the collisionless drift-kinetic equation applies,

$$\partial_t \tilde{f} + \frac{1}{B_0} [\phi, \tilde{f}] + v_{\parallel} \nabla_{\parallel} \tilde{f} = \frac{e}{m_e} (\partial_t \psi - \nabla_{\parallel} \phi) \frac{\partial \tilde{f}}{\partial v_{\parallel}}. \quad (6.1)$$

The brackets are defined as $[A, B] = \mathbf{e}_z \cdot \nabla A \times \nabla B$, and $\nabla_{\parallel} = \partial_z + [\psi, \cdot]$ is the derivative along the total magnetic field \mathbf{B} . Ion Larmor radius effects are neglected here, and the magnetic moment is considered an ignorable coordinate in phase space and has been integrated over.

If we assume the z -coordinate to be ignorable, or $\partial_z = 0$, and we change coordinates to the canonical momentum,

$$v_z = v_{\parallel} + \frac{e}{m} \psi,$$

we can write Eq. (6.1) as

$$\partial_t f + [\Phi, f] = 0, \quad (6.2)$$

with $f = f(t, \mathbf{x}, v_z) \equiv \tilde{f}(t, \mathbf{x}, v_{\parallel})$ and $\Phi = (\phi + v_z \psi - (e/2m_e)\psi^2)/B_0$ a v_z -dependent stream-function. This describes the advection of Lagrangian invariants, conserving an infinite number of fluid type distributions $f(\mathbf{x}, v_z)$. It implies furthermore that any function of $G(f, v_z)$ is a solution of Eq. (6.2). The first two moments of the new electron distribution function,

$$\int dv_z f = n_0 + \frac{1}{ev_A^2} \nabla^2 \phi, \quad (6.3)$$

$$-e \int dv_z v_z f = \nabla^2 \psi - d_e^{-2} \psi, \quad (6.4)$$

where $d_e = \sqrt{m/e^2 n_0}$ the electron inertial skin depth, and $v_A = B_0/\sqrt{n_0 m_i}$ the Alfvén velocity, provide the sources for the electric and magnetic fields in the plasma.

6.3 Initial conditions

We can solve Eq. (6.2) for f by creating regions of finite area where the distribution function is uniform. We assume f to be of the form $f(x, y, v_z, t) = f_0(v_z) + f_1(x, y, v_z, t)$, where f_0 is the solution of $[\Phi, f_0] = 0$, and can be chosen to be of Maxwellian type. We approximate f_1 by a sum of δ -functions in v_z , with weights $f_{1,i}$, that may depend on space and time. These weights can change from one area to the other, creating regions with a perturbed distribution function. We define

$$f_0(v_z) = \frac{n}{\sqrt{\pi} v_t} e^{-v_z^2/v_t^2}, \quad (6.5)$$

$$f_1(x, y, v_z, t) = \sum_{i=0}^{N-1} f_{1,i}(t, x, y) \delta(v_z - v_i), \quad (6.6)$$

with v_t the electron thermal velocity. The function that describes an excursion from equilibrium $f_{1,i}(x, y, t) \delta(v_z - v_i)$ is the boundary of a region with uniform f , and will be called a *contour*. With this discretization, the drift kinetic equation, Eq. (6.2), reduces to N evolution equations

$$\partial_t f_{1,i} + [\Phi(v_i), f_{1,i}] = 0, \quad i = 0, \dots, N-1, \quad (6.7)$$

which describes the evolution of regions with uniform f as they are advected by N different streamfunctions $\Phi(v_0), \dots, \Phi(v_{N-1})$. The macroscopic quantities are retrieved by taking the moments of the perturbed distribution function,

$$h_j = \int dv_z v_z^j f_1 = \sum_{i=0}^{N-1} v_i^j f_{1,i}(t, \mathbf{x}). \quad (6.8)$$

So when we make use of N support velocities v_0, \dots, v_{N-1} , imposing the first N moments h_0, \dots, h_{N-1} results in the weights $f_{1,0}, \dots, f_{1,N-1}$. This leaves the choice of the support velocities v_i as a degree of freedom in this system.

A method to determine these velocities is based on the point that low order moments should correspond to basic deviations from a Maxwellian distribution function. Here, the orthogonal Hermite polynomials $H_n(v_z/v_t)$ are used to redefine the moments, with $H_n(x)$ satisfying

$$\int_{-\infty}^{\infty} H_m(x) H_n(x) e^{-x^2} dx = 2^n \sqrt{\pi} n! \delta_{m,n}. \quad (6.9)$$

The j -th Hermite moment is then defined as

$$h_j^H = \int H_j(v/v_t) f_1 dv, \quad j = 0, \dots, N-1. \quad (6.10)$$

In this way a perturbation of the distribution function proportional to $v^m \exp(-v^2/v_t^2)$ only perturbs the lowest $m+1$ moments h_0^H, \dots, h_m^H .

By choosing the N support velocities v_i to be the zeroes of the N -th Hermite polynomial $H_N(v_z/v_t)$, the N -th moment vanishes: $h_N^H = 0$. The first N moments do not vanish, and are given by

$$h_j^H = \sum_{i=0}^{N-1} f_i H_j(v_i/v_t), \quad j = 0, \dots, N-1. \quad (6.11)$$

The first four moments have their usual meaning, viz. perturbation of density, current density, temperature and heat flow.

For $N = 1$, the 2-D Eulerian fluid flow is described, as no current density is possible. The region limited by the contour then corresponds to a finite area vorticity region. With $N = 2$ the isothermal two-fluid plasma model is retrieved [8, 10, 11]. The areas can now be enclosed by two types of contours, corresponding to plus and minus the thermal velocity, where we have a finite generalized vorticity $\Omega_{\pm} = \nabla^2 \phi \mp v_t (v_A/v_t)^2 \nabla_e^2 \psi$. The perturbations can be such that in a region where there is a negative deviation for the negative velocity and a positive deviation for the positive velocity (or vice versa) a finite current density occurs. The case with $N = 3$ may capture thermal effects, but also corresponds to the isothermal three-field model [10, 14], that also models the time evolution of the ion response, but with a different electron temperature with respect to the $N = 2$ case. For $N \geq 4$ a truly kinetic model arises.

6.4 Contour Dynamics

The Lagrangian formulation of Eq. (6.2) allows the simplification that is exploited when using contour dynamics. Inverting Eq. (6.2), we obtain the stream functions for every parallel

velocity v_z as integrals over the distribution function $f(\mathbf{x}, v_z, t)$,

$$\Phi(\mathbf{x}, v, t) = \int_C d^2x' \int_{-\infty}^{\infty} dv' G_{vv'}(|\mathbf{x} - \mathbf{x}'|) f(\mathbf{x}', v', t), \quad (6.12)$$

with G the Green's function for the unbounded domain, given by [11]

$$G_{vv'}(r) = \frac{1}{2\pi} \left(\ln r + \frac{vv'}{v_A^2} K_0\left(\frac{r}{d_e}\right) \right), \quad (6.13)$$

with K_0 the modified Bessel function of the second kind. By assuming the distribution function to be constant within a well-defined region C , bounded by a contour ∂C , the dynamics are completely defined. A piecewise uniform distribution function will remain piecewise uniform by Eq. (6.2), and so the topology of the initial distribution is also conserved in time. The Green's function $G_{vv'}$ is the streaming potential of the contour corresponding to velocity v at \mathbf{x} as a consequence of a contour with support velocity v' at \mathbf{x}' .

When we apply this to the discretized form of f_1 consisting of N δ -functions at v_0, \dots, v_N , we get

$$\Phi_j(\mathbf{x}, t) = \sum_{i=1}^N f_{1,i} \int_{C_i(t)} d^2\mathbf{x}' G_{v_i v_j}(|\mathbf{x} - \mathbf{x}'|), \quad (6.14)$$

with $C_i(t)$ a piecewise uniform electron velocity distribution with parallel velocity $v_z = v_i$. The velocity of the j -th contour is then calculated by applying Stokes' theorem and integrating by parts,

$$\mathbf{u}_j(\mathbf{x}, t) = - \sum_{i=1}^N f_{1,i} \oint_{\partial C_i(t)} d\mathbf{x}' G_{v_i v_j}(|\mathbf{x} - \mathbf{x}'|), \quad (6.15)$$

where the summation is over all contours ∂C_i and v_i is the support velocity of the i -th contour. This implies that the time evolution of a contour depends only of the location of the contours, including its own location.

The plasma in the region that is bounded by ∂C_i corresponds to a flux $f_{1,i}$. Because the surface enclosed by ∂C_i is conserved, all linear combinations of fluxes $F(f_{1,i})$ are also conserved.

6.5 Equilibrium, linear stability

We will study an equilibrium with an annular current layer, yielding a ψ -profile comparable to that of a flux function ψ^* corresponding to a flux surface with a rational value of the safety factor $q = m/n$, where m, n are the poloidal and toroidal mode number, respectively.

The equilibrium is constituted by overlaying two concentric circular patches with radii R_1, R_2 , ($R_1 < R_2$). We impose the first moment of the outer patch, h_{1,R_2}^H , to have a positive value, and the first moment of the inner patch to have the same value, only negative, $h_{1,R_1}^H = -h_{1,R_2}^H$. Furthermore, we can simulate a density and temperature gradient by specifying jumps of the zeroeth and second moments at R_j : h_{0,R_j}^H, h_{2,R_j}^H , resulting in a staircase or wedding cake structure. In this paper, we only consider equilibria with jumps in the temperature.

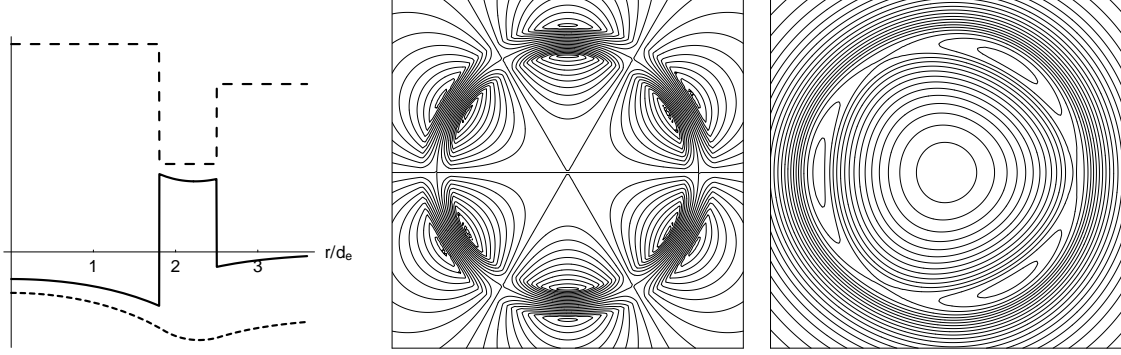


Figure 6.1: On the left the fields of a current annulus equilibrium. The dashed curve shows the x -dependence of the total generalized vorticity, the solid curve shows the current density $\nabla^2\psi_0$ as a layer between R_1 and R_2 that is shielded on a length scale d_e , and the dotted curve is ψ_0 . Next is shown the linear $m = 3$ mode in a cylindrical current annulus, with eigenfunctions for the electrostatic potential ϕ (middle) and the magnetic potential ψ (right).

The perturbed first moment yields a current density j_j , resulting in a magnetic vector potential given by

$$\psi_{0,j} = -d_e^2 j_j \begin{cases} 1 - \frac{R_j}{d_e} K_1\left(\frac{R_j}{d_e}\right) I_0\left(\frac{r}{d_e}\right) & \text{if } r < R_j, \\ \frac{R_j}{d_e} I_1\left(\frac{R_j}{d_e}\right) K_0\left(\frac{r}{d_e}\right) & \text{if } r > R_j, \end{cases}$$

for $j = 1, 2$, with I_m, K_m modified Bessel functions of the first and second kind. The current profile as depicted in Fig. 6.1 is peaked, and shows the shielding effects on a length scale d_e caused by the electron inertia. However, the corresponding ψ_0 is smooth and its derivative with respect to r continuous. The quantities

$$\begin{aligned} \hat{j}_1 &= \frac{\psi'_0(R_1)}{R_1} = j_1 I_{11} K_{11} + j_2 I_{11} K_{12} \frac{R_2}{R_1}, \\ \hat{j}_2 &= \frac{\psi'_0(R_2)}{R_2} = j_1 I_{11} K_{12} \frac{R_1}{R_2} + j_2 I_{12} K_{12}, \end{aligned}$$

give the relative gradient at R_1 and R_2 , the edges of the annulus. When they are of opposite sign we have a neutral line within the annular region $R_1 < r < R_2$, or, in other words, ψ_0 will have a minimum there. This is equivalent to requiring $j_1 < 0 < j_2$ or $h_{1,R_1}^H < 0 < h_{1,R_2}^H$. Here,

$$I_{mj} = I_m(R_j/d_e), \quad K_{mj} = K_m(R_j/d_e), \quad j = 1, 2.$$

This equilibrium can only be perturbed at the location of the contours, because of the absence of gradients in f . Away from the contours we find solutions for ϕ_1 and ψ_1 that are regular in $r \rightarrow 0, r \rightarrow \infty$,

$$\nabla^2 \phi_1 = 0,$$

gives

$$\phi_1(r, \theta) = e^{i(m\theta - \omega t)} \sum_{j=1,2} \frac{\phi_{j,m}}{2m} \begin{cases} \left(\frac{r}{R_j}\right)^m, & r \leq R_j, \\ \left(\frac{R_j}{r}\right)^m, & r \geq R_j. \end{cases} \quad (6.16)$$

Similarly

$$\nabla_e^2 \psi_1 \equiv \nabla^2 \psi_1 - d_e^{-2} \psi_1 = 0,$$

has a continuous solution

$$\psi_1(r, \theta) = e^{i(m\theta - \omega t)} \sum_{j=1,2} \psi_{j,m} \begin{cases} K_{mj} I_m(\frac{r}{d_e}), & r \leq R_j, \\ I_{mj} K_m(\frac{r}{d_e}), & r \geq R_j, \end{cases} \quad (6.17)$$

where m is the poloidal mode number of the excitation. Evaluating the jumps at the inner and outer surfaces $r = R_1$ and $r = R_2$,

$$\begin{aligned} \psi'_0(R_j) &= R_j \hat{j}_j, \\ \nabla_e^2 \psi'_0 &= \sum_{j=1,2} h_{1,R_j}^H = \sum_j -j_j \delta(r - R_j), \\ \nabla^2 \phi_1 &= \sum_{j=1,2} -\frac{2m}{R_i} \phi_{i,m} \delta(r - R_i), \\ \nabla_e^2 \psi_1 &= \sum_{j=1,2} -\frac{\psi_{i,m}}{d_e} \delta(r - R_i). \end{aligned}$$

These are the relations that couple the perturbed field as a consequence of the dislocated contours back to the evolution equation (6.2).

In this way, a dispersion relation can be obtained. However, when this is attempted for the full drift-kinetic system, in cylindrical geometry difficulties arise that have not yet been overcome. For the linear periodic slab a dispersion relation has been obtained [9]. A closed expression for the cylindrical dispersion relation cannot be obtained with the same approach. Here, the dispersion relation for the discretized system with $N = 2$, the isothermal two-fluid equations, will be given.

For $N = 2$, the zeroth and first moment of the drift-kinetic equation, Eq. (6.2), reduce to

$$\partial_t \nabla^2 \phi + [\phi, \nabla^2 \phi] = v_A^2 [\psi, \nabla_e^2 \psi], \quad (6.18)$$

$$\partial_t \nabla_e^2 \psi + [\phi, \nabla_e^2 \psi] = -\frac{v_t^2}{v_A^2} [\nabla^2 \phi, \psi], \quad (6.19)$$

with $\rho_s = \sqrt{m_e m_i v_t} / e B_0$ the ion-sound Larmor radius. Linearizing and filling in the jump conditions at R_1 and R_2 leads to a set of four equations,

$$\omega \begin{pmatrix} \phi_{1,m} \\ \phi_{2,m} \end{pmatrix} = \mathbf{M}_\psi \begin{pmatrix} \psi_{1,m} \\ \psi_{2,m} \end{pmatrix}. \quad (6.20)$$

$$\omega \begin{pmatrix} \psi_{1,m} \\ \psi_{2,m} \end{pmatrix} = \mathbf{M}_\phi \begin{pmatrix} \phi_{1,m} \\ \phi_{2,m} \end{pmatrix}, \quad (6.21)$$

with

$$\begin{aligned} \mathbf{M}_\psi &= -\frac{v_A^2}{2} \begin{pmatrix} j_1 I_{m1} K_{m1} - \hat{j}_1 & j_1 I_{m1} K_{m2} \\ j_2 I_{m1} K_{m2} & j_2 I_{m2} K_{m2} - \hat{j}_2 \end{pmatrix} \\ \mathbf{M}_\phi &= m \begin{pmatrix} j_1 + 2m \hat{j}_1 v_t^2 / v_A^2 & j_1 (R_1 / R_2)^m \\ j_2 (R_1 / R_2)^m & j_2 + 2m \hat{j}_2 v_t^2 / v_A^2 \end{pmatrix} \end{aligned} \quad (6.22)$$

Matching the jumps in the derivatives in the eigenfunctions at R_1 and R_2 leads to the dispersion relation in ω and k ,

$$\omega^4 + \omega^2 \text{Tr}(\mathbf{M}) + \det(\mathbf{M}) = 0, \quad (6.23)$$

with $\mathbf{M} = \mathbf{M}_\psi \mathbf{M}_\phi$. The value of ω is determined by h_{1,R_j}^H , the ratio v_A/v_t and the geometric details of R_j, d_e and $k = 2m/(R_1 + R_2)$. This relation reveals the existence of at least one unstable tearing mode, that manifests itself as a chain of magnetic islands with m -fold periodicity in the poloidal direction.

The influence of a temperature gradient on the evolution of the tearing mode that may be excited by an infinitesimally small seed perturbation has been studied in slab geometry [9]. Though the results are not expected to apply fully on the cylindrical equilibrium studied here, they will be used to compare the numerics to.

The jumps in the temperature $\Delta T_j = h_{2,R_j}^H$ lead to a diamagnetic drift in the form of a poloidal rotation with frequency $\omega_* = kT'_0/eB_0$, where T'_0 corresponds to an effective temperature gradient

$$T'_0 = \frac{\Delta T_1 + \Delta T_2}{R_2 - R_1}. \quad (6.24)$$

This diamagnetic frequency ω_* enters Ampère's equation (6.4), resulting in a modified wavelength $2\pi/k$ for perturbations in the magnetic potential ψ . In the early, linear stage of the mode, the rotation frequency of the chain of magnetic islands becomes

$$\omega_c = \begin{cases} \omega_* & \gamma \gg \omega_c, \\ (\omega_*(\gamma A + B))^{1/3} & \gamma \ll \omega_c \end{cases} \quad (6.25)$$

where A, B are functions of $\tilde{k}, R_2 - R_1, d_e$, and $\gamma = \text{Im}(\omega)$. This results in a phase shift of the magnetic island with respect to the external perturbation of

$$\delta y = -\frac{|x|}{k} \times \begin{cases} \omega_*/(2\gamma\tilde{k}d_e^2), & \gamma \gg \omega_c, \\ \gamma\omega_c/2(\gamma A + B)\tilde{k}d_e^2, & \gamma \ll \omega_c. \end{cases} \quad (6.26)$$

The last expression shows that the phase shift vanishes for small growth rates. When the mode saturates and no longer grows, the shift remains and becomes

$$\delta y = \begin{cases} C\omega_*/k^2\gamma w, & \gamma \gg k_{\parallel}v_t/kw, \\ D\omega_*/kk_{\parallel}v_t, & \gamma \ll k_{\parallel}v_t/kw, \end{cases} \quad (6.27)$$

where C, D are functions of order unity of kd_e and $(R_2 - R_1)/d_e$.

6.6 Numerical method

The numerical implementation of the contour dynamics method is not new. The code used by the authors is based on an existing code which is described in detail in [11, 12]. Some changes had to be made to adapt it to dealing with an arbitrary number of types of contours, as every support velocity v_i corresponds to a different conserved flux and a different streamfunction Φ_i . Some relevant or newly added features will be outlined here.

The number of support velocities, or abscissas, N , is entered, and the imposed jumps in the first moments of the distribution function, h_i^H , based on which the zeroes of $H_N(x)$ and their respective weights are calculated. Then, for each patch, N circular contours are generated with a sinusoidal perturbation $\sim \epsilon \sin(m\theta)$ along the contour. Note that all contours $f_{1,i}$ are initially equally deformed. Each contour is defined by a discrete set of points $h_i(j)$. These points, or *nodes*, define line segments whose evolution in time is given by Eq. (6.2) with a velocity solely dependent on the location of the set of contours, as expressed in Eq. (6.15). The discretization of a contour is reconsidered by the code every timestep, inserting more nodes when the local curvature of a segment becomes too large, or when a line segment of the same type comes close, and deleting nodes in the opposite cases. The velocity field of the discretized system is shown to be divergence-free nevertheless [12]. We stress that line segments of contours of different type are allowed to cross, whereas segments of contours with the same support velocity, or segments that belong to the same contour, are not, as they are advected by the same potential flow.

The implicit predictor-corrector scheme using a second-order midpoint rule that is used to calculate the motion of the line segments is symplectic, and therefore conserves the area of the initial contours to a high degree [12].

When the number of nodes per contour exceeds a preselected limit, the code breaks off. The intricate features can pose considerable computational cost when a highly nonlinear stage is reached, with the amount of computations scaling roughly with the amount of nodes squared.

The computational cost is not so much of an issue, since it takes the code generally a few hours to reach the stage where the maximum number of nodes is used. Increasing the maximum number will in general only lead to a few more timesteps, because the structure of the contours will have become so complex and filamentary that every timestep a large number of nodes will be added. By this time the simulated dynamics have become so deeply nonlinear that chaotic phase-mixing has taken over, passing beyond the phenomena this paper is focussing on.

The code harbours the possibility for Contour Surgery, meaning that when the tolerance for the closeness of two parts of a contour is surpassed, the code cuts the structure loose and ties the enclosing ends together. This leads to the loss of topological conservation of the generalized fluxes, and the loss of thin structures. These thin filaments may contain populations of electrons that can be of crucial importance for the kinetic modelling that is pursued here. Therefore, this feature is not used in our simulations and will not be discussed further, for details see [11].

The electrostatic potential ϕ and magnetic potential ψ can be calculated as a function of \mathbf{x} by testing whether \mathbf{x} is in- or outside a contour, and subsequently performing the integral

$$\Phi_j(\mathbf{x}) = \sum_i f_{1,i} \int_{C_i} d^2\mathbf{x}' G_{ij}(|\mathbf{x} - \mathbf{x}'|),$$

which is equivalent to

$$\Phi_j(\mathbf{x}) = \sum_i f_{1,i} \oint_{\partial C_i} d\mathbf{l}' \times (\mathbf{x} - \mathbf{x}') F_{ij}(|\mathbf{x} - \mathbf{x}'|),$$

with

$$F_{ij}(r) = \frac{1}{r^2} \int_0^r dr' r' G_{ij}(r').$$

Because of the representation of this integral as a contour integral instead of a two-dimensional integral over the infinite plain, it is not necessary to adapt the computational domain to include the dominant part of the integrand. Thus no assumptions need to be made as to at what distance from the contours the velocity fields they create become negligible. Furthermore, line integrals require less computational cost than surface integrals.

Aside of the electrostatic and magnetic potential, the first four moments of the distribution function are given as output of this routine. The density, current density, temperature (if $N > 2$) and heat flow (if $N > 3$) are calculated on a grid for a given time t . Furthermore, the code tracks the location of the x- and o-points. The amount of reconnected flux is calculated as the difference in magnetic flux between the x- and o-point,

$$\psi_{\text{rec}} = \psi_X - \psi_O.$$

Finally, the angle of the external perturbations with respect to the initial situation is calculated. To have an idea of how the excited mode is rotating with respect to the field perturbations as perceived far away from the patch, the m -th coefficient of the K_m expansion of the whole structure is calculated,

$$\mathcal{I}_m = \sum_i f_{1,i}(-env_i) \oint dr r \int d\theta I_m\left(\frac{r}{d_e}\right) e^{im\theta}, \quad (6.28)$$

so that

$$\theta_{\text{ext}} = \arctan\left(\frac{\text{Im}(\mathcal{I}_m)}{\text{Re}(\mathcal{I}_m)}\right). \quad (6.29)$$

Now we can compare the rotation of the x- and o-points to the rotation of the perturbations of the external field. This is the quantity that will be identified as the phase shift δy as discussed in Eq. (6.26).

6.7 Numerical results

The numerical simulations were performed for different poloidal mode numbers, and different levels of discretization. The radii of the annulus were chosen such that the excited poloidal mode number corresponds to the fastest growing mode in the equilibrium.

Here we stress that we did not obtain a dispersion relation for the drift-kinetic model in cylindrical geometry. To investigate the numerical results of the N -fold discretized system, we assess the correspondence with the exact results obtained for two-fluid theory, and we compare the non-isothermal results with the effects that were predicted in [9] for equilibria in slab geometry.

6.7.1 Comparison with the two-fluid model

The results that are generated by the code are illustrated in Figs. 6.2, 6.3 and 6.4 for a tearing mode with poloidal mode number $m = 3$, resp. for the cases with $N = 5$ and $N = 2$ without an applied temperature gradient, and for $N = 5$ with a small temperature gradient.

We calculated the growth rate for different values of the discretization level N , and for different values of the poloidal mode number m . The growth rate of the mode is measured by the rate of change of the reconnected flux, $\psi_{\text{rec}}(t)$, in the time interval where the amount

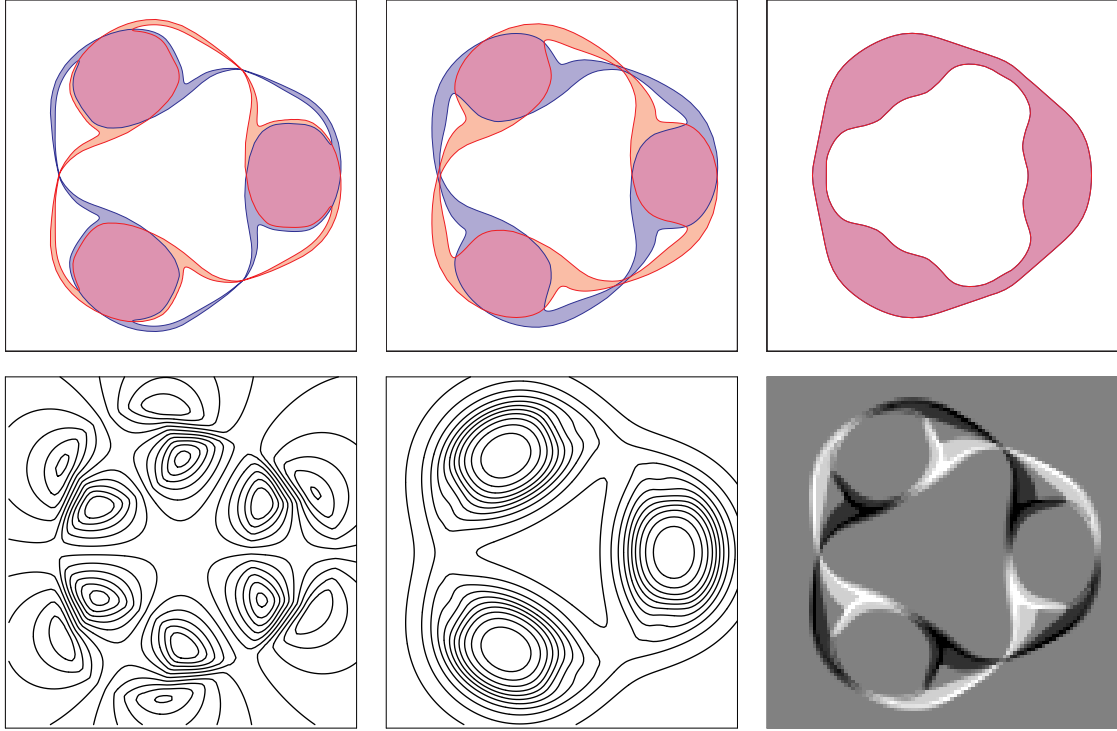


Figure 6.2: Here we see the contours that are produced by the numerical code for discretization level $N = 5$. In this case no temperature gradient has been applied. A $m = 3$ mode has been excited, which is shown here at $t = 10.0\tau_A$. The left figure shows the contours that correspond to velocities $v_i = \pm 2.02v_t$, and with resp. weights $w_i = \pm 0.091$. The middle figure shows the contours with $v_i = \pm 0.96v_t$, and $w_i = \pm 0.85$, and in the right figure $v_i = 0, w_i = 0$. The red coloured areas correspond to electrons with $\omega_i = \nabla^2\phi - v_i\nabla_e^2\psi$, advected by $\Phi_i = \phi + v_i\psi$, and the blue areas have $\omega_i = \nabla^2\phi + v_i\nabla_e^2\psi, \Phi_i = \phi - v_i\psi$. The purple areas correspond to areas where the vorticities cancel, and only current is carried, except in the right figure, where $v_i = 0$, and the corresponding electrons only move along with the $\mathbf{E} \times \mathbf{B}$ motion in the plasma. The bottom row shows the isolines of ϕ , which can be interpreted as the flowlines of the $\mathbf{E} \times \mathbf{B}$ velocity, and the isolines of ψ mark the flux surfaces. On the right we see the temperature profile.

of reconnected flux increases exponentially. This is adjusted by deducting the effect of the excited exponentially damped mode, assuming that initially

$$\psi_1(t) = \psi_1(0) \cosh(\gamma t),$$

with $\psi_1(0)$ the perturbation at $t = 0$ and $\gamma = \text{Im}(\omega)$, the imaginary part of the eigenvalue corresponding to the tearing mode solution. Then the growth rate as predicted by the dispersion relation is given by

$$\gamma t = \log \left(\frac{\psi(t)}{\psi_1(0)} + \sqrt{\left(\frac{\psi(t)}{\psi_1(0)}\right)^2 - 1} \right). \quad (6.30)$$

The results are given in Table 6.1.

m	R_1/d_e	R_2/d_e	N	γ_{dis}	γ_{num}	$\omega_{*,\text{est}}$	$\omega_{*,\text{num}}$	δy_{est}	δy_{num}
3	4.0	5.5	2	0.391	0.345				
3	4.0	5.5	3	0.391	0.399	0.0197	0.0295	-0.0346	-0.0440
3	4.0	5.5	5	0.391	0.395	0.0197	0.0181	-0.0346	-0.0342
3	4.0	5.5	7	0.391	0.383	0.0197	0.0172	-0.0346	-0.0333
3	4.0	5.5	10	0.391	0.383	0.0197	0.0168	-0.0346	-0.0335
5	4.0	4.8	2	0.656	0.620				
5	4.0	4.8	3	0.656	0.630	0.0663	0.0349	-0.0557	-0.0342
5	4.0	4.8	5	0.656	0.618	0.0663	0.0256	-0.0557	-0.0307
5	4.0	4.8	7	0.656	0.616	0.0663	0.0256	-0.0557	-0.0297
5	4.0	4.8	10	0.656	0.616	0.0663	0.0256	-0.0557	-0.0305

Table 6.1: Comparison of the growth rates of the numerically simulated modes γ_{num} for different discretization level N and poloidal mode number m . Also, the analytically obtained growth rates from the linear dispersion relation γ_{dis} are given. Furthermore, for $N > 2$ the analytical estimate of ω_c (cf. Eq. (6.25)) is given as $\omega_{*,\text{est}}$ next to the frequency obtained by the simulation, $\omega_{*,\text{num}}$, as well as for δy , with δy_{est} from Eq. (6.26), and δy_{num} from the code. For $N = 2$ the plasma is isothermal, hence $\omega_c = 0$, $\delta y = 0$.

First, if we look at Table 6.1 and Figs. 6.2 and 6.3, we note the good correspondence between the theoretical linear $N = 2$ fluid predictions and the results from the non-linear code in the early, linear regime. Furthermore, the growth rate converges for increasing N .

The simulations with the two-fluid conditions display a slightly smaller growth rate, so in Fig. 6.3 the results of a later timestep is shown for comparison. The contours in the two-fluid model with $v_i = \pm v_t$ look similar to the contours of the $N = 5$ simulation with $v_i = \pm 0.96v_t$ (Fig. 6.2, top row, middle picture).

In general, we observe that the fields of the electrostatic and magnetic potential ϕ and ψ are qualitatively very similar for the cases $N = 2$ and $N = 10$. The kinetic effects that may play a role for large N do not alter the basic features of the mode much. This is not very surprising, as for slab geometry the fluid dispersion relation is a limiting case of the kinetic version.

Also, if we look at the spatial distribution of the current-carrying electrons, denoted by the coloured areas in the contour plots, we can see that for small N (notably $N \leq 3$), these areas do not cover the whole magnetic island and x-point region. Holes can start to appear in the electron distribution before the magnetic island saturates. This seems not to lead to obvious artefacts in the ϕ, ψ -fields, but it is clear that the kinetic approach smoothes the dynamics and corresponds to a more physical picture.

Furthermore, we note that for large N , the numerical method is faced with more extreme deformation of the contours than with the two-fluid or $N = 2$ case. The contours that correspond to large $|v_i|$ are advected by streamfunctions that have a larger magnitude $|\phi_i|$. Those contours tend to follow the magnetic field lines more than the $\mathbf{E} \times \mathbf{B}$ -flow, which results in the alignment with the magnetic separatrices. This motion brings the line-segments of the

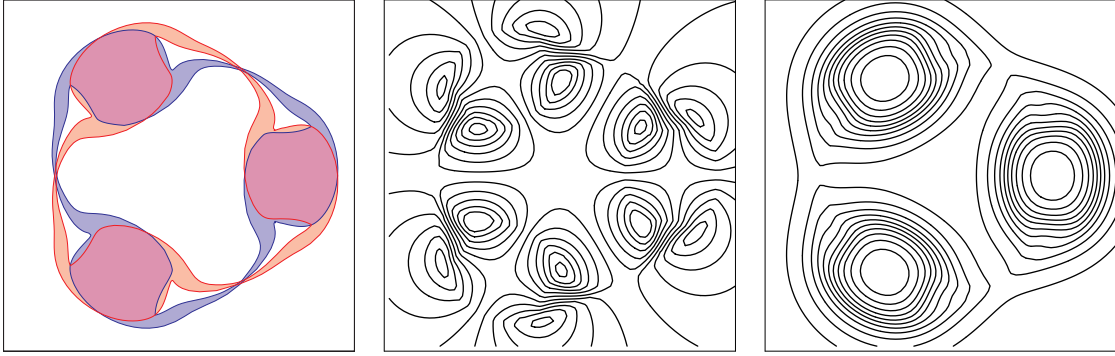


Figure 6.3: The numerical results of the two-fluid model ($N = 2$) at $t = 12\tau_A$, with on the left the contours that correspond to $v_{\pm} = \pm v_t$ next to isolines of the electrostatic and magnetic potential ϕ and ψ .

contours very close, resulting in a fast multiplication of the number of nodes that define the contour, and therefore the code breaks off because of exceeding the maximum number of nodes soon in comparison to the case with $N = 2$. Still, the code manages to realise a relatively large number of timesteps for $N \leq 10$, reaching the stage where the tearing mode starts to saturate. Simulations with $N > 10$ have not been performed yet.

6.7.2 Comparison with ∇T -effects in slab geometry

The application of a temperature gradient becomes straightforward with this version of the code. The outer area ($r > R_2$) has no temperature perturbation, but the contours of the outer and the inner contours can both be adjusted in such a way that their weights correspond to a finite step in the temperature ΔT_j , at radii $j = 1, 2$, by imposing the second moment of the perturbed distribution function to assume some input value. This leads to a double temperature step in the radial temperature profile. To be able to compare the movement of the island chain as produced by the code to the expressions (6.25) and (6.26), that contain $\omega_* = kT'_0/eB_0$, this temperature profile is approximated by Eq. (6.24). The temperature profile for simulations with different N is shown in greyscale in Fig. 6.5. The spatial distribution of temperature becomes smoother for increasing N . Where for $N = 3$ we see at $t = 10\tau_A$ broad regions of black and white, indicating the temperature extremes, and a well delineated region corresponding to the region of negative current density at the clockwise flank of the magnetic island, this has become an almost featureless monochromatic region for $N = 10$. We also note that the regions with negative temperature perturbation at the outboard side of the islands become smaller for increasing N .

The effects of a temperature gradient that were described in [9] are a phase velocity ω_c and a shift with respect to the perturbed field as perceived in the external region δy . To be able to quantify these, the timetraces of the relative angle of the x-point θ_X , the o-point θ_O and the angle of the coefficient of the Bessel-expansion for poloidal mode number m , θ_{ext} , as given in Eq. (6.29) are shown in Fig. 6.6. This is for the case where $m = 3, N = 3, 5, 7$. The phase velocity ω_c is given by the slope of θ_X, θ_O during the time before saturation sets in, here at $t = 7\tau_A$. The shift δy is the angle between θ_X, θ_O and θ_{ext} . This is not a constant shift, as it becomes irregular from the point where saturation sets in, and it starts with a bit

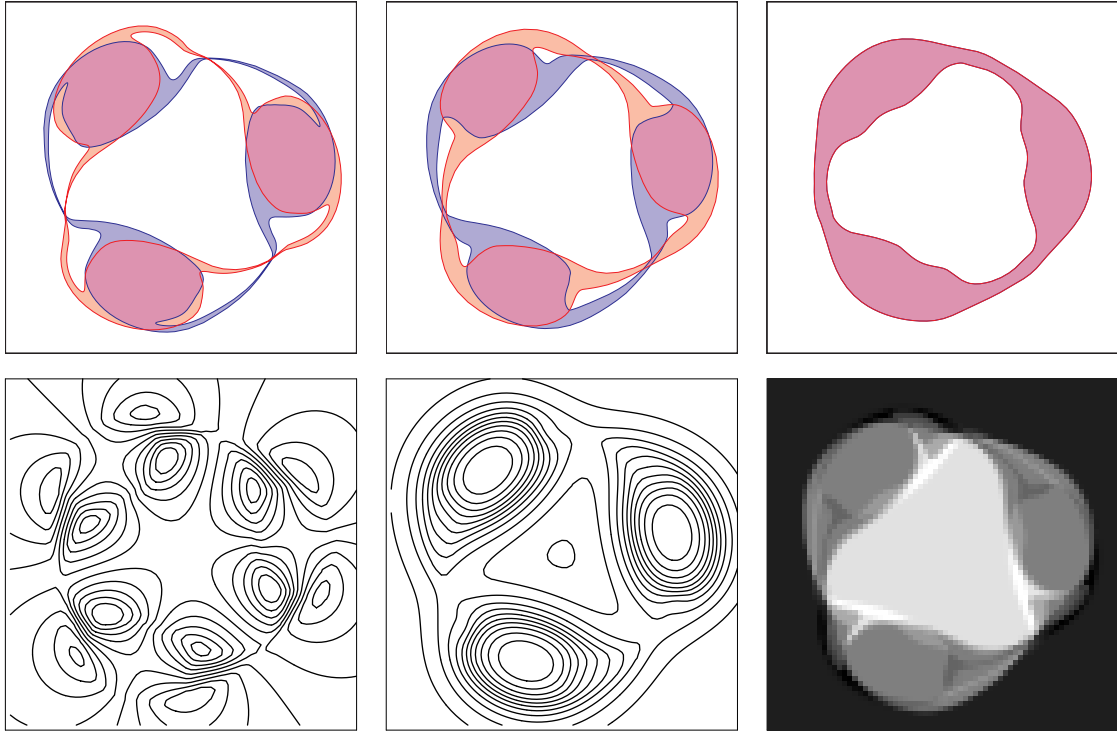


Figure 6.4: Here we see the contours that are produced by the numerical code for the same parameters and the same timestep as in Fig. 6.2, $t = 10.0\tau_A$, again discretization level $N = 5$. In this case a small temperature gradient has been applied by two finite jumps at the initial contours at $r = R_1$ and R_2 . The left figure shows the contours that correspond to velocities $v_i = \pm 2.02v_t$, and with resp. weights $w_i = \pm 0.17$ and ∓ 0.01 . The middle figure shows the contours with $v_i = \pm 0.95v_t$, and $w_i = \pm 1.05$ and ∓ 0.67 , and in the right figure $v_i = 0, w_i = -0.53$. The bottom row shows the isolines of ϕ and ψ and on the right the temperature profile is given.

smaller value than during the interval between roughly $t = \tau_A$ and the time that the mode starts to saturate. The value that we will take here is measured over this interval.

In Tab. 6.1 the results are given for various parameters. From the contour and fieldplots it is already clear that the velocity with which the structure is rotating, $\omega_{*,\text{num}}$, is considerably smaller than the phase velocity of the mode, $\sim \gamma$, as there are several turnover times of the mode whereas the island chain only turns by less than half a radian. This means that by (6.25) we should compare ω_c to ω_* . This gives reasonable correspondence to the linear estimate for the diamagnetic shift of the magnetic island chain ω_c for the case with $m = 3$ and a value of the right order of magnitude for $m = 5$.

In general we can say that we have qualitative resemblance of the deformation of the magnetic island as predicted in [9] and the shape of the magnetic islands as depicted in Fig. 6.4. The deformation can be quantified as the difference in the relative phase angle $\theta_X - \theta_O$. This becomes evident when saturation has set in, when θ_X starts to move faster than θ_O , clearly seen in Fig. 6.6. This will be next topic of scrutiny.



Figure 6.5: Here the temperature profiles are shown for an $m = 3$ perturbed equilibrium at $t = 10.0\tau_A$, where temperature jumps were applied at the original contours at $r = R_1, R_2$. The left figure corresponds to a simulation with discretization level $N = 3$, the middle for $N = 5$ and the right figure for $N = 10$. Note that the middle figure corresponds to the contours shown in Fig. 6.4.

6.7.3 Dynamical behaviour of the X-point

In Fig. 6.6, the angles of the x- and o-points are given as a function of time, as well as the relative shift of the external field θ_{ext} from Eq. (6.29), for $N = 3, 5, 10$. The $\omega_{*,\text{num}}$, listed in Table 6.1 is calculated as the time-derivative of the angle of the o-point, $\partial_t\theta_O$, in the time interval where the mode can be assumed to be linear, so before the nonlinear saturation sets in. The shift of the chain of magnetic islands with respect to the external perturbations, $\theta_{X,O} - \theta_{\text{ext}}$, is determined by the value at $t = 0$ of the fit of $\theta_{\text{ext}}(t)$ in the linear regime, approximately $\tau_A < t < 6\tau_A$.

Looking at Fig. 6.6, we notice several things. First of all, in the linear stage of the mode, the whole structure is shown to rotate approximately rigidly. The x-point and the o-point do not deviate from one another, and θ_{ext} moves with the same frequency. Already in the first few timesteps a finite phase shift δy between the magnetic islands and the external perturbed field develops, which remains approximately constant until $t \approx \tau_A$. The magnitude of the shift agrees with the estimate based on the linear dispersion relation of the straight current slab, expressed in Eq. (6.26). This correspondence is less precise for the case with $m = 5$ (see Table 6.1), but still of the right order of magnitude.

When nonlinear saturation of the mode sets in, we see the following: $\theta_{\text{ext}}(t)$ becomes irregular, and $\theta_X(t)$ starts to accelerate in what seems to be two distinct phases: first θ_X deviates linearly with a slightly larger velocity than θ_O , but approximately τ_A later it accelerates again. This is not visible when we only take three contours, $N = 3$. This stage of steep acceleration is followed by saturation, where $\theta_X - \theta_O$ actually decreases again.

The fact that the rotational frequency of the x-points starts to increase can be explained by the observation that at $t \approx 6\tau_A$, the contours of v_i start to deform in such a way that the jumps in temperature ΔT_i , carried by the contours, are closing in, so that the temperature gradient estimated by Eq. (6.24) is no longer accurate, but should be adjusted by substituting $R_2 - R_1$ by $R_2(t) - R_1(t)$ to take into account the actual position of the contours. However, one might expect the opposite to happen for the o-points, a deceleration as a consequence of a decreasing diamagnetic frequency because the contours come further apart as the magnetic

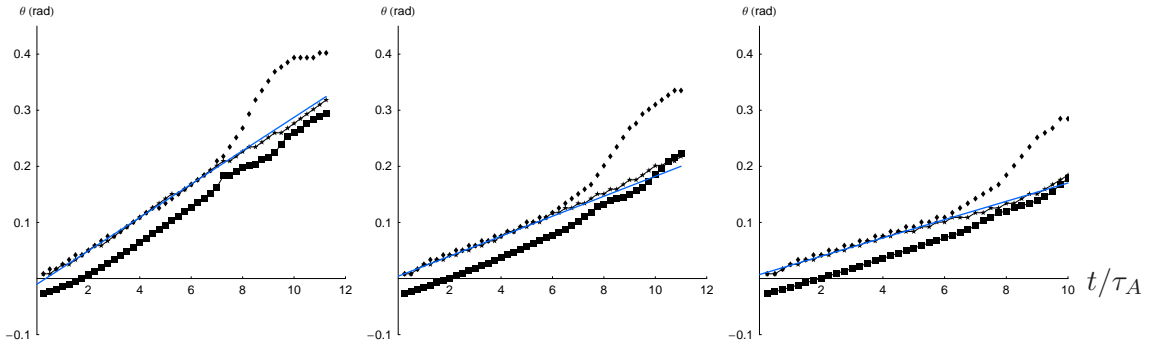


Figure 6.6: Above are the timetraces of the deviation of the angles of the x-point, the o-point and the angle of the external perturbations, θ_X , θ_O and θ_{ext} , resp. the upper, middle and lower trace in the figures, given in radians. The straight line is a fit of θ_O in the time interval where the mode is assumed to be linear, i.e. before it nonlinearly saturates. From left to right the figures correspond to $m = 3, N = 3, 5, 10$. Again, the middle figure corresponds to the same case as Fig. 6.4.

island grows. This is not the case, or very mildly so, not comparable to the change of the phase velocity of the x-points.

To understand the decrease of the frequency of the x-points from $t \approx 9\tau_A$ onwards, we take a look at the shape of the contours and how they constitute the total current density, as shown in Fig. 6.7. Here we depicted the contours and the current in the \mathbf{e}_z -direction j_z for the case with $N = 5$, $m = 3$, for three different timesteps, starting at $t = 9\tau_A$. From this point onward an asymmetry between the clockwise and the counterclockwise side of the magnetic island starts to appear. The separatrices on the counterclockwise side of the x-point are broader than on the other side. This effect was already predicted in [6], as the result of a current perturbation caused by the difference in parallel electron velocity of the population on the warm and the cold side of the current layer.

At $t = 10\tau_A$, we see that within the magnetic island, at the clockwise side, a region appears with negative current density. To explain how this can occur, we turn to Fig. 6.1. On the lengthscale d_e , the current layer (solid curve) is shielded by an exponentially decaying current sheet in the opposite direction. If the contours of two separate current regions (e.g. the red and the blue area) are close with respect to d_e , these shielding current sheets overlap and can cause a region with negative current density. This current structure has a diameter of the order of d_e , and though the effect is most pronounced for small N , it converges to a finite negative current region for large N . The appearance of structures on lengthscale d_e has already been reported for monopolar current-vortices in [11].

The fact that this only happens at the clockwise side of the magnetic island is a direct result of the temperature-induced asymmetry of the contours. On this side the current filaments remain broader and the distance between the current regions smaller than on the counterclockwise side.

This region of negative current interacts with the large region of positive current, which pushes it away, like two electric wires that carry opposite current. This in turn pushes the x-point away from the o-point, resulting in the decrease of the rotational velocity and in some

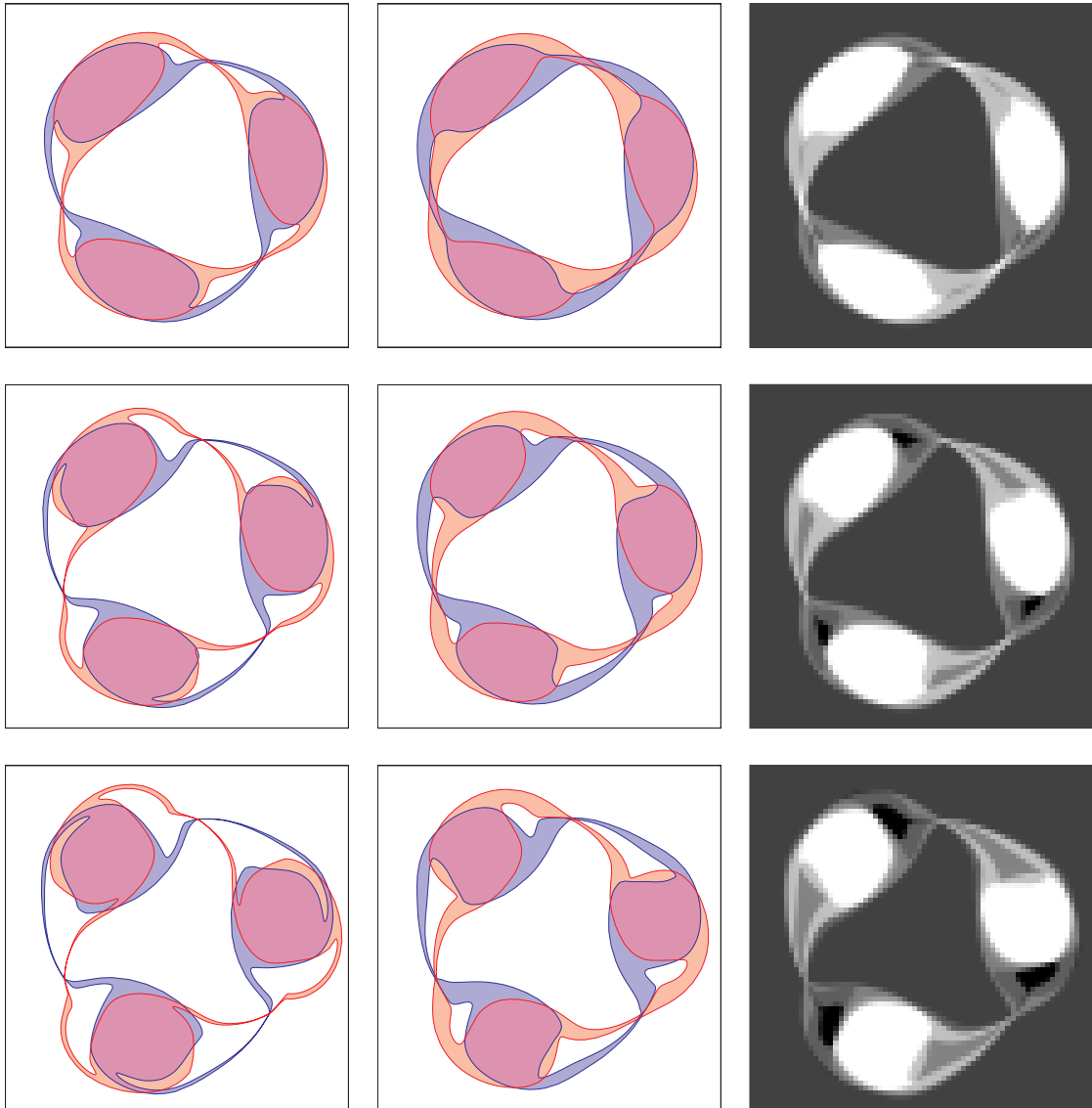


Figure 6.7: Above figures pertain to the simulation with $N = 5$ and $m = 3$. On the left we see the contours that contribute to the current density, with left $v_i = \pm 2.02v_t$ and in the middle figure with $v_i = \pm 0.95v_t$. On the right we see the total current density in the \mathbf{e}_z -direction, where it is noted that $j = 0$ away from the current layer. The top row corresponds to $t = 9\tau_A$, middle for $t = 10\tau_A$, bottom for $t = 11\tau_A$.

cases even to the complete halt of the x-point. This effect is present in all simulations that we performed that include a temperature gradient.

6.8 Discussion

This paper presented a novel method to study collisionless magnetic reconnection within the framework of the drift-kinetic equations. The discretization of the perturbed electron velocity distribution function both in space and in velocity space is possible because of the fact that the drift-kinetic equation can be cast in a purely advective form, as in Eq. (6.2). This is equivalent to the 2D Euler equation, describing the time evolution of vorticity, only now an infinite class of conserved quantities emerges because of the v_{\parallel} dependence of both f and Φ . This formalism was already studied in Ref. [7]. It enables us to use the powerful Contour Dynamics method [12, 15] to calculate the evolution in time of the boundaries of areas with a uniform electron distribution function. These boundaries, or contours, completely determine the entire dynamics of the system.

By imposing the moments of f , such as current density and temperature perturbations, the distribution of the support velocities that shape f_1 is still arbitrary. Once those are specified, the corresponding weights are fully determined. We have chosen the v_i to be the zeroes of the N -th Hermite polynomial, so that with N contours the $N + 1$ -th moment vanishes. This yields an intuitive distribution of the v_i , with more supports where there are more electrons, and vice versa. Thus, we construct a system where the distribution function becomes a foliation of a finite number of conserved fluid type distributions.

The numerical results obtained by the contour dynamics code can be divided into two groups: isothermal and non-isothermal. The isothermal results show to a high degree resemblance with the two-fluid simulations that were performed earlier. Qualitatively we see the same structures appear in the macroscopic fields. The magnitude of the growth rates and the timetraces of the amount of reconnected flux are also very much alike. However, in the kinetic case the distribution of small scales that appear in the nonlinear stage of the mode becomes broader, which can be considered to be the effect of thermal spreading. The development of small scale structures in the contours thus becomes an irreversible process, that is the spatial variant of velocity phase space mixing.

The non-isothermal results show evidence that supports the analysis that was presented in [9]. The magnetic island chain initially rotates with a velocity that is comparable to the diamagnetic velocity, as predicted in Eq. (6.25), and displays a shift δy with respect to the external perturbed field. The estimates given by Eqs. (6.25) and (6.26) are based on an equilibrium in slab geometry, but agree to the numerical results in cylindrical geometry in order of magnitude. Even though the simulations performed with a higher mode number m could be expected to bear more resemblance to the slab results, this does not seem to be the case when we compare the diamagnetic frequencies $\omega_{*,\text{est}}$ to $\omega_{*,\text{num}}$, or the linear shifts δy_{est} to δy_{num} . The non-diagonal elements in $\mathbf{M}_{\psi}, \mathbf{M}_{\phi}$ that account for the cylindrical coupling of the kink and tearing solution may play a role in the deviation of those results.

Finally, we observe that in the nonlinear stage of the mode the magnetic islands start to deform, and assume a ‘droplet’-like shape, as in [9]. This is attributed to the generation of a current in the island region as a consequence of the fact that fast electrons from the region in the plasma with higher temperature, here bounded by the contours at $r = R_1$, fill up the magnetic island faster than the electrons from the colder region, $r > R_2$. The analysis that predicted this effect was first described in [6].

The subsequent deceleration of the x-point is a consequence of the appearance of a region of negative current inside the magnetic island structure, as shown in Fig. 6.7. This exerts a repulsive magnetic force on the central positive current structure, thus pushing the x-point

away from the o-point. The negative current is an effect of the screening of the current density on a scale length d_e , which can result in a negative current when the contours that carry positive current are sufficiently close, so that the shielding currents overlap. The emergence of structures of a size of order d_e in contour dynamics has already been demonstrated as a peeling effect of monopolar current vortices [11].

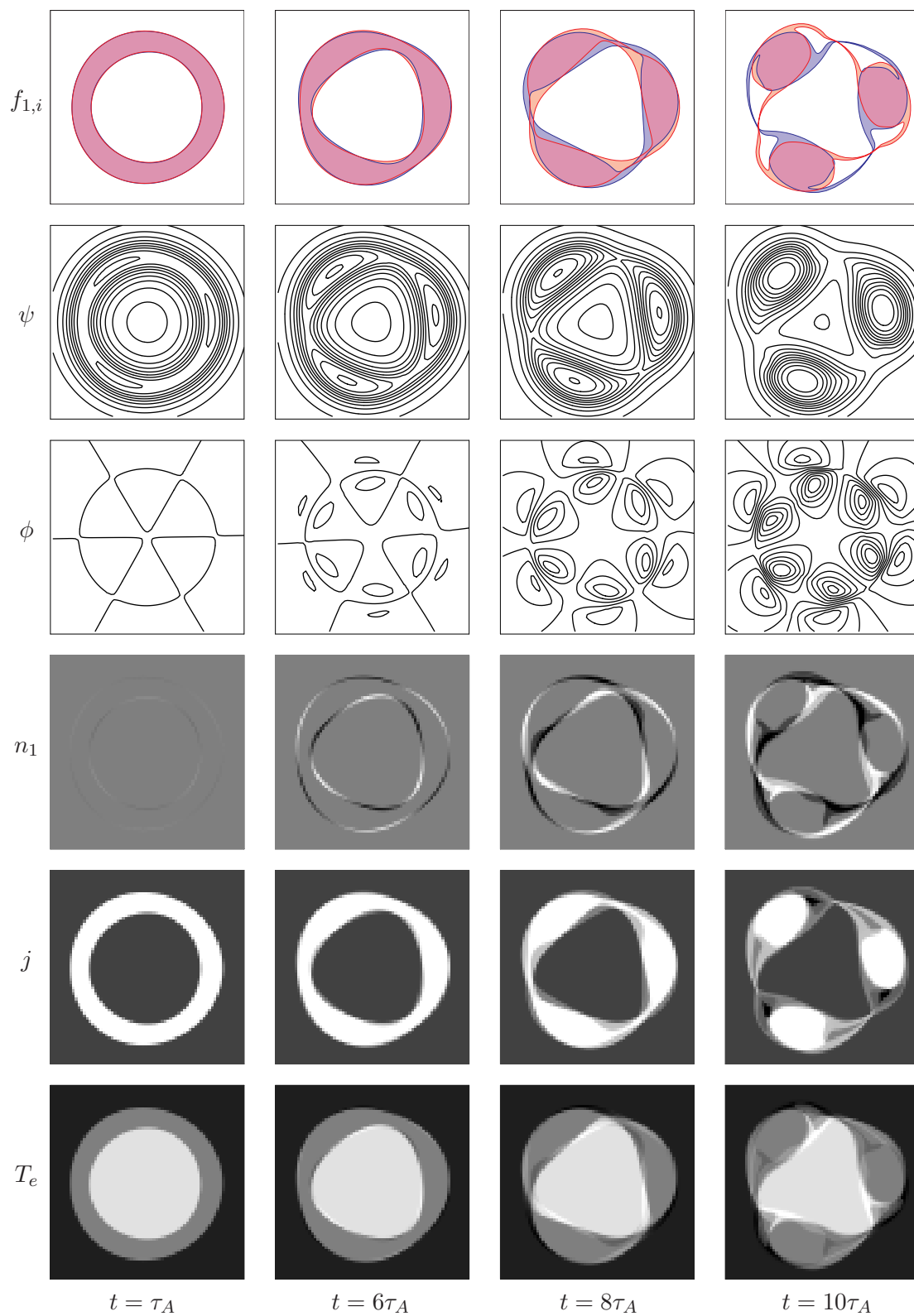
Acknowledgements

This work, supported by the European Communities under the contract of Association between EURATOM/FOM, was carried out within the framework of the European Fusion Programme with financial support from NWO. The views and opinions expressed herein do not necessarily reflect those of the European Commission.

References

- [1] V. M. Vasyliunas. *Rev. Geophys. Space Phys.*, 13:303, 1975.
- [2] T. G. Cowling. Magnetic Stars. In L. H. Aller and D. B. McLaughlin, editors, *Stellar Structure - Stars and Stellar Systems*, page 425, 1965.
- [3] M. Ottaviani and F. Porcelli. *Phys. Rev. Lett.*, 71:3802, 1993.
- [4] E. N. Parker. *Astrophys. J. Suppl.*, 8:177, 1963.
- [5] M. Ottaviani and F. Porcelli. *Phys. Plasmas*, 2:4104, 1995.
- [6] H. J. de Blank and G. Valori. *Plasma Phys. Control. Fusion*, 45:A309, 2003.
- [7] T. V. Liseikina, F. Pegoraro, and E. Yu. Echkina. *Phys. Plasmas*, 11:3535, 2004.
- [8] T. J. Schep, F. Pegoraro, and B. N. Kuvshinov. *Phys. Plasmas*, 1:2843, 1994.
- [9] E. V. van der Plas and H. J. de Blank. *Phys. Rev. Lett*, 98:265002, 2007.
- [10] J. Bergmans, B. N. Kuvshinov, V. P. Lakhin, and T. J. Schep. *Phys. Plasmas*, 7:2388, 2000.
- [11] J. H. Mentink, J. Bergmans, L. P. J. Kamp, and T. J. Schep. *Phys. Plasmas*, 12:052311, 2005.
- [12] P. W. C. Vosbeek and R. M. M. Mattheij. *J. of Comput. Phys.*, 133:222, 1997.
- [13] R. D. Hazeltine, M. Kotschenreuther, and P. J. Morrison. *Phys. Fluids*, 28(8):2466–2477, 1985.
- [14] B. N. Kuvshinov, V. P. Lakhin, F. Pegoraro, and T. J. Schep. *J. Plasma Physics*, 59:727, 1998.
- [15] N. J. Zabusky, M. H. Hughes, and K. V. Roberts. *J. of Comput. Phys.*, 30:96, 1979.

6.A Evolution of the macroscopic quantities



7 Discussion and conclusions

The chapters of this thesis are ordered in such a way that they are in roughly chronological order of the work done, as well as a logical order, going from simple to more detailed modelling, ending with the numerical nonlinear kinetic modelling of reconnecting modes. Here, the conclusions will be presented by subject, discussing the method, the linear, the nonlinear and the numerical results, indicating the role of a temperature gradient where applicable.

7.1 Method

In this thesis, the problem of collisionless magnetic reconnection is investigated using contour dynamics to study the drift-kinetic model of a strongly magnetized plasma [1, 2]. The term contour dynamics is used for a variety of approaches of the drift-kinetic equation, pertaining to either discretization in velocity space or real space, or both. When only discretization of the perturbed distribution function in velocity space is applied the drift-kinetic equation reduces to a fluid model. If only two or three discrete velocities are chosen, the result consists of the two-fluid drift-Alfvén equations [3].

In Chapter 3 and 4 the distribution function is discretized only spatially, leaving the smooth distribution in velocity space intact. The equilibrium that was considered could be regarded as being built up by an infinity of velocity contours that constitute current jumps located at two instances in space initially.

The number of contours necessary to model kinetic effects that differ from the fluid model is at least four. The discretization in velocity space is essentially arbitrary. When the value of a moment of the total distribution function is fixed this determines a combination of weights w_i of the support velocities v_i . We have chosen the orthogonal Hermite polynomials to determine the v_i .

The calculation of the fields that result from the locations of the contours using the Green's function, as given in Eq. (5.7), can be done using line integrals over the contributing patches instead of surface integrals. This has numerical benefits.

7.2 Linear stability

Exact linear dispersion relations for equilibria with slab and cylindrical geometries were obtained, Eq. (3.21) for the full drift-kinetic model and Eq. (5.21) for the two-fluid model respectively. It was found that a current layer in both slab and cylindrical geometry is unstable for a tearing mode with a sufficiently long wavelength. In slab geometry it can be proven for parameters within reasonable bounds that this is the only unstable mode present within the drift-kinetic model. This excludes beam-type instabilities.

We explicitly assume that $\beta \ll 1$, so that the Hall-term does not lead to whistler-type instabilities. This stresses that the formulation of the drift-kinetic model that is used throughout this thesis and the conclusions that are drawn are restricted to the low- β regime of the tokamak ordering.

Though in slab geometry only the tearing mode is unstable, the kink and tearing parities are coupled as a kinetic effect. In a cylindrical equilibrium, additional coupling occurs as a consequence of the geometry. This means that even if only the tearing mode is unstable, some

kink-character mixes into the mode. Thus, even without the kinetic kink-tearing coupling, in a cylinder there is no analogy of the left-right (anti-) symmetry of the straight current layer instability. This lack of symmetry in the cylinder results in the x- and o-points of a magnetic island chain to be at slightly different radii.

In slab geometry, the fluid and the kinetic approaches lead to the same stability boundary, which depends only on the ratios of the current layer width, the wavelength and the electron inertial skin depth. The kinetic and fluid dispersion relations have identical behaviour for high frequency phenomena with low plasma β . Away from the particle-wave resonance the fluid description of an isothermal plasma is sufficient to capture the essential dynamics.

Influence of a temperature gradient

When a small temperature gradient is present in the straight current layer, a modified dispersion relation is found. This leads to a different point of marginal stability, and a phase shift of the magnetic island chain with respect to the initial perturbation. This shift in the electron diamagnetic drift direction is calculated here for both the regime with small and large growth rate compared to the the diamagnetic drift frequency ω_* .

The oscillation in the eigenfunctions as reported in [4] is a manifestation of the same effect. The x -dependent shift in the y -direction results in an oscillatory behaviour of the eigenfunctions when they are viewed at a constant value of y .

7.3 Nonlinear effects of a temperature gradient

Once the growing magnetic island has reached a finite width, the difference between the mean particle velocities of electrons originating from the side with high and low temperature induces a current perturbation inside the magnetic island, breaking the up-down symmetry. This has already been shown for a simplified geometry in which only the neighborhood of the x-point is modelled [2], but is now established for a complete island chain. We observe that the magnetic island is deformed: the magnetic separatrix angle at one side of the x-point widens, whereas it narrows on the other side. This can also be understood as the x-point region experiencing a larger ω_* -drift than the o-point because the local temperature gradient at the x-point steepens due to the motion of flux surfaces towards the x-point.

Furthermore, it is shown that when the magnetic island saturates, i.e. for vanishing reconnection rate, a phase shift of the island with respect to the external perturbed fields remains. This result is established for saturated reconnecting instabilities. It is expected that it also applies to island chains caused by external magnetic perturbations e.g. by other island chains, leading to forced magnetic reconnection. The shift is relevant for the process of magnetic field ergodization, because it means that finite size, saturated islands can still be shifted with respect to other island chains. The consequences are still under investigation, as the effect can either be that this leads to a form of self-organization through feedback of diamagnetic shift and local temperature gradient, or leads to enhanced ergodization as some preliminary calculations seem to show. In this way this shift can have consequences for the confinement in tokamak plasmas in this regime.

7.4 Numerical results

The numerical simulation code for the two-fluid drift-Alfvén system has been used before, mainly for studying the interaction between current-vortex tubes [5, 6]. This thesis presents the first systematic investigation of reconnection using this method. The annular current layer equilibrium could straightforwardly be studied, as this is equivalent to a four-vortex system with partly overlapping vortex regions. The initial linear growth rates that are in good agreement with the analytic values that are given by the linear dispersion relation.

In the nonlinear regime, the reconnection rate was seen to saturate. After some time, no flux was reconnected anymore, although the contours clearly did not reach a steady state. At this point the contours become very filamentary and stretched, and are advected to areas that are far from their initial location. This amounts to an irreversible transfer of energy to small scales.

In cylindrical geometry there is no symmetry between the inner and outer contours, compared to the left and right contour in slab geometry. The breaking of this symmetry prevents the x-point from collapsing, which is the process where the characteristic length scales keep shrinking indefinitely, almost resembling finite-time singularity, as reported in [2]. The shrinking part of the contours are advected away from each other, preventing a scale collapse.

It was seen that by varying the ratio of the electron thermal velocity and the growth rate, the electrons follow the field lines more closely for higher temperatures, and follow the $\mathbf{E} \times \mathbf{B}$ drift streamlines more closely for lower temperatures. This extends a result that was reported for slab geometry [7]. We also observed that when the electrons deviate strongly from the magnetic separatrix, the highly localized current density deforms the separatrix, stretching the x-point to a ribbon-like structure.

The code was successfully extended to handle an arbitrary number of N contours. There is a high degree of qualitative and quantitative agreement between the two-fluid simulations and the kinetic simulations there where it was expected from an analytical point of view, as for isothermal applications and away from particle-wave resonances the kinetic equations are only slightly different from the fluid equations.

A notable difference is that for higher N , we observe that the profiles of the macroscopic fields become smoother. This is due to the fact that the different contours are advected by different stream functions, so that they generally spread out. The contours that correspond to the largest $|v_i|$ are the first ones to become thin and filamentary, leading to small scales at different places for different v_i , thus transferring energy to smaller scales in an irreversible manner. This spatial mixing at small scales is the contour dynamics version of kinetic phase mixing.

The contours that correspond to the largest $|v_i|$ require the most computational effort. This may be solved by using contour surgery, a technique already available for the single-fluid version of the contour dynamics code [6]. However, the criteria for contour surgery in plasma modelling should be different from those in hydrodynamics or monopolar problems, as in general the plasma model deals with overlapping and intersecting contours, as opposed to the hydrodynamical case. The present implementation would remove all the contours that are stretched to thin filaments, but in practice the x-point region in an advanced stage of the simulation consists of such contours. Applied indiscriminately, contour surgery would remove the locus of collisionless reconnection from the simulation.

Influence of a temperature gradient

When the weights of the contours are chosen such that the contours correspond to a temperature jump, the chain of magnetic islands starts to rotate with a frequency that agrees with an estimated diamagnetic frequency given by the modified linear dispersion relation for a slab equilibrium. Also the analytically predicted phase shift with respect to the external perturbations is found, and of the same order of magnitude as analytically estimated. The fact that we do not have a very good correspondence may be attributed to the different geometry of the equilibrium, resulting in a.o. coupling effects.

When the mode starts to saturate, the x-points rotate faster than the o-points and far-field perturbations, resulting in the deformation of the magnetic island. The start of the acceleration coincides with the constriction of the contours, which results in a higher local temperature gradient and therefore a higher diamagnetic frequency. This acceleration is eventually slowed down or even stopped as a result of the emergence of a region of negative current inside the magnetic island. This is a skin or shielding effect, that leads to a current structure of approximately the size of d_e , that experiences repulsion from the larger positive current channel around the o-point.

7.5 Discussion and outlook

The application of contour dynamics to non-thermal kinetic effects in magnetic reconnection is new. There are many more approaches to model collisionless magnetic reconnection kinetically, such as particle simulations [8, 9], that can resolve the dynamics of the parallel electron motion during reconnection.

Before we can make claims as to the correctness of the qualitative description of the magnetic field and quantitative results of growth rates compared to those measured in real tokamak plasma discharges, we shall need to compare the data to results of other studies that use the same model, and focus on the same unstable initial equilibria, but choose a different approach to determine the temporal evolution of the system. The same set of drift-kinetic equations was studied in [1], where it was applied to a double periodic equilibrium. Similar qualitative features were observed, such as the shape of the v_z -dependent streamfunctions. The study of the same formulation of the drift-kinetic system is also discussed in [10] and Ref. [45] therein. Here, the breaking of symmetry of the tearing parity is already reported.

Though the model that was developed was primarily intended to generate a better understanding of the various aspects of collisionless reconnection and the influence of temperature gradients on this process, the research is ultimately aimed at contributing to the feasibility of nuclear fusion as a commercial energy source. Therefore, the applicability of the results presented here on current or future tokamak plasma conditions needs to be investigated more thoroughly.

Furthermore, during the research that is presented here, several issues came up that are still unresolved.

With respect to linear stability, we have studied the two-fluid dispersion relation in cylindrical geometry in Chapter 5. This relation, given in Eq. (5.21), formally seems to give way to overstable modes: modes that are oscillatory and damped or growing at the same time. However, no parameters have been found that generate a mode in this regime, so the question rises whether they exist or not. Also, we can obtain a kinetic dispersion relation for an annular current layer, but not in a closed form, as in Chapter 4, Eq. (4.11). Still it can be useful

to solve a kinetic dispersion relation numerically, to be able to quantify possible differences with its fluid counterpart.

The parameter space of the system of equations that was used throughout this work is huge. One particular regime that is worth investigating is that of modes closer to marginal stability. In Chapter 6 we have studied the temperature gradient effects on a mode with a significantly larger growth rate than the diamagnetic frequency. In Chapter 3 analysis of the nonlinear kinetic behaviour of a tearing mode in slab geometry near marginal stability showed that it matches the case for $\gamma \gg |\omega_*|$, and it is important to investigate whether numerical simulations support this model.

The possibilities of the contour dynamics method are numerous. In this thesis we have only studied equilibria with two interfaces, viz. slab and annular current regions, which yielded basic results on reconnecting instabilities. By adding more contours at different locations many more interesting phenomena can be studied. If we add more contours that induce current density inside and outside of the annulus, we could construct a more realistic current profile, simulating an equilibrium that corresponds more to a tokamak q -profile, the magnetic winding number as a function of radius. We could also add contours inside of the current annulus that do not make a current jump, but do impose small temperature differences, causing a smoother temperature gradient instead of two discrete temperature jumps. And if we would make one extra current jump of similar size, the equilibrium would correspond to a q -profile with a local minimum, so with a region of negative magnetic shear, that could be unstable with respect to a double tearing mode. This is the case when two flux surfaces with a finite distance in between have the same magnetic winding number, and can become unstable to perturbations of the same poloidal mode number. Experimental evidence of such modes exists [11], and they are of particular relevance to future tokamak operation scenarios since regions of negative magnetic shear also may improve the magnetic confinement properties of a tokamak.

At this moment the numerical code is based on the idea that there is one equilibrium electron distribution function, and the contours constitute a perturbation of this distribution based on imposing moments. However, the fact that resistivity decreases with temperature, or v_{\parallel} , means that a totally different population of electrons might build up with a velocity far from the thermal velocity of the equilibrium distribution. These electrons are also called *runaway* electrons [12], and may have a significant influence on reconnection processes in the core of the plasma. They require an extension of our models to include magnetic curvature effects, which seems much more feasible than including e.g. ∇B -effects. It needs to be demonstrated whether phase-space effects such as (inverse) Landau damping are indeed captured by the contour dynamics method, and if so, how many contours are needed to do this properly.

At present, the contour dynamics method, while limited to very specific plasma models and initial conditions, is computationally much more efficient than methods based on grids or basis functions in (v_{\parallel}, x, y) -space. Still, the numerical code can be improved and optimized on several accounts. At this moment, all the contours interact with each other, and are treated on equal footing. However, when the discretization level N increases, the contours with largest $|v_i|$ represent a decreasing number of electrons. Because of their large velocity, they may still have a substantial effect on the general structure of the magnetic field, but the interaction with other small fractions of fast electrons may prove superfluous. Exactly those contours also experience the highest degree of filamentation, which means that they need the largest number of nodes to support structure of the contour. Cutting back on the interactions between the contours with the largest $|v_i|$ saves considerable computational cost.

Furthermore, the code is not completely free of numerical dissipation, which is manifested as a slight decrease in the total area enclosed by a contour. This is a result of the algorithm that decides when and where to place the additional supporting nodes on the contour, based on the local curvature and the proximity of a contour segment with the same v_i .

In conclusion, the kinetic contour dynamics method opens up a whole new area of investigation, with some exciting new physics that can be studied. The numerical code is directly mirrored in tractable analysis, making it easy to interpret the various outcomes, that come at relatively low computational cost. The results thus obtained can be compared to the results that are generated by the codes that model the reconnection region as a boundary layer [1, 10].

Much remains to be learned about the importance of magnetic turbulence in anomalous electron heat transport in tokamaks. Large gyrokinetic [13, 14], gyro-fluid, and two-fluid [15] simulations of tokamak turbulence and anomalous transport typically use spatial resolutions that do not resolve the width of a typical reconnection layer in a near-collisionless plasma. If reconnection plays a significant role in anomalous transport, e.g. via magnetic turbulence, an open problem is how to include these effects of reconnection in such large scale turbulence simulations. The approach in the present thesis, to focus on the increase of fundamental understanding of (in this case, collisionless) reconnection, is based on the view that such understanding may lead to basic models of reconnection processes that are suitable for inclusion into larger turbulence and transport models.

References

- [1] T. V. Liseikina, F. Pegoraro, and E. Yu. Echkina. *Phys. Plasmas*, 11:3535, 2004.
- [2] H. J. de Blank and G. Valori. *Plasma Phys. Control. Fusion*, 45:A309, 2003.
- [3] T. J. Schep, F. Pegoraro, and B. N. Kuvshinov. *Phys. Plasmas*, 1:2843, 1994.
- [4] G. Ara, B. Basu, B. Coppi, G. Laval, M. N. Rosenbluth, and B. V. Waddell. *Ann. Phys.*, 112:443, 1978.
- [5] J. Bergmans, B. N. Kuvshinov, V. P. Lakhin, and T. J. Schep. *Phys. Plasmas*, 7:2388, 2000.
- [6] J. H. Mentink, J. Bergmans, L. P. J. Kamp, and T. J. Schep. *Phys. Plasmas*, 12:052311, 2005.
- [7] E. Cafaro, D. Grasso, F. Pegoraro, F. Porcelli, and A. Saluzzi. *Phys. Rev. Lett.*, 80:4430, 1998.
- [8] R. Horiuchi and T. Sato. *Phys. Plasmas*, 4(2):277–289, 1997.
- [9] M. Tanaka. *Phys. Plasmas*, 3(11):4010–4017, 1996.
- [10] M. Ottaviani, N. Arcis, D. F. Escande, D. Grasso, P. Maget, F. Militello, F. Porcelli, and W. Zwingmann. *Plasma Phys. Control. Fusion*, 46(12B):B201–B212, 2004.
- [11] H. P. Furth, P. H. Rutherford, and H. Selberg. *Phys. Fluids*, 16(7):1054–1063, 1973.

- [12] R. M. Kulsrud, Y.-C. Sun, N. K. Winsor, and H. A. Fallon. Runaway electrons in a plasma. *Phys. Rev. Lett.*, 31(11):690–693, 1973.
- [13] Z. Lin, T. S. Hahm, W. W. Lee, W. M. Tang, and R. B. White. *Science*, 281:1835 – 1837, 1998.
- [14] W. M. Nevins, J. Candy, S. Cowley, T. Dannert, A. Dimits, W. Dorland, C. Estrada-Mila, G. W. Hammett, F. Jenko, M. J. Pueschel, and D. E. Shumaker. *Phys. Plasmas*, 13:122306, 2006.
- [15] P. Mantica, A. Thyagaraja, J. Weiland, G. M. D. Hogewij, and P. J. Knight. *Phys. Rev. Lett.*, 95(18):185002, 2005.

A Cylindrical limit of slab results

The linear two-fluid dispersion relation of the tearing mode that is found in cylindrical geometry should become identical to the fluid version of the one found in the periodic slab. To understand how the dispersion relation of the current annulus relates to the one of the current slab, we have to take the limit $R \rightarrow \infty$, or

$$R_i = R_0 \pm L, \quad r = R_0 + x,$$

and let R_0 go to infinity. First we shall compare the equilibria, and then the actual mode.

A.1 Equilibrium

There are three regions to be considered,

I: $r < R_1$, the inner region, or $x < -L$,

II: $R_1 < r < R_2$ or $-L < x < L$, the current region,

III: $r > R_2$, the outer region, or $x > L$,

Here, it is convenient to adopt some more slab nomenclature,

$$j = \text{sign}(r - R_1)j_- - \text{sign}(r - R_2)j_+,$$

so that

$$\begin{array}{ll} \text{I} & j_1 + j_2 = j_+ - j_-, \\ \text{II} & j_2 = j_+ + j_-, \\ \text{III} & 0 = -j_+ + j_-. \end{array}$$

We see that because of the asymmetry between inner and outer region that the current patch has an extra degree of freedom in which it is possible that $j_1 + j_2 \neq 0$. For proper comparison, however, we can put $j_1 = -j_2$.

In region I:

$$\begin{aligned} \psi_{\text{I}} &= \psi_{01} + \psi_{02}, \\ &= -d_e^2 \left\{ (j_1 + j_2) - j_1 \frac{R_1}{d_e} \text{K}_1\left(\frac{R_1}{d_e}\right) \text{I}_0\left(\frac{r}{d_e}\right) - j_2 \frac{R_2}{d_e} \text{K}_1\left(\frac{R_2}{d_e}\right) \text{I}_0\left(\frac{r}{d_e}\right) \right\}. \end{aligned}$$

We note that

$$\begin{aligned} (\text{detail}) \quad &= \frac{R_1}{d_e} \text{K}_1\left(\frac{R_1}{d_e}\right) \text{I}_0\left(\frac{r}{d_e}\right), \\ &= \frac{R_0 - L}{d_e} \text{K}_1\left(\frac{R_0 - L}{d_e}\right) \text{I}_0\left(\frac{R_0 + x}{d_e}\right), \\ R_0 \rightarrow \infty \quad &\approx \frac{R_0 - L}{d_e} \frac{e^{-(R_0 - L)/d_e}}{\sqrt{2(R_0 - L)/d_e}} \frac{e^{(R_0 + x)/d_e}}{\sqrt{2(R_0 + x)/d_e}}, \\ &! \frac{R_0 - L}{d_e} \frac{e^{-(R_0 - L)/d_e}}{\sqrt{2(R_0 - L)/d_e}} \frac{e^{(R_0 + x)/d_e}}{\sqrt{2(R_0)/d_e}}, \\ &\approx \frac{1}{2} e^{(x+L)/d_e}. \end{aligned}$$

where at the ! we reckoned that

$$\lim_{R \rightarrow \infty} \partial_x e^{R+x} \gg \lim_{R \rightarrow \infty} \partial_x \frac{1}{\sqrt{R+x}},$$

and took the limits for large arguments and fixed m of $I_m(x), K_m(x)$,

$$\begin{aligned} I_m(x) &\Rightarrow \frac{e^x}{\sqrt{2\pi x}}, \\ K_m(x) &\Rightarrow \frac{e^{-x}}{\sqrt{2x/\pi}}, \end{aligned}$$

So,

$$\psi_I/d_e^2 = -(j_1 + j_2) + \frac{1}{2}j_1 e^{(x+L)/d_e} + \frac{1}{2}j_2 e^{(x-L)/d_e}.$$

In region II:

$$\begin{aligned} \psi_{II} &= \psi_{01} + \psi_{02}, \\ &= -d_e^2 \left\{ (j_2) + j_1 \frac{R_1}{d_e} I_1\left(\frac{R_1}{d_e}\right) K_0\left(\frac{r}{d_e}\right) + j_2 \frac{R_2}{d_e} K_1\left(\frac{R_2}{d_e}\right) I_0\left(\frac{r}{d_e}\right) \right\}. \end{aligned}$$

As before, we approximate

$$\begin{aligned} \text{(detail)} \quad &= \frac{R_1}{d_e} I_1\left(\frac{R_1}{d_e}\right) K_0\left(\frac{r}{d_e}\right), \\ &= \frac{R_0 - L}{d_e} I_1\left(\frac{R_0 - L}{d_e}\right) K_0\left(\frac{R_0 + x}{d_e}\right), \\ R_0 \rightarrow \infty \quad &\approx \frac{R_0 - L}{d_e} \frac{e^{(R_0-L)/d_e}}{\sqrt{2(R_0 - L)/d_e}} \frac{e^{-(R_0+x)/d_e}}{\sqrt{2(R_0 + x)/d_e}}, \\ &! \frac{R_0 - L}{d_e} \frac{e^{(R_0-L)/d_e}}{\sqrt{2(R_0 - L)/d_e}} \frac{e^{-(R_0+x)/d_e}}{\sqrt{2(R_0)/d_e}}, \\ &\approx \frac{1}{2} e^{-(x+L)/d_e}. \end{aligned}$$

So,

$$\psi_{II}/d_e^2 = -j_2 - \frac{1}{2}j_1 e^{-(x+L)/d_e} - \frac{1}{2}j_2 e^{(x-L)/d_e}.$$

As for region III,

$$\begin{aligned} \psi_{III} &= \psi_{01} + \psi_{02}, \\ &= -d_e^2 \left\{ j_1 \frac{R_1}{d_e} I_1\left(\frac{R_1}{d_e}\right) K_0\left(\frac{r}{d_e}\right) + j_2 \frac{R_2}{d_e} I_1\left(\frac{R_2}{d_e}\right) K_0\left(\frac{r}{d_e}\right) \right\}. \end{aligned}$$

This becomes

$$\psi_{III}/d_e^2 = -\frac{1}{2}j_1 e^{-(x+L)/d_e} - \frac{1}{2}j_2 e^{-(x-L)/d_e}.$$

If we were to put $j_2 = -j_1 = 2j_0$,

$$\begin{aligned} \psi_I/d_e^2 &= -j_0 \left\{ e^{(x+L)/d_e} - e^{(x-L)/d_e} \right\}, \\ \psi_{II}/d_e^2 &= -2j_0 + j_0 \left\{ e^{-(x+L)/d_e} - e^{(x-L)/d_e} \right\}, \\ \psi_{III}/d_e^2 &= j_0 \left\{ e^{-(x+L)/d_e} - e^{-(x-L)/d_e} \right\}, \end{aligned}$$

When we compare this to the slab equilibrium,

$$\begin{aligned}\psi_{\text{I}}/d_e^2 &= -j_0 \left\{ e^{(x+L)/d_e} - e^{(x-L)/d_e} \right\}, \\ \psi_{\text{II}}/d_e^2 &= -2j_0 + j_0 \left\{ e^{-(x+L)/d_e} + e^{(x-L)/d_e} \right\}, \\ \psi_{\text{III}}/d_e^2 &= j_0 \left\{ e^{-(x+L)/d_e} - e^{-(x-L)/d_e} \right\},\end{aligned}$$

we see there we get the same result as the solution in the slab,

$$\psi_{0,\text{slab}} = -\frac{d_e^2}{2} j_0 \left[\text{sign}(x+L)(1 - e^{-|x+L|/d_e}) - \text{sign}(x-L)(1 - e^{-|x-L|/d_e}) \right].$$

A.2 Perturbations

Here, it is prudent to consider the radius of the patch as of being built up by the wavelength of the perturbation, so

$$R_0 = m \frac{\lambda}{2\pi} = \frac{m}{k}.$$

The perturbations of the electrostatic potential can be written (e.g. for $r < R_1$),

$$\begin{aligned}\phi_{1,m} &= \left(\frac{r}{R_1} \right)^m, & &= \left(\frac{R_0 + x}{R_0 - L} \right)^m, \\ &= \left(\frac{m + kx}{m - kL} \right)^m, & &= \left(1 + \frac{k}{m}(x+L) \right)^m, \\ &\Rightarrow e^{k(x+L)},\end{aligned}$$

just as for $r > R_1$

$$\begin{aligned}\phi_{1,m} &= \left(\frac{R_1}{r} \right)^m, & &= \left(\frac{R_0 - L}{R_0 + x} \right)^m, \\ &= \left(\frac{m - kL}{m + kx} \right)^m, & &= \left(\frac{1}{1 + \frac{k}{m}x} - \frac{k}{m}L \right)^m, \\ &\Rightarrow e^{-k(x+L)},\end{aligned}$$

for $m \rightarrow \infty$, or

$$\phi_{1,m} \sim e^{-k|x+L|}.$$

The magnetic perturbations of the equilibrium are to be handled with a bit more care. Because of the fact that the radius goes to infinity but the wavelength of the perturbation goes to zero,

$$\psi_m \sim \text{I}_m\left(\frac{R_0 + x}{d_e}\right) = \text{I}_m\left(\frac{m + kx}{kd_e}\right),$$

both the order of the Besselfunction as the argument go to infinity. Following [1], we have that for large m (9.7.7, 9.7.8),

$$\text{I}_m(mz) \sim \frac{1}{\sqrt{2\pi m}} \frac{e^{m\eta}}{(1+z^2)^{1/4}} \left\{ 1 + \sum_{k=1}^{\infty} \frac{u_k(t)}{m^k} \right\}, \quad (\text{A.1})$$

$$\text{K}_m(mz) \sim \sqrt{\frac{\pi}{2m}} \frac{e^{-m\eta}}{(1+z^2)^{1/4}} \left\{ 1 + \sum_{k=1}^{\infty} (-)^k \frac{u_k(t)}{m^k} \right\}, \quad (\text{A.2})$$

and (9.7.9, 9.7.10),

$$I'_m(mz) \sim \frac{1}{\sqrt{2\pi m}} \frac{e^{m\eta}}{z} (1+z^2)^{1/4} \left\{ 1 + \sum_{k=1}^{\infty} \frac{v_k(t)}{m^k} \right\}, \quad (\text{A.3})$$

$$K'_m(mz) \sim -\sqrt{\frac{\pi}{2m}} \frac{e^{-m\eta}}{z} (1+z^2)^{1/4} \left\{ 1 + \sum_{k=1}^{\infty} (-)^k \frac{v_k(t)}{m^k} \right\}, \quad (\text{A.4})$$

where

$$\eta = \sqrt{1+z^2} + \ln \frac{z}{1+\sqrt{1+z^2}}, \quad t = \frac{1}{\sqrt{1+z^2}},$$

and $u_k(t)$ and $v_k(t)$ come from Debye's asymptotic expansions of J_m , [1], 9.3.9. If we take $\psi_{1,m}(r, \theta)$ for $r < R_1$ as an example, we have

$$\psi_{1,m} \sim \frac{R_1}{d_e} K_m\left(\frac{R_1}{d_e}\right) I_m\left(\frac{r}{d_e}\right),$$

so if we split this up in the constant and the variable part for legibility, and we expand around R_0 ,

$$\begin{aligned} \frac{R_1}{d_e} K_m\left(\frac{R_1}{d_e}\right) &= \frac{m-kL}{kd_e} K_m\left(\frac{m-kL}{kd_e}\right), \\ &\approx \frac{m-kL}{kd_e} K_m\left(\frac{m}{kd_e}\right) - \frac{kL}{kd_e} K'_m\left(\frac{m}{kd_e} + \dots\right), \\ &\approx \frac{m}{kd_e} \left[\sqrt{\frac{\pi}{2m}} \frac{e^{-m\eta}}{\sqrt[4]{1+(kd_e)^{-2}}} \left\{ \dots \right\} \right. \\ &\quad \left. + \frac{kL}{kd_e} \sqrt{\frac{\pi}{2m}} \frac{e^{-m\eta}}{z} \sqrt[4]{1+(kd_e)^{-2}} \left\{ \dots \right\} + \dots \right], \\ &= \sqrt{\frac{\pi}{2m}} e^{-m\eta} \left\{ \dots \right\} \frac{m}{kd_e} \sqrt{\frac{k}{mk_e}} (1+k_e L + \dots), \end{aligned}$$

where $\{\dots\}$ is shorthand for the $u_k(t)$ expansion, we assumed $m \gg kL$, and the ratio k/k_e enters through

$$\sqrt[4]{1+(kd_e)^{-2}} = \sqrt{\frac{k_e}{k}}.$$

Similarly, the other part is

$$\begin{aligned} I_m\left(\frac{r}{d_e}\right) &= I_m\left(\frac{m+kx}{kd_e}\right), \\ &\approx I_m\left(\frac{m}{kd_e}\right) + \frac{kx}{kd_e} I'_m\left(\frac{m}{kd_e} + \dots\right), \\ &\approx \sqrt{\frac{1}{2\pi m}} \frac{e^{m\eta}}{\sqrt[4]{1+(kd_e)^{-2}}} \left\{ \dots \right\} + \frac{kx}{kd_e} \sqrt{\frac{1}{2\pi m}} \frac{e^{m\eta}}{z} \sqrt[4]{1+(kd_e)^{-2}} \left\{ \dots \right\} + \dots, \\ &= \sqrt{\frac{1}{2\pi m}} e^{m\eta} \left\{ \dots \right\} \sqrt{\frac{k}{mk_e}} (1+k_e x + \dots), \end{aligned}$$

so if we multiply the above

$$\begin{aligned}\psi_{1,m} &\sim \frac{1}{2} \frac{m}{kd_e} \frac{k}{mk_e} (1 + k_e L + \dots)(1 + k_e x + \dots), \\ &\approx \frac{1}{2k_e d_e} e^{k_e(x+L)}.\end{aligned}$$

Note that the $\{\dots\}$ expansion is irrelevant because all terms with $k > 0$ go to zero as m^{-k} for $m \rightarrow \infty$. Furthermore is the somewhat complex expression for η also circumvented because the modified Besselfunctions always show up in pairs.

For the expression for $r > R_1$, the I_m and K_m are reversed, and we get two minus signs,

$$\psi_{1,m} \sim \frac{1}{2k_e d_e} e^{-k_e(x+L)},$$

so, compactly, for large radius but small wavelength, (large m),

$$\psi_{1,m} \sim \frac{1}{2k_e d_e} e^{-k_e|x+L|}.$$

A.3 Boundary conditions: the dispersion relation

To see if the dispersion relation Eq. (5.21) becomes the dispersion relation of the fluid case of the current slab for large radius, or large m , we will fill in the boundary conditions at $r = R_i$ and take the proper limit.

First, we look at the terms with the $I_i(x_1)K_i(x_2)$ for finite (fixed) i , and at the same radius j :

$$\begin{aligned}\bar{R}_j I_{ij} K_{ij} &= \frac{R_j}{d_e} I_i\left(\frac{R_j}{d_e}\right) K_i\left(\frac{R_j}{d_e}\right), \\ &\approx \frac{m \pm kL}{kd_e} \frac{e^{(m \pm kL)/kd_e}}{\sqrt{2(m \pm kL)/kd_e}} \frac{e^{-(m \pm kL)/kd_e}}{\sqrt{2(m \pm kL)/kd_e}}, \\ &= \frac{1}{2},\end{aligned}$$

for $m \rightarrow \infty$, i fixed, $j \in \{1, 2\}$. If the radii are different ($j \neq h$), we get

$$\begin{aligned}\bar{R}_j I_{ij} K_{ih} &= \frac{R_j}{d_e} I_i\left(\frac{R_j}{d_e}\right) K_i\left(\frac{R_h}{d_e}\right), \\ &\approx \frac{m \pm kL}{kd_e} \frac{e^{(m \pm kL)/kd_e}}{\sqrt{2(m \pm kL)/kd_e}} \frac{e^{-(m \mp kL)/kd_e}}{\sqrt{2(m \mp kL)/kd_e}}, \\ &= \frac{1}{2} e^{\pm 2L/d_e},\end{aligned}$$

For terms with $I_{mj}K_{mh}$ it also depends. When $j = h$ we have

$$\begin{aligned}\bar{R}_j I_{mj} K_{mj} &= \frac{R_j}{d_e} I_m\left(\frac{R_j}{d_e}\right) K_m\left(\frac{R_j}{d_e}\right), \\ &\approx \frac{m \pm kL}{kd_e} \frac{1}{\sqrt{2\pi m}} \frac{e^{m\eta}}{\sqrt[4]{1 + (kd_e)^{-2}}} \left(e^{\pm k_e L}\right) \sqrt{\frac{\pi}{2m}} \frac{e^{-m\eta}}{\sqrt[4]{1 + (kd_e)^{-2}}} \left(e^{\mp k_e L}\right), \\ &\approx \frac{1}{2k_e d_e},\end{aligned}$$

using the same relations as before, and for $j \neq h$ we have

$$\begin{aligned}\bar{R}_j \mathbf{I}_{mj} \mathbf{K}_{mh} &= \frac{R_j}{d_e} \mathbf{I}_m \left(\frac{R_j}{d_e} \right) \mathbf{K}_m \left(\frac{R_h}{d_e} \right), \\ &\approx \frac{m \pm kL}{kd_e} \frac{1}{\sqrt{2\pi m}} \frac{e^{m\eta}}{\sqrt[4]{1 \pm (kd_e)^{-2}}} \left(e^{\pm k_e L} \right) \sqrt{\frac{\pi}{2m}} \frac{e^{-m\eta}}{\sqrt[4]{1 + (kd_e)^{-2}}} \left(e^{\pm k_e L} \right), \\ &\approx \frac{1}{2k_e d_e} e^{-2k_e L}.\end{aligned}$$

See for details of this limit the notation given in the previous (sub)section. The limits for the elements containing ratios of R_1 and R_2 are readily evaluated as

$$\left(\frac{R_1}{R_2} \right)^m = \left(\frac{m - kL}{m + kL} \right)^m \Rightarrow e^{-2kL}.$$

So we have

$$\left(\frac{R_1}{R_2} \right)^m \Rightarrow e^{-2kL}, \quad (\text{A.5})$$

$$R_j \mathbf{I}_{m1} \mathbf{K}_{m2} \Rightarrow \frac{1}{2} \frac{e^{-2k_e L}}{k_e d_e}, \quad (\text{A.6})$$

$$R_j \mathbf{I}_{mi} \mathbf{K}_{mi} \Rightarrow \frac{1}{2} \frac{1}{k_e d_e}, \quad (\text{A.7})$$

$$\begin{aligned}R_j \mathbf{I}_{kl} \mathbf{K}_{gh} &\Rightarrow \frac{1}{2}, && \text{for } k, g \text{ fixed, } l = h, \\ &\Rightarrow \frac{1}{2} e^{-2L/d_e}, && \text{for } k, g \text{ fixed, } l \neq h, (l = 1, \quad h = 2).\end{aligned} \quad (\text{A.8})$$

and $m/R_j \rightarrow kd_e$ for $m \rightarrow \infty$. Now we can fill in the matrix elements of the cylindrical two-fluid dispersion relation Eq. (5.21), given by

$$\omega^4 + \omega^2 \text{Tr}(\mathbf{M}) + \det(\mathbf{M}) = 0,$$

with

$$\begin{aligned}\mathbf{M}_\psi &= -\frac{v_A^2}{2} \begin{pmatrix} j_1 \mathbf{I}_{m1} \mathbf{K}_{m1} - \hat{j}_1 & j_1 \mathbf{I}_{m1} \mathbf{K}_{m2} \\ j_2 \mathbf{I}_{m1} \mathbf{K}_{m2} & j_2 \mathbf{I}_{m2} \mathbf{K}_{m2} - \hat{j}_2 \end{pmatrix} \\ \mathbf{M}_\phi &= m \begin{pmatrix} j_1 + 2m \hat{j}_1 \rho_s^2 / d_e^2 & j_1 (R_1 / R_2)^m \\ j_2 (R_1 / R_2)^m & j_2 + 2m \hat{j}_2 \rho_s^2 / d_e^2 \end{pmatrix}\end{aligned}$$

and

$$\begin{aligned}\hat{j}_1 &= \frac{\psi'_0(R_1)}{R_1} = j_1 \mathbf{I}_{11} \mathbf{K}_{11} + j_2 \mathbf{I}_{11} \mathbf{K}_{12} \frac{R_2}{R_1}, \\ \hat{j}_2 &= \frac{\psi'_0(R_2)}{R_2} = j_1 \mathbf{I}_{11} \mathbf{K}_{12} \frac{R_1}{R_2} + j_2 \mathbf{I}_{12} \mathbf{K}_{12},\end{aligned}$$

using the substitutions (A.5) - (A.8). This gives

$$\begin{aligned} M_{\psi,11} &= \frac{v_A^2}{4} \left(j_1 \left(1 - \frac{1}{k_e d_e} \right) + j_2 e^{-2L/d_e} \right), \\ M_{\psi,12} &= -\frac{v_A^2}{4} \frac{j_1}{k_e d_e} e^{-2k_e L}, \\ M_{\psi,21} &= -\frac{v_A^2}{4} \frac{j_2}{k_e d_e} e^{-2k_e L}, \\ M_{\psi,22} &= \frac{v_A^2}{4} \left(j_2 \left(1 - \frac{1}{k_e d_e} \right) + j_1 e^{-2L/d_e} \right), \end{aligned}$$

and

$$\begin{aligned} M_{\phi,11} &= j_1 k d_e \left(1 + \frac{\rho_s^2}{d_e^2} k d_e \left(1 + \frac{j_2}{j_1} e^{-2L/d_e} \right) \right), \\ M_{\phi,12} &= j_1 k d_e e^{-2kL}, \\ M_{\phi,21} &= j_2 k d_e e^{-2kL}, \\ M_{\phi,22} &= j_2 k d_e \left(1 + \frac{\rho_s^2}{d_e^2} k d_e \left(1 + \frac{j_1}{j_2} e^{-2L/d_e} \right) \right), \end{aligned}$$

and calculate the corresponding dispersion relation. Setting also $j_1 = -j_2$ we should arrive at the exact same dispersion relation as given in Eq. (3.16). Because in that case $M_{\psi,11} = -M_{\psi,22}$, $M_{\psi,12} = -M_{\psi,21}$, $M_{\phi,11} = -M_{\phi,22}$ and $M_{\phi,12} = -M_{\phi,21}$, the dispersion relation reduces to

$$\omega^4 - 2(M_{\psi,11}M_{\phi,11} + M_{\psi,12}M_{\phi,21})\omega^2 + (M_{\psi,11}^2 - M_{\psi,12}^2)(M_{\phi,11}^2 - M_{\phi,21}^2) = 0,$$

or

$$\begin{aligned} \mathcal{D}(\omega) &= (\omega^2 - (M_{\psi,11} - M_{\psi,12})(M_{\phi,11} - M_{\phi,21})) \times \\ &\quad (\omega^2 - (M_{\psi,11} + M_{\psi,12})(M_{\phi,11} + M_{\phi,21})) \\ &= 0. \end{aligned}$$

If we expand these expressions (use the shorthand $\epsilon = 1 - \exp(-2L/d_e)$) we get the solutions

$$\omega_{\pm}^2 = -\frac{v_A^2}{4} j_0^2 \frac{k}{k_e} \left(k_e d_e \epsilon - (1 \pm e^{-2k_e L}) \right) \left(\frac{\rho_s^2}{d_e^2} k d_e \epsilon + (1 \mp e^{-2kL}) \right),$$

which are exactly the same as Eq. (3.16) from the current slab analysis. Here, ω_+ corresponds to the tearing configuration and ω_- to the kink.

References

- [1] M. Abramowitz and I. A. Stegun. *Handbook of mathematical functions*. 1964.

Summary

A long time ago, mankind was a pretty pathetic species. We were cold, dependent on the sun for light and heat, and our diet was abhorrent. Fortunately, Prometheus felt sorry for us, and presented us the gift of fire. Zeus was not too keen on letting humans set fire to just about everything they could, and Prometheus paid dearly for his act of compassion by being chained to a mountain ridge in the Caucasus, where his liver got eaten out every single day by a large eagle, after which it grew back on again. Mankind, on the other hand, were having a ball [1].

To a certain extent, this is still the situation today. Mankind sets fire to anything that provides comfort, to make it warm when it is cold, to make it cold when it is warm, using small explosions inside cylinders of a car to make a baby sleep because it likes the humming sound. And of course, Prometheus would still be up there somewhere if it were not for Heracles. But in this day and age, we start to feel that the gift of Prometheus may no longer be enough to lavish our lust for energy and we start to realize that we need to redirect our looting frenzy towards a new source of energy if we want to sustain the luxury and abundance as we have known the last decades. Of some sources we can see the bottom, of some we are not sure under what restrictions we will be able to buy them, and in general we can see the side-effects of the waste that we produce.

Therefore, we turn to Helios, the Sun. Not to become dependent once again on when and where he will shine, but to usher him to reveal his secrets, so that we can make a sun of our own. He has been relatively forthcoming in providing us with the theory of what is supposed to happen: in a process called *nuclear fusion* two light atomic nuclei collide and merge into a heavier one. The reaction products carry the energy that is released in such a process as kinetic energy, i.e. by going extremely fast. The process that seems the most likely or feasible candidate to produce fusion power in a reactor here on earth is between two hydrogen isotopes, deuterium (D) and tritium (T) to yield helium (what's in a name) and a neutron,



Deuterium is a hydrogen isotope, and consists of a nucleus with a positively charged proton and a neutron and a negatively charged electron surrounding it, whereas tritium has a proton and two neutrons in the nucleus, which makes it unstable, so that it suffers from radio-active decay.

If we know what the reaction is, what is stopping us? The resources will not run out for the next couple of thousand years, as lithium is widely available to breed tritium from the neutron shower inside the reactor, and deuterium can be extracted from sea water easily for many more thousands of years. Also the reaction products are relatively clean: helium is used to fill balloons at children's parties, and the neutrons do cause radio-active activation of the steel of which the reactor is built, but this is mildly radio-active and can be safely stored.

By blowing up innocent islands in the southern Pacific in the early 1950s it has been proven in a most dramatic way that nuclear fusion does indeed work, and ever since the challenge has become to master this process so that we can make it evolve in a controlled and orderly, *non-violent* fashion. This is non-trivial, because the nuclei need to overcome the electric repulsion, or the Coulomb interaction, to get close enough to merge. This requires a very high mean velocity, or equivalently, temperature. At these high temperatures the

electrons are separated from their nuclei, and the fuel mixture becomes a (hot) *plasma*, in which the nuclei, or ions, and electrons can move independently but under the influence of each others electromagnetic field.

This brings us back to Helios once more. Confiding in us as far as the energy source was concerned may have seemed relatively safe. Zeus' wrath is not yet upon him, as for us it is not a matter of fusing the particles, but *how* we do this to create an efficient cycle. The Sun confines plasma in its core at roughly 15 million degrees Kelvin, with its huge gravity field pulling the plasma inward, which leads to a relatively slow, smouldering reaction.

We have to do better. And hotter. We want to maintain a fusion reaction with minimum input power and maximum yield, which means that we have to heat the D-T plasma to 150 million degrees Kelvin. To keep it there, away from cold, melting walls, our present day fusion reactor concepts make use of a magnetic field. Charged plasma particles in a magnetic field describe gyrating orbits around magnetic field lines, so if the magnetic field does not touch the walls of the containing vessel, neither will the particles. This can be achieved by giving the vessel and the magnetic field a toroidal shape.

The best candidates for delivering net fusion power in the near future is called the *tokamak*, a machine that is based on producing a strong, dominant, magnetic field in the *toroidal* direction (the long way around the torus), and the ability to draw a current through the plasma, either inductively or non-inductively, resulting in a smaller *poloidal* component. The now helical magnetic field lines are thus neatly organized on nested concentric surfaces, also called *flux surfaces*.

Here is where magnetic reconnection enters the story. When the magnetic field would conserve this nested topology, like a toroidal magnetic Russian matruschka doll, the confinement of the particles and the heat would be excellent. But it does not. With all those particles racing along magnetic field lines, the plasma actually becomes a wildly turbulent, swirling mass, pushing those flux surfaces to and fro. When magnetic field lines that are not aligned are pushed together, not only pressure builds up, but the magnetic tension of the field as well, resulting in a large electric field hurling the electrons in place to shield the surfaces from one another. If somehow this sheet of electrons does not do its shielding job properly, the magnetic field finds its own way to release the pressure, by untying the magnetic field lines and connect them to other field lines in a way that there is less magnetic stress. This is called *magnetic reconnection*. It happens when e.g. the current sheet between the flux surfaces degrades by resistivity, so when the electrons and the ions collide so much that the sheet becomes too weak, or by turbulent eddies dislocating the meandering electrons. The once neatly organized flux surfaces break up, and what used to be in- and outside the flux surface is no longer clear: regions appear that no longer belong to the original surfaces, and the new boundaries are now called *separatrices*. In a toroidal plasma these regions form helical ribbons around the original surface, and when one looks at a cross section of the plasma, they can be identified as a chain of *magnetic islands*, with an o-point in the middle, and an x-point where the field lines break open and reconnect again. The release of magnetic tension then may result in a pressure drop, sucking more plasma and magnetic field into this pit of magnetic annihilation, and thus the process can feed itself, in a vicious cycle that because of the tearing of the flux surfaces is called a *tearing mode*.

The effects of such a process are destructive for the confinement of hot particles that should stay in the core of the plasma to eventually fuse together, which is the whole idea behind a fusion reactor. It may result in (more) turbulence, it may induce other flux surfaces to start tearing up, and when the magnet islands start to overlap this leads to magnetic field

ergodization, which means that field lines become randomly displaced from their original flux surface. They can fill up a three dimensional volume, and because particles race along them, they can race out of the plasma (not the other way around, because the pressure inside is much higher). When the islands grow really large, chances are that the plasma ends in a disruption. All the energy that was stored in the magnetic field is released at once, leading to considerable damage to the fusion reactor.

This may sound as if we have a pretty good idea of what is going on during reconnection inside a tokamak plasma. But, as was mentioned before, a fusion plasma is very hot. Very hot. In very hot plasmas the electron mass plays an important role in causing of magnetic reconnection. In that case, we call this process *collisionless magnetic reconnection*, as in cooler plasmas a more straightforward reconnection mechanism is more important, caused by the collisions between the plasma particles. It was shown that collisionless reconnection can explain the fast reconnection rates that have been measured in the centre of tokamak plasmas. The model that is studied in this thesis relies on this mechanism for magnetic reconnection.

To model the effect that electrons do not collide but can have different temperatures, the equations that determine the dynamics of electrons in a plasma with a dominant magnetic field in one direction, make use of a distribution function that specifies how many electrons have a certain velocity parallel to the magnetic field with respect to the bulk of the plasma. They look like the equations that determine vorticity (the amount of rotation) in a two dimensional, shallow, fluid system. Vorticity is generally dragged along or *advected* by a stream function, or a flow field, like storms are advected by the wind. The difference is that in this equation, the *drift-kinetic* equation, for each parallel velocity we have a different type of vorticity, advected by a different stream function. To keep the metaphor of the weather, it is analogous to having a different wind for each height, where height would correspond to parallel velocity. This correspondence is very real: indeed storms are advected differently at different heights, and are described by very similar equations.

This observation opens the way to make use of similar tools as in fluid theory to study plasma, such as *contour dynamics*. Vorticity in two dimensions can be thought of of being built up like a topographical map: a mountain is described with a line or contour that corresponds to 100 meter altitude, and within this contour lies another contour corresponding to 200 meter altitude and so forth. The same is true for vorticity. One can draw a contour that corresponds to a certain amount of vorticity, and within a contour that corresponds to more vorticity etc. The locations of these contours may change in time, as vorticity evolves, but it is clear that these contour lines cannot cross: on a map one can think of strangely shaped mountains, but with vorticity this is just impossible. For plasma, we can draw these contours for every different type of vorticity, i.e. for every parallel velocity. For different types, they are allowed to cross, for the same type they may not. Very important is the fact that in this way, all of the plasma dynamics is now captured by the location of the contours, and the interaction between them and themselves.

Back to parallel electron velocities. A contour now describes the jump in the parallel electron velocity. If we construct an area where electrons move with respect to the bulk in a certain direction, this is equivalent to saying that there is a current density. Actually, it is a bit more subtle, because electrons interact with the plasma by their electrical charge and, if they move, by the magnetic field they generate, so we have ‘pure’ current if n less electrons move in the negative direction and n electrons more move in the positive direction (or vice versa).

If we construct a straight or annular layer with a current density in this way, this layer

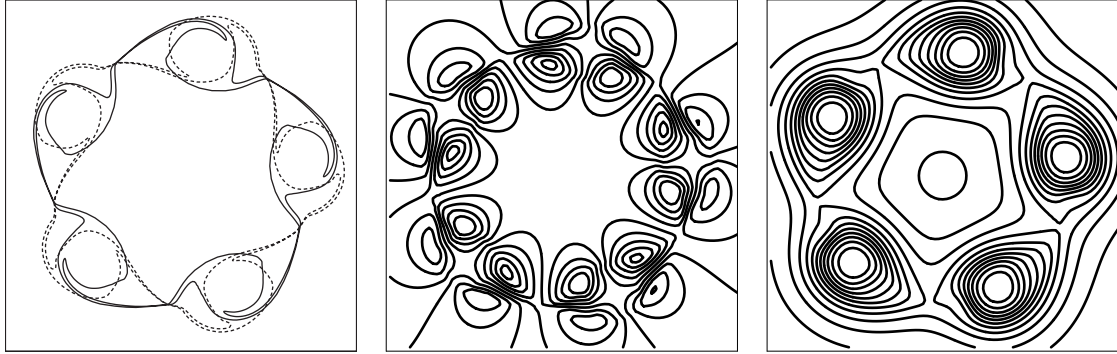


Figure S.1: From left to right: the contours of the electrons with the highest velocities for a simulation where the mode number of the perturbation is $m = 5$, and the distribution function is replaced by $N = 5$ contours that mark the boundaries of the 5 corresponding parallel electron velocities. The middle figure shows the isolines of the electrostatic potential (or the altitude lines of the electric field) along which slow electrons drift, and the right figure shows the isolines of the magnetic potential, or a top view of the flux surfaces along which the magnetic field is confined. Fast electrons tend to move along these lines.

stays just as it is. Nothing happens. All the equations need an excursion from symmetry, because there is no gradient or gradual change anywhere, except at the location of the jumps. We can only excite or perturb the system at these contours, and then calculate what happens. There are three possibilities: when the contours are dislocated they can bend back again, resulting in a (damped) wave, like in a guitar string. Then the system is called stable. The contours can be moved and still nothing happens, like a ball on a horizontal plane, which is called metastable. But if the contours are moved and they start moving in the same direction of the perturbation, the perturbation grows exponentially. The system is then linearly unstable.

In Chapter 3 and 4 the stability of an equilibrium that consists of a straight slab of plasma with in the middle a region with an electrical current is investigated. It is found that it can be unstable with respect to a tearing mode, and *only* to a tearing mode. This leads to a chain of magnetic islands through the middle of the current layer, whose growth rate depends on the amount of current, the magnitude of the magnetic field and the electron mass and density. The equation that links the linear growth rate to the other parameters is the linear *dispersion relation*.

When a temperature difference across this layer is applied, having warmer plasma on one side of the current layer than on the other, the island chain starts to move in the direction perpendicular to both the magnetic field and the direction of the temperature gradient. And if the islands have already obtained a finite width, and the dynamics of the island becomes dependent on the width of the island, so in the nonlinear regime, a shift with respect to the external perturbation remains. This shift is important, because if there are multiple chains of magnetic islands next to each other, the local temperature gradient will depend on the location of the islands. This can lead to self-organization of magnetic islands, so that they fit better, or so that they start to overlap sooner. The onset of magnetic field ergodization can depend on the way these islands shift with respect to each other. The magnetic island

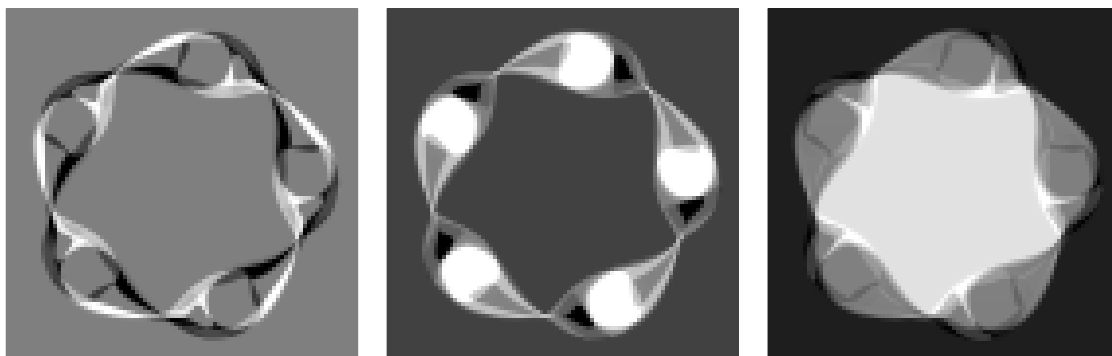


Figure S.2: These are resp. the density, current and temperature distributions of the same mode as shown in the previous figure.

becomes ‘droplet’ (or onion) shaped, because the x-point is shifted more than the o-point.

In Chapter 5, the linear stability analysis of Chapter 3 and 4 is applied to an equilibrium that is circular instead of straight. This was done for the two-fluid variant of the drift-kinetic equation, using only two contours to describe the perturbed parallel velocity of the electrons. For this shape of equilibria, the computer code that was developed in Eindhoven could be used to calculate the evolution of those contours in time. The growth rates that we found in this way showed good agreement with the theoretical predictions made by the linear dispersion relation. The numerical code is fully nonlinear, which means that it can calculate the evolution of the contours self-consistently, without assuming that they only move a little bit. One purely nonlinear effect is that after a certain amount of time, the reconnection stops, or in other words, the magnetic island saturates. And though the two-fluid model is essentially isothermal, it is possible to study the effect of the ratio of the thermal velocity of the electrons and the mode velocity with which the island grows. The simulations show that when the electrons move fast compared to the velocity of the mode, they move more along the separatrices of the magnetic island, following the magnetic field lines, whereas if they are slow compared to the mode, they drift along isolines of the electrostatic potential, perpendicular to the electric field.

The numerical code was extended so that we could use more than two types of contours, and simulate the effect of a temperature gradient on the process of collisionless magnetic reconnection. The rotation of the island chain with the diamagnetic velocity and the deformation of the magnetic island are found to be in pretty good agreement with the predictions that were made in Chapter 3 and 4. The x-point, that rotates faster than the o-point because there the same temperature difference occurs over a shorter distance, is observed to decelerate again after some time. This is attributed to the appearance of a region with negative current density that pushes the x-point away from the o-point, because the o-point corresponds to a region with positive current.

This concludes the work that was done for this thesis, which was done as part of a project that should contribute to a working nuclear fusion device. But browsing through the contents of this thesis the image of a power plant may not surface very often. However, magnetic reconnection can lead to some of the most violent phenomena in magnetized plasmas, that need to be controlled if we want to use nuclear fusion as an energy source. It has the power

to reshape the magnetic configuration within the plasma, ultimately destroying confinement altogether, and it may have the subtle, even useful effect of removing the Helium ‘ash’ out of the core of the plasma, saving it from extinction.

It is essential to have a deeper knowledge of this process to be able to control it or prevent it from happening. We have to understand how it works, what the electrons that are involved in this process do and how they influence the evolution of the reconnection process, and how important parameters like the temperature gradient may play a role, keeping in mind that a tokamak generates the largest temperature gradient known in the universe. This was the main question that was addressed in this thesis.

References

- [1] Hesiod. *Theogony*.

Samenvatting

Lang geleden was de mensheid maar een erbarmelijke soort. We hadden het koud, waren afhankelijk van de zon voor licht en warmte en ons dieet was weezinwekkend. Gelukkig had Prometheus medelijden met ons, en gaf ons macht over het vuur. Zeus was het hier duidelijk niet helemaal mee eens, aangezien we alles wat ook maar een beetje wilde branden in lichterlaaie hebben gezet, en liet Prometheus boeten voor zijn verraad. Hij ketende hem aan de Kaukasus vast, en een grote arend at dagelijks van zijn lever, die vervolgens 's nachts gewoon weer aangroeide. De mensheid daarentegen kon zijn lol niet op [1].

Tot op zekere hoogte is dit nog steeds aan de gang. Mensen verbranden alles wat maar branden wil om comfortabel te kunnen leven, om het warm te maken als het koud is, om het koud te maken als het warm is, om kleine explosies in cilinders te veroorzaken in de motor van een auto, zodat een baby van het licht ronkende geluid in slaap kan vallen. En Prometheus zou nog aan de berg vastgeketend zijn als Heracles hem er niet een keer afgehaald had. Tegenwoordig is het offer van Prometheus wellicht niet meer genoeg om onze honger naar energie te stillen. Het besef gloort dat we een nieuwe bron van energie zullen moeten gaan plunderen om de levensstijl die we ons de afgelopen decennia hebben aangemeten te kunnen blijven volhouden. Van sommige bronnen ervaren we inmiddels de eindigheid, van andere weten we nog niet of we ze kunnen veroorloven, en van de meeste beginnen we de gevolgen van het grootschalige gebruik te zien.

Dus wenden wij ons tot Helios, de zon. Niet om weer afhankelijk te worden van waar en wanneer hij schijnt, maar om hem de geheimen te ontfutselen hoe hij aan zijn energie komt, zodat we zelf een zon kunnen maken. Wat er in theorie zou moeten gebeuren heeft hij al een keer losgelaten: in een proces dat we *kernfusie* noemen smelten twee lichte atoomkernen samen tot een zwaardere. De energie die daarbij vrijkomt wordt aan de reactieproducten meegegeven als kinetische energie (ze bewegen heel snel). Het meest veelbelovende fusieproces dat we in een reactor hier op aarde zouden kunnen bewerkstelligen is tussen twee waterstof-isotopen, deuterium en tritium, wat bij versmelting (niet geheel toevallig) helium en een neutron oplevert,



Deuterium lijkt op waterstof, maar heeft een extra neutron in zijn kern zitten, en tritium heeft een proton en twee neutronen in zijn kern, waardoor het instabiel is en radio-actief kan vervallen.

Als we weten hoe het werkt, wat houdt ons dan nog tegen? Er is genoeg brandstof voor duizenden jaren als we lithium gebruiken om tritium te genereren met de neutronen die uit de reactor komen. Deuterium kan schier oneindig uit zeewater gewonnen worden. Het afval, of de as, is relatief schoon: helium wordt gebruikt voor kinderballonnen. De neutronen maken de reactor weliswaar voor tamelijk korte tijd licht radio-actief, maar als de reactor afgebroken wordt kan het afval veilig opgeslagen worden.

Dat fusie inderdaad werkt, is op nietsontziende wijze aangetoond door het her en der oplazen van een atol in de Grote Oceaan. Sinds die tijd ligt de uitdaging met name daarin om dit proces op een gecontroleerde en niet al te gewelddadige manier te laten verlopen. Het probleem is dat de atoomkernen elkaar elektrisch afstoten, zodat we een hele hoge temperatuur nodig hebben om de deeltjes genoeg snelheid te geven om de elektrische afstoting te overwinnen. Onder deze omstandigheden worden de brandstoffen een (heet) *plasma*, waarin

de atoomkernen los kunnen bewegen van de elektronen, maar wel onder invloed van elkaars elektromagnetische veld.

En zo komen we weer bij Helios. De toorn van Zeus heeft hem nog niet geraakt, aangezien we alleen nog maar weten wat er zich ongeveer afspeelt in het middelpunt van de zon. Het plasma wordt hier door het enorme zwaartekrachtsveld onder niet al te hoge temperaturen (pakweg 15 miljoen graden) bij elkaar gehouden, zodat de fusiereacties daar langzaam verlopen en *smeulend* genoemd mogen worden. Hoe we op aarde een efficiënte reactor in elkaar moeten zetten is een heel ander verhaal.

Op aarde moet dat vooral heter. Om een fusiereactie aan de gang te houden willen we een minimale hoeveelheid energie toevoegen en er zoveel mogelijk uitkrijgen, moet het D-T plasma tot zo'n 150 miljoen graden worden gestookt. Om dat voor elkaar te krijgen moet het plasma weggehouden worden van de koude en smeltende wanden van de reactor, en dat wordt tegenwoordig gedaan met behulp van een magnetisch veld. Ieder geladen plasmadeeltje draait in een kurkentrekkerbaan rond een magnetische veldlijn, zodat als de veldlijn de wand niet raakt, de deeltjes dat ook niet doen. Dit is mogelijk als we de reactor en het veld een torus-vorm geven.

Op dit moment is de *tokamak* de beste kandidaat om binnen afzienbare tijd fusiestroom te kunnen leveren aan het elektriciteitsnet. Het idee is dat magneetspoelen een sterk magnetisch veld in de toroidale richting (de lange weg rond de torus) genereren, en dat een toroidale stroom een kleiner, poloidaal (de korte weg rond de torus) veld maakt. De veldlijnen gaan zo helisch de torus rond, en blijven keurig op tweedimensionale, geneste *flux-oppervlakken* liggen.

Nu komt magnetische reconnectie in beeld. Als de geneste topologie van het magnetische veld behouden zou blijven, als een soort magnetische Russische matruschka-pop, zou de opsluiting van deeltjes en warmte geweldig zijn. Maar dat is niet het geval. Met al die plasmadeeltjes die langs de magneetveldlijnen spoeden, wordt het plasma een kolkende, turbulente massa die de flux-oppervlakken heen en weer schudden. Als magneetveldlijnen met een verschillende richting tegen elkaar aan geduwd worden, wordt niet alleen de druk daar heel hoog, maar ook de magnetische energie. Dit leidt tot nieuwe elektrische stromen in het plasma die het magnetische veld zó veranderen dat de flux-oppervlakken intact blijven. Als deze beschermende stroom zijn werk niet goed doet, kan de magnetische energie vrijkomen doordat veldlijnen elkaar naderen, openbreken, en op andere manieren weer versmelten. Dit heet *magnetische reconnectie*. Dit gebeurt als de stroomlaag bijvoorbeeld afgebroken wordt doordat de deeltjes teveel botsen, oftewel door resistiviteit, of als turbulente wervels de elektronen uit hun baan schudden. De eerst zo keurig geneste flux-oppervlakken vallen lokaal uiteen, en het is niet langer duidelijk wat de binnen- en wat de buitenkant van die flux-oppervlakken was: er ontstaan gebieden in het plasma die niet meer bij de oorspronkelijke oppervlakken horen, en de randen daarvan heten nu *separatrices*. In een toroidaal plasma zijn deze nieuwe gebieden helische slingers rond het oorspronkelijke oppervlak, en als we naar een doorsnede van de plasma-torus kijken zien ze eruit als *magnetische eilanden*, met een o-punt in het midden en een x-punt waar de veldlijnen opengesneden en weer aan elkaar geknoopt zijn. Doordat er daar nu minder magnetische druk heerst, kan er opnieuw plasma, met daarin magnetische veldlijnen, naartoe gezogen worden, zodat het proces zichzelf blijft voeden in een vicieuze cirkel die in het Engels een *tearing mode* genoemd wordt vanwege het openscheuren van de flux-oppervlakken.

De gevolgen van dit proces zijn dramatisch voor de opsluiting van hete deeltjes die in een reactor, net als in de zon, zouden moeten fuseren in het centrum van het plasma. Het kan

leiden tot meer turbulentie, het kan ervoor zorgen dat flux-oppervlakken op andere locaties open gaan breken, en als de magnetische eilanden van verschillende oppervlakken elkaar raken kunnen die ook weer openbreken: veldlijnen liggen dan niet meer op een oppervlak maar kunnen dwars door het plasma heen liggen, zodat de deeltjes die langs de magneetveldlijnen racen ook zo het plasma uit kunnen racen. En als de eilanden te groot worden kan het plasma eindigen in een disruptie, waarbij alle energie die in het magnetische veld zit in een keer losbarst, wat stevige schade aan de binnenwand van een reactor kan toebrengen.

Tot dusver lijkt het alsof we tamelijk goed weten wat er zoal aan de hand is tijdens reconnectie in een tokamakplasma. Maar een fusieplasma is heet. Echt heet. In hele hete plasma's is een belangrijke oorzaak van reconnectie te herleiden tot de massa van de elektronen. In dat geval noemen we dat *botsingsloze magnetische reconnectie*, omdat in minder hete plasma's een meer voor de hand liggend reconnectiemechanisme belangrijker is, dat veroorzaakt wordt door de botsingen tussen de plasmadeeltjes. Het is aangetoond dat in hele hete tokamakplasma's botsingsloze reconnectie de experimentele waarnemingen kan verklaren. Het model dat in dit proefschrift bestudeerd is, maakt gebruik van dit mechanisme om reconnectie te veroorzaken.

De methode die we gebruikt hebben om dit proces te bestuderen is nieuw. Elektronen van verschillende veldlijnen botsen nauwelijks met elkaar maar kunnen wel verschillende temperaturen hebben. Om deze eigenschappen te kunnen combineren maken we gebruik van vergelijkingen die gebaseerd zijn op een distributiefunctie die bepaalt hoeveel elektronen een bepaalde snelheid parallel aan het magneetveld hebben. Deze vergelijkingen lijken op de vergelijkingen die de vorticeiteit (de mate van draaiing of werveling) bepalen in een tweedimensionale of ondiepe vloeistof. Over het algemeen wordt vorticeiteit meegeleurd door de stroming, zoals stormen worden meegevoerd door wind. Het verschil is dat in de plasmavergelijkingen, of om precies te zijn de *drift-kinetische* vergelijkingen, we voor elke parallelle snelheid een andere soort vorticeiteit hebben, die wordt meegevoerd door zijn eigen snelheidsveld. Het is te vergelijken met dat er op elke hoogte andere wind waait. De overeenkomst met weersystemen is niet uit de lucht gegrepen: stormen worden inderdaad op verschillende hoogtes door verschillende winden meegevoerd, wat beschreven kan worden met vergelijkbare vergelijkingen.

Deze beschrijving maakt het mogelijk om voor onze plasmafysica gebruik te maken van *contourdynamica*, zoals die ook toegepast wordt in de vloeistofdynamica. Als we vorticeiteit in twee dimensies willen beschrijven, kunnen we dat doen zoals we een topografische kaart met hoogteverschillen maken: een berg ziet er bijvoorbeeld uit als een hoogtelijn of contour die aangeeft waar het 100 meter hoog is, daarbinnen ligt een contour die aangeeft waar het 200 meter hoog is etcetera. Dat kan ook met vorticeiteit. We kunnen een contour tekenen waarbinnen massa met een bepaalde snelheid ronddraait, en daarbinnen een contour die aangeeft dat daar massa sneller ronddraait, die dus duidt op een hogere vorticeiteit. Deze contourlijnen mogen elkaar niet snijden. Een berg kan een rare vorm hebben, zodat hoogtelijnen dat wel zouden kunnen, maar voor vorticeiteit kan dit niet. Voor plasma kunnen we voor elk type vorticeiteit, dus voor elke parallelle snelheid, een eigen contour trekken, waarbij contouren van dezelfde parallelle snelheid elkaar niet mogen kruisen, maar van verschillende snelheid wel. Alle dynamica van het plasma is nu vastgelegd in de ligging van deze contouren en hun onderlinge interacties.

Terug naar plasma en parallelle snelheden. Een contour beschrijft in dit model een sprong in de parallelle elektronensnelheid. Als een gebied binnen zo'n contour ligt, hebben elektronen daar een snelheid ten opzichte van de gemiddelde snelheid, en dus heerst daar een stroomdichtheid. Eigenlijk ligt het iets subtieler, aangezien elektronen met hun lading een

elektrische en door hun snelheid een magnetische interactie hebben. We kunnen zeggen dat er alleen een stroomdichtheid is als er evenveel elektronen extra in de positieve richting bewegen als er minder in de negatieve richting bewegen (of vice versa).

Als we op deze manier een rechte stroomlaag of een ronde stroomring in een plasma aanleggen gebeurt er niks. Hij blijft daar gewoon liggen, omdat de contouren de enige plekken zijn waar iets verandert, en die zo'n symmetrische vorm hebben. Als we die contouren een klein zetje geven kunnen we berekenen wat er gebeurt. Er zijn globaal drie mogelijkheden: als de contouren van hun plek getrokken zijn buigen ze weer terug, wat leidt tot een (gedempte) golf, zoals in een gitaarsnaar. Dan is het systeem stabiel. Als de contouren verschoven worden en er gebeurt nog steeds niets, zoals een bal op een horizontaal veld, heet het systeem metastabiel. Maar als de contouren nadat ze verplaatst zijn verder bewegen in de richting van de verplaatsing zodat de verstoring exponentieel groeit, heet het systeem (lineair) instabiel.

In Hoofdstuk 3 en 4 is de stabiliteit onderzocht van een evenwicht in een oneindige, periodieke vlakke laag met in het midden een stroomlaag. Hier is aangetoond dat in deze laag de tearing mode instabiel is. Deze mondt uit in een keten van magnetische eilanden in het midden van die laag. De groeisnelheid is afhankelijk van de oorspronkelijke stroomdichtheid, de sterkte van het magnetische veld en de elektronenmassa en -dichtheid. De vergelijking die de groeisnelheid en golflengte koppelt aan de andere parameters is de *dispersierelatie*.

Als er een temperatuurgradiënt wordt aangebracht over de laag, zodat het plasma aan de ene kant warmer is dan aan de andere, begint de eilandketen te bewegen in de richting die loodrecht staat op die van het magneetveld en van de temperatuurgradiënt. En als de eilanden al een zekere dikte hebben, zodat de dynamica van het eiland afhankelijk wordt van zijn dikte, blijft deze verschuiving ten opzichte van de verstoring in het buitengebied bestaan. Deze verschuiving is belangrijk omdat als er verschillende eilandketens naast elkaar ontstaan, de lokale temperatuurgradiënt afhankelijk zal zijn van de onderlinge ligging van de eilandketens. Dit kan zorgen voor zelforganisatie van de eilanden zodat ze beter in elkaar passen, of juist eerder overlappen. De mate van ergodisatie van het magnetische veld kan dus afhangen van de manier waarop de eilanden ten opzichte van elkaar verschuiven. Onder invloed van een temperatuurgradiënt wordt het magnetische eiland 'druppel'- (of ui-)vormig, omdat het x-punt sneller beweegt dan het o-punt.

In Hoofdstuk 5 wordt de lineaire stabiliteitsanalyse van Hoofdstuk 3 en 4 toegepast op een evenwicht dat cirkelvormig is in plaats van recht. Hiervoor hebben we de twee-vloeistof variant van de drift-kinetische vergelijking toegepast, waarbij slechts twee soorten contouren worden gebruikt. Voor deze vorm kon de simulatiesoftware gebruikt worden die aan de TU Eindhoven ontwikkeld is om de beweging van contouren als functie van de tijd te berekenen. De groeisnelheden die op deze manier gevonden zijn zijn in goede overeenstemming met de theoretische waarden die volgen uit de lineaire dispersierelatie. De numerieke code is volledig niet-lineair, wat betekent dat deze de evolutie van de contouren geheel zelf-consistent kan uitrekenen zonder uit te gaan van slechts kleine afwijkingen van de beginposities. Eén puur niet-lineair effect is dat na een bepaalde tijd de reconnectie stopt, met andere woorden dat er saturatie van het magnetische eiland optreedt. En hoewel het twee-vloeistof model essentieel isotherm is, is het mogelijk om de invloed van de verhouding van de thermische snelheid van de elektronen ten opzichte van de snelheid van de verstoring te bestuderen. Simulaties laten zien dat als de elektronen snel gaan vergeleken met de snelheid van de verstoring, ze meer de magneetveldlijnen volgen, terwijl als de elektronen langzaam zijn ten opzichte van de verstoring ze meer langs lijnen van constante elektrische potentiaal drijven, dus loodrecht op het elektrische veld.

De numerieke code is uitgebreid zodat we meer dan twee soorten contouren kunnen gebruiken. Zo kunnen we door de sprongen in de parallelle snelheid niet exact even groot te maken aan de twee kanten van de stroomlaag de invloed van een temperatuurgradiënt op botsingsloze magnetische reconnectie bestuderen. De rotatie van de eilandketen met de diamagnetische snelheid en de vervorming van de magnetische eilanden komen best goed overeen met de voorspellingen die gemaakt zijn in hoofdstukken 3 en 4 voor de vlakke laag. Het x-punt, dat op een gegeven moment sneller beweegt dan het o-punt omdat hetzelfde temperatuurverschil over een kleinere afstand wordt verdeeld, wordt na een tijdje weer afgeremd. Dit wordt toegeschreven aan het verschijnen van een gebied met negatieve stroomdichtheid, dat het x-punt wegduwt van het o-punt, aangezien het o-punt een gebied met positieve stroomdichtheid is.

Hoewel het onderzoek waaruit dit proefschrift is ontstaan, bij het project hoort dat aan een werkende fusiereactor dient bij te dragen, zal er bladerende door dit proefschrift niet dikwijls een beeld van een energiecentrale opgeborreld zijn. De relevantie van magnetische reconnectie is echter aanzienlijk, aangezien het kan leiden tot een paar van de heftigste verschijnselen in fusieplasma's, die beheerst moet worden voor de implementatie van fusie als energiebron. Het kan de magnetische configuratie van het plasma vervormen, een volledig eind maken aan magnetische opsluiting, maar ook het subtiele, nuttige effect hebben van het regelmatig naar buiten werken van de helium-'as', zodat het plasma niet uitdooft.

Het is essentieel een beter begrip te krijgen van dit proces om het te kunnen beheersen of zelfs te voorkomen. We moeten begrijpen hoe het werkt, wat de elektronen die erbij betrokken zijn doen en hoe ze het verloop van het reconnectieproces beïnvloeden. En we willen graag weten welke rol belangrijke parameters zoals de temperatuurgradiënt spelen, als we bedenken dat de grootste temperatuurgradiënt van het heelal gegenereerd wordt in een tokamak. Dit was de hoofdvraag die in dit proefschrift aan de orde gekomen is.

References

- [1] Hesiod. *Theogony*.



Acknowledgements

Adde parvum parvo magnus acervus erit.

(Add little to little and there will be a big pile.)

Ovid.

The work that is bundled in this thesis would probably be just a big pile of little things if it were not for the considerable number of people that have contributed to it in one way or the other. I feel fortunate to have been surrounded by so many people that offered guidance, help or distraction whenever I needed it.

First of all I would like to thank my promotores, professor Niek Lopes Cardozo and professor Wim Goedheer, who gave me the confidence and freedom to pursue the research as I saw fit. The question “where can I stop reading this manuscript” still burns in my mind as a challenge to write things in a (more) compelling way.

But there would be nothing to write about without my supervisor, Hugo ‘the grandfather of all knowledge’ de Blank. Not only did he make time whenever I was misguided and revelling in my lack of knowledge or mathematical rigour, but he also knew everything about everything. And apart from all that he also has a good sense of humour, taste in cartoons and he is perplexingly relaxed. It was a pleasure to work with him, and I will certainly miss the enlightening discussions, coffee breaks and walks through the park.

I would like to thank professor GertJan van Heijst, professor Howard Wilson and professor Karl-Heinz Spatschek for carefully reading the manuscript, and sharing their comments and suggestions. Also, I would like to extend my gratitude to professor Theo Schep, who brought the numerical Contour Dynamics method to our attention.

The meetings of the group in which I was embedded, formerly known as Nonlinear Dynamics and Transport, which merged into the Computational Plasma Physics department, were always inspiring. I learned a lot of the interpretations of experiments of Dick Hogeweij, Erik Min’s hardships to simulate tokamak plasmas, the complex Brunt-Väisälä frequencies of Jan-Willem Blokland and the disarmingly simple though unanswerable questions of Kees de Meijere, Esq. After the merger such pleasantries were shared with Victor Land, Dagmar de Rooij, Zakaria Meliani and Rob Wiegers.

Here, I would like to extend a special thanks to Jan-Willem Blokland, who introduced me into the wondrous world of supercomputing, and helped me on numerous occasions when my FORTRAN code fell apart under the harsh regime of yet another compiler. Without your help it would probably be a sorry excuse for a code, that would only work on one specific, outdated computer, maybe.

Erik Min has been the roommate anyone could wish for. Joining me in laughter and misanthropy, introducing me to Hertzfeldt (“my spoon is *too* big”) and Too Much Coffee Man and sharing the wonders of fatherhood, he made me appreciate the luxury of having a friend as a roommate.

Rijnhuizen is in a sense the ivory tower that every scientist dreams of, as a patch of scientific paradise immersed in the wastelands of Nieuwegein. Here the bitter woes of the Ph.D. student are easily soothed during coffee breaks or over a beer by solidarity of the fellow inmates, like Amy Shumack, Wouter Vijvers, Jeroen Westerhout, Hans van Eck, Maarten de

Bock and Ivo Classen and senior scientists Gerard van Rooij and Marco de Baar. And of course, Hajnal Vörös illuminated it all with her presence, and brightens the darkest of days.

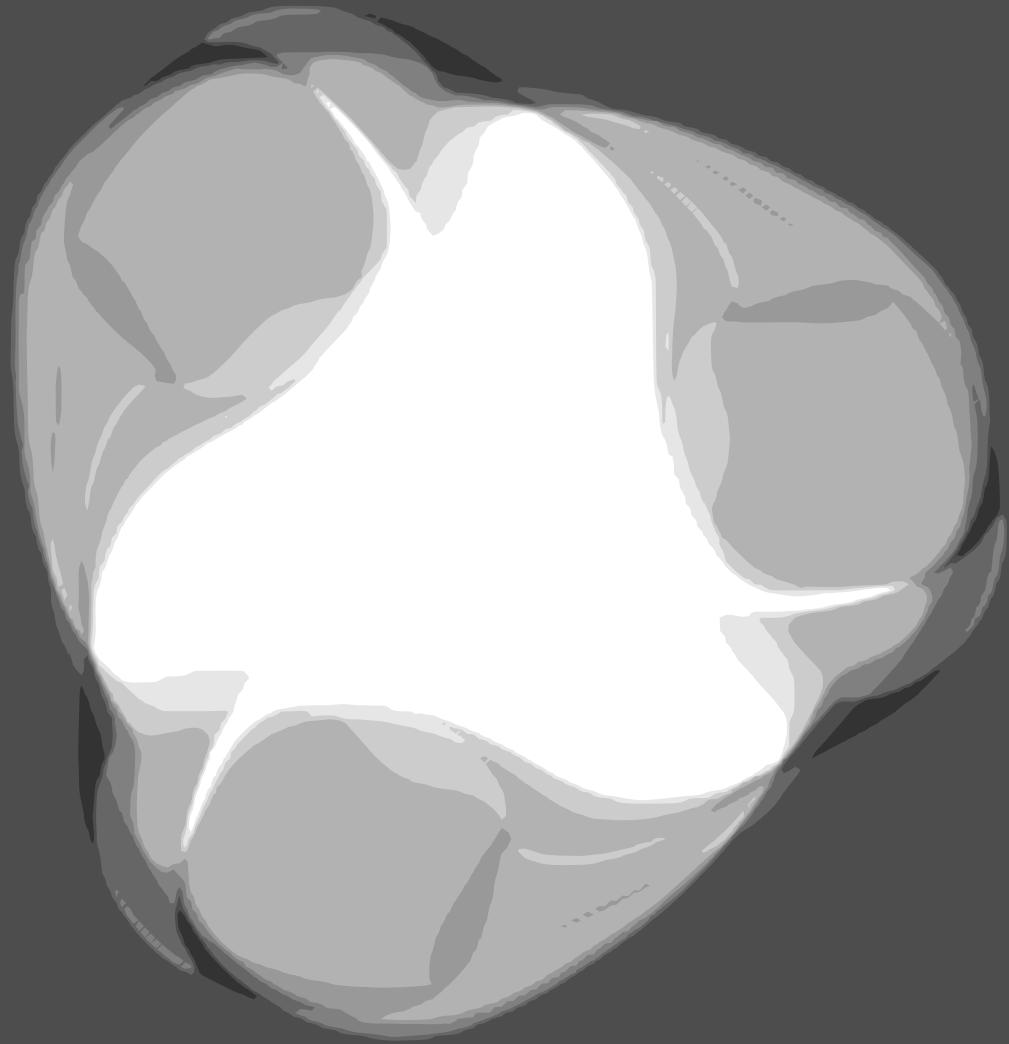
Fortunately, there is more to life than sitting behind a computer or sipping coffee exchanging small talk: there are friends with whom I can share that I have been doing this. I enjoy the pointless though sometimes sharp discussions with Aschwin Wijnsma, Frans Kooiman, Rick Bethlem and Peter van der Kamp, though the latter lacked physical presence the recent years. Thank you for your patience and understanding, and reading my incoherent e-mail. I will not even try to mention all the people that I have shamefully neglected the recent period, but I hope you will forgive me my lack of determined concreteness, which I plan to compensate with chaotic impulsivity.

I am very grateful to my parents, for producing me, and supporting me in many material and immaterial ways throughout my life. I consider myself a very lucky person to have been raised in your love and undivided attention. Attention, shared only by my brother, whom I thank for his many tips and tricks on how to survive a Ph.D. period. I would also like to thank my parents-in-law, who provided me with time and opportunity to spend my weekends writing all this.

Dear Titia, I think there are no words that can express the gratitude for your patience, support and help during this whole ordeal. But most of all, thank you for having given me a daughter, the light of my life, Isis.

Curriculum Vitae

I was born on November 20, 1972 in Amsterdam and grew up in Uithoorn, which lies approximately 15 km south of Amsterdam. At the secondary school the ‘Hermann Wesselink College’ in Amstelveen I obtained my ‘gymnasium- β ’ diploma in 1991. I studied theoretical physics at the Vrije Universiteit in Amsterdam. The research for my master’s thesis, ‘Global Alfvén phenomena in toroidal geometry’, was done at the FOM-Institute for Plasma Physics Rijnhuizen, under supervision of J.P. Goedbloed. After graduating in 1997, I worked as a trainee at the Global Transaction Services department of the ABN AMRO bank, until the turn of the millennium. I quit this job to travel through South Asia. In the fall of 2000, I took up a Ph.D. position at the TU Delft to investigate the influence of magnetic fields on turbulent Rayleigh-Bénard convection with an experimental set-up. Unfortunately, I could not complete the research there because of suffering from Lyme’s disease for a prolonged period. In October 2003 I started working as a Ph.D. student at the FOM-Institute for Plasma Physics Rijnhuizen under supervision of dr. H.J. de Blank. I performed theoretical analysis on the influence of temperature gradients on collisionless magnetic reconnection in tokamak plasmas using the Contour Dynamics method. The results of this research are described in this thesis.



Magnetic reconnection in plasmas is the process where magnetic field lines break open and reconnect in a different way, transforming magnetic into kinetic energy. In fusion plasmas, reconnection can degrade the magnetic confinement of the plasma necessary to achieve efficient nuclear fusion. In this thesis reconnection is studied analytically and numerically with the theoretical technique of Contour Dynamics. This approach made it possible to use a kinetic model to study the influence of temperature gradients on the nonlinear reconnection process.